Analysis of the Rolling Motion of Loaded Hoops

Willem F.D. Theron

Dissertation presented for the degree
Doctor of Philosophy
at the Department of Applied Mathematics of the
University of Stellenbosch, South Africa

Supervisor : Dr MF Maritz

March 2008

Declaration

I, the undersigned, hereby declare that the work contained in this dissertation is my own original work and that I have not previously in its entirety or in part submitted it at any university for a degree.

Signature: _____ Date: _____

Abstract

This dissertation contains a detailed report on the results of a research project on the behaviour of a dynamical system consisting of a hoop to which a heavy particle is fixed at the rim. This loaded hoop rolls on a rough surface while remaining in the vertical plane. The motion of the hoop consists of various, possibly alternating, phases consisting of rolling without slipping, spinning or skidding motion and in some cases ends by hopping off the surface.

A general mathematical model is developed, consisting of a system of second order ordinary differential equations, one for each of the three degrees of freedom. Analytic solutions are obtained in some cases; otherwise numerical solutions are used.

Three specific applications of the general model are dealt with.

In the first application the problem of massless hoops is investigated. The main emphasis is on the somewhat controversial question of what happens after the normal reaction becomes zero in a position where the particle is still moving downwards. A new result shows that the hoop can continue to move horizontally in a motion defined as skimming.

The second application deals with rigid hoops and a large number of detailed results are presented. Classification schemes for the different types of behaviour are introduced and summarised in the form of phase diagrams. Some emphasis is placed on the rather amazing number of different patterns of motion that can be obtained by varying the parameters.

In the third application two elastic models are analysed, with the primary purpose of explaining one aspect of the reported behaviour of experimental hoops, namely hopping while the particle is moving downwards.

A chapter on experimental models rounds off the project.

Opsomming

In hierdie verhandeling word verslag gedoen oor 'n navorsingsprojek oor die gedrag van 'n dinamiese stelsel wat bestaan uit 'n swaar partikel wat geheg word op die rand van 'n ronde hoepel. Hierdie gelaaide hoepel rol in die vertikale vlak op 'n ruwe oppervlakte. Die beweging van die hoepel bestaan uit verskeie, moontlik alternerende, fases wat insluit suiwer rol beweging en twee tipes gly beweging. In sommige gevalle verlaat die hoepel die oppervlakte.

'n Algemene wiskundige model is ontwikkel, bestaande uit 'n tweede orde gewone differensiaalvergelyking vir elk van die drie vryheidsgrade. In sommige gevalle word 'n analitiese oplossing verkry; andersins word numeriese oplossings gebruik.

Drie spesifieke gevalle word ondersoek.

In die eerste toepassing word die probleem van massalose hoepels ondersoek. Die klem is hoofsaaklik op die ietwat kontroversiele vraagstuk oor die beweging van die hoepel nadat die reaksiekrag tussen die oppervlakte en die hoepel nul word terwyl die partikel afwaarts beweeg. Daar word aangetoon dat die hoepel kan voortgaan om horisontaal vorentoe te beweeg terwyl dit roteer; hierdie nuwe tipe beweging word "skimming" genoem.

Starre hoepels is die onderwerp van die tweede toepassing, en die beweging word in fyn besonderhede ontleed. Die verskillende tipes beweging word geklassifiseer en opgesom in fase-diagramme. Klem word geplaas op die verrassend groot aantal bewegings-patrone wat verkry word deur die parameters te verander.

In die derde toepassing word twee elastiese modelle ge-analiseer, met die hoof doel om 'n verklaring te vind vir die waargenome verskynsel dat eksperimentele hoepels kan hop terwyl die partikel afwaarts beweeg.

Die projek word afgerond met 'n hoofstuk oor eksperimentele modelle.

Acknowledgements

This dissertation is the result of a decision taken nearly five years ago. The author hereby wishes to express his gratitude towards

- Dr Milton Maritz for his insight, patience and diligence. Our regular interviews invariably provided positive and constructive suggestions on his part. It was a truly great pleasure working with him on this project.
- Proff. Andre Weideman and Willy Heremans for originally suggesting that the previously published articles be combined in a dissertation.
- Prof. Tadashi Tokieda, whose article inspired this research project, and for his continued interest in the subject.
- The Department of Applied Mathematics for the use of their computing facilites.
- My wife, Mercia, and our two children for all their support and encouragement.

.

Preface

This dissertation is based on a personal research project which culminated in four articles, with the possibility of a fifth.

The following ten pages contain information to aid the reader, culminating in the Table of Contents. This is followed by nine chapters plus five appendices.

Chapter 1 of this dissertation is an introduction in which the project is described in some detail, including a literature survey.

Chapter 2 contains the derivation of the mathematical model for the most general case, using Newtonian dynamics.

Chapter 3 is a slightly extended version of the article on massless hoops, [2].

Chapters 4 to 6 contain a detailed analysis of rigid hoops and include all the results in [1]. Many new results, some of which are included in [6], are obtained.

Chapter 7 is an extended version of the article on elastic hoops, [3].

Chapter 8 contains some results for experimental examples of hopping hoops.

Chapter 9 contains some final discussion and conclusions.

Appendix A contains three alternative derivations of certain equations.

Appendix B contains an extensive review of a number of aspects related to the torque equation as used in Newtonian Dynamics. An article, [7], based on this review has been submitted for publication.

Appendix C contains a summary of the general theory of the Lagrange method. This method is then used to derive the equations for elastic hoops.

Appendix D contains the derivation of the moment of inertia of an elastic hoop.

Appendix E contains computer code of selected functions used to obtain the numerical results.

The text of the original articles has been re-written to a large extent, with a number of changes and corrections. In most cases more mathematical detail is given here (compared with the original articles). All the numerical results have been re-calculated and the graphical representation thereof re-plotted. The new results are similar, but not necessarily identical, to the original results.

A number of new insights that were not recognised in the articles are included in the dissertation. This is especially true for the rigid hoop of Chapters 4 to 6 and the models for elastic hoops in Chapter 7.

Typesetting

The following general conventions regarding typesetting are used in this dissertation :

Latin letters
Physical values such as forces, coordinates, kinematic quantities and other physical parameters are denoted by latin letters.

Greek letters and calligraphic characters
Dimensionless quantities are usually denoted by small Greek letters - for example δ and τ denote non-dimensional distance and time respectively.
In cases where a suitable Greek letter is not available, calligraphic characters are used - for example, $\mathcal{E}$, $\mathcal{F}$ and $\mathcal{N}$ are used to denote non-dimensional energy, friction force and normal reaction respectively. (Unfortunately the calligraphic font style of the graphics program differs from that in the main text. This difference is ignored.)

Differentiation
Differentiation with respect to time is denoted by an over dot; for example $\dot{x}$ is used for $\frac{\mathrm{d}\,x}{\mathrm{d}\,t}$.

Differentiation with respect to dimensionless time is denoted by a prime; for example δ' is used for $\frac{\mathrm{d}\,\delta}{\mathrm{d}\,\tau}$.

Framed boxes

- Pedagogical aspects.

  One of the features of this dissertation is to accentuate pedagogical aspects as they arise. Such remarks should be of interest to teachers of Classical Mechanics and also occasionally to teachers of Numerical Mathematics. However, these remarks can be ignored without affecting the understanding of the main theme of the dissertation.

- Algorithms and numbered results.

  Algorithms and important results that are numbered for ease of reference are also placed in boxes.

Spelling

U.K. orthography is used throughout.

Decimal points (not commas) are used in real numbers.

Nomenclature

Precise definitions for a number of concepts are given here.

Firstly, in connection with hoops, note that hoops can be categorised as being either elastic or rigid; they can also be considered to be with or without mass. The following nomenclature is used in this dissertation :

- A *massless hoop* refers to a hypothetical hoop-and-particle system in which the mass of the hoop is zero; i.e. the total mass equals the mass of the particle. Only rigid massless hoops will be considered.
- A *real hoop* refers to a hoop-and particle system in which the mass of the hoop is non-zero; a real hoop can be either rigid or elastic.
- A *rigid hoop* refers to a real hoop which is considered to be rigid.
- An *elastic hoop* refers to a real hoop which is considered to be elastic.
- Two *elastic models* are analysed. The external model consists of a rigid hoop rolling on an elastic surface. The internal model consists of an elastic hoop rolling on a rigid surface.
- A *non-elastic hoop* is either a massless or a rigid hoop.

The term *rolling* is used in two slightly differing contexts.

- For the greatest part of this dissertation the term rolling or rolling motion refers to the motion of the hoop in which it rotates without slipping. This implies zero velocity of the contact point, and could also be referred to as "pure" rolling.
- In some case however, the term rolling is used in a slightly more general sense, namely to describe the planar motion of the hoop. In these cases the various different phases of the motion are not important. An example of this usage is to be found in the definition of the elastic models above.

Finally, a number of concepts used in this dissertation to derive the mathematical models are defined precisely.

- The *moment* of a vector quantity $\mathbf{V}$ around a reference point A is the cross-product $\mathbf{r} \times \mathbf{V}$, where $\mathbf{r}$ is the position vector from point A to the vector.
- *Torque* is the moment of a force.
- The *torque equation* is a form of Newton's second law in which the total torque acting on a body is equated to kinematic quantities.
- The *equation of motion* is a differential equation that can be solved to obtain the velocity or angular velocity.

Notation; List of Symbols

The notation used here for the general model inevitably differs from the notation used in the original articles in a few respects. The assumption used here is that the reader will *not* attempt to read the articles at the same time; however, if he should wish to do so, the table below can be used to identify the differences.

The notation used in this dissertation is defined in the first two columns in Table 0.1 below, in chronological order as defined in the text. The third column shows the notation in the original article [3]. In cases where this differs from the notation in articles [1] and [2], the notation of the latter is given in the last two columns.

The abbreviation n-d is used to identify non-dimensional variables.

Note the following regarding the notation :

- The sign of the *elastic displacement* d is opposite to that used in [3]. In the original article, a negative value of d denoted compression of the hoop. The convention used here corresponds to the more physical interpretation that a positive value of d denotes compression.
- The concept of *non-dimensional variables* was used slightly differently in [1, 2], where all differentiation was done with respect to real time t; here non-dimensional time is defined and used in the derivatives.
- Three different symbols are used to denote the *non-dimensional angular acceleration.*
  θ'' is used in the kinetic equations;
  ω' is used in the first order differential equations;
  α is used in the text and in the graphs.
- Certain special positions, and the corresponding variables, are denoted by specific subscripts.
  $\theta_0 = 0$ defines the initial position;
  θ_r establishes the position where a rolling phase commences;
  θ_s establishes the position where a slipping phase commences;
  θ_f denotes the final position, where the analysis of the motion ends;
  θ_* establishes the position where the hoop hops;
  θ_+ establishes the position where the hop ends;
  θ_m denotes the first minimum in the normal reaction.
- Discontinuities are indicated by superscript $^-$ and superscript $^+$ to indicate a value just before and immediately after the discontinuity; for example $\alpha(\theta_s^+) - \alpha(\theta_s^-)$ denotes a (possible) discontnuity in the angular acceleration when slipping starts.

Symbol	Definition	[3]	[2]	[1]
r	radius of hoop	r		
ψ	slope of the ramp	φ		
θ	angular displacement of hoop	θ		
γ	eccentricity of hoop; O-G $= \gamma r$	γ		
$\mathcal{H}$	n-d height of G	h		
m_h	mass of hoop	m_h		
m_p	mass of particle	m_p		
m	total mass; $m = m_h + m_p$; $\gamma = m_p/m$	M		
I	moment of inertia of hoop	I		
κ	inertia factor; $I = \kappa\, mr^2$	κ		
ϵ	moment of inertia of particle : $I_P = \epsilon\, mr^2$	ϵ		
$\mathbf{e}_t; \mathbf{e}_n$	Cartesian unit vectors	$\mathbf{i}; \mathbf{j}$		
$X; Y$	coordinates of point O	$X; Y$		
d	elastic displacement; $Y = r - d$	$-d$		
$x; y$	coordinates of point G	$x; y$		
a	acceleration of G			ag
$\mathcal{X}; \mathcal{Y}$	n-d coordinates of point O; $\mathcal{X} = (X/r); \mathcal{Y} = (Y/r)$			
$\mathcal{V}$	n-d velocity of O; $\mathcal{V}_x = \mathcal{X}'; \mathcal{V}_y = \mathcal{Y}'$			
δ	elastic deformation; $\delta = d/r$	δ		
mg	total weight	Mg		
F_n	normal force between track and hoop	N		
F_f	friction force between track and hoop	F		
μ	friction coefficient; $F_f \leq \mu F_n$	μ		
$\mathcal{N}$	n-d normal reaction : $\mathcal{N} = F_n/mg$			
$\mathcal{F}$	n-d friction : $\mathcal{F} = F_f/mg$			
τ	n-d time; $\tau = \sqrt{g/r}\, t$	τ		
ω	n-d angular velocity; $\omega = \sqrt{r/g}\, \dot{\theta}$	ω		
ω_0	initial angular velocity; $\omega_0 = \sqrt{r/g}\, \dot{\theta}(0)$	ω_0		
$\alpha = \omega' = \theta''$	n-d angular acceleration : $\theta'' = r\ddot{\theta}/g$	ω'	ζ	ζ
ω^2	n-d centripetal acceleration : $\omega^2 = r\dot{\theta}^2/g$		η	η
E; $\mathcal{E} = E/mgr$	Energy (Potential plus Kinetic)			
E_1; $\mathcal{E}_1 = E_1/mgr$	Initial energy (Potential plus Kinetic)			
E_0; $\mathcal{E}_0 = E_0/mgr$	Initial Potential energy			
S	slip factor; $S = \gamma \sin\theta - \mu\mathcal{H}$	S		
$\mathcal{S}_1$, $\mathcal{S}_2$, $\mathcal{S}_T$	n-d range of the particle; $\mathcal{S}_T = \mathcal{S}_1 + \mathcal{S}_2$		S_T	
$\mathcal{T}_2$	elapsed time of the hop; $\mathcal{T}_2 = \tau_2 - \tau_s$		T_2	
k	stiffness coeff. in Hooke's law; $F_n = kd$	k		
d_s	static deformation; $d_s = mg/k$	d_s		
e	elastic constant; $e = r/d_s$; $\mathcal{N} = e\delta$	e		

Table 0.1 : Notation for Loaded Hoops

Table of Contents

List of numbered boxes

Algorithms

Results

List of Tables

Chapter 1

Introduction

In this dissertation the general problem of the two-dimensional dynamic behaviour of *loaded hoops* is investigated. By this is meant a dynamical system in which a heavy particle is fixed to the rim of a light hoop, or in general, an eccentrically loaded wheel in which the centre of mass does not coincide with the axis of rotation. The hoop or wheel is given an initial velocity to start it rolling on a rough, possibly sloping, planar surface, and the resulting two-dimensional motion is analysed. This purely academic exercise culminated in three articles [2, 1, 3], on massless, rigid and elastic hoops respectively.

1.1 Background to the problem of Hopping Hoops

This section contains a general discussion of the phenomenon of *hopping hoops* (without going into detail); this is followed by an overview of the literature on this phenomenon and related issues.

This project started with a chance reading of an obituary to the American mathematician Fred Almgren [11]. In this article passing reference is made to an experiment in collaboration with Tadashi Tokieda, to verify the phenomenon of "The Hopping Hoop" as analysed by Tokieda [9]. In the experiment they ".. taped a battery to a hula hoop and rolled it down a hallway. The hoop hopped, just as predicted." [11]

I found this result intriguing and consulted the paper by Tokieda. And so started a research project that has fascinated me for almost ten years.

The hypothetical problem of a rigid, massless hoop, loaded with a particle fixed to the rim, and which rolls without slipping on a horizontal surface, has been used for very many years as an interesting class-room problem for planar motion of rigid bodies, and was first published by J.E. Littlewood [8] in 1953 in "A Mathematician's Miscellany". The following formulation and "solution" is from p. 37 of the recently published revised edition [8] of this book.

'*A weight is attached to a point of a rough weightless hoop, which then rolls in a vertical plane, starting near the point of unstable equilibrium. What happens, and is it intuitive ?*

The hoop lifts off the ground when the radius vector to the weight becomes horizontal. I don't find the lift directly intuitive; one can however "see" that the motion is equivalent to the weight's sliding smoothly under gravity on the cycloid it describes, and it is intuitive that it will sooner

or later leave that. *(But the "seeing" involves the observation that P is instantaneously rotating about C (Fig.1).)*

Mr H.A. Webb sets the question annually to his engineering pupils, but I don't find it in books.

In actual practice the hoop skids first.'

The same problem is considered by Tokieda [9], whose analysis is based on the geometric aspects of the motion. Both Littlewood and Tokieda conclude that the hoop will hop after rolling through 90° after starting from rest with the particle at the highest point of its cycloidal path.

This conclusion has troubled me and others, it being counter intuitive that the hoop can hop while the particle is moving downwards. In the first version of the paper on massless hoops, [2], I attempted to prove that the hoop could not hop as predicted. A reviewer pointed out an error in the proof, and insisted that hopping was a possibility, just as the new skimming motion derived in [2] is a possible motion. The same error was made by Butler [12], as discussed later.

There is no dispute that the normal reaction becomes zero; in the skimming motion derived in [2] the hoop remains in contact with the surface even though the reaction force between surface and hoop is zero.

When discussing these issues with Tokieda, he responded as follows [10] : "By 'hopping', what is mathematically meant is of course not that the hoop acquires an upward velocity, but rather that the vertical reaction on the floor vanishes; the point of contact hovers as if in zero gravity. Physically, any tiny irregularity on the floor is enough to push up the hoop, and in practice the hoop hops. "

In this dissertation the above interpretation is not used; here *hopping* is defined precisely as a motion in which the centre of the hoop does acquire an upward velocity. Conditions in which this happens are derived for real hoops (with mass). In the case of rigid hoops, it is shown in [1] that hopping can occur under certain conditions after rotating more than 270°, i.e. while the particle is moving *upwards*. In the case of elastic hoops, it is shown in [3] that hopping can occur under certain conditions while the particle is moving *downwards*.

A conclusive proof that the truly singular problem of a massless, rigid hoop loaded with a particle does not hop when the normal reaction becomes zero has not yet been published. The current understanding is that both skimming and hopping are possible motions, due to the singularity inherent to the problem. These issues are discussed again in more detail in later chapters.

1.2 Literature overview

The phenomenon of the "hopping hoop" has received some attention recently [9, 1, 2, 3, 12, 13], many years after first being published in 1953 in "A Mathematician's Miscellany" by J.E. Littlewood [8].

The quotation given in the previous section is all that Littlewood says about the problem in this book. His remarks seem to have been accepted (or unnoticed !) for more than forty years, until 1997 when Tokieda [9] published an ingenious analysis based on the fact that the path of the particle changes from a cycloid to a parabola. He interpreted this as supporting Littlewood's statement that the hoop lifts off the ground, or *hops*, after rotating through 90°.

Tokieda's article prompted a flurry of interest [1, 2, 3, 12, 13], mainly regarding the question of whether the hoop lifts off the ground (i.e. *hops*) or not.

Massless hoops are analysed by Butler [12] and Theron [2]. Butler sets out to prove that Littlewood's hoop cannot hop; unfortunately his proof contains a serious error which will be discussed later. In [2], Littlewood's problem is generalised slightly by including the effects of non-zero initial velocities and realistic friction coefficients. The main result of this paper is a somewhat unusual motion called "skimming", which is found to be an alternative to hopping after the normal reaction becomes zero. At this stage there is no formal proof that the massless hoop will *not* hop, although there are strong indications that it will rather skim. These aspects are discussed in detail in later chapters.

In all the above references to massless hoops, it was assumed that the hoop was also rigid.

Pritchett [13] and Theron [1] consider various aspects of the behaviour of *rigid hoops*, i.e. real, rigid models in which the mass of the hoop and the effect of friction are taken into account. Pritchett proves formally that such hoops cannot hop from the rolling motion, but have to slide first. An important aspect of his proof is a model where the "particle" is a body with non-zero moment of inertia. Clearly, Littlewood also realised that the hoop would "skid first", as seen in the last sentence in the quotation from his book.

Theron uses mainly numerical solutions to analyse a number of interesting phenomena in great detail. His results are in agreement with Pritchett in showing that a real hoop will always start sliding before the normal reaction becomes zero. However, the two papers present conflicting results for the motion after sliding starts; Theron maintains that the hoop cannot hop after rotating through approximately 90°, whereas Pritchett shows a graphic result in which it does. This discrepancy is presumably due to the different numerical algorithms used to solve the sliding motion.

The main focus in [1] is on cases with very large eccentricities, such as obtained when a heavy particle is fixed to the rim of a light hoop. Hopping can occur in such cases after rotating through approximately 270°, and the initial conditions which are necessary to cause this are derived and presented as the main result of this analysis.

A second interesting feature of such hoops is that they provide another example of a "faster than gravity" model (see [15, 16]), in which the acceleration of the particle can exceed the acceleration due to gravity even though gravity is the only active force.

A third point of interest is the number of different modes of motion and the large variety of sequences in which they can occur. This is the subject of a recent article, [6].

All three the above mentioned aspects are discussed in detail in Chapters 4 to 6.

Tokieda [9] reports having witnessed an experiment by Fred Almgren [11] in which a hula-hoop was loaded with a battery and hopped as predicted by Littlewood, namely that the hoop leaves the ground when the radius to the particle is approximately horizontal and the particle is moving downwards. Pritchett [13] also shows a stroboscopic photograph of the same phenomenon, in which a plastic hula-hoop is loaded with brass rods. It is noteworthy that in both cases a hula-hoop, which can surely not be considered to be rigid, was used.

Theron's article [3] on *elastic hoops* is the first to develop a model which gives a reasonable explanation of the abovementioned phenomenon by taking the elasticity of the hoop into account. An extremely simple elastic model is considered, in which it is assumed inter alia that the deformation of the hoop does not affect the moment of inertia. In spite of its simplicity,

this model yields the desired results as discussed in Chapter 7.

The subject of eccentrically loaded hoops, wheels or cylinders is still receiving attention, as shown by the following papers published in 2004 and 2005. Liu and Xue [17] describe a model identical to the author's [1] for a rigid hoop loaded with a particle on its rim. The presentation of results in terms of phase diagrams of angular velocity versus angular displacement in [17] differs from the presentation of results in [1]; however, the model and conclusions in [17] are the same as those in [1], without making any reference to [1].

Carnevali and May [18] show that an asymmetric cylinder can, under the correct conditions, roll down a slope in a shorter time than a symmetric cylinder.

1.3 A similar project

An earlier project (which is not included in this dissertation) analysed somewhat similar models for a more practical project, culminating in two articles [4, 5]. The two projects are similar in a number of aspects : in both cases, the rolling motion of a wheel is considered; the motion takes place in a vertical plane (i.e. only two-dimensional motion is considered); the elasticity of the wheel is a very important feature; the wheel is loaded in some manner and in certain circumstances the wheel can hop (or bounce) (i.e. it leaves the surface on which it is rolling).

The earlier project was done in collaboration with civil engineers who were investigating techniques for testing the condition of (road) pavements. One such technique is based on millions of wheel loads being applied to the pavement by an apparatus known as the 'Accelerated Loading Facility', or ALF, in which a heavily loaded wheel rolls down a circular track onto a horizontal section of road. The wheel has a surprisingly large response to the sudden change in acceleration at the end of the circle. The author's contribution to the project was a computer simulation of this dynamic response of the ALF.

The load consists of a large external mass above the wheel, connected to the axis by a suspension mechanism, which is usually modelled as a linear spring and damper system.

The system has the capacity to store elastic potential energy while rolling down the circular track. When it reaches the point where the circular track changes to a flat surface (i.e. the point where the curvature of the track suddenly becomes zero), the wheel is subjected to an 'infinite jerk' which releases the stored energy and causes vertical oscillations while the wheel rolls along the horizontal pavement.

Typical graphs of the normal force between the track and the wheel during the motion show an increase in this force due to the centrifugal effect while rolling down the circular track, followed by severe oscillations starting suddenly at the point where the circle ends. The initial amplitude of this vertical oscillation essentially reflects the effect of the jerk. In cases where this initial amplitude is large enough, the first minimum in the normal force is negative, indicating that the wheel has bounced off the pavement; in [4] the conditions that are required for the wheel to bounce are analysed. Two simplified models are analysed in more detail in [5].

Chapter 2

General mathematical model of a loaded hoop

This chapter contains the general mathematical model of a loaded hoop. The model is general in the sense that it contains elasticity; in later chapters detailed results are obtained for the special cases of massless, rigid and elastic hoops respectively, corresponding to the results in [2, 1, 3].

This general model consists of a rigid hoop rolling on a deformable surface, and will also be referred to as the *external elastic model*. This is the simplest manner in which elasticity can be included. An alternative model is developed in Chapter 7.

2.1 The mathematical model

The analysis is done in terms of forces rather than the energy of the system, because the different phases of the motion are identified in terms of the forces. The equations of motion are therefore derived using Newton's second law in the standard manner by taking moments around the centre of mass. Alternative derivations are given in Appendix A.

The main purpose of the analysis is to investigate the behaviour of the system, in which time does not play an essential part. All the differential equations are therefore formulated in terms of position rather than time, leading in general to simpler solutions.

2.1.1 Geometry of the hoop

Figure 2.1 shows a loaded hoop (or wheel) with radius r rolling down a surface which makes an angle ψ with the horizontal plane.

Point O is the centre of the hoop, which is loaded with a particle at point P on the rim.

Point C is the point of contact between the hoop and the track. In the case of rolling without slipping point C is also the instantaneous centre of rotation.

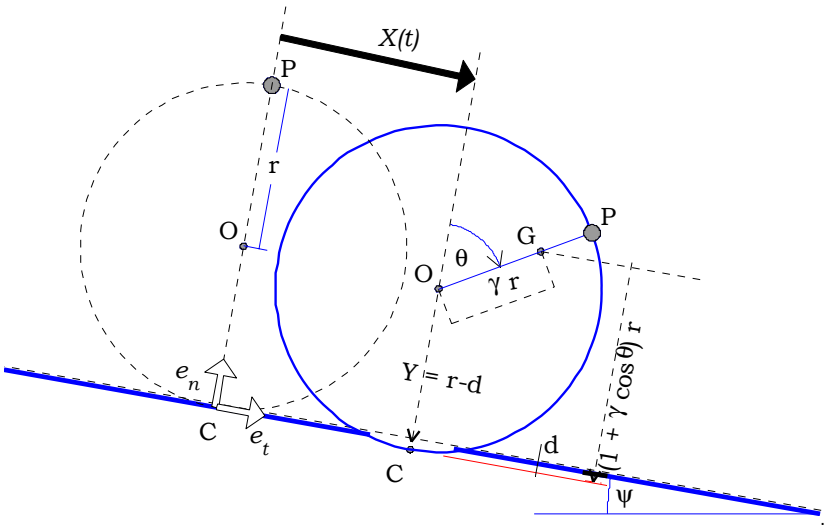

Figure 2.1: Geometry of a Loaded Hoop

The position of the hoop is determined by the angular displacement θ, with the initial position $\theta = 0$ being taken as the position when the radii C-O-P form a straight line. The analysis is restricted to $\theta < \pi$ in the case of a massless hoop (Chapter 3). In the case of real hoops (Chapters 4 to 7) however, this restriction is lifted, and the analysis is for $\theta \in [0,\ 2\pi]$.

The centre of mass is at point G at a radial distance γr from point O, where the *eccentricity* γ is defined by

$$\gamma = \mathrm{OG}/r. \tag{2.1}$$

Let m_h denote the mass of the hoop, m_p the mass of the particle and $m = m_h + m_p$ the total mass; then

$$\gamma = m_p/m.$$

The cases of interest for the analysis which follows are for large eccentricities, approximately in the range $\gamma \in (0.5,\ 1)$. For example, in the *equal mass* case, $m_p = m_h$ and $\gamma = 0.5$; in the case of Littlewood's hoop, $m_h = 0$ and $\gamma = 1$. If $m_p = 2m_h$, $\gamma = 2/3$; this is the case used in many of the numerical results.

A useful geometric quantity is the component in the normal direction of the vector CG, denoted by $\mathcal{H}\, r$; i.e. we write

$$\mathrm{CG} = \gamma r \sin\theta\, \mathbf{e}_t + \mathcal{H} r\, \mathbf{e}_n,$$

and refer to $\mathcal{H}$ as *the non-dimensional height* of point G.
Using Figure 2.1, $\mathcal{H}\, r = r + \gamma\, r\, \cos\theta$, i.e.

$$\mathcal{H} = 1 + \gamma\, \cos\theta. \tag{2.2}$$

This expression applies to all cases of rigid hoops.

Moments of inertia are defined in terms of a factor κ such that the moment of inertia, I, is given by $\kappa\, mr^2$; i.e.

$$\kappa = I/mr^2.$$

This concept of defining the moment of inertia as a dimensionless factor multiplied by the mass multiplied by a length squared is not commonly used in the literature on Dynamics. Most textbooks use k to denote the radius of gyration (with unit of length); in this dissertation the symbol κ is used for the non-dimensional factor.
In the case of the loaded hoop the moment of inertia is given by $\kappa\, mr^2$.
Other well known examples are the moments of inertia of a circular disk and a rod about axes through their centre of mass, namely $\frac{1}{2}mr^2$ and $\frac{1}{12}mL^2$; i.e. $\kappa = \frac{1}{2}$ and $\frac{1}{12}$ respectively.
Clearly, this factor will always be a positive real number.
The main advantage of this definition occurs when equations are non-dimensionalised. This definition can also be used for the second moment of area by simply replacing the mass by the area.

In all cases the axis around which the moments are taken is perpendicular to the plane containing the hoop. The hoop is approximated as a rigid circular wire so that $I_{O(hoop)} = m_h\, r^2$.

In articles [1, 2] an infinitely small particle with $I_{P(particle)} = 0$ was used; in [3] we followed Pritchett [13] and defined $I_{P(particle)} = \epsilon\, mr^2$. Usually ϵ will be a small number with very little influence on the numerical results; it was used by Pritchett in his proof that the massless hoop always slides before hopping. Then the total moment of inertia around point O is

$$I_O = m_h\, r^2 + \epsilon\, mr^2 + m_p\, r^2 = (1+\epsilon)\, m\, r^2.$$

Using the parallel axes theorem, $I_O = I_G + m(\gamma\, r)^2$, or

$$I_G = (1 + \epsilon - \gamma^2)\, m\, r^2.$$

The dimensionless moment of inertia factor for G is therefore

$$\kappa_G = 1 + \epsilon - \gamma^2. \tag{2.3}$$

Here the significance of ϵ becomes clear: κ_G remains positive even when $\gamma = 1$ for the massless case.

Clearly, for $m_h > 0$, $\gamma < 1$ and $\kappa_G > 0$. In the case of the massless hoop, $\gamma = 1$ and $\kappa_G = \epsilon$. It is possible to envisage a model with $\gamma > 1$ by placing a heavy particle on a spoke outside the rim of the hoop; however this case is not included in this analysis. Note that the above expressions for the moments of inertia, and (2.3) in particular, no longer apply if $\gamma > 1$.

It is also useful to use the moment of inertia around the axis through C, calculated as $I_C = I_G + m(\mathrm{GC})^2$. Noting from Figure 2.1 that $(\mathrm{GC})^2 = (r\,\gamma\,\sin\theta)^2 + (r\,\mathcal{H})^2$, and using (2.3) and (2.2), the dimensionless moment of inertia factor simplifies to

$$\kappa_C = 2\,\mathcal{H} + \epsilon. \tag{2.4}$$

The geometry [1] of a hoop is conveniently summarised by three values, namely $\mathcal{H}$, the non-dimensional height of G from (2.2), and the moment of inertia factors κ_G from (2.3) and κ_C from (2.4).

The mathematical model in this chapter is derived for the most general geometry, with $\epsilon \geq 0$ and $\psi \geq 0$. However, in Chapters 3 and 7 a simpler model with $\epsilon = 0$ and $\psi = 0$ is used. In Chapter 4 the general model is derived, but the numerical results in almost all the examples in Chapters 5 and 6 use $\epsilon = 0$ and $\psi = 0$.

2.1.2 Kinematics

With t denoting time, the co-ordinates of O are $(X(t), Y(t))$ in a fixed Cartesian co-ordinate system with axes parallel and perpendicular to the plane as indicated by unit vectors $\mathbf{e}_t$ and $\mathbf{e}_n$, and with origin at the contact point in the initial position on an un-deformed surface. Differentiation with respect to t is denoted by a dot, for example $\dot{X}$; as usual, g denotes the gravitational acceleration.

The fundamental assumption regarding elasticity in this model is that the surface deforms elastically. The downward displacement perpendicular to the surface at point C is denoted by d as shown in Figure 2.1. Because of this deformation of the surface

$$Y(t) = r - d(t); \quad \dot{Y} = -\dot{d}; \quad \ddot{Y} = -\ddot{d}. \tag{2.5}$$

The variable $d(t)$ is interpreted as follows:

- In the massless and rigid models, $d(t) = 0$.
- In the elastic models, $d(t) \geq 0$ implies contact between the hoop and the surface and positive values of $d(t)$ denote elastic deformation, which should be recognised as compression of the surface. [2]
- Negative values of d have no physical interpretation.

The co-ordinates of the centre of mass G are $(x(t), y(t))$ relative to the same axes. Then the rigidity of the hoop enforces the following constraints on $x(t)$ and $y(t)$:

$$x(t) = X(t) + \gamma\, r\, \sin\theta(t); \qquad y(t) = Y(t) + \gamma\, r\, \cos\theta(t). \tag{2.6}$$

Differentiation of (2.6) with respect to time t gives the velocity components as

$$\dot{x} = \dot{X} + \gamma\, r\, \dot{\theta}\, \cos\theta; \qquad \dot{y} = \dot{Y} - \gamma\, r\, \dot{\theta}\, \sin\theta(t); \tag{2.7}$$

and the acceleration components as

$$\ddot{x} = \ddot{X} + \gamma\, r\ddot{\theta}\, \cos\theta - \gamma\, r\dot{\theta}^2\, \sin\theta; \qquad \ddot{y} = \ddot{Y} - \gamma\, r\ddot{\theta}\, \sin\theta - \gamma\, r\dot{\theta}^2\, \cos\theta. \tag{2.8}$$

The magnitude of the acceleration of G is denoted by a:

$$a = \sqrt{(\ddot{x})^2 + (\ddot{y})^2}.$$

The general model has three degrees of freedom, which are here selected as X, Y and θ.

[1] In this dissertation the term 'geometry' is used in a slightly broader sense than normal so as to include the quantities $\mathcal{H}$ and κ_C that are functions of time.

[2] In the original article [3] the sign of d is reversed.

2.1.3 Initial conditions

The initial position and velocity must be given for each of the three degrees of freedom.

We assume that the motion commences at $t = 0$ from an initial position defined by

$$\theta(0) = 0; \quad X(0) = 0; \quad Y(0) = r - d_0.$$

The origin of the axes in Figure 2.1 was defined at the point $d(0) = 0$. However, this value is not used in the subsequent analysis and the specification of d_0 is left for Chapter 7.

The initial angular velocity $\dot{\theta}_0$ is given as an input variable. We assume rolling from the start for all cases, therefore $\dot{X}(0) = r\dot{\theta}_0$. Finally, $\dot{Y}(0) = \dot{d}(0) = 0$ is assumed throughout. To summarise:

$$\dot{\theta}(0) = \dot{\theta}_0; \quad \dot{X}(0) = r\dot{\theta}_0; \quad \dot{Y}(0) = 0.$$

The model therefore requires the input of two possibly non-zero initial values, namely d_0 and $\dot{\theta}(0)$.

2.1.4 Kinetics

Figure 2.2 shows the three forces acting on the hoop while moving in contact with the surface. These are the weight mg, the normal reaction F_n, and the friction force F_f. The reaction forces F_n and F_f act at point C in the direction of the co-ordinate axes.

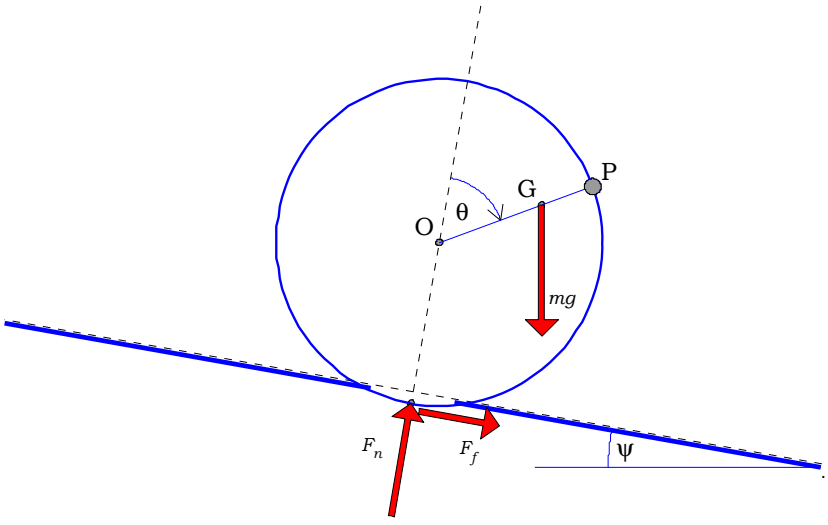

Figure 2.2: Forces on a Loaded Hoop

In the elastic model the normal reaction is due to the elastic deformation, and the relationship between the force F_n and deformation d is modelled very simply by Hooke's law. This issue will be discussed in detail in Chapter 5.

The maximum value of the friction force places a constraint on the forces. Denoting the coefficient of friction by μ, Coulomb's law states that

$$|F_f| \leq \mu\, F_n. \tag{2.9}$$

In classical mechanics it is normal to distinguish between static and dynamic friction coefficients. Although this has very little influence on the results, it does not complicate the model and will be included where appropriate. This was not done in [1, 2], but in [3] it was, following the example set by Pritchett [13] . In this thesis, this distinction is taken into account for rigid hoops, Chapter 4, but is ignored in the case of massless hoops and the elastic models, Chapters 3 and 7.

Newton's second law determines the relationship between the forces and the accelerations. In the two-dimensional problem being considered there are three independent equations. Taking components in the transverse direction, $mg\sin\psi + F_f = m\ddot{x}$, or dividing by m and using (2.8)

$$F_f/m = \ddot{X} + \gamma\, r\ddot{\theta}\, \cos\theta - \gamma\, r\dot{\theta}^2\, \sin\theta - g\sin\psi. \tag{2.10}$$

Taking components perpendicular to the plane, $F_n - mg\cos\psi = m\ddot{y}$, or, dividing by m and using (2.8)

$$F_n/m = \ddot{Y} - \gamma\, r\ddot{\theta}\, \sin\theta - \gamma\, r\dot{\theta}^2\, \cos\theta + g\cos\psi. \tag{2.11}$$

Taking clock-wise moments about the centre of mass,

$$F_n\ \gamma\, r\ \sin\theta - F_f\ r\,\mathcal{H} = I_G\ \ddot{\theta}.$$

Dividing by mr and using (2.3),

$$(F_n/m)\,\gamma\ \sin\theta - (F_f/m)\ \mathcal{H} = \kappa_G\, r\ddot{\theta}. \tag{2.12}$$

Equations (2.10), (2.11) and (2.12), and various forms thereof, will be referred to collectively as the *kinetic equations*. Equation (2.12), and various forms thereof, will be referred to as the *torque equation*.

2.2 Non-dimensional formulation

In later chapters the mathematical formulation, as well as the numerical solution, is simplified by using non-dimensional variables. Defining non-dimensional time as

$$\tau = \sqrt{g/r}\ t,$$

and denoting derivatives with respect to τ by $(\ )'$, it follows that

$$\frac{\mathrm{d}(\ )}{\mathrm{d}\tau} = (\ )' = \sqrt{r/g}\ \frac{\mathrm{d}(\ )}{\mathrm{d}t} = \sqrt{r/g}\ \dot{(\ )}.$$

This implies inter alia that $x'' = (r/g)\ddot{x}$ or $(x/r)'' = \ddot{x}/g$.

It is convenient to denote the non-dimensional angular velocity by ω, where

$$\omega = \theta' = \sqrt{r/g}\ \dot{\theta},$$

with initial value denoted by $\omega_0 = \theta'(0) = \sqrt{r/g}\ \dot{\theta}(0)$.

The non-dimensional angular acceleration is defined and denoted by

$$\alpha = \omega' = \theta'' = (r/g)\ \ddot{\theta}.$$

Also, $\omega^2 = (r/g)\ \dot{\theta}^2$ can be interpreted as the non-dimensional centripetal acceleration.

Noting that $\frac{\mathrm{d}(\ )}{\mathrm{d}\theta} = \frac{\mathrm{d}(\ )}{\mathrm{d}\tau}\frac{\mathrm{d}\tau}{\mathrm{d}\theta} = \frac{\mathrm{d}(\ )}{\mathrm{d}\tau}\,\omega^{-1}$, the following useful relationship is obtained:

$$\frac{\mathrm{d}\omega^2}{\mathrm{d}\theta} = 2\omega' \quad \text{or} \quad \omega' = \tfrac{1}{2}\ \frac{\mathrm{d}\omega^2}{\mathrm{d}\theta}. \tag{2.13}$$

This is the non-dimensional form of the well known technique for converting a differential equation w.r.t. time into a differential equation w.r.t. position.

The position of point O is denoted by the non-dimensional coordinates

$$\mathcal{X} = (X/r); \quad \mathcal{Y} = (Y/r);$$

and the velocity by the non-dimensional components

$$\mathcal{V}_x = \mathcal{X}' = (X/r)'; \quad \mathcal{V}_y = \mathcal{Y}' = (Y/r)'.$$

Defining the *elastic deformation* δ as

$$\delta = d/r,$$

equation (2.5) in non-dimensional form becomes

$$\mathcal{Y} = 1 - \delta; \quad \mathcal{V}_y = -\delta'; \quad \mathcal{Y}'' = -\delta''. \tag{2.14}$$

The rigidity constraints (2.6) can be written in non-dimensional form as

$$x/r = \mathcal{X} + \gamma\,\sin\theta; \qquad y/r = 1 - \delta + \gamma\,\cos\theta. \tag{2.15}$$

Differentiation of (2.15) with respect to τ then gives the non-dimensional velocity and acceleration components as

$$(x/r)' = \mathcal{V}_x + \gamma\,\omega\,\cos\theta; \qquad (y/r)' = -\delta' - \gamma\,\omega\,\sin\theta; \tag{2.16}$$

$$(x/r)'' = \mathcal{X}'' + \gamma\,\theta''\,\cos\theta - \gamma\,\omega^2\,\sin\theta; \qquad (y/r)'' = -\delta'' - \gamma\,\theta''\,\sin\theta - \gamma\,\omega^2\,\cos\theta. \tag{2.17}$$

In addition, the magnitude of the acceleration of G is of some interest. The non-dimensional value of this acceleration is given by

$$a/g = \sqrt{((x/r)'')^2 + ((y/r)'')^2}. \tag{2.18}$$

The non-dimensional form of the kinetic equations (2.10), (2.11) and (2.12) are

$$\mathcal{F} = F_f/mg = \mathcal{X}'' + \gamma\,\theta''\,\cos\theta - \gamma\,\omega^2\,\sin\theta - \sin\psi; \tag{2.19}$$

$$\mathcal{N} = F_n/mg = -\delta'' - \gamma\,\theta''\,\sin\theta - \gamma\,\omega^2\,\cos\theta + \cos\psi; \tag{2.20}$$

$$\mathcal{N}\,\gamma\,\sin\theta - \mathcal{F}\,\mathcal{H} = \kappa_G\,\theta''. \tag{2.21}$$

2.3 Total energy

The total energy of the system is frequently found useful in the interpretation of results.

In general, the total energy being considered here is the sum of the potential and kinetic energies, and can be written as

$$E = mgH + \tfrac{1}{2}mv_G^2 + \tfrac{1}{2}I_G\dot{\theta}^2,$$

where H is the vertical height of point G above some reference plane.

Using Figure 2.1, and taking the origin of the axes as reference, the initial energy is

$$E_1 = mg(r - d_0 + \gamma r)\cos\psi + \tfrac{1}{2}m(\dot{x}_0^2 + \dot{y}_0^2) + \tfrac{1}{2}I_G\dot{\theta}_0^2.$$

Using non-dimensional variables and (2.16), together with the previously defined initial conditions, this simplifies to

$$\mathcal{E}_1 = E_1/mgr = (1 - \delta_0 + \gamma)\cos\psi + \tfrac{1}{2}(\mathcal{V}_{x0} + \gamma\omega_0)^2 + \tfrac{1}{2}\kappa_G\omega_0^2. \tag{2.22}$$

Similarly, the total energy after a rotation θ, in non-dimensional form $\mathcal{E} = E/mgr$, is

$$\mathcal{E} = (1-\delta)\cos\psi + \gamma\cos(\theta+\psi) - \mathcal{X}\sin\psi + \tfrac{1}{2}(\mathcal{V}_x + \gamma\omega\cos\theta)^2 + \tfrac{1}{2}(-\delta' - \gamma\omega\sin\theta)^2 + \tfrac{1}{2}\kappa_G\omega^2. \tag{2.23}$$

2.4 Rolling motion

As stated previously, the first phase of the motion is always rolling without slipping, and it is convenient at this stage to develop the equations for rolling motion.

Rolling is characterised by the constraints that contact is maintained and that the contact point C does not slip, i.e. that $\dot{X} = r\dot{\theta}$ and $\ddot{X} = r\ddot{\theta}$.

The non-dimensional specification for rolling motion is therefore

$$\mathcal{V}_{x0} = \omega_0; \qquad \mathcal{V}_x = \omega; \qquad \mathcal{X}'' = \theta''. \tag{2.24}$$

Note that the torque equation for rolling can always be reduced to an equation for moments around point C, in which case the moment of inertia around the axis through C is

$$I_C = I_G + m(\mathrm{GC})^2 = \kappa_C\, mr^2,$$

where $\kappa_C = 2\,\mathcal{H} + \epsilon$ from (2.4).
Because I_C is not constant, the simple form of the torque equation, namely total moment around C $= I_C\ \ddot{\theta}$, is incorrect. This issue is discussed in more detail in Appendix B.

Using (2.19) and (2.20) to eliminate the reaction forces from the torque equation (2.21), together with (2.24), the torque equation becomes

$$\begin{gathered}\gamma\,\sin\theta(-\delta'' - \gamma\,\theta''\,\sin\theta - \gamma\,\omega^2\,\cos\theta + \cos\psi) \\ -\mathcal{H}\,((1 + \gamma\,\cos\theta)\theta'' - \gamma\,\omega^2\,\sin\theta - \sin\psi) = \kappa_G\,\theta''.\end{gathered}$$

Collecting terms containing θ'' and simplifying by using (2.4)

$$(\kappa_G + (\gamma \sin\theta)^2 + \mathcal{H}^2)\,\theta'' = \kappa_C\,\theta''.$$

After simplifying the ω^2-terms in a similar fashion, the torque equation for rolling becomes

$$\kappa_C\,\theta'' + \gamma \sin\theta\,\delta'' = \gamma \sin\theta\,\omega^2 + \gamma \sin\theta\,\cos\psi + \mathcal{H} \sin\psi. \tag{2.25}$$

In the case of rigid hoops, δ and all its derivatives are zero, and the torque equation during rolling is

$$\kappa_C\,\theta'' = \gamma \sin\theta\,\omega^2 + \gamma \sin\theta\,\cos\psi + \mathcal{H} \sin\psi. \tag{2.26}$$

2.5 Spinning and skidding

When the friction force reaches a maximum, the rolling motion ends and the hoop starts *slipping.*

In the case of massless hoops, Chapter 3, this slipping motion is characterised by the phenomenon that the reaction force (normal and friction) is zero, and a motion called *skimming* is defined. In the case of real hoops, Chapters 4 to 7, this maximum friction force may be either positive or negative depending on the values of the parameters and initial values, and the following two cases are identified.

If the friction force is positive when slipping starts, $r\,\dot\theta > \dot X$ and the subsequent motion is defined as *spinning.* From (2.9), $\mathbf{F_f} = +\mu_k\,F_n\,\mathbf{e}_t$, where μ_k is the kinetic coefficient of friction. The torque equation (2.21) now becomes

$$\mathcal{N}\,(\gamma \sin\theta - \mu_k\,\mathcal{H}) = \kappa_G\,\theta''.$$

Defining the non-dimensional *spin factor* S_+ as

$$S_+(\theta) = \gamma \sin\theta - \mu_k\ \mathcal{H},$$

the torque equation for spinning becomes

$$\kappa_G\,\theta'' = \mathcal{N}\,S_+(\theta).$$

Similarly, if the friction force is negative the subsequent motion is defined as *skidding* and $r\,\dot\theta < \dot X$, with $\mathbf{F_f} = -\mu_k\,F_n\,\mathbf{e}_t$, and the *skid factor* S_- is defined as

$$S_-(\theta) = \gamma \sin\theta + \mu_k\ \mathcal{H},$$

whereby the torque equation for skidding becomes

$$\kappa_G\,\theta'' = \mathcal{N}\,S_-(\theta).$$

The formulation is simplified a great deal by using the following mathematical definitions to combine spinning and skidding in one equation.
In the case of spinning, define $\mu = +\mu_k$;
in the case of skidding, define $\mu = -\mu_k$.

Then $\mathbf{F_f} = \mu\,F_n\,\mathbf{e}_t$, the *slip factor* S is defined as

$$S = \gamma \sin\theta - \mu\,\mathcal{H}, \tag{2.27}$$

and the torque equation for slipping becomes $\kappa_G\,\theta'' = \mathcal{N}\,S$.

Using (2.20), $\mathcal{N} = -\delta'' - \gamma\,\theta''\,\sin\theta - \gamma\,\omega^2\,\cos\theta + \cos\psi$, this becomes $\kappa_G\,\theta'' = S(-\delta'' - \gamma\,\theta''\,\sin\theta - \gamma\,\omega^2\,\cos\theta + \cos\psi)$, or

$$(\kappa_G + S\,\gamma\,\sin\theta)\,\theta'' + S\delta'' = S\,(\cos\psi - \gamma\,\omega^2\,\cos\theta). \tag{2.28}$$

Equations (2.13) to (2.28) and the corresponding definitions constitute the mathematical model for the loaded hoop. These will be simplified in the following two chapters for the special cases of massless and rigid hoops, and developed further in Chapter 7 to solve the equations for the elastic model.

2.6 Immediate hopping

A phenomenon that occurs in all the models is that of *immediate hopping*, by which is meant that the hoop leaves the surface immediately after time $t = 0$.

The fundamental equation is (2.8):

$$F_n/m = \ddot{Y} - \gamma\,r\ddot{\theta}\,\sin\theta - \gamma\,r\dot{\theta}^2\,\cos\theta + g\cos\psi, \quad \text{or} \quad \mathcal{N} = \mathcal{Y}'' - \gamma\,\alpha\,\sin\theta - \gamma\,\omega^2\,\cos\theta + \cos\psi.$$

In the initial position where $\theta = 0$, this simplifies to:

$$\mathcal{N}(0^+) = \mathcal{Y}''(0^+) - \gamma\,\omega_0^2 + \cos\psi, \tag{2.29}$$

where (0^+) indicates possible discontinuities in the forces and accelerations. (Note that initial equilibrium implies $F_n(0^-) = mg\cos\psi$, i.e. $\mathcal{N}(0^-) = \cos\psi$.)

At this point the models containing elasticity behave differently to those that do not. For the elastic models, $\mathcal{N}(0^+)$ can never be zero and is always positive if the initial deformation is non-zero, as discussed later in Chapter 7.

For the models without elasticity, only one of two possibilities exist for (2.29):

- either $\mathcal{N}(0^+) = 0$, in which case $\mathcal{Y}''(0^+) = \gamma\,\omega_0^2 - \cos\psi \geq 0$;
- or $\mathcal{Y}''(0^+) = 0$, in which case $\mathcal{N}(0^+) = -\gamma\,\omega_0^2 + \cos\psi \geq 0$.

It is convenient, also for later results, to define $\hat{\omega}_0$, the *critical initial velocity*, as

$$\hat{\omega}_0 = \sqrt{(1/\gamma)\,\cos\psi}. \tag{2.30}$$

Noting that neither $\mathcal{N}(0^+)$ nor $\mathcal{Y}''(0^+)$ can be negative, it follows that:

- if $\omega_0 > \hat{\omega}_0$, then $\mathcal{Y}''(0^+) > 0$ and the hoop hops;
- if $\omega_0 < \hat{\omega}_0$, then $\mathcal{N}(0^+) > 0$ and the hoop rolls;
- if $\omega_0 = \hat{\omega}_0$, then $\mathcal{N}(0^+) = 0$, and $\mathcal{Y}''(0^+) = 0$. In this case the third and fourth time derivatives are required to determine whether the hoop will hop; this detail is not included in this dissertation.

These observations can be summarised in the following result:

Result 2.1 : Immediate hopping of non-elastic hoops
A non-elastic hoop will leave the surface at position $\theta = 0$
if the initial angular velocity exceeds the critical initial velocity; i.e. if

$$\omega_0 > \sqrt{(1/\gamma)\,\cos\psi}.$$

2.7 D'Alembert's principle

Where-as Newton's second law is formulated as $\mathbf{F} = m\mathbf{a}_G$, D'Alembert's principle is formulated as a "dynamic equilibrium" equation in the form

$$\mathbf{F} - m\mathbf{a}_G = \mathbf{0};$$

see for example [33], page 240.

In other words, the negative of the product of the mass and the acceleration of G is considered to be a "fictitious" or "inertia" force which is in dynamic equilibrium with the real forces. An example of such a fictitious force is the well-known "centrifugal force" in circular motion.

Drawings in which these fictitious forces are included together with the real forces provide a visual aid to understanding many of the phenomena occurring during the motion of loaded hoops, and are used in later chapters as an aid in interpreting certain results. In this dissertation such drawings will be referred to as *D'Alembert diagrams*.

Taking $\ddot{Y} = 0$ for the case of a rigid hoop, the acceleration of the mass centre G, as given by (2.8), can be written in the alternative form of $\mathbf{a}_G = \ddot{X}\mathbf{e}_t + \gamma\, r\ddot{\theta}\,\mathbf{e}_\theta + \gamma\, r\dot{\theta}^2\,\mathbf{e}_r$, or in non-dimensional form as

$$\mathbf{a}_G/g = \mathcal{X}''\mathbf{e}_t + \gamma\,\alpha\,\mathbf{e}_\theta + \gamma\,\omega^2\,\mathbf{e}_r. \tag{2.31}$$

The transverse and radial unit vectors, $\mathbf{e}_\theta$ and $\mathbf{e}_r$, [3] are shown in Figure 2.3(a) together with the three components of the non-dimensional acceleration.

For a loaded hoop D'Alembert's principle therefore becomes

$$m\,\mathbf{g} + F_n\mathbf{e}_n + F_f\mathbf{e}_t - m\mathbf{a}_G = 0,$$

where $\mathbf{g}$ is the gravity vector. In non-dimensional form, using (2.31), this becomes

$$1\,(\mathbf{g}/g) + \mathcal{F}\,\mathbf{e}_t + \mathcal{N}\,\mathbf{e}_n - \mathcal{X}''\,\mathbf{e}_t - \gamma\,\alpha\,\mathbf{e}_\theta - \gamma\,\omega^2\,\mathbf{e}_r = 0. \tag{2.32}$$

Figure 2.3(b) is a typical D'Alembert diagram for a rotation of 40°, showing the vectors in 2.32. The lengths of the vectors are drawn to scale for an actual example. Note that the weight-vector is a unit vector in the non-dimensional diagram. [4] The $\gamma\,\omega^2$-component is the "centrifugal force", and in later sections reference will be made to the *centrifugal effects* when discussing some of the results.

[3] Here θ and r do not have the usual connotation of polar coordinates.

[4] Unfortunately the calligraphic font style for $\mathcal{F}$ and $\mathcal{N}$ of the graphics program differs from that in the main text.

Figure 2.3(c) is the corresponding vector diagram, illustrating that the sum of the vectors in (2.32) is zero.

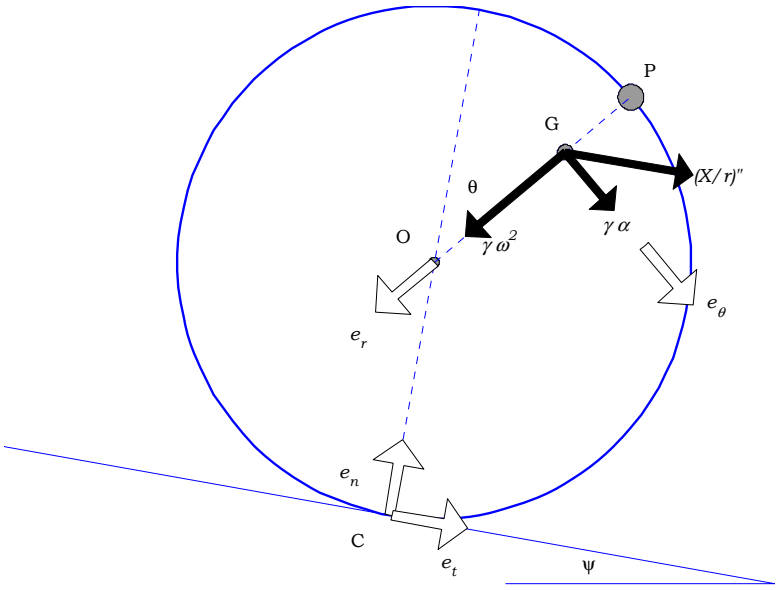

(a) : Unit vectors and acceleration components

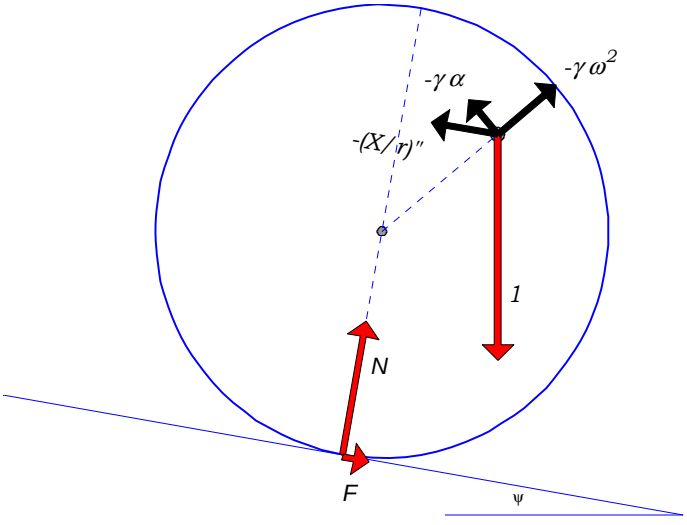

(b) : D'Alembert diagram

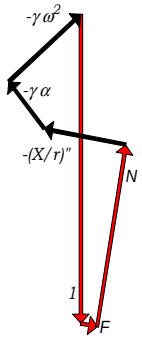

(c) : Vector diagram

Figure 2.3 : D'Alembert's principle applied to a rigid hoop, for $\theta = 40°$

Chapter 3

Dynamics of a massless rigid hoop

3.1 Introduction

In this chapter the behaviour of a massless hoop is analysed, as was done in [2], with the main purpose of establishing whether a rigid, massless hoop can hop as suggested by Littlewood. This chapter therefore contains a detailed analysis of the motion of a rigid, massless hoop which is loaded by a particle fixed to its rim and which is rolling on a rough flat surface. Only the case of a horizontal plane will be considered here.

The problem as introduced by Littlewood was for a point particle so that the model has the important characteristic that the moment of inertia of the system around an axis through its centre of gravity is zero. In addition, the original problem was for zero initial velocity and large friction coefficient. In this chapter the problem is generalised by including the effects of non-zero initial velocities and realistic friction coefficients. This model will be referred to as *Littlewood's hoop*, and is the model analysed in [2].

A slight variation of the problem is obtained by replacing the point particle with a body that has a non-zero moment of inertia. This will be referred to as *Pritchett's hoop* [13]. (The load will however still be referred to as a particle).

The behaviour of massless hoops can be derived by considering the limiting case of a real hoop as the hoop mass tends to zero; in the case of Pritchett's hoop the moment of inertia around G is non-zero. Littlewood's hoop can then be considered as a limiting case of Pritchett's hoop in which the dimensions of the particle also tend to zero.

These are clearly hypothetical models that have no physical counterpart, but they raise a number of very interesting and subtle aspects of Newtonian dynamics. It is shown inter alia that in the case of Littlewood's hoop there is an alternative to hopping after the normal reaction becomes zero, namely a somewhat unusual motion called "skimming", in which the hoop continues rotating with non-zero angular acceleration while its centre moves forward parallel to the plane, but the constraint of pure rolling is absent and the particle follows a parabolic rather than a cycloidal path.

An important by-product of this analysis is the conclusion that the vanishing of the normal reaction is only a necessary but not a sufficient condition for hopping.

The first objective is to obtain expressions for the angular velocity and angular acceleration as

functions of the angular displacement; i.e. $\omega = \omega(\theta)$ and $\alpha = \alpha(\theta)$, for each of the different phases of the motion.

In this chapter the equations for Littlewood's hoop are derived and solved, this being the historical source for this whole investigation and also being the simplest model from a mathematical point of view. Further analysis of Pritchett's hoop is left for Chapter 6, because the equations for Pritchett's hoop are the same as those for a real rigid hoop.

3.2 The mathematical model

The rigidity of the hoop is modelled by setting d, and all the derivatives of d, to zero in the equations of Chapter 2.

The massless hoop is modelled by setting $m_h = 0$, i.e. $\gamma = 1$, in the equations of Chapter 2. Similarly, the particle is modelled by setting $\epsilon = 0$ for Littlewood's hoop.

Also, only motion on a horizontal plane is considered; therefore $\psi = 0$, as shown in Figure 3.1. This simplifies the detail of the equations without affecting the nature or structure of the solutions.

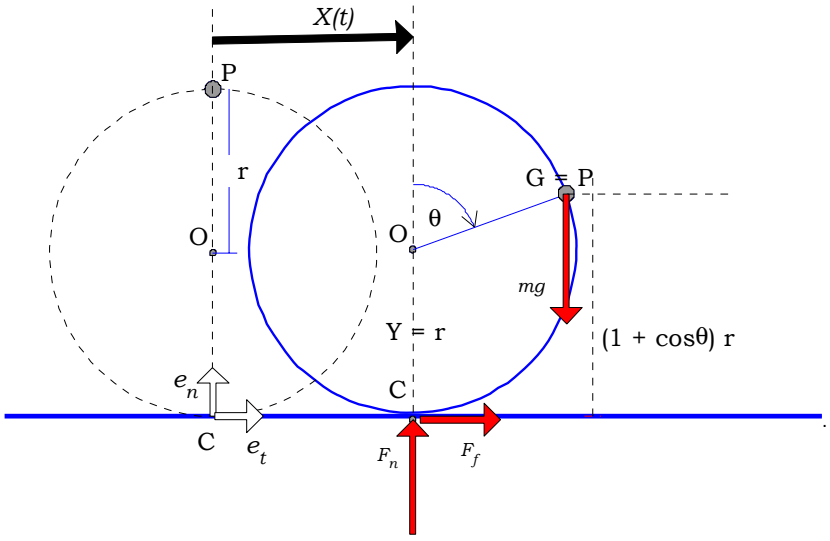

Figure 3.1 : The massless hoop

The geometry of this model is summarised by

$$\mathcal{H} = 1 + \cos\theta\,; \quad \kappa_G = 0\,; \quad \kappa_C = 2\,(1 + \cos\theta) = 2\mathcal{H}. \tag{3.1}$$

3.2.1 Kinematics and Kinetics

Only the final non-dimensional equations are simplified for use in this chapter.

Setting the modelling assumptions into the kinematic equations (2.16) and (2.17) results in the following non-dimensional velocities and accelerations :

$$(x/r)' = \mathcal{V}_x + \omega\,\cos\theta; \qquad (y/r)' = \mathcal{V}_y - \omega\,\sin\theta; \tag{3.2}$$

and

$$(x/r)'' = \mathcal{X}'' + \theta''\,\cos\theta - \omega^2\,\sin\theta; \qquad (y/r)'' = \mathcal{Y}'' - \theta''\,\sin\theta - \omega^2\,\cos\theta. \tag{3.3}$$

The kinetic equations (2.19) and (2.20) become

$$\mathcal{F} = \mathcal{X}'' + \theta''\,\cos\theta - \omega^2\,\sin\theta; \tag{3.4}$$

$$\mathcal{N} = -\theta''\,\sin\theta - \omega^2\,\cos\theta + 1; \tag{3.5}$$

Note that in all cases where $\mathcal{N} > 0$, $Y = r$ and $Y'' = 0$ has been used in (3.5).

3.2.2 The torque equation for a massless hoop

The torque equation for moments around G, equation (2.21), now simplifies to

$$\mathcal{N}\,\sin\theta - \mathcal{F}\,(1 + \cos\theta) = 0. \tag{3.6}$$

The torque equation can normally be used to obtain an expression for the angular acceleration. However, in the case of Littlewood's hoop, with $\kappa_G = 0$, this equation *can not be used to find* $\ddot{\theta}$. The author gratefully acknowledges this insight provided by M.S. Tiersten, a reviewer of an earlier version of [2]. This seemingly obvious fact was not noted in some instances, which resulted in erroneous attempts by Theron [14] and Butler [12] to prove that Littlewood's hoop can not hop.

Equation (3.6) requires that $(\mathcal{F}/\mathcal{N}) = \sin\theta/(1 + \cos\theta)$, or

$$\mathcal{F} = \tan(\theta/2)\,\mathcal{N}, \quad \theta < \pi. \tag{3.7}$$

From a physical point of view, equation (3.7) can be derived by noting that zero moment around G can only be obtained if the line of action of the resultant reaction force is along the line CG, as shown in the figure alongside. Noting further that angle OCG is $\theta/2$, (3.7) follows directly.

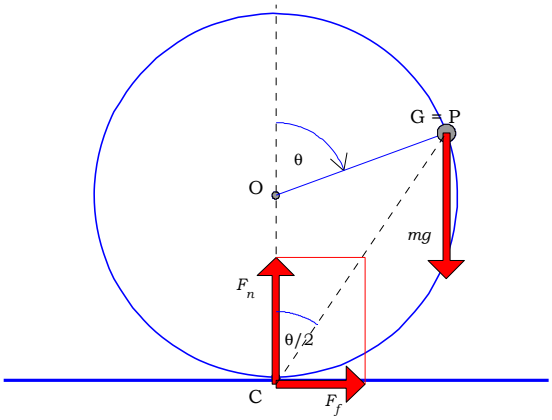

Therefore the friction force is non-negative for $\theta \in [0,\ \pi)$. Ignoring the difference between static and kinetic friction, Coulomb's law for this case becomes

$$0 \leq \mathcal{F} \leq \mu \mathcal{N}. \tag{3.8}$$

Now there are two restrictions on the friction force, namely Coulomb's law (3.8) and the torque equation (3.7). These two restrictions can be satisfied simultaneously only if

$$\tan\theta/2 \leq \mu,\ \mathcal{N} > 0; \quad \text{or} \ \ \mathcal{F} = 0,\ \mathcal{N} = 0. \tag{3.9}$$

Clearly, from (3.7), the subsequent analysis of Littlewood's hoop is restricted to $0 \leq \theta < \pi$.

3.3 Phase 1 : Rolling

The first phase of the motion is rolling without slipping, resulting from the initial conditions that $\dot{X}(0) = r\dot{\theta}(0)$, or $\mathcal{X}'(0) = \mathcal{V}_x(0) = \mathcal{V}_{x0} = \omega(0) = \omega_0$. This motion is governed by the restriction in (2.24) which simplifies to

$$\mathcal{X}'' = \theta'' \quad \text{with} \quad \mathcal{V}_{x0} = \omega_0. \tag{3.10}$$

The path of the particle is obtained from (2.6). During rolling, $X = r\,\theta$ and $Y = r$, and with $\gamma = 1$ this results in

$$x(t) = r(\theta + \sin\theta); \qquad y(t) = r(1 + \cos\theta).$$

Therefore the path of the particle during rolling is a cycloid, as noted by Littlewood [8] and Tokieda [9].

In the next section equations (2.24) to (2.26) of the previous chapter are simplified for the case of Littlewood's hoop. This is followed by an alternative solution using energy methods.

3.3.1 Solution of equations of motion

The torque equation (2.26) now simplifies to $\kappa_C\,\theta'' = (1 + \omega^2)\,\sin\theta$, with $\kappa_C = 2\,(1 + \cos\theta)$ from (2.4). This can be re-written as

$$\omega' = \tfrac{1}{2}\,(1 + \omega^2)\,\tan\theta/2, \tag{3.11}$$

and then be converted to a differential equation w.r.t. θ by using (2.13) to obtain

$$\frac{\mathrm{d}(\omega^2)}{\mathrm{d}\theta} = (1 + \omega^2)\,\tan\theta/2.$$

Separating the variables in order to integrate,

$$\int \frac{\mathrm{d}(\omega^2)}{(1 + \omega^2)} = \int \tan(\theta/2)\,\mathrm{d}\theta,$$

and using the initial condition $\omega(0) = \omega_0$, this results in

$$1 + \omega^2 = (1 + {\omega_0}^2)\,\sec^2(\theta/2),$$

or, using the identity $\sec^2(\theta/2) = 2/(1+\cos\theta)$,

$$\omega^2 = \frac{2\,(1+{\omega_0}^2)}{(1+\cos\theta)} - 1. \tag{3.12}$$

Equations (3.11) and (3.12) can be used to obtain an expression for the normal reaction from (3.5), which simplifies to

$$\begin{aligned}
\mathcal{N} &= 1 - \tfrac{1}{2}\,(1+\omega^2)\,\sin^2\theta/(1+\cos\theta) - \omega^2\,\cos\theta \\
&= \tfrac{1}{2}\,(1+\cos\theta)\,(1-\omega^2) \\
&= \tfrac{1}{2}\,(1+\cos\theta)\,(1-2\,(1+{\omega_0}^2)\,(1+\cos\theta)^{-1}+1) \\
&= 1+\cos\theta-(1+{\omega_0}^2),
\end{aligned}$$

or

$$\mathcal{N} = \cos\theta - {\omega_0}^2. \tag{3.13}$$

This implies that ω_0 needs to be less than 1 for $\mathcal{N}(0) > 0$. Unless specified otherwise, it is assumed throughout that this is the case; the situation where $\omega_0 > 1$ is discussed separately as a special case.

Similarly, substituting (3.11) and (3.12) in (3.4) for the friction force results in

$$\begin{aligned}
\mathcal{F} &= \theta''\,(1+\cos\theta) - \omega^2\,\sin\theta \\
&= \tfrac{1}{2}\,(1+\omega^2)\,\tan\theta/2\,(1+\cos\theta) - \omega^2\,\sin\theta \\
&= \tfrac{1}{2}\,(1-\omega^2)\,\sin\theta \\
&= \tfrac{1}{2}\,(1-2\,(1+{\omega_0}^2)\,(1+\cos\theta)^{-1}+1)\,\sin\theta,
\end{aligned}$$

or

$$\mathcal{F} = (\cos\theta - {\omega_0}^2)\,\tan\theta/2. \tag{3.14}$$

Equations (3.13) and (3.14) clearly satisfy (3.7), the restriction resulting from the torque equation.

Equations (3.10) to (3.14) constitute the solution for rolling motion of Littlewood's hoop.

3.3.2 Solution using energy methods

Because this is a conservative motion, the solution above can also be obtained by applying the principle of energy conservation.

Using $\mathcal{V}_{x0} = \mathcal{V}_x(0) = \omega_0$ in (2.22), or directly from Figure 3.1, the initial energy relative to the surface can be written as

$$E_1 = mg2r + \tfrac{1}{2}m(2r\dot{\theta}_0)^2 = 2\,mgr\,(1+{\omega_0}^2\,).$$

The potential energy of the hoop after a rotation through θ is $mgr\mathcal{H}$. Noting that the particle is rotating around point C with angular velocity $\dot{\theta}$, and that $(\mathrm{CG})^2$ can be simplified to $(2r^2\mathcal{H})$, the kinetic energy of the system can be written as $\frac{1}{2}m(2r^2\mathcal{H})\dot{\theta}^2 = mgr\mathcal{H}\,\omega^2$. The total energy in position $\theta > 0$ is the sum of the potential and kinetic energies, namely

$$E = mgr\mathcal{H}\,(1+\omega^2).$$

Setting $E = E_1$ and solving for ω^2 results in

$$\omega^2 = 2\,(1+{\omega_0}^2)\,(1+\cos\theta)^{-1} - 1, \quad \theta \neq \pi,$$

which is the same as (3.12).

Differentiation w.r.t. τ gives $2\omega\omega' = 2\,(1+{\omega_0}^2)\,(\sin\theta)\,(1+\cos\theta)^{-2}\,\theta'$;
i.e. the angular acceleration is $\omega' = (1+{\omega_0}^2)\,(\sin\theta)\,(1+\cos\theta)^{-2}, \quad \theta \neq \pi$.
Using (3.12), this can also be written as

$$\omega' = \tfrac{1}{2}\,(1+\omega^2)\,(1+\cos\theta)\,(\sin\theta)\,(1+\cos\theta)^{-2} = \tfrac{1}{2}\,(1+\omega^2)\,\tan(\theta/2), \quad \theta \neq \pi,$$

which is the same as (3.11).

It was pointed out by Tokieda [10] that "... something dramatic must happen if the hoop can roll until the weight reaches the bottom," because both the potential energy and the kinetic energy are zero at this point. However, if the friction coefficient is limited to realistic values, the hoop has to stop rolling before this point is reached and therefore the energy is no longer conserved.

3.3.3 Pritchett's hoop

In the case of Pritchett's hoop $\kappa_C = 2\,(1+\cos\theta) + \epsilon$, and the differential equation (3.11) w.r.t. θ becomes

$$\frac{\mathrm{d}(\omega^2)}{\mathrm{d}\theta} = (1+\omega^2)\,\sin\theta/(1+\cos\theta+\epsilon/2).$$

The solution is $\omega^2 = (C_1 - \cos\theta)/(1+\cos\theta+\epsilon/2)$, with $C_1 = 1+\omega_0^2\,(2+\epsilon/2)$. This is the same as solution (3.12) for the case when $\epsilon = 0$. Further analysis of the motion of a Pritchett hoop will be left for Chapter 6.

3.4 Phase 2 : Motion after the rolling phase ends

The main contribution of this chapter is the analysis of the motion of Littlewood's hoop once the rolling phase ends, hereafter referred to as phase 2. The position where phase 1 ends will be denoted by θ_s, occurring at time t_s:

$$\theta_s = \theta(t_s).$$

Before analysing this motion, it is convenient to emphasise some aspects of the problem. Then solutions are obtained in terms of θ_s, and finally θ_s is obtained in terms of μ and ω_0.

3.4.1 General remarks

- **Remark 1.** Continuity at $\theta = \theta_s$.
  a) All velocities will be continuous functions of time or position through θ_s, due to the absence of impulsive forces. Therefore $\omega_s = \omega(\theta_s)$ is known from (3.12), the solution for rolling motion.
  b) The reaction forces and accelerations may be discontinuous, in which case the angular acceleration immediately before this point will be denoted by $\alpha_s^- = \omega'(\theta_s)$, and is known from (3.11), the solution for rolling.

- **Remark 2.** For systems with zero moment of inertia and $\mathcal{N} = 0$, therefore $\mathcal{F} = 0$, when $t \geq t_s$, Newton's second law in the form of the torque equation (2.21) provides no information whatsoever regarding the angular acceleration α_s^+.

- **Remark 3.** For real hoops where $I_G > 0$ and $\mathcal{N} = 0$, therefore $\mathcal{F} = 0$, the torque eq. (2.21) implies that $\theta'' = 0$. This observation formed the basis of our earlier attempt [14] to prove that Littlewood's hoop cannot hop, and was used for the same purpose in Butler's proof [12]. However, as pointed out above, this argument can not be used when $I_G = 0$.

  This argument is also used (correctly) by Pritchett [13] to show that sliding occurs before hopping, also in the case of a massless hoop. Because his hoop is loaded with a body (and not a particle), $I_G > 0$ even for the massless hoop.

- **Remark 4.** Finally, the obvious fact is repeated that the rigidity of the hoop and the surface implies that there are only two possibilities when $t \geq t_s$: either the hoop leaves the surface (i.e. hops), so that $Y(t) > r$ for a while, or $Y(t) = r$ irrespective of the normal reaction.

3.4.2 Zero reaction force

It follows from (3.9) that, after the hoop stops rolling, the requirements of zero moment around G and Coulomb's law can be satisfied simultaneously for $\theta > \theta_s$ only if $\mathcal{N} = 0$ and $\mathcal{F} = 0$.

Because these reaction forces are zero for $\theta > \theta_s$, the weight of the particle is the only force on the system and the acceleration of the centre of mass G is given by the components

$$\ddot{x} = 0 \quad ; \quad \ddot{y} = -g, \tag{3.15}$$

resulting in a parabolic trajectory for the particle, *irrespective of the motion of the hoop.* This well-known trajectory is analysed in section 3.6. This leaves the unresolved issue of how the hoop rotates about the particle, or, equivalently, the motion of point O for $\theta > \theta_s$.

Phase 2 motion for the hoop is therefore characterised by the fact that the reaction force is zero, and the only component of acceleration is $\ddot{y} = -g$. Using this in (3.3) results in $-1 = \mathcal{Y}'' - \theta'' \sin\theta - \omega^2 \cos\theta$, or

$$\theta'' = (\mathcal{Y}'' - \omega^2 \cos\theta + 1)/\sin\theta, \tag{3.16}$$

which may be considered to be the governing equation for phase 2.

Note that this is a purely kinematic relationship, based only on the earlier assumptions that OP $= r$ (i.e. rigid) and $\gamma = 1$, and for situations with zero reaction force so that $\ddot{y} = -g$.

3.4.3 Angular acceleration at position θ_s.

Expressions for the angular acceleration at position θ_s are derived next. The value at the start of phase 2 is denoted by α_s^+, and the discontinuity in the angular acceleration is defined as

$$\Delta\alpha = \alpha_s^+ - \alpha_s^-.$$

As noted in remark 1, the values of ω_s and α_s^- are known in terms of θ_s. Using (3.12),

$$\omega_s^2 = 2\,(1+{\omega_0}^2)\,(1+\cos\theta_s)^{-1} - 1, \tag{3.17}$$

and from (3.11),

$$\alpha_s^- = \tfrac{1}{2}\,(1+\omega_s^2)\,\tan\theta_s/2. \tag{3.18}$$

As pointed out in remark 4, there are only two possibilities for Y, the first of which is $Y = r$, therefore $Y'' = 0$. Using $Y'' = 0$ in (3.16), $\theta'' = (1-\omega^2\,\cos\theta)/\sin\theta$, and the value at the start of phase 2 is

$$\alpha_s^+ = (1-\omega_s^2\,\cos\theta_s)/\sin\theta_s. \tag{3.19}$$

Using (3.18) and (3.19), the discontinuity in the angular acceleration is

$$\Delta\alpha = (1-\omega_s^2\,\cos\theta_s)/\sin\theta_s - \tfrac{1}{2}\,(1+\omega_s^2)\,\tan\theta_s/2,$$

which simplifies to $\Delta\alpha = (1-\omega_s^2)\,\cot\theta_s/2$. Using (3.17), this can be simplified further to give

$$\Delta\alpha = (\cos\theta_s - \omega_0^2)/\sin\theta_s. \tag{3.20}$$

3.4.4 Skimming motion of the hoop

An expression for the angular velocity as a function of θ is derived next, based on the assumption that $Y(t) = r$, therefore $Y'' = 0$, for $t > t_s$. Using (3.16) with $Y'' = 0$,

$$\theta'' + \omega^2\,\cot\theta = \csc\theta, \quad \theta > \theta_s. \tag{3.21}$$

Using (2.13) in (3.21), the first order differential equation

$$\frac{\mathrm{d}(\omega^2)}{\mathrm{d}\theta} + 2\omega^2\,\cot\theta = 2\csc\theta \tag{3.22}$$

is obtained, with initial condition $\omega_s = \omega(\theta_s)$ from (3.17).

Using the integrating factor $e^{\int 2\,\cot\theta \mathrm{d}\theta} = \sin^2\theta$, the solution is

$$\omega^2 = (C_1 - 2\cos\theta)\;/\;\sin^2\theta; \quad C_1 = \omega_s^2\,\sin^2\theta_s + 2\cos\theta_s. \tag{3.23}$$

Using (2.13) and differentiating (3.23), or substituting (3.23) in (3.21), gives

$$\omega' = (1+\cos^2\theta - C_1\,\cos\theta)\;/\;\sin^3\theta. \tag{3.24}$$

Using $\ddot{x} = 0$ from (3.15), together with (3.23) and (3.24) in (3.3), the acceleration of point O is

$$\begin{aligned} \mathcal{X}'' = \ddot{X}/g &= -\theta''\,\cos\theta + \omega^2\,\sin\theta \\ &= (C_1 - \cos\theta(2+\sin^2\theta))\;/\;\sin^3\theta. \end{aligned}$$

Note that the above solutions only apply for $\theta < \pi$, and that ω, ω' and $\mathcal{X}''$ all tend to infinity as θ goes to π.

The angular position can be obtained as a function of time by integrating (3.21) with respect to time after substituting $u = \cos\theta$, to obtain [1]

$$\cos\theta(\tau) = \cos\theta_s - \omega_s(\tau - \tau_s)\sin\theta_s - \tfrac{1}{2}(\tau - \tau_s)^2. \tag{3.25}$$

The motion described above is termed *"skimming"*, being a motion in which the massless hoop whips round the particle at just the right angular velocity to ensure horizontal motion of point O while the particle is falling along the parabolic trajectory. Note that the hoop maintains geometric contact with the surface even though the normal reaction is zero. The skimming motion continues up to $\theta = \pi$, at which point the particle collides with the surface, with the hoop directly above it. This statement will be shown to be true in section 3.6.

The "discovery" of this skimming motion is the most significant contribution of this chapter and article [2].

3.4.5 Hopping

Equations (3.19) to (3.25) were derived on the assumption that $Y = r$. The only other possibility (remark 4) is that $Y > r$. And because $Y(\theta_s) = r$ and $\dot{Y}(\theta_s) = 0$, a necessary condition for this is that $\ddot{Y}_s^{\,+} > 0$, or, from (3.16), $\alpha_s^+ > (1 - \omega_s^2\cos\theta_s)/\sin\theta_s$.

To hop therefore, using (3.20), the discontinuity in the angular acceleration must satisfy

$$\Delta\alpha > (\cos\theta_s - \omega_0^2)/\sin\theta_s. \tag{3.26}$$

Because this value is undeterminable, nothing more can be said about this motion !

3.4.6 Immediate hopping

In the previous analysis $\omega_0 < 1$ was assumed in order to ensure contact during phase 1, as implied by (3.13).

In section 2.6 it was shown that a non-elastic hoop will hop immediately at $\theta = 0$ if

$$\omega_0 > \hat{\omega}_0 = \sqrt{(1/\gamma)\,\cos\psi}.$$

In the case of a massless hoop on a horizontal plane the critical initial velocity simplifies to

$$\hat{\omega}_0 = 1;$$

i.e. immediate hopping occurs if $\omega_0 > 1$. This can be interpreted physically by noting the large initial centrifugal effect as illustrated in the D'Alembert diagram.

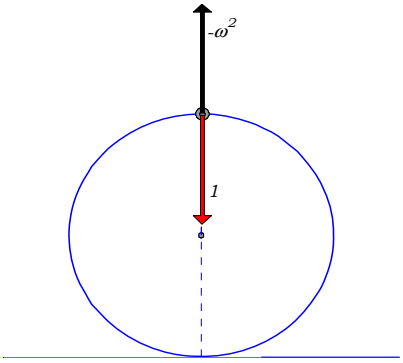

D'Alembert diagram for $\theta = 0$

[1] This solution is due to N.M. du Plessis, the co-author of [2].

3.4.7 Summary

The results of section 3.4 can be summarised as:

Result 3.1 : Motion of a massless hoop after the normal reaction becomes zero

- Skimming motion as defined by equations (3.21) to (3.25) can occur after the normal reaction becomes zero.
- Alternatively, an undefinable hop is possible.
- Zero normal reaction is a necessary but not sufficient condition for hopping.
- Immediate hopping at $\theta = 0$ occurs if $\omega_0 > 1$.

3.5 Transition from rolling to skimming

The transition from rolling to skimming is analysed next by returning to the conditions at the end of phase 1. Depending on the initial velocity and the friction coefficient, the rolling motion comes to an end at position $\theta = \theta_s$ (at time t_s) in one of two circumstances:

- when the friction force reaches its maximum value before $\mathcal{N}$ becomes zero; from (3.9), this will be when $\tan\theta_s/2 = \mu$;
- when the normal reaction becomes zero; from (3.13), this will be when $\cos\theta_s = {\omega_0}^2$.

The values of μ and ω_0 therefore determine which will happen first.

3.5.1 Critical friction coefficient

Using elementary trigonometry, it follows that:

$$\text{if} \quad \tan(\theta_s/2) = \mu, \quad \text{then} \quad \sin\theta_s = 2\mu/(1+\mu^2) \quad \text{and} \quad \cos\theta_s = (1-\mu^2)/(1+\mu^2). \tag{3.27}$$

It is convenient to define the value $\bar{\omega}_0$ in terms of the last expression,

$$\bar{\omega}_0 = \sqrt{(1-\mu^2)/(1+\mu^2)}. \tag{3.28}$$

It is clear from (3.9) that rolling will stop when maximum friction is reached at position θ_s where

$$\tan(\theta_s/2) = \mu,$$

in which case, using (3.28),

$$\cos\theta_s = (\bar{\omega}_0)^2. \tag{3.29}$$

Alternatively, rolling will stop when $\mathcal{N} = 0$ at θ_s, where, from(3.13),

$$\cos\theta_s = \omega_0^2. \tag{3.30}$$

Therefore the rolling phase ends with maximum friction if $\omega_0 < \bar{\omega}_0(\mu)$, and ends with zero reaction if $\omega_0 > \bar{\omega}_0(\mu)$.

Equivalently, the rolling phase ends with maximum friction if $\mu < \bar{\mu}$ where, for a given initial velocity, the *critical friction coefficient* is defined as

$$\bar{\mu} = \sqrt{(1-{\omega_0}^2)/(1+{\omega_0}^2)}. \tag{3.31}$$

Note that the expressions for $\bar{\omega}_0$ and $\bar{\mu}$ are symmetrical, and that $\bar{\omega}_0$ varies between 1 and 0 as μ varies between 0 and 1.

This result is illustrated by Figure 3.2, where the region below the curve $\omega_0 = \bar{\omega}_0(\mu)$ represents parameter values of μ and ω_0 that will result in maximum friction being reached at the end of the rolling phase, and the shaded region above the curve represents values that will result in zero reaction.

The values of ω_s^2 and α_s^- on the curve where $\omega_0 = \bar{\omega}_0$ are found from (3.12) together with (3.30) and (3.11) together with (3.27) respectively, simplifying to

$$\omega_s^2 = 1; \quad \alpha_s^- = \mu.$$

Therefore, for all cases in the region below the curve, $\omega_s < 1$ and $\alpha_s^- < \mu$.

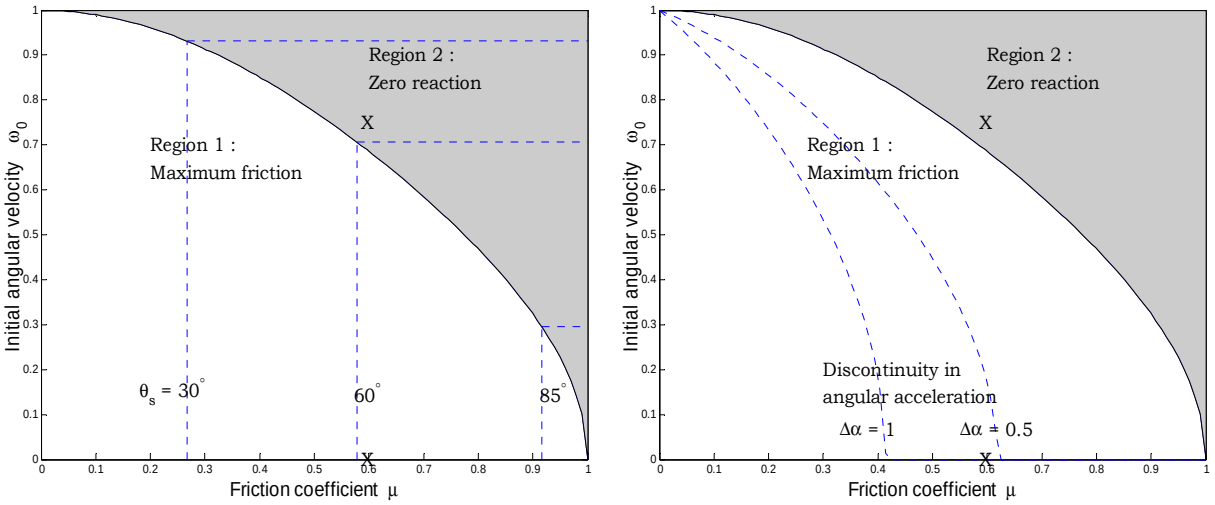

(a) : Contours of θ_s (b) : Discontinuity in α

Figure 3.2 : Two regions in the (μ, ω_0)-parameter space, separated by the curve $\omega_0 = \bar{\omega}_0(\mu)$

In the case of real hoops, Pritchett [13] and Theron [1] show that the rolling phase always ends when maximum friction is reached. It has been shown here that in the case of a massless hoop this only occurs if the initial velocity is smaller than a critical value that is a function of the friction coefficient.

Expressions in terms of the initial parameters μ and ω_0 will be derived next for all the variables at the end of the rolling phase for the two cases.

3.5.2 Case 1 : Low initial velocity

As shown above, the rolling motion comes to an end when maximum friction is reached if $\omega_0 < \bar{\omega}_0$; this will be called a case of *low initial velocity*, with the initial velocity being less than the critical value for a given value of μ, and (3.29) defining the value of θ_s.

Alternatively, this situation can also be called a case of *light friction*, with μ relatively small for a given initial velocity.

From (3.27), $\theta_s = 2\arctan(\mu)$; therefore $\theta_s = 0$ when $\mu = 0$, $\theta_s = \pi/2$ when $\mu = 1$ and θ_s approaches π as μ goes to infinity. The vertical lines in Figure 3.2(a) are the contours for three other constant values of θ_s.

The angular velocity at the point where phase 1 ends, using (3.29) in (3.17), is
$\omega_s^2 = 2\,(1+{\omega_0}^2)\,(1+\mu^2)/2 - 1$, or

$$\omega_s^2 = {\omega_0}^2\,(1+\mu^2) + \mu^2. \tag{3.32}$$

The angular acceleration just before this point is reached, using (3.18), is

$$\alpha_s^- = \tfrac{1}{2}\,\mu\,(1+{\omega_0}^2)\,(1+\mu^2).$$

The discontinuity in the angular acceleration, as given by (3.20), becomes

$$\Delta\alpha = (\cos\theta_s - \omega_0^2)(1+\mu^2)/(2\mu) = (1-\mu^2-\omega_0^2(1+\mu^2))/(2\mu).$$

This can be re-written as $\omega_0^2 = (1-\mu^2-2\,\mu\,\Delta\alpha)/(1+\mu^2)$, and used for plotting on Figure 3.2(b), where dotted curves show the cases $\Delta\alpha = 0.5$ and $\Delta\alpha = 1$. Note that $\Delta\alpha = 1$ corresponds to a discontinuity in the tangential acceleration equal to g; i.e. $\Delta(r\ddot{\theta}) = g$.

Clearly also from (3.20), $\Delta\alpha = 0$ on the curve $\omega_0 = \bar{\omega}_0(\mu)$.

The normal reaction just before this point is reached, from (3.13), is

$$\mathcal{N}_s^- = \cos\theta_s - {\omega_0}^2 = \bar{\omega}_0^2 - {\omega_0}^2.$$

Clearly, this situation can only occur if $\mathcal{N}_s^- > 0$, which confirms that $\omega_0 < \bar{\omega}_0$.

As discussed previously, $\mathcal{N} = 0$ and $\mathcal{F} = 0$ for $\theta \geq \theta_s$. The reaction force therefore undergoes a discontinuous drop to $\mathcal{N}_s^+ = 0$ and $\mathcal{F}_s^+ = 0$. This discontinuity in the reaction force is the cause of the corresponding discontinuity in the acceleration.

Also, if $\mu = 0$, then $\theta_s = 0$, $\alpha_s^- = 0$, $\mathcal{N}_s^- = (1-{\omega_0}^2)$, $\bar{\omega}_0 = 1$ and $\Delta\alpha$ tends to infinity.
If $\mu = 1$, then $\theta_s = \pi/2$, $\alpha_s^- = 1$, $\mathcal{N}_s^- = 0$, $\bar{\omega}_0 = 0$ and $\Delta\alpha = 0$. This is the extreme case; for $\mu > 1$ this situation of maximum friction can never arise, and the second situation described next will always occur.

3.5.3 Case 2 : High initial velocity

In cases where $\omega_0 > \bar{\omega}_0$, the normal reaction becomes zero before maximum friction is reached, and according to (3.30) the rolling phase ends at the point where $\cos\theta_s = \omega_0^2$. The horizontal lines in this region are the contours for constant θ_s.

This will be called a case of *high initial velocity*, or, equivalently, a case of *heavy friction* with $\mu > \bar{\mu}$, and is shown as the shaded region in Figure 3.2.

In some respects this is the most interesting situation arising from this model, as it can occur only in the hypothetical case under discussion; it never occurs for real hoops, as will be seen in the next chapter.

Using (3.30), (3.17) becomes $\omega_s^2 = 2\,(1+{\omega_0}^2)\,(1+\cos\theta_s)^{-1} - 1 = 1$,
(3.18) becomes $\alpha_s^- = \frac{1}{2}\,(1+\omega_s^2)\tan\theta_s/2 = \tan\theta_s/2$,
and (3.20) is $\Delta\alpha = (\cos\theta_s - \omega_0^2)/\sin\theta_s = 0$.

To summarise the above, for the case of high initial velocity or heavy friction

$$\mu > \bar{\mu}\,; \quad \cos\theta_s = \omega_0^2\,; \quad \omega_s = 1\,; \quad \Delta\alpha = 0. \tag{3.33}$$

Note that in this case there is no discontinuity in the angular acceleration required for skimming motion.

If $\omega_0 = 0$ then Littlewood's original problem is obtained, as discussed below. If $\omega_0 = 1$ then $\theta_s = 0$ and $\bar{\mu} = 1$; this is the limit for the previous solution; values of $\omega_0 > 1$ are dealt with later as a special case.

3.5.4 Zero initial velocity

Littlewood [8] and Tokieda [9] both considered the special case of zero initial velocity and large friction coefficient.

Taking $\omega_0 = 0$ in the previous analysis for heavy friction, $\bar{\mu} = 1$ and $\theta_s = \pi/2$; this means that if $\mu \geq 1$, the normal reaction becomes zero when the radius between the centre of the hoop and the particle is horizontal, in agreement with Littlewood's original statement. [8]

Also, from (3.33), $\omega_s = 1$, $\alpha_s^- = 1$ and $\Delta\alpha = 0$. Clearly therefore, continuity in the angular acceleration results in skimming, whereas hopping can only occur if there is a positive discontinuity so that $\alpha_s^+ > 1$.

3.5.5 Numerical examples

To conclude this section, two examples illustrating the behaviour of massless hoops are presented. A friction coefficient of $\mu = 0.6$ is used; this results in a large discontinuity for the low velocity case.

In example 1 the initial velocity is taken as zero, the same as in Littlewood's case. However, because the friction coefficient is less than 1, skimming starts at a much earlier angle. The second example is for $\omega_0 > \bar{\omega}_0$.

Table 3.1 shows the input data for the two examples, as well as the values of $\bar{\omega}_0$, θ_s and $\Delta\alpha$ as calculated from (3.28), (3.29) or (3.30), and (3.20) respectively.

μ	$\bar{\omega}_0$	ω_0	θ_s	$\Delta\alpha$
0.6	0.686	0	61.9°	0.533
		0.75	55.8°	0.0

Table 3.1 : Parameter values and calculated values for the examples shown in Figure 3.3

The two data-points are also marked in Figure 3.2 by crosses. Note that the calculated values in Table 3.1 are in agreement with the contours for θ_s and $\Delta\alpha$ in Figure 3.2.

The low velocity example is shown in Figures 3.3(a) and (b), with the graphs for the reactions in Figure 3.3(a). The horizontal line at 0.6 indicates the value of μ; clearly, the rolling motion in the first phase continues until $\mathcal{F} = \mu\mathcal{N}$, i.e. $\mathcal{F}/\mathcal{N} = \mu$, as illustrated by the curve labelled $\mathcal{F}/\mathcal{N}$. At this point $\theta = \theta_s$ and the reaction force drops to zero instantaneously.

The kinematic quantities ω and α are shown in Figure 3.3(b), and the large discontinuity in α is clearly noticeable. Both curves tend to infinity as θ approaches π.

In the second example the rolling phase ends when N becomes zero, before maximum friction is reached, as shown in Figure 3.3(c). Figure 3.3(d) shows that in this case the angular acceleration is continuous through the point $\theta = \theta_*$.

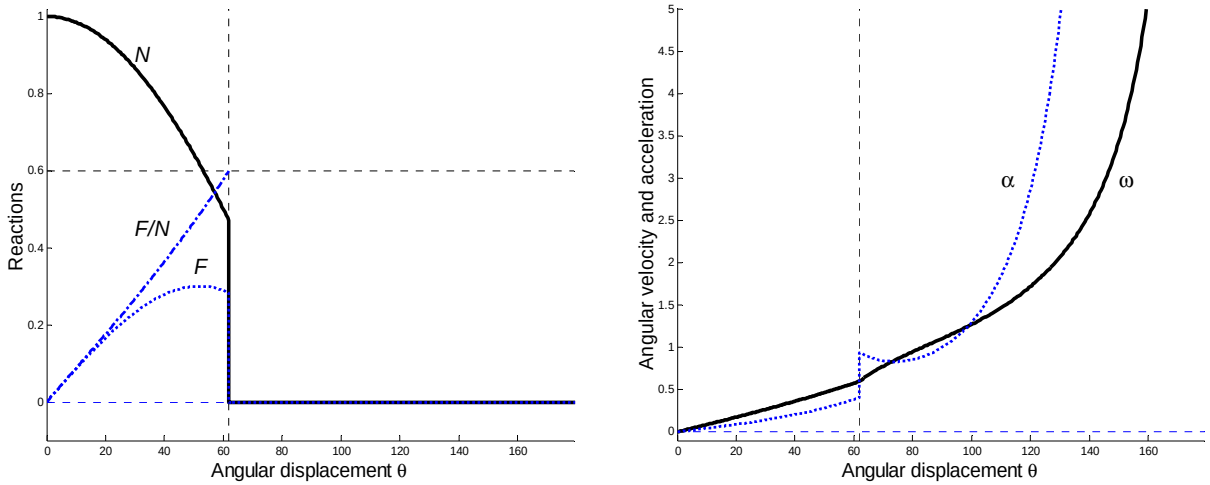

(a) : Reaction forces (b) : Kinematic quantities

Case 1 : $\omega_0 = 0$, low initial velocity

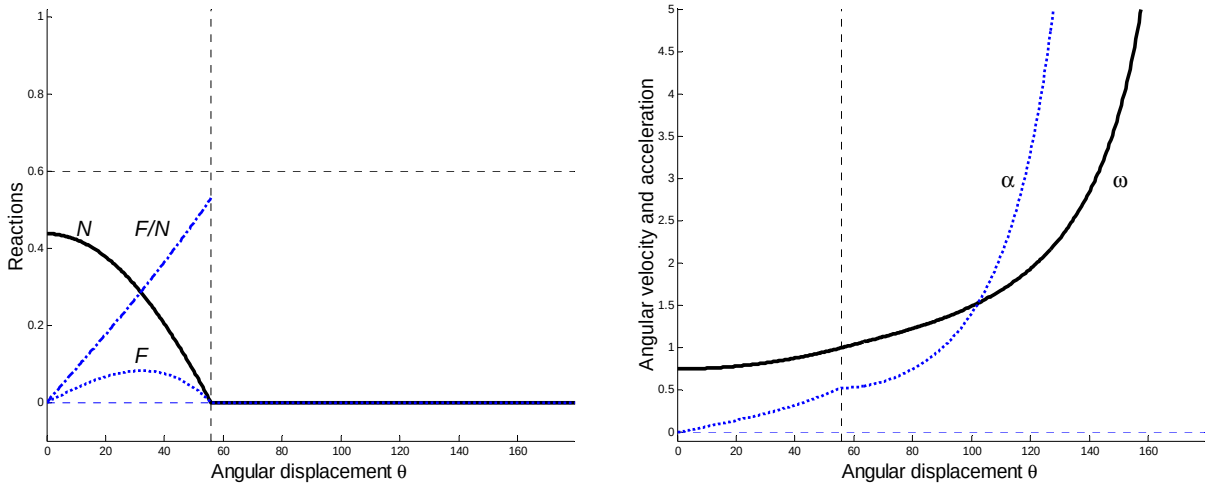

(c) : Reaction forces (d) : Kinematic quantities

Case 2 : $\omega_0 = 0.75$, high initial velocity

Figure 3.3 : Detailed results for two examples of massless hoops

3.6 Parabolic motion of the particle

The parabolic path of the particle for $t > t_s$ is examined to round off this analysis of the massless hoop.

It is convenient to denote the *range on the cycloid* by $\mathcal{S}_1$, and the non-dimensional height of the particle when it leaves the cycloid by $\mathcal{H}_1$; Then the position of the particle at the end of the rolling phase is

$$\mathcal{S}_1 = (x_s/r) = \theta_s + \sin\theta_s; \quad \mathcal{H}_1 = (y_s/r) = 1 + \cos\theta_s.$$

Using (3.2) with $\mathcal{V}_x = \omega$ and $\mathcal{V}_y = 0$ during phase 1, the components of velocity at the end of the rolling phase are

$$(x/r)'(\theta_s) = \omega_s\,\mathcal{H}_1; \qquad (y/r)'(\theta_s) = -\omega_s\,\sin\theta_s.$$

These values are the initial conditions for the parabolic motion of the particle.

Integrating $\ddot{x} = 0$ and $\ddot{y} = -g$ w.r.t. t, or in non-dimensional form, integrating $(x/r)'' = 0$ and $(y/r)'' = -1$ w.r.t. τ, and using the initial conditions above, the velocity of the particle is

$$(x/r)' = \omega_s\,\mathcal{H}_1; \qquad (y/r)' = -\omega_s\,\sin\theta_s - (\tau - \tau_s).$$

Likewise, one more integration gives the trajectory of the particle as

$$(x/r) = \mathcal{S}_1 + \omega_s\,\mathcal{H}_1\,(\tau - \tau_s); \qquad (y/r) = \mathcal{H}_1 - \omega_s\,\sin\theta_s\,(\tau - \tau_s) - \tfrac{1}{2}\,(\tau - \tau_s)^2. \tag{3.34}$$

This phase of the motion comes to an end when the particle collides with the rigid surface, say at position $(x_2,\ 0)$, causing an impulse on the particle. The *range on the parabola*, and the elapsed time between positions 1 and 2, are defined as the non-dimensional values

$$\mathcal{S}_2 = (x_2 - x_s)/r \ \text{ and } \ \mathcal{T}_2 = \tau_2 - \tau_s.$$

When solving for $\mathcal{T}_2$ from the quadratic equation

$$\tfrac{1}{2}\,\mathcal{T}_2^2 + \omega_s\,\sin\theta_s\,\mathcal{T}_2 - \mathcal{H}_1 = 0,$$

it is convenient to use the following factor in the discriminant:

$$D_1 = \sqrt{1 + 2\mathcal{H}_1/(\omega_s^2\,\sin^2\theta_s)}.$$

Then

$$\mathcal{T}_2 = \omega_s\,\sin\theta_s\,(D_1 - 1)$$

and

$$\mathcal{S}_2 = \omega_s^2\,\sin\theta_s\,\mathcal{H}_1\,(D_1 - 1).$$

The components of velocity just before the impact are

$$\omega_s\,\mathcal{H}_1 \ \text{ and } \ -D_1\,\omega_s\,\sin\theta_s$$

in the x- and y-directions respectively. Using the above values in (3.25),

$$\cos\theta(t_2) = \cos\theta_s - \omega_s\,\mathcal{T}_2\,\sin\theta_s - \tfrac{1}{2}\,\mathcal{T}_2^2 = \cos\theta_s - \omega_s^2\,\sin^2\theta_s\,(D_1 - 1)(1 + \tfrac{1}{2}(D_1 - 1)).$$

Using $\theta_2 = \theta(t_2)$, this simplifies to $\cos\theta_2 = -1$; i.e. $\theta_2 = \pi$, implying that the hoop is directly above the particle as previously stated in section 3.4.4 when describing the skimming motion. The velocity of the particle at this point is known; the velocity just after the impact depends on the nature of the particle and the surface. Depending on the elasticity of the impact the hoop is likely to hop at $\theta = \pi$.

A final result of some interest is the total range of the particle. The *total range* is defined as $\mathcal{S}_T = \mathcal{S}_1 + \mathcal{S}_2$, and $r\,\mathcal{S}_T$ is the horizontal distance the particle travels from the initial position until it hits the surface. Using the previous results,

$$\mathcal{S}_T = \theta_s + \sin\theta_s + \omega_s^2 \sin\theta_s(1 + \cos\theta_s)(D_1 - 1). \tag{3.35}$$

Figure 3.4 shows a few examples of the path travelled by the particle when fixed to a massless hoop. In figure (a) the dotted curve shows the cycloid, with range π. Because $\theta_s < \pi$ as shown above, the particle on a massless hoop will always leave the cycloid before $\theta = \pi$. (However, in the next chapter it will be shown that real hoops can roll through this position, in which case the particle remains on the cycloid.)

The curve labelled a, just to the right of the cycloid, represents the path of the particle for Littlewood's hoop with zero initial velocity. The position where the particle leaves the cycloid and the parabola begins is marked by the +-sign and the verticle and horizontal dotted lines. The co-ordinates of this point, $(\mathcal{S}_1,\ \mathcal{H}_1)$, are tabulated in the first line of Table 3.2.

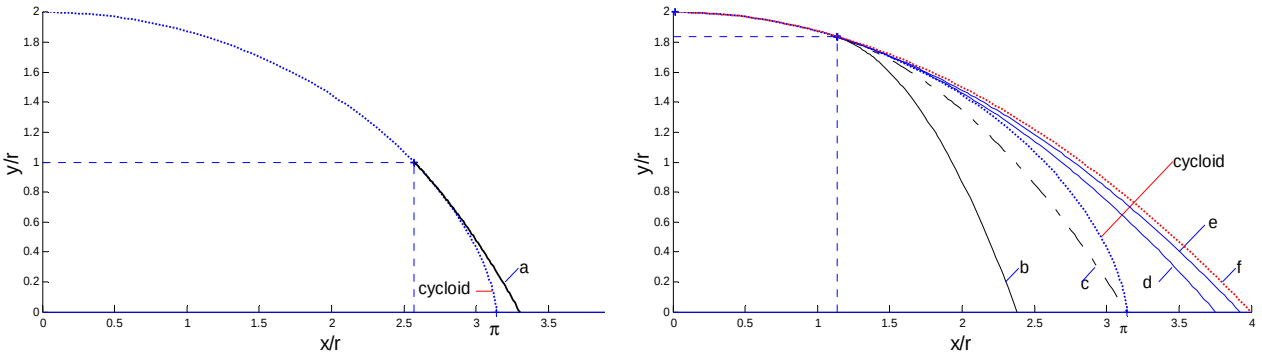

(a) : Littlewood's case, $\mu = 1$ (b) : Cases b to f

Figure 3.4 : Path of the particle

Ex	μ	$\bar{\omega}_0$	θ_s	$\mathcal{S}_1$	$\mathcal{H}_1$	ω_0	ω_s	$\mathcal{S}_2$	$\mathcal{S}_T$
a	1	0	$\pi/2$	$\pi/2+1$	1	0	1	$\sqrt{3}-1$	3.3
b	0.3	0.9137	33.4^o	1.133	1.835	0.25	0.3976	1.247	2.38
c						0.6027			π
d						0.9	0.9864	2.62	3.75
e						0.99	1.0762	2.79	3.97
f	0	1	0	0	2	1	1	4	4

Table 3.2 : Parameter values and ranges for the examples shown in Figure 3.4

Five graphs are shown in Figure 3.4(b) for the remaining values shown in the table, with cases b to e being for $\mu = 0.3$. Note that the values of $\bar{\omega}_0$, θ_s and $\mathcal{S}_1$ are functions of μ alone and are independent of the initial velocity. The cycloid is again shown by the dotted curve.

The first graph, labelled b, is for a very low initial velocity, $\omega_0 = 0.25$. Because μ is much smaller than in the case of Littlewood's hoop, slipping starts much earlier and the angular velocity during the hop is lower. Consequently the total range is also less as shown.

The curve labelled c is for the special case where the initial velocity is selected so that the total range equals the range of half a cycloid; i.e. so that $\mathcal{S}_T = \pi$. This is achieved by using the definitions for $\mathcal{S}_1$, $\mathcal{S}_T$ and D_1, and defining constants $a_1 = (1+\cos\theta_s))/\sin^2\theta_s$ and $b_1 = (\pi - \mathcal{S}_1)/(\sin\theta_s\,(1+\cos\theta_s))$. Then $\omega_s^2 = \frac{1}{2}\,b_1^2/(a_1 - b_1)$ and $\omega_0^2 = (\omega_s^2 - \mu^2)/(1+\mu^2)$. For $\mu = 0.3$, the required initial velocity is $\omega_0 = 0.6027$, and the path is shown with a dash-dot curve.

Curve d is for $\omega_0 = 0.9$, which is still less than $\bar{\omega}_0$ and therefore a case of low initial velocity. Due to the higher initial velocity the range on the parabola is much larger than the previous examples and the total range exceeds that of the cycloid.

The next example, labelled e, is a case of high initial velocity, with $\omega_0 = 0.99 > \bar{\omega}_0$ and a total range that is larger than the previous cases.

The last example is shown as a dotted curve labelled f, and is the limiting case when $\mu = 0$, $\theta_s = 0$ and the particle leaves the cycloid immediately and follows a parabolic path for the whole trajectory. The previous solutions in terms of D_1 are no longer valid, because D_1 tends to infinity as θ_s goes to zero. Now $\omega_s = \omega_0$, and the linear term in the quadratic equation for $\mathcal{T}_2$ disappears, so that $\mathcal{T}_2 = \sqrt{2(y_s/r)} = 2$ and $\mathcal{S}_T = \mathcal{S}_2 = 4\omega_0$. The graph is drawn for $\omega_0 = 1$, giving a range of $\mathcal{S}_T = 4$ which is the maximum achievable if the initial angular velocity is restricted to $w_0 \leq 1$.

Each of these graphs is a point on the (ω_0, $\mathcal{S}_T$)-plane in Figure 3.5, which shows some graphs of $\mathcal{S}_T$ as a function of the initial velocity ω_0 for a few values of μ.

The lowest graph, for $\mu = 0$ (and therefore $\theta_s = 0$) is also the graph obtained for a free projectile fired horizontally with initial velocity $\dot{x}(0) = 2r\dot{\theta}(0)$ from a height $2r$ above the horizontal plane. In non-dimensional form, $(y_s/r) = 2$, $\mathcal{T}_2 = 2(y_s/r)$, $\mathcal{S}_2 = 4\omega_0$ and $\mathcal{S}_T = 4\omega_0$. In this case the range increases linearly with increasing ω_0, and is not affected by the hoop. Graph f in Figure 3.4(b) corresponds with the + -sign at point (1, 4) in Figure 3.5.

For positive values of the friction coefficient, the effect of the hoop is to increase the range by prolonging the rolling phase. The + - signs are drawn on the abscissa $\bar{\omega}_0(\mu)$ and indicate the parameter values which separate the low and high initial angular velocity situations. For

$\mu = 0.3$, $\bar{\omega}_0 = 0.9137$; for $\mu = \frac{1}{2}$, $\bar{\omega}_0 = \sqrt{3/5}$. For $\omega_0 > \bar{\omega}_0$ (high velocity situations) the range is independent of the friction coefficient, as shown by the fact that the curves are the same.

Three graphs in Figure 3.4(b) correspond to the points marked with crosses on the curve for $\mu = 0.3$ in Figure 3.5, for $\omega_0 = 0.25$, 0.9 and 0.99 respectively.

The upper limit is reached with $\mu = 1$, when case 2 applies for all initial velocities. In this case the + - sign also represents Littlewood's model, with $\omega_0 = 0$ and $\theta_s = \pi/2$, resulting in a range of $\mathcal{S}_T = \pi/2 + \sqrt{3} \approx 3.3$ as shown previously.

Finally, the dashed horizontal line at $\mathcal{S}_T = \pi$ shows the range obtained for a real hoop [1] that rolls without slipping through 180°, being the "range" of half a cycloid.

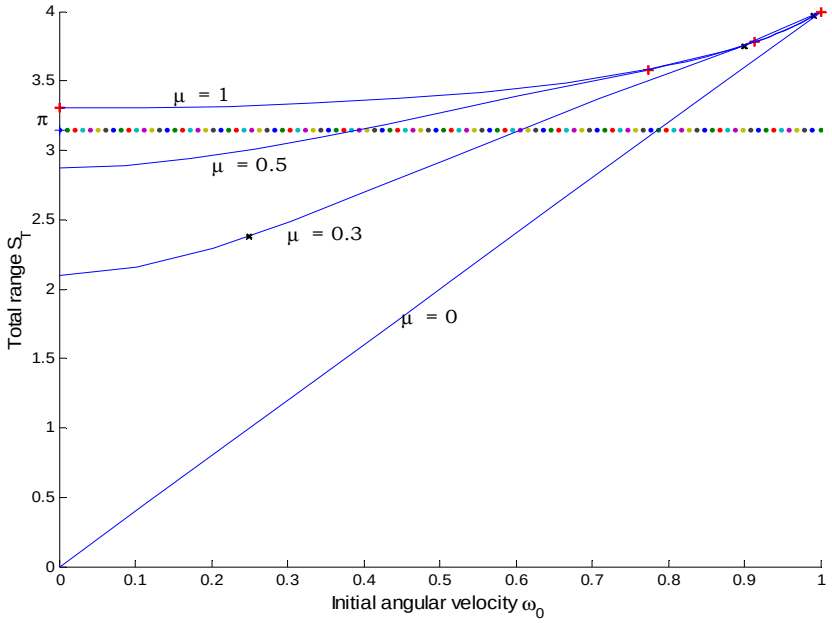

Figure 3.5 : Total range $\mathcal{S}_T$ as a function of initial velocity ω_0, for different values of the friction coefficient μ

3.7 Summary and Conclusions

In this analysis of a rigid, massless hoop rolling on a rough horizontal surface while loaded by a heavy particle on its rim, it has been shown that the previously held understanding that the hoop will hop with $\theta \leq \pi/2$ is not the only possible motion. An alternative motion called skimming has been derived; during this motion the hoop continues moving horizontally after the normal reaction becomes zero. During this skimming motion, the hoop rotates around the free-falling particle at exactly the correct angular velocity to remain in geometric contact with the surface.

Two cases have been identified depending on whether the initial velocity is less than or greater than the critical value, which is a function of the friction coefficient. Case 1 refers to situations with low initial velocity (or light friction) in which a massless hoop (as well as a real hoop) stops rolling due to maximum positive friction. In case 2 situations a massless hoop stops rolling when the normal reaction becomes zero.

The question on whether the hoop will hop or skim can not be decided by Newton's second law, which provides no information regarding the angular acceleration in the case of a massless hoop. It is suggested however that the following arguments are plausible, if not conclusive, reasons why the (hypothetical) massless hoop will skim rather than hop.

- In all cases the angular acceleration required for skimming is smaller than that required for hopping. Hopping always requires a discontinuous increase in the angular acceleration; in case 1, the discontinuity for skimming is smaller; in case 2, skimming occurs without a discontinuity. It seems reasonable to accept that the hoop will continue moving with a minimum change in the acceleration, as there is no physical moment causing such a change.

- The skimming motion is properly defined, and ensures that the hoop rotates around the particle at exactly the right angular velocity to ensure that it remains above the particle and the surface up to the moment when the particle hits the surface at $\theta = \pi$. The hopping motion on the other hand is completely undefined as far as the rotation of the hoop is concerned, and there is no way of determining when the hoop will hit the surface.

- The governing equation for skimming, (eq. 3.21), is obtained by setting the hoop mass equal to zero in the corresponding equation for real hoops, for $\theta > \theta_s$. This is true for both cases, and it will be shown later in section 6.4 that the numerical solutions for real hoops approximate skimming for very small values of the hoop mass. Because real hoops do not hop when $\theta \leq \pi/2$ it seems reasonable to suggest that a massless hoop will skim and not hop.

Finally, this skimming motion illustrates the principle that zero normal reaction is a necessary but not sufficient condition for hopping.

Chapter 4

Dynamics of a rigid hoop - mathematical model

The purpose of the following three chapters is to analyse the behaviour of real, rigid hoops, as was done in [1]. In this chapter the mathematical model is derived and analysed. In Chapter 5 results based on numerical solutions of the equations are given and the different behavioural patterns are classified. A number of additional results based on the numerical solutions are given in Chapter 6.

In contrast to the previous chapter, the analysis is not restricted to $\theta < \pi$, and interesting behaviour is identified in the region $\theta \approx 3\pi/2$. Also, the equations are developed for motion on a slope, with $\psi \geq 0$, and for a particle with $\epsilon \geq 0$. However, nearly all the numerical solutions are for $\psi = 0$ and $\epsilon = 0$.

4.1 The mathematical model

The rigidity of the hoop is modelled by setting d, and all the derivatives of d, to zero in the equations of Chapter 2. Only the final non-dimensional equations are simplified for use in this chapter.

Using (2.3), (2.15) and (2.4), or Figure 4.1, the height $\mathcal{H}$ and the moment of inertia factors now simplify to

$$\mathcal{H} = 1 + \gamma \cos\theta, \quad \kappa_G = 1 + \epsilon - \gamma^2, \quad \kappa_C = 2\mathcal{H} + \epsilon. \tag{4.1}$$

The non-dimensional kinematic equations (2.15) to (2.17) are still

$$x/r = \mathcal{X} + \gamma \sin\theta, \qquad y/r = \mathcal{Y} + \gamma \cos\theta, \tag{4.2}$$

$$(x/r)' = \mathcal{V}_x + \gamma\,\omega \cos\theta, \qquad (y/r)' = \mathcal{V}_y - \gamma\,\omega \sin\theta, \tag{4.3}$$

$$(x/r)'' = \mathcal{X}'' + \gamma\,\theta'' \cos\theta - \gamma\,\omega^2 \sin\theta, \qquad (y/r)'' = \mathcal{Y}'' - \gamma\,\theta'' \sin\theta - \gamma\,\omega^2 \cos\theta. \tag{4.4}$$

Note that these equations are applicable in all cases, whether $Y = r$ while the hoop is in contact with the surface, or whether $Y > r$ during a hop.

The kinetic equations (2.19) to (2.21) are only applicable while $Y = r$. Using $Y'' = 0$ in (2.20), these equations are

$$\mathcal{F} = \mathcal{X}'' + \gamma\,\theta''\,\cos\theta - \gamma\,\omega^2\,\sin\theta - \sin\psi, \tag{4.5}$$

$$\mathcal{N} = -\gamma\,\theta''\,\sin\theta - \gamma\,\omega^2\,\cos\theta + \cos\psi, \tag{4.6}$$

$$\mathcal{N}\,\gamma\,\sin\theta - \mathcal{F}\,\mathcal{H} = \kappa_G\,\theta''. \tag{4.7}$$

As before, X, Y and θ are chosen as the degrees of freedom.

For a rigid hoop, the expressions for the total energy, (2.22) and (2.23), simplify to

$$\mathcal{E}_1 = (1+\gamma)\cos\psi + \tfrac{1}{2}(\mathcal{V}_{x0} + \gamma\omega_0)^2 + \tfrac{1}{2}\kappa_G\omega_0^2, \tag{4.8}$$

$$\mathcal{E} = (1+\gamma\cos\theta)\cos\psi - \mathcal{X}\sin\psi + \tfrac{1}{2}(\mathcal{V}_x + \gamma\omega\cos\theta)^2 + \tfrac{1}{2}(-\gamma\omega\sin\theta)^2 + \tfrac{1}{2}\kappa_G\omega^2,$$

or

$$\mathcal{E} = (1+\gamma\cos\theta)\cos\psi - \mathcal{X}\sin\psi + \tfrac{1}{2}\mathcal{V}_x^2 + \mathcal{V}_x\gamma\omega\cos\theta + \tfrac{1}{2}(1+\epsilon)\omega^2. \tag{4.9}$$

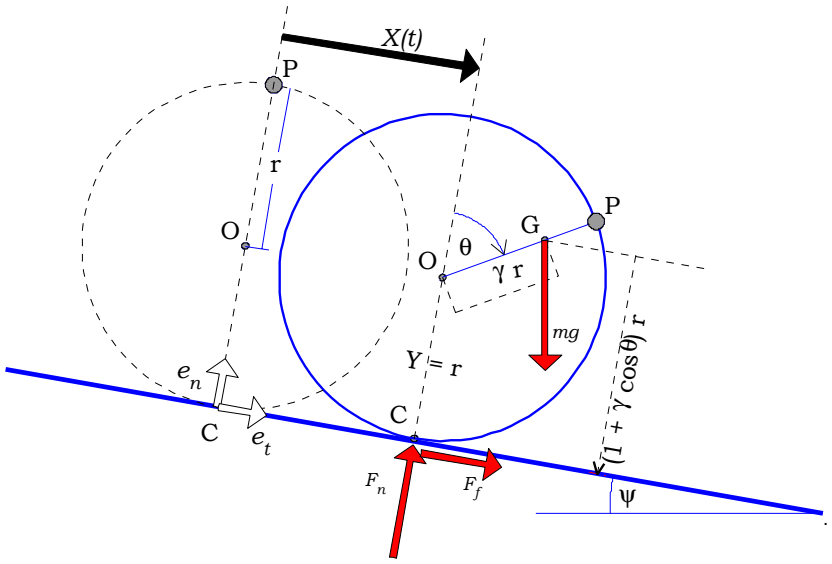

Figure 4.1 : The rigid hoop - geometry and forces

4.2 Different modes of motion

As stated earlier, the initial conditions are always selected so as to ensure rolling motion to start with. Later results will show that a surprisingly large number of variations in the subsequent sequence of modes of motion is possible.

It is clear that hopping can occur only after the normal reaction $\mathcal{N}$ has become zero. For realistic values of the friction coefficient the friction force $\mathcal{F}$ must reach its maximum value of $\mu_s \mathcal{N}$ before $\mathcal{N}$ becomes zero; therefore the hoop must slip before hopping. This was realised by Littlewood and formally proven by Pritchett that it also applies in the case of a massless hoop.

Therefore rolling motion can end with either a spinning (i.e. positive friction force) or a skidding (i.e. negative friction force) phase, depending on the values of μ_s and the initial velocity.

The second phase (spinning or skidding) usually ends with another rolling phase, followed by further spinning or skidding.

4.2.1 Final conditions

The analysis ends when the sequence of alternating rolling and slipping phases reaches a final condition at a position denoted by θ_F. This final condition is taken as one of the following:

- $\theta_F = 2\pi$, implying that a complete revolution has been completed.
- $\omega_F = \omega(\theta_F) = 0$, i.e. the hoop stops rotating and will start rotating backwards. Note that $\omega_F = 0$ does not imply that $\mathcal{V}_x$ is also zero; the hoop may still be moving forwards while rotating anti-clockwise.
- $\mathcal{N}_F = \mathcal{N}(\theta_F) = 0$, i.e. the normal reaction becomes zero and the hoop hops.

4.2.2 Rolling

The non-dimensional form of the acceleration for rolling motion, after simplifying (2.24) for a rigid hoop, is

$$\mathcal{X}'' = \theta''. \tag{4.10}$$

The torque equation for rolling, (2.26), is $\kappa_C\, \theta'' = \gamma \sin\theta\, \omega^2 + (\gamma \sin\theta \cos\psi + \mathcal{H} \sin\psi)$. The last term in brackets, which is the term associated with the weight mg, simplifies to $(\gamma \sin\theta \cos\psi + \sin\psi(1 + \gamma \cos\theta)) = \gamma \sin(\theta + \psi) + \sin\psi$. Therefore

$$\kappa_C\, \theta'' = \gamma \sin\theta\, \omega^2 + \gamma \sin(\theta + \psi) + \sin\psi. \tag{4.11}$$

The equation above was derived by the standard method of taking moments around the centre of mass and then eliminating the forces using Newton's second law for translation. It is of some interest to consider the many different ways in which this equation can be derived; this is done in some detail in Appendix A.

Using (2.13), $\frac{\mathrm{d}\omega^2}{\mathrm{d}\theta} = 2\omega'$, with (4.11), this can be written as

$$\frac{\mathrm{d}\omega^2}{\mathrm{d}\theta} = \frac{2}{\kappa_C} (\gamma \sin\theta\, \omega^2 + \gamma \sin(\theta + \psi) + \sin\psi).$$

Using $\kappa_C = 2 + \epsilon + 2\gamma \cos\theta$ from (4.1), this linear first order differential equation in ω^2 can be integrated with respect to θ to give the analytic solution

$$\omega^2 = \frac{2}{\kappa_C} \left(-\gamma \cos(\theta + \psi) + \theta \sin\psi + C\right). \tag{4.12}$$

The integration constant C is found from the conditions at the point where rolling starts. Initially this is at the point $\theta = 0$, where $C = C_0$ is used, with

$$C_0 = (1 + \epsilon/2 + \gamma)\,\omega_0^2 + \gamma\,\cos\psi.$$

As shown later, the rolling motion can resume at position θ_r where $\omega(\theta_r) = \omega_r$, in which case

$$C = (1 + \epsilon/2 + \gamma\,\cos\theta_r)\,\omega_r^2 + \gamma\cos(\theta_r + \psi) - \theta_r\,\sin\psi.$$

While the friction force is less than the maximum permissible value, equation (4.12) gives ω as a function of θ; with this known, (4.11) can be used to find θ'', (4.10) to find X'', (4.6) to find $\mathcal{N}$, and (4.7) or (4.5) can be used to find $\mathcal{F}$, all as functions of θ.

The rolling motion will continue up to one of the final conditions defined in section 4.2.1, or until $|\mathcal{F}| = \mu_s\mathcal{N}$ at some stage of the motion, and the hoop starts slipping.

4.2.3 Spinning and skidding

Assume that the wheel rolls until the angular displacement is θ_s when slipping commences with $\mathcal{N}(\theta_s) > 0$ and $|\mathcal{F}(\theta_s)| = \mu_s\,\mathcal{N}(\theta_s)$. The initial conditions for the slipping motion are defined by $\omega_s = \omega(\theta_s)$ and $\mathcal{V}_s = \mathcal{V}(\theta_s) = \omega_s$.

The two possibilities for the orientation of the friction force were considered separately in section 2.5. To reiterate, the hoop is said to be spinning if $\mathbf{F}_f = +\mu_k\,F_n\,\mathbf{e}_t$, with $r\,\dot\theta > \dot X$. Similarly, motion is defined as skidding if the friction force is negative, $\mathbf{F}_f = -\mu_k\,F_n\,\mathbf{e}_t$, with $r\,\dot\theta < \dot X$. By defining $\mu = \mu_k$ in the case of spinning, and $\mu = -\mu_k$ in the case of skidding, the two cases are handled by one differential equation.

For a rigid hoop the slip factor S in (2.27) becomes

$$S = \gamma\sin\theta - \mu\,(1 + \gamma\,\cos\theta),$$

and (2.28) becomes

$$(\kappa_G + S\,\gamma\,\sin\theta)\,\theta'' = S\,(\cos\psi - \gamma\,\omega^2\,\cos\theta),$$

or, using (2.13),

$$\frac{\mathrm{d}\omega^2}{\mathrm{d}\theta} = \frac{2S\,(\cos\psi - \gamma\,\omega^2\,\cos\theta)}{\kappa_G + S\,\gamma\,\sin\theta}. \tag{4.13}$$

No analytical solution could be found for (4.13), and this equation is integrated numerically, using the initial condition $\omega(\theta_s) = \omega_s$.

With ω known at a specific position, θ'' is calculated by using (2.13) and re-writing (4.13) as

$$\theta'' = \frac{S\,(\cos\psi - \gamma\,\omega^2\,\cos\theta)}{\kappa_G + S\,\gamma\,\sin\theta}. \tag{4.14}$$

The normal reaction $\mathcal{N}$ is obtained from (4.6), and the friction force $\mathcal{F}$ is obtained from Coulomb's law: $\mathcal{F} = \mu\mathcal{N}$. (Note that the correct sign of $\mathcal{F}$ is obtained, because of the definition of μ.) Equation (4.5) is now used to calculate X'',

$$\mathcal{X}'' = \sin\psi - \gamma\theta''\cos\theta + \gamma\omega^2\sin\theta + \mathcal{F}, \tag{4.15}$$

and the values of $\mathcal{V}_x$ and $\mathcal{Y}$ can then be obtained by numerical integration.

The slipping motion will continue up to one of the final conditions defined in section 4.2.1, or until $\mathcal{X}'(\theta_r) = \omega(\theta_r)$ at some stage of the motion, and the hoop starts rolling again.

4.2.4 Hopping

The necessary conditions for hopping are that $\mathcal{N} = 0$ and that point O acquires a positive velocity normal to to the surface. The following derivation is based on three sets of values or equations, namely the values immediately before the hop, the equations during the hop, and the values immediately after the hop commences.

- The position where hopping commences is denoted by θ_*, at time τ_*, and is found as the position where $\mathcal{N}(\theta_*) = \mathcal{N}(\tau_*^-) = 0$. [1] The friction force at this moment, $\mathcal{F}(\tau_*^-)$, must also be zero, therefore $\alpha(\tau_*^-) = 0$ from (4.7). Also, $\mathcal{V}_y(\theta_*) = 0$ and $\mathcal{Y}''(\tau_*^-) = 0$.

  The angular velocity $\omega_* = \omega(\theta_*)$ is known from the solution of the preceding slipping motion, and using (4.6) for $\mathcal{N} = 0$ and $\alpha = 0$, obeys the relationship $\omega_*^2\,\gamma\,\cos\theta_* = \cos\psi$.

  To summarise, the known values at the end of the phase just before the reaction becomes zero are

$$\omega_*^2\,\gamma\,\cos\theta_* = \cos\psi; \quad \alpha(\tau_*^-) = 0; \quad \mathcal{V}_y(\theta_*) = 0; \quad \mathcal{Y}''(\tau_*^-) = 0. \tag{4.16}$$

- For $t \geq t_*$ the weight acting at the centre of mass G is the only force and, from Newton's second law, the acceleration components are $\ddot{x} = g\,\sin\psi, \quad \ddot{y} = -g\,\cos\psi, \quad \ddot{\theta} = 0$. As discussed previously, the last result applies only if $\kappa_G > 0$. In terms of the non-dimensional values, these accelerations and their derivatives are

$$(x/r)'' = \sin\psi; \quad (y/r)'' = -\cos\psi; \quad (y/r)''' = 0; \quad \alpha = 0; \quad \alpha' = 0. \tag{4.17}$$

  Clearly, the centre of mass G follows a parabolic trajectory and the hoop rotates with a constant angular velocity ω_*. Some of the properties of this parabolic path were derived in [2] and are given in Chapter 3.

  The motion of the centre of the hoop needs to be analysed in order to establish whether the hoop leaves the surface or not. The component of the acceleration perpendicular to the surface is given by the second relationship in (4.4):

$$(y/r)'' = \mathcal{Y}'' - \alpha\,\gamma\,\sin\theta - \omega^2\,\gamma\,\cos\theta.$$

  The jerk (third derivative of position) is also required:

$$(y/r)''' = \mathcal{Y}''' + (\omega^3 - \alpha')\,\gamma\,\sin\theta - 3\omega\alpha\,\gamma\,\cos\theta.$$

  Using (4.17), the acceleration and jerk of point O for $t \geq t_*$ are therefore

$$\mathcal{Y}'' = \omega^2\,\gamma\,\cos\theta - \cos\psi; \qquad \mathcal{Y}''' = -\omega^3\gamma\,\sin\theta; \qquad \theta \geq \theta_*. \tag{4.18}$$

- At the moment when the hop commences at τ_*^+, the acceleration is given by

$$\mathcal{Y}''(\tau_*^+) = \omega_*^2\,\gamma\,\cos\theta_* - \cos\psi, \text{ therefore, } \mathcal{Y}''(\tau_*^+) = 0,$$

  using the first of (4.16). This can be interpreted by noting that $\omega_*^2\,\gamma\,\cos\theta_* = \cos\psi$ is equivalent to $m\,\gamma r\,\dot{\theta}_*^2\,\cos\theta_* = mg\,\cos\psi$ in terms of the physical variables. At the instant

[1] As before, possible discontinuities in the forces and accelerations at this point are allowed for by using this notation. Here it is convenient to use (non-dimensional) time as the independent variable to indicate the discontinuity. Note that position and velocity are continuous functions of time.

when $\mathcal{N}$ becomes zero the normal component of the "centrifugal force" therefore equals the normal component of the weight; this can only be the case if $\theta_* < \pi/2$ or if $\theta_* > 3\pi/2$, as clearly shown in the D'Alembert diagram.

The jerk at this moment is given by

$$\mathcal{Y}'''(\tau_*^+) = -\omega_*^3 \gamma \sin\theta_*.$$

- The necessary kinematic criterion for hopping of a rigid hoop is clearly that $Y(\tau) > r$ for $\tau > \tau_*$. Because $Y(\tau_*) = r$, $\mathcal{V}_y(\tau_*) = 0$ and $\mathcal{Y}''(\tau_*^+) = 0$, a sufficient condition for hopping is that the third derivative or jerk be positive. Therefore the criterion for hopping is

$$\mathcal{Y}'''(\tau_*^+) = -\omega_*^3 \gamma \sin\theta_* > 0. \tag{4.19}$$

Clearly this criterion will be satisfied if $\omega_* > 0$ and $\theta_* \in (\pi, 2\pi)$. Furthermore, if $\theta_* \in (3\pi/2, 2\pi)$ then $\mathcal{Y}'' = \omega_*^2 \gamma \cos\theta - \cos\psi$ will become positive for $\theta > \theta_*$ and the centrifugal effect of the heavy particle lifts the hoop off the surface. These aspects are illustrated by the Dalembert representation for $\theta_* > 3\pi/2$, where the lengths of the vectors are drawn to scale for the values calculated for a later example where hopping occurs.
Hopping always follows a slipping phase, therefore ω_* can only be calculated numerically.

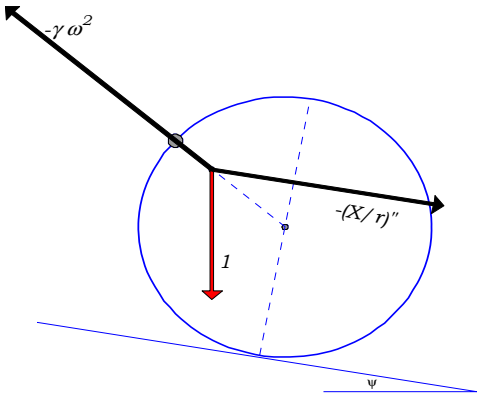

D'Alembert diagram for $\theta_* > 3\pi/2$

4.2.5 Immediate hopping

Result 2.1 in section 2.6 shows that a rigid hoop will hop in position $\theta = 0$ if

$$\omega_0 > \hat{\omega}_0 = \sqrt{(1/\gamma)\,\cos\psi}.$$

This places an upper bound on the initial velocity for initial contact to be maintained, as $\mathcal{N}(0) > 0$ only if $\omega_0 < \hat{\omega}_0$.
Conversely, if $\omega_0 > \hat{\omega}_0$, then $\mathcal{Y}''(0) = \gamma\omega_0^2 - \cos\psi > 0$ from (4.18) and the hoop will hop at $\theta = 0$ due to the large initial centrifugal effect as shown in the D'Alembert diagram.

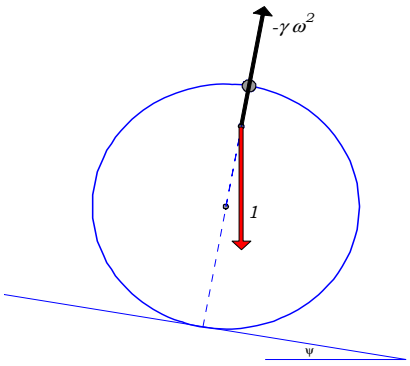

D'Alembert diagram for $\theta = 0$

4.2.6 Summary

The results of the previous two sections on hopping can be summarised as:

Result 4.1 : Hopping of a rigid hoop

- A rigid hoop will hop at $\theta = 0$ if $\omega_0 > \sqrt{(1/\gamma)\,\cos\psi}$.
- For $\omega_0 < \sqrt{(1/\gamma)\,\cos\psi}$, a rigid hoop will leave the surface at position $\theta_* \in (3\pi/2,\, 2\pi)$, provided that ω_0 is greater than a value to be determined numerically.

4.3 Analysis of a simplified model and special cases

It is possible to obtain additional analytical results in certain simplified or special situations. A significant simplification occurs if the load is considered as a particle; in other words, if $\epsilon = 0$. The numerical results show that small values of ϵ have a negligible influence on the behaviour of the hoop, except for very extreme cases where the mass of the hoop tends to zero. Therefore ϵ will be taken as zero to obtain the analytical results in the following sections; this will be termed the *simplified model*.

The important implication is that the moment of inertia factors in (4.1) now simplify to

$$\kappa_G = 1 - \gamma^2 \; ; \quad \kappa_C = 2\mathcal{H} = 2(1 + \gamma \cos\theta). \tag{4.20}$$

Eight situations are considered. Firstly, the initial position ($\theta = 0$) is considered and a critical value of the friction coefficient is derived. Next, rolling motion on a horizontal plane ($\psi = 0$) is considered, and the extreme points on the graph of $\mathcal{N}$ as a function of θ are identified. The $\mathcal{F}/\mathcal{N}$-ratio receives some special attention. The specific situations of small displacements and rolling through the lowest position, still on a horizontal plane, are considered next; the large velocities and accelerations in the region of $\theta = \pi$ are analysed. Next, the completely smooth case ($\mu = 0$) is considered, and finally the special case of a concentric hoop ($\gamma = 0$) is analysed. The other extreme of the massless hoop ($\gamma = 1$) was analysed in the previous chapter, and the limiting case as $\gamma \to 1$ is dealt with separately.

4.3.1 Initial position

It is of some interest to analyse the reactions and accelerations in the initial position. Using $\theta = 0$ in (4.20), $\kappa_C(0) = 2(1 + \gamma)$.

It was shown in section 4.2.5 that there exists an upper bound on the initial velocity for initial contact to be maintained, namely that

$$\mathcal{N}(0) = \gamma(\hat{\omega}_0^2 - \omega_0^2)$$

is positive only if $\omega_0 < \hat{\omega}_0$. Note that this is also applicable for $\epsilon \neq 0$.

Similarly, using $\theta = 0$ in (4.11), the initial angular acceleration is

$$\theta''(0) = (1/\kappa_C)\,(1 + \gamma)\,\sin\psi = (1 + \gamma)\,\sin\psi/(2 + 2\gamma + \epsilon).$$

For the simplified model this becomes

$$\theta''(0) = \tfrac{1}{2}\,\sin\psi.$$

The initial acceleration is therefore zero on a horizontal surface, and positive on a slope, as expected.

Using (4.5) with $\theta = 0$ and (4.10) on the assumption of initial rolling, the initial friction force is given by $\mathcal{F}(0) = (1 + \gamma)\,\theta''(0) - \sin\psi$, or

$$\mathcal{F}(0) = -\tfrac{1}{2}(1 - \gamma)\,\sin\psi.$$

This clearly shows that the initial friction force is negative if the hoop is rolling down a slope, and that it is zero for rolling on a horizontal plane. This will be confirmed in the graphs showing numerical results in later sections.

If $\omega_0 < \hat{\omega}_0$ the hoop can start rolling in the initial position provided that $\mu_s \geq |\mathcal{F}(0)| / \mathcal{N}(0)$, or, using the above expressions,

$$\mu_s \geq \hat{\mu} = \frac{(1-\gamma)\,\sin\psi}{2\gamma\,(\hat{\omega}_0^2 - \omega_0^2)}. \tag{4.21}$$

Here $\hat{\mu}$ denotes the *critical friction coefficient*. In the special cases of $\gamma = 1$ or $\psi = 0$ this value is zero. Note that (4.21) is valid only for the simplified model with $\epsilon = 0$.

To summarise: the hoop will start rolling from the initial position if the following three conditions apply:

$$\mathcal{V}_x(0) = \omega_0; \quad \omega_0 < \hat{\omega}_0 = \sqrt{(1/\gamma)\cos\psi}; \quad \mu_s \geq \hat{\mu}. \tag{4.22}$$

The reactions and acceleration of the simplified model in the initial position are:

$$\mathcal{N}(0) = \gamma(\hat{\omega}_0^2 - \omega_0^2); \quad \mathcal{F}(0) = -\tfrac{1}{2}(1-\gamma)\,\sin\psi; \quad \theta''(0) = \tfrac{1}{2}\,\sin\psi. \tag{4.23}$$

For $\omega_0 < \hat{\omega}_0$ with $\gamma < 1$ and $\psi > 0$, (4.21) shows that increasingly large friction coefficients are required to ensure initial rolling as ω_0 increases, and that this value tends to infinity as $\omega_0 \to \hat{\omega}_0$ For finite values of μ_s therefore, a range of values $\omega_0 \leq \hat{\omega}_0$ exist for which the hoop will not roll initially, but will slip from the start if the surface is not horizontal.

On the other hand, for a horizontal plane with $\psi = 0$, $\hat{\mu} = 0$ for $\omega_0 < \hat{\omega}_0 = 1/\sqrt{\gamma} > 1$, and the hoop will roll in the initial phase for any $\mu_s > 0$, provided that $\mathcal{V}_x(0) = \omega_0$.

4.3.2 Reactions for rolling on a horizontal plane

In the special case of a horizontal plane the equations for rolling are readily analysed for the simplified model and yield a number of useful results. In this section the reaction forces are analysed, based on the assumption that the friction coefficient is large enough to prevent slipping.

During rolling, use of $\psi = 0$ in (4.12) results in $\omega^2 = \frac{2}{\mathcal{K}_C}\,(C_0 - \gamma\,\cos\theta)$; using (4.20) this becomes

$$\omega^2 = \frac{1}{\mathcal{H}}\,(C_0 - \gamma\,\cos\theta), \quad \text{and therefore} \quad \omega^2 + 1 = (C_0 + 1)/\mathcal{H}.$$

Note that in (4.12) the integration constant for this simplified model is

$$C_0 = (1+\gamma)\omega_0^2 + \gamma.$$

For $\psi = 0$, (4.11) simplifies to

$$\theta'' = \frac{\gamma\,\sin\theta}{\kappa_c}\,(\omega^2 + 1) = \gamma\,\sin\theta(C_0 + 1)/(2\mathcal{H}^2).$$

Using $\psi = 0$ and (4.10) in (4.5), the latter becomes $\mathcal{F} = (1 + \gamma\,\cos\theta)\,\theta'' - \gamma\,\omega^2\,\sin\theta$, or, substituting for θ'' in terms of ω^2,

$$\mathcal{F} = \mathcal{H}\,\gamma\,\sin\theta\,(\omega^2 + 1)/\kappa_c - \gamma\,\omega^2\,\sin\theta,$$

which simplifies to [2]

$$\mathcal{F} = \tfrac{1}{2}\gamma \sin\theta\,(1-\omega^2) = \tfrac{1}{2}\gamma \sin\theta\,(2\gamma\cos\theta + (1-C_0))\,/\mathcal{H}. \tag{4.24}$$

The first equation shows that the friction force for rolling on a horizontal surface will be positive as long as $\omega < 1$ and $0 < \theta < \pi$, and that it is initially zero as already found in the previous section. Also, $\mathcal{F}(\pi) = 0$ and the graph is skew-symmetric.

These characteristics are confirmed in the graphs shown in Figure 4.2, using a typical value of $\gamma = 2/3$ for the eccentricity and three initial velocities.

Further analysis requires the derivative of $\mathcal{F}$ w.r.t. θ, using the second expression in (4.24):

$$\omega^{-1}\mathcal{F}' = \tfrac{1}{2}\mathcal{H}^{-2}\left(2\gamma^3\cos^3\theta + 4\gamma^2\cos^2\theta + (1-C_0)\gamma\cos\theta - \gamma^2(1+C_0)\right). \tag{4.25}$$

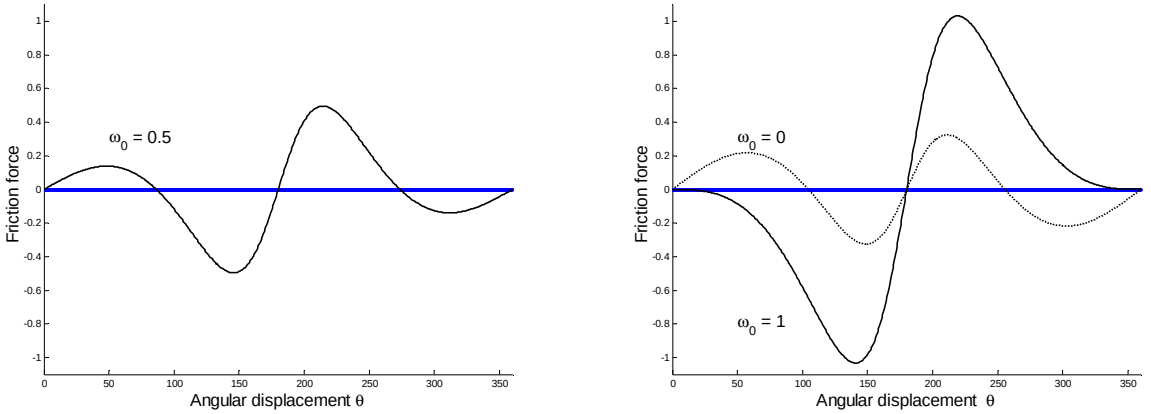

(a) : $\omega_0 = 0.5$ (b) : $\omega_0 = 0,\ 1$

Figure 4.2 : Graphs of $\mathcal{F}$ as functions of θ for $\gamma = 2/3$

For rolling on a horizontal plane, the expression for the normal reaction, (4.6), becomes

$$\mathcal{N} = 1 - \gamma\sin\theta\,\theta'' - \gamma\cos\theta\,\omega^2,$$

which, using the above expressions for ω^2 and θ'', can be plotted as shown in Figure 4.3.

[2] The first form of the equation is incorrect in the original paper [1], where the sign is reversed.

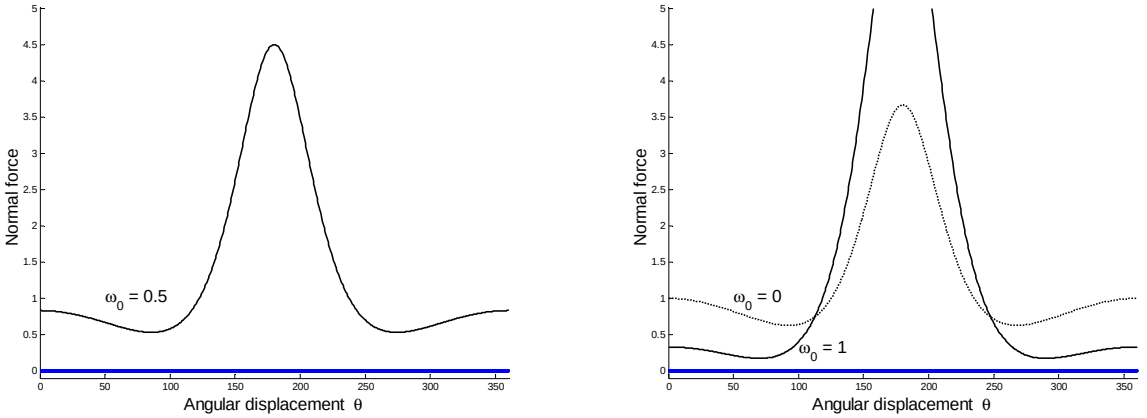

(a) : $\omega_0 = 0.5$ (b) : $\omega_0 = 0,\ 1$

Figure 4.3 : Graphs of $\mathcal{N}$ as functions of θ for $\gamma = 2/3$

These graphs are symmetrical with a large maximum at $\theta = 180°$, and show a relative minimum value for $\theta \in (0, 180°)$. [3]

For further analysis the expressions for ω^2 and θ'' are substituted and the equation for $\mathcal{N}$ becomes

$$\mathcal{N} = 1 - \frac{(\gamma \sin\theta)^2 (C_0 + 1)}{2\mathcal{H}^2} + \frac{\gamma \cos\theta (\gamma \cos\theta - C_0)}{\mathcal{H}}.$$

The third term can be written as $\gamma \cos\theta (\mathcal{H} - 1 - C_0)/\mathcal{H}$, and after some manipulation the expression simplifies to

$$\mathcal{N} = \mathcal{H} + \frac{(1-\gamma^2)(C_0+1)}{2\mathcal{H}^2} - \frac{1}{2}(C_0 + 1).$$

Defining the positive constant ξ as

$$\xi^3 = (1-\gamma^2)(C_0+1) = (1-\gamma)(1+\gamma)^2(1+\omega_0^2),$$

this becomes

$$\mathcal{N} = \mathcal{H} + \frac{\xi^3}{2\mathcal{H}^2} - \frac{1}{2}(C+1). \tag{4.26}$$

The first two derivatives of $\mathcal{N}$ (w.r.t. τ) can be written as

$$\mathcal{N}' = \omega\,\gamma \sin\theta\,(-1 + \xi^3\,\mathcal{H}^{-3}),$$

$$\mathcal{N}'' = \omega^2 (\gamma \sin\theta)^2\,\xi^3\,3\mathcal{H}^{-4} + \omega^2\,\gamma \cos\theta\,(-1 + \xi^3\,\mathcal{H}^{-3}) + \omega'\,\omega^{-1}\,\mathcal{N}',$$

for $\omega > 0$.

[3] For the remainder of this dissertation, angles are given in degrees rather than radians in all cases referring to actual examples and graphs; radians are used in analytic work.

The above expression for $\mathcal{N}'$ can be re-written as

$$\omega^{-1}\,\mathcal{N}' = \frac{\gamma\,\sin\theta}{\mathcal{H}^3}\,(\xi^3 - \mathcal{H}^3). \tag{4.27}$$

Noting that $\mathcal{H} = 1 + \gamma\cos\theta > 0$ for $\gamma < 1$, (4.27) shows that there are three possible extrema for $\mathcal{N}$:

i) In position $\theta = 0$, $\mathcal{N}'(0) = 0$ and $\mathcal{N}''(0) = 0 + \omega_0^2\,\gamma\,(-1 + \xi^3\,\mathcal{H}^{-3}) + 0$, which simplifies to

$$\mathcal{N}''(0) = -\omega_0^2\,\gamma\,(2\gamma - \omega_0^2(1-\gamma))/(1+\gamma).$$

For values of $\omega_0^2 < 2\gamma/(1-\gamma)$, this is therefore a relative maximum position with value $\mathcal{N}(0) = (1+\gamma) + \frac{1}{2}\xi^3/(1+\gamma)^2 - \frac{1}{2}(C_0+1) = (1+\gamma) + \gamma\,(C_0+1)/(1+\gamma)$, or

$$\mathcal{N}(0) = 1 - \gamma\,\omega_0^2,$$

which agrees with the value found at the beginning of the previous section.

ii) $\mathcal{N}' = 0$ in position $\theta_m = \arccos((\xi-1)/\gamma)$, found from $\mathcal{H} = \xi$ i.e. $(1 + \gamma\,\cos\theta_m) = \xi$. Then $\mathcal{N}''(\theta_m) = 3\,\xi^{-1}\,(\omega\,\gamma\,\sin\theta_m)^2$, which is clearly positive, indicating that this is a minimum point. The angle at this point, and the corresponding value of the normal reaction, are

$$\theta_m = \cos^{-1}((\xi-1)/\gamma); \qquad \mathcal{N}_m = \mathcal{N}(\theta_m) = \tfrac{1}{2}\,(3\,\xi - C_0 - 1). \tag{4.28}$$

For small enough values of γ and ω_0 the first local minimum at θ_m exists.

iii) In position $\theta = \pi$, $\mathcal{N}'(0) = 0$, $\mathcal{H} = 1 - \gamma$ and $\mathcal{N}''(0) = -\omega^2\,\gamma\,(-1 + \xi^3\,\mathcal{H}^{-3})$ or $\mathcal{N}''(0) = -\omega^2\,\gamma\,(1+\gamma)(C_0+\gamma)/(1-\gamma)^2$. This is clearly a maximum point for all situations, with value from (4.26)

$$\mathcal{N}(\pi) = (C_0+1)\gamma/(1-\gamma) + 1 - \gamma = 1 + \gamma\,(C_0+\gamma)/(1-\gamma).$$

Clearly, this value tends to infinity as γ tends to 1. In Figure 4.3, with $\gamma = 2/3$, this maximum value is $\mathcal{N}(\pi) = 1 + \frac{2}{3}(5\,\omega_0^2 + 4)$. For $\omega_0 = 0$, 0.5 and 1 this maximum value is therefore 11/3, 9/2 and 7 respectively.

4.3.3 The first minimum of $\mathcal{N}$

It is of some interest to analyse the values of the reactions at θ_m as found in (4.28). As found above,

$$\mathcal{N}_m = \tfrac{1}{2}(3\,\xi - C_0 - 1) \quad \text{and} \quad \mathcal{N}'(\theta_m) = 0.$$

Similarly, using (4.24),

$$\mathcal{F}_m = \mathcal{F}(\theta_m) = \tfrac{1}{2}\gamma\,\sin\theta_m\,(2\xi - C_0 - 1)/\xi.$$

It is found that this value is negative in the examples shown later in Figure 4.6. Noting that the constants were defined as

$$C_0 = (1+\gamma)\omega_0^2 + \gamma \quad \text{and} \quad \xi^3 = (1-\gamma^2)(C_0+1) = (1-\gamma)\,(1+\gamma)^2\,(1+\omega_0^2),$$

these expressions are functions of γ and ω_0, and further analysis of the $(\gamma,\,\omega_0)$-parameter space is of some interest for the numerical results obtained later.

Figure 4.4 shows a number of interesting curves and contours on the $(\gamma,\,\omega_0)$-parameter plane.

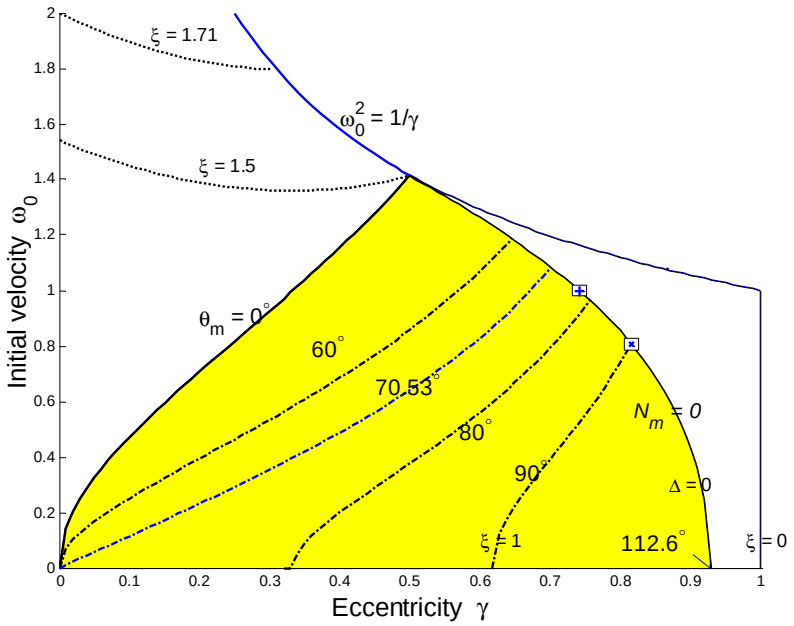

Figure 4.4 The (γ, ω_0)-parameter plane, showing the region where $\mathcal{N}$ reaches a positive minimum while rolling, and the corresponding contours of θ_m

The upper limit for ω_0 is defined by (2.30), in this case by $\omega_0 = 1/\sqrt{\gamma}$.

The shaded region in Figure 4.4 shows the parameter values for which positive values of the first minimum of $\mathcal{N}$ exists. This region is bounded by the contour for $\theta_m = 0$ and the curve where $\mathcal{N}_m = 0$.

For initial velocities above the $\theta_m = 0$-contour, the minimum in the $\mathcal{N}$-function does not exist. For eccentricities greater than those on the $\mathcal{N}_m = 0$-curve, it is impossible to roll in the position $\theta = \theta_m$. It will be shown later that rolling in this position requires infinite friction.

Three sets of contours are shown:

- Contours for constant θ_m are obtained by re-writing the first equation in (4.28) as

$$\gamma \cos\theta_m = \xi - 1, \quad \text{or} \quad \omega_0^2 = -1 + (1 + \gamma\cos\theta_m)^3/((1-\gamma)(1+\gamma)^2). \tag{4.29}$$

  The origin at (0, 0) satisfies this equation for all values θ_m; i.e. one of the branches of every contour goes through the origin.

  For $\theta_m = 0$ the equation for the contour simplifies to $\omega_0^2 = 2\gamma/(1-\gamma)$; the endpoints of this curve are (0, 0) and $(0.5, \sqrt{2})$ as shown in Figure 4.4.

  Using the first equation in (4.29), the contour $\theta_m = 90°$ corresponds with the curve where $\xi = 1$, given by

$$\omega_0^2 = \gamma(\gamma^2 + \gamma - 1)/((1-\gamma)(1+\gamma)^2).$$

  The positive branch starts at the point $(0.618, 0)$, with the incidental curiosity that the positive root of $\gamma^2 + \gamma - 1$ is $(\sqrt{5}-1)/2 = 0.618$ is the "golden ratio" of ancient Greek architecture!

Similar expressions can be derived for other contours of θ_m, such as $\theta_m = 60^\circ$ and 80°, as shown in Figure 4.4.

The case when $\cos\theta_m = 1/3$, i.e. when $\theta_m = 70.53^\circ$, has a number of interesting characteristics. For $\theta_m \leq 70.53^\circ$ the positive branch of the contour starts at the origin; for θ_m greater than this value the positive branch starts with a positive eccentricity. This can be shown by setting the derivative of (4.29) w.r.t. γ equal to zero to obtain the equation

$$3\cos\theta_m\left(1+\gamma^2+2\gamma^3+\gamma\cos\theta_m(\text{terms containing } \gamma \text{ and } \cos\theta_m)\right) = 1-2\gamma-\gamma^2-2\gamma^3.$$

For $\cos\theta_m = 1/3$, a root is clearly $\gamma = 0$, [4] implying that the origin is an extreme point on the contour. This case therefore separates the situations where the negative minimum value is to the left or right of the origin.

- The curve where $\mathcal{N}_m = 0$ is obtained from (4.28), and is given by $3\,\xi = C_0 + 1$, or

$$(\omega_0^2+1)^2 = 27(1-\gamma)/(1+\gamma).$$

As shown in Figure 4.4, this curve starts at (13/14, 0), at which point $\xi = 9/14$ and the angle is $\theta_m = \cos^{-1}(-5/13) = 112.6^\circ$. This curve ends at the point $(0.5, \sqrt{2})$, at which point it has also been shown that $\theta_m = 0$.

Two more points are marked on this curve in Figure 4.4. For $\omega_0 = 1$ the +-symbol at (23/31, 1) results in values of $\xi = 36/31$ and $\theta_m = \cos^{-1}(5/23) = 77.4^\circ$. The cross at point $(\sqrt{(2/3)}, 0.807)$ marks the parameters where $\mathcal{N}_m$ becomes zero at position $\theta_m = 90^\circ$. These points are referred to again in a later section.

The positive values of $\mathcal{N}_m$ are not of any interest and therefore no more contours of $\mathcal{N}_m$ are shown.

- Contours for constant ξ are obtained by re-writing the definition in (4.26), namely $\xi^3 = (1-\gamma)(1+\gamma)^2(1+\omega_0^2)$, as

$$\omega_0^2 = -1 + \xi^3/\left((1-\gamma)\,(1+\gamma)^2\right).$$

It also follows from (4.26) that $\xi = 0$ when $\gamma = 1$, as shown in Figure 4.4.

The dotted curve starting at point (0, 2) in Figure 4.4 is the contour for $\xi = 5^{1/3} = 1.71$. Also shown in Figure 4.4 is the contour for $\xi = 1.5$, between points $(0, \sqrt{19/8})$ and $(0.5, \sqrt{2})$.

Clearly Figure 4.4 does not apply if the hoop starts slipping before θ_m is reached.

4.3.4 The rolling curve

The graph of the $\mathcal{F}/\mathcal{N}$-ratio as a function of θ is fundamental in the analysis of the different patterns of motion found later. For cases where the hoop rolls without slipping through a full 360°, this graph is called the *rolling curve*.

In this section the rolling curve is analysed for the simplified model and horizontal plane and a friction coefficient that is large enough to ensure rolling.

[4] Using Mathematica, it can be shown that this is the only real, non-negative root.

Using (4.24) and (4.26), the $\mathcal{F}/\mathcal{N}$-ratio can be written as

$$\mathcal{F}/\mathcal{N} = \gamma \sin\theta \frac{\mathcal{H}\,(2\gamma\,\cos\theta + 1 - C_0)}{(2\mathcal{H}^3 - (1+C_0)\mathcal{H}^2 + \xi^3)}. \tag{4.30}$$

In Figure 4.5 a few examples of rolling curves are shown for typical values of the parameters.

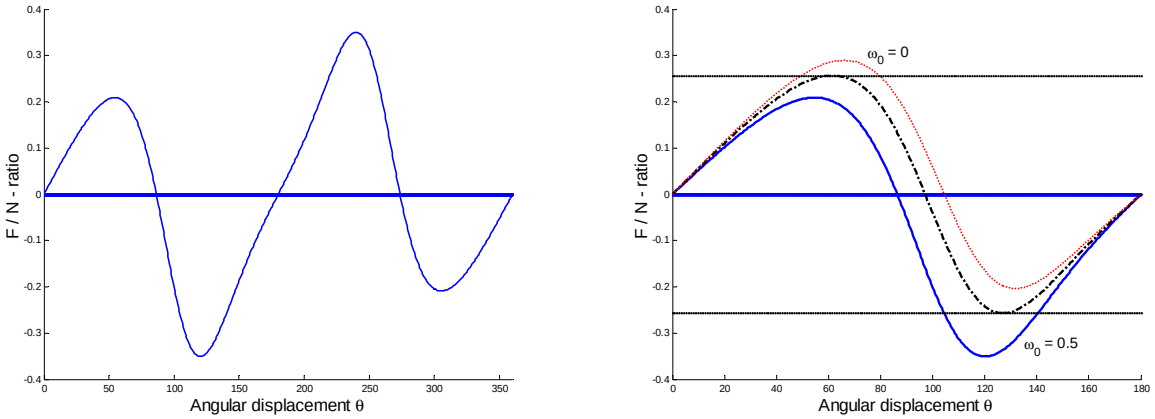

(a) : $\omega_0 = 0.5$ (b) : $\omega_0 = 0.5,\ 0.317,\ 0$

Figure 4.5 : Rolling curves for $\gamma = 2/3$

The properties of these curves are discussed in numerical terms in the next chapter, section 5.3.1. In the remainder of this section some additional analysis is performed.

Figure 4.5(a) shows two maximum points and two minima. These extrema are found where $\mathcal{N}\,\mathcal{F}' - \mathcal{N}'\,\mathcal{F} = 0$. Using (4.25) and (4.26),

$$\left(2\mathcal{H}^4\,\omega^{-1}\right)\mathcal{N}\mathcal{F}' = \tfrac{1}{2}\left(2\mathcal{H}^3 - (C_0+1)\mathcal{H}^2 + \xi^3\right)\left(2\gamma^3\cos^3\theta + 4\gamma^2\cos^2\theta - c_1\cos\theta - \gamma^2(1+C_0)\right).$$

Noting that $\mathcal{H}^3 = (\gamma\cos\theta)^3 + 3(\gamma\cos\theta)^2 + 3\gamma\cos\theta + 1$, this becomes

$(2\mathcal{H}^4\,\omega^{-1})\,\mathcal{N}\mathcal{F}' = 2(\gamma\cos\theta)^6$ + terms of degree five in θ and less.

Similarly, using (4.27) and (4.24), the second term simplifies to

$$\left(2\mathcal{H}^4\,\omega^{-1}\right)\mathcal{N}'\mathcal{F} = \gamma^2\left(1-\cos^2\theta\right)\left(\xi^3 - \mathcal{H}^3\right)\,(2\gamma\,\cos\theta + 1 - C_0)\,,$$

or $(2\mathcal{H}^4\,\omega^{-1})\,\mathcal{N}'\mathcal{F} = 2(\gamma\cos\theta)^6$ + terms of degree five in θ and less.

It is convenient to define $\Delta = (2\mathcal{H}^4\,\omega^{-1})\,(\mathcal{N}\,\mathcal{F}' - \mathcal{N}'\,\mathcal{F})$. As shown above, this is a fifth degree polynomial in $\cos\theta$ and the positions of the extrema are found from the zeros of Δ.

Further analysis of the above relationships does not seem warranted, and the later use of the $\mathcal{F}/\mathcal{N}$-ratio is all based on numerical calculations. However, the $\mathcal{F}/\mathcal{N}$-ratio at the point where the first minimum in $\mathcal{N}$ is zero is of some interest. This was shown as the curve demarcating the right hand side of the shaded region in Figure 4.4. For parameters on this curve, $\mathcal{N} = 0$

and $\mathcal{N}' = 0$, which implies that $\Delta(\theta_m) = 0$. Therefore an extremum of the $\mathcal{F}/\mathcal{N}$-ratio occurs at this point and $\to \infty$. Four examples of this situation are shown in Figure 4.6, namely where $\theta_m = 0°,\ 77.4°,\ 90°,\ 112.6°$ respectively. In cases (b) to (d) the vertical dotted lines mark the values of θ_m.

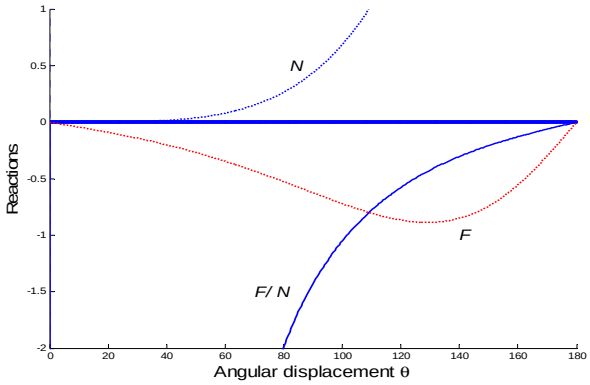

(a) : $\theta_m = 0°$, $\gamma = 0.5$ and $\omega_0 = \sqrt{2/3}$

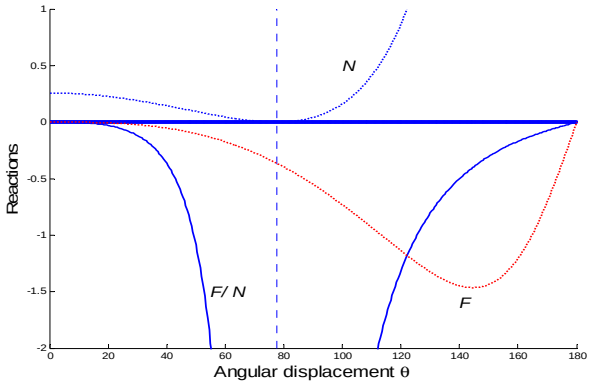

(b) : $\theta_m = 77.4°$, $\gamma = 23/31$ and $\omega_0 = 1$

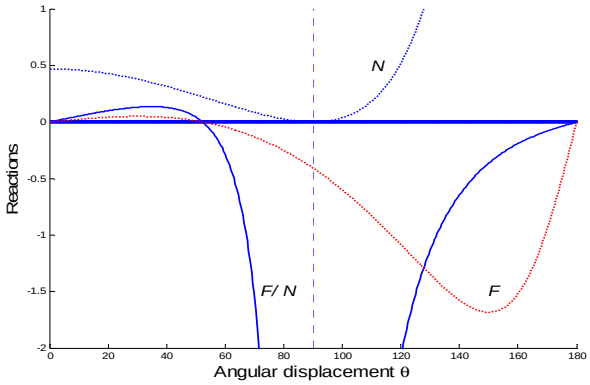

(c) : $\theta_m = 90°$, $\gamma = \sqrt{2/3}$, and $\omega_0 = 0.807$

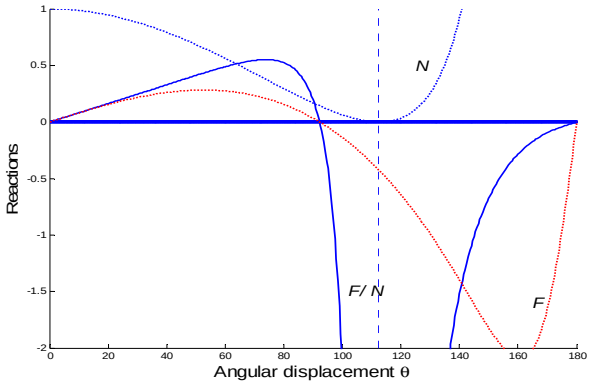

(d) : $\theta_m = 112.6°$, $\gamma = 13/14$, and $\omega_0 = 0$

Figure 4.6 : Reactions as a function of θ for cases where $\mathcal{N}_m = 0$, showing $\mathcal{N}$ as a solid curve, $\mathcal{F}$ as a dotted curve and $\mathcal{F}/\mathcal{N}$ as the dash-dot curve

These graphs confirm that the minimum of $\mathcal{N}$ is indeed zero at the positions θ_m as found analytically. Figure 4.6 (b) to (d) also show that $\mathcal{F}(\theta_m) < 0$, which was not evident from the earlier analysis in section (4.3.3). The first minimum of the rolling curve therefore tends to negative infinity in these cases. Case (a), where $\theta_m = 0$, is a special case with $\mathcal{F}(\theta_m) = 0$ and $\mathcal{N}(\theta_m) = 0$ and the ratio is undetermined.

It should be realised that the curves shown in Figure 4.6 are of an extreme situation, and that a normal hoop will start slipping before θ_m is reached. It will be shown later in section 6.1 that infinitely large friction is required to reach the curve $\mathcal{N}_m = 0$.

4.3.5 Analysis for small displacements on horizontal plane

It is instructive for later interpretation of the results to analyse the motion during the early stages, for small values of θ, for a horizontal plane and the simplified model. The approximations

$$\sin\theta \approx \theta; \quad \cos\theta \approx 1,$$

are used. Assuming the initial condition for rolling, namely $\mathcal{V}_x = \omega_0$,

$$C = C_0 = (1+\gamma)\,\omega_0^2 + \gamma.$$

Then $\mathcal{H} = 1+\gamma$ and $\kappa_C = 2(1+\gamma)$ in (4.1), and the angular acceleration from (4.11) is

$$\theta'' \approx \tfrac{1}{2}\,\gamma\,\theta\,(1+\omega^2)/(1+\gamma).$$

Clearly, the angular acceleration is zero initially, and increases as θ increases; therefore the angular velocity will also increase, starting from the initial value of ω_0.

Using (4.5), the friction force is $\mathcal{F} \approx (1+\gamma)\,\theta'' - \gamma\,\omega^2\,\theta$, which simplifies to

$$\mathcal{F} \approx \tfrac{1}{2}\gamma\,\theta\,(1-\omega^2).$$

Therefore the friction force (on a horizontal plane) is initially zero, and is positive as long as $\omega < 1$, as found previously in (4.24).

4.3.6 Rolling through $\theta = \pi$ on horizontal plane

In all cases where the hoop rolls through position $\theta = \pi$ on a horizontal plane, the solutions found in 4.3.2 may be used after substituting the integration constant C for C_0.

When $\theta = \pi$, $\mathcal{N}(\pi) = 1+\gamma\omega^2$, from (4.6), and as shown in 4.3.2 this is a maximum value. Also, from (4.24), the friction force is zero at this point.

An additional point of interest is the very large angular velocity that occurs at this point. In position $\theta = \pi$, $\mathcal{H}$ becomes $\mathcal{H}(\pi) = 1-\gamma$, and the solution for rolling becomes

$$\omega^2(\pi) = \frac{C+\gamma}{1-\gamma}.$$

Equation (4.11) simplifies to $\theta''(\pi) = 0$; therefore this is a position of maximum angular velocity.

Similarly, the non-dimensional acceleration of the centre of gravity, can be found by using (4.4) and (4.10) and simplifying:

$$(x/r)''(\pi) = 0; \qquad (y/r)''(\pi) = \gamma\,\omega^2(\pi) = a(\pi); \qquad a(\pi)/g = \gamma\,\omega^2(\pi).$$

The graphs drawn for the numerical results in later sections clearly show that this is also a maximum value. [5]

To summarise, $\alpha(\pi) = 0$, $\mathcal{F}(\pi) = 0$ and

$$\omega^2(\pi) = \frac{C+\gamma}{1-\gamma}; \quad a(\pi)/g = \gamma\,\omega^2(\pi); \quad \mathcal{N}(\pi) = 1 + a(\pi)/g. \tag{4.31}$$

[5] This can be confirmed analytically with rather laborious manipulations not included here.

In cases where the hoop does not slip before reaching his position, the integration constant as defined in section 4.2.2 is

$$C = C_0 = (1+\gamma)\,\omega_0^2 + \gamma,$$

and the expressions simplify to

$$\omega^2(\pi) = \omega_0^2 + \frac{2\gamma(1+\omega_0^2)}{1-\gamma}; \quad a(\pi)/g = \gamma\,\omega^2(\pi); \quad \mathcal{N}(\pi) = 1 + a(\pi)/g. \tag{4.32}$$

4.3.7 Zero Friction

As shown in section 4.3.1, the hoop will start rolling if $\mu_s > 0$. If however $\mu_s = 0$, the hoop will start slipping immediately at $\theta = 0$, and will continue doing so for the full 360° without any loss of energy because $\mathcal{F} = 0$.

It is of some interest to analyse the effect of the friction coefficient tending to zero. Then the change from rolling to slipping will take place at an angle tending to zero, and

$$\mathcal{F} = \tfrac{1}{2}\gamma\theta(1-\omega^2),$$

as shown in section 4.3.5 for small displacements on a horizontal plane. This implies that rolling changes to spinning if $\omega_0 \in (0,1)$, and that rolling changes to skidding if $\omega_0 \in (1,\hat{\omega}_0)$.

4.3.8 Concentric hoop

It is instructive to also analyse the well-known problem of an unloaded hoop, with $m_p = 0$ and therefore $\gamma = 0$, $\kappa_G = 1$ and $(x,\, y) = (X,\, Y)$. The dynamic equations (4.5) to (4.7) now become

$$\mathcal{F} = \mathcal{X}'' - \sin\psi; \quad \mathcal{N} = \cos\psi; \quad -(\mathcal{F}) = \theta''. \tag{4.33}$$

Three cases will be considered, namely initial conditions such that the hoop rolls; initial conditions such that the hoop spins initially; initial conditions such that the hoop skids initially.

Case 1: Rolling Assume that $\dot{X}(0) = r\dot{\theta}(0)$, i.e. $\mathcal{V}_x(0) = \omega_0$, so that the hoop starts rolling. Then $\mathcal{X}'' = \theta'' = \frac{1}{2}\sin\psi$, i.e. constant acceleration and $\mathcal{F} = -\frac{1}{2}\sin\psi$, provided that $\mu_s \geq \tan\psi$. If the rolling occurs on a horizontal plane, all three values are zero and the hoop continues rolling with constant speed and zero friction.

Case 2: Spinning Assume that $\dot{X}(0) = 0$ and $\dot{\theta}(0) > 0$, i.e. $\mathcal{V}_x(0) = 0$ and $\omega_0 > 0$, so that the hoop starts spinning with $\mathcal{F} = \mu_k\ \mathcal{N}$. Then $\mathcal{X}'' = \sin\psi + \mu_k\ \cos\psi$ and $\theta'' = -\mu_k\ \cos\psi$. The spinning will change to rolling when $\dot{X} = r\dot{\theta}$ or $\mathcal{V}_x = \omega$, say at time t_1 such that $(\sin\psi + \mu_k\ \cos\psi)\ t_1 = \omega_0 - \mu_k\ \cos\psi\ t_1$, or $t_1 = \omega_0/(\sin\psi + 2\mu_k\ \cos\psi)$.

At this moment the hoop starts rolling again, and the angular acceleration changes instantaneously from $\theta'' = -\mu_k\ \cos\psi$ to $\theta'' = \frac{1}{2}\sin\psi$, using the above expressions for rolling. A discontinuity of $\Delta\theta'' = \frac{1}{2}\sin\psi + \mu_k\ \cos\psi$ therefore occurs, with similar discontinuities in the acceleration, $\Delta\mathcal{X}'' = -(\frac{1}{2}\sin\psi + \mu_k\ \cos\psi)$ and friction force $\Delta(\mathcal{F}) = -(\frac{1}{2}\sin\psi + \mu_k\ \cos\psi)$.

For motion on the horizontal plane, $t_1 = \omega_0/2\mu_k$ and the magnitude of the discontinuities equal μ_k. Now the angular velocity when the change occurs is $\omega_1 = \frac{1}{2}\omega_0$, and the position where this happens is $\theta_1 = \frac{3}{8}{\omega_0}^2/\mu_k$.

Case 3: Skidding Assume that $\dot{X}(0) > 0$ and $\dot{\theta}(0) = 0$, i.e. $\mathcal{V}_{x0} = \mathcal{V}_x(0) > 0$ and $\omega_0 = 0$, so that the hoop starts skidding with $\mathcal{F} = -\mu_k\, \mathcal{N}$. Then $\mathcal{X}'' = \sin\psi - \mu_k\, \cos\psi$ and $\theta'' = \mu_k\, \cos\psi$. The skidding will change to rolling when $\dot{X} = r\dot{\theta}$ or $\mathcal{X}' = \theta'$, say at time t_1 such that $\mathcal{V}_{x0} + (\sin\psi - \mu_k\, \cos\psi)\, t_1 = \mu_k\, \cos\psi\, t_1$, or $t_1 = \mathcal{V}_{x0}/(2\mu_k\, \cos\psi - \sin\psi)$, provided that $\tan\psi < 2\mu_k$. If this last condition does not apply, the hoop will continue skidding and cannot start rolling again.

At the moment when the hoop starts rolling again, the angular acceleration changes instantaneously from $\theta'' = \mu_k\, \cos\psi$ to $\theta'' = \frac{1}{2}\sin\psi$, using the above expressions for rolling. A discontinuity of $\Delta\theta'' = -(\mu_k \cos\psi - \frac{1}{2}\sin\psi)$ therefore occurs, with similar discontinuities in the acceleration, $\Delta\mathcal{X}'' = \mu_k \cos\psi - \frac{1}{2}\sin\psi$ and friction force $\Delta(\mathcal{F}) = \mu_k \cos\psi - \frac{1}{2}\sin\psi$. Comparison with the expressions for spinning show that the discontinuity is smaller in the case of skidding.

For motion on the horizontal plane, $t_1 = \mathcal{V}_{x0}/2\mu_k$ and the magnitude of the discontinuities equal μ_k, the same as for spinning. Now the velocity when the change occurs is $\mathcal{V}_{x1} = \frac{1}{2}\mathcal{V}_{x0}$, and the position where this happens is $\theta_1 = \frac{1}{8}\mathcal{V}_{x0}^2/\mu_k$.

Note that in all cases (spinning and skidding) the discontinuity is *"inwards"*; i.e. towards the zero.

In the case of the loaded hoops with $\gamma > 0$, the numerical solutions given in later sections show similar discontinuities when the motion changes from spinning or skidding to rolling.

4.4 Solution algorithm

The mathematical model derived in this chapter can be summarised in the form of the algorithm given below. The computer programs that were used to obtain the numerical results are based on this algorithm.

Control over the program is maintained by using so-called condition codes, abbreviated as CC's, for the different modes of motion and the different final conditions, as follows:

CC = 'R' implies rolling;	'S' for spinning;	'D' for skidding;
CC = 'T' implies $\theta_F = 2\pi$;	'Z' for $\omega_F = 0$;	'H' for $\mathcal{N}_F = 0$.

Algorithm 4.1 : Solution algorithm for a rigid hoop

- Input or assign all parameter values: γ, μ_s, μ_k, ψ, ϵ;
  Calculate constants from (4.1): $\kappa_G = 1 + \epsilon - \gamma^2$
  and (4.22): $\hat{\omega}_0 = \sqrt{(1/\gamma)\,\cos\psi}$.

- Input or assign the initial values for the rolling phase:
  $\theta(0) = 0; \quad \theta'(0) = \omega_0; \quad \mathcal{X}(0) = 0; \quad \mathcal{V}_x(0) = \omega_0.$
  .
  Calculate the integration constant $C = (1 + \epsilon/2 + \gamma)\,\omega_0^2 + \gamma\,\cos\psi$.
  Calculate critical μ from (4.21): $\hat{\mu} = (1-\gamma)/(2\gamma).\sin\psi/(\hat{\omega}_0^2 - \omega_0^2)$.

  IF $\omega_0 > \hat{\omega}_0$: Immediate hopping; STOP.
  IF $\mu_s < \hat{\mu}$: Immediate slipping; STOP.

- REPEAT
  - IF CC == 'R'
    Solve the equations for rolling.
    Rolling stops when $\|\mathcal{F}\| = \mu_s\mathcal{N}$: $\theta = \theta_s$; CC = 'S' or 'D';
    or when $\theta = \theta_F$; CC = 'T' or 'Z' or 'H'.
  - IF CC == 'S' or 'D'
    Solve the equations for slipping.
    Slipping stops when $\mathcal{V}_x = \omega$: $\theta = \theta_r$; CC = 'R';
    or when $\theta = \theta_F$; CC = 'T' or 'Z' or 'H'.

  UNTIL CC = 'T' or 'Z' or 'H'.

The system of second order differential equations for slipping can be solved numerically in the standard manner by writing them as a system of first order equations. The vector of unknown variables includes the horizontal displacement X, and is defined as

$$Z = [\theta,\, \omega,\, \mathcal{X},\, \mathcal{V}_x].$$

The first derivative is given by

$$Z' = [\omega,\, \theta'',\, \mathcal{V}_x,\, \mathcal{X}''],$$

with θ'' and $\mathcal{X}''$ being calculated from (4.14) and (4.15) respectively.

The ODE45 solver in MATLAB [19] was used. This is a fourth order Runge-Kutta algorithm with automatic adaptation of step size. It also has a facility for finding the zero's of a specified function; this is called an "event". This facility is used in determining the point where slipping stops by defining the event as the function $f = (\omega - \mathcal{V}_x)\,\omega\,\mathcal{N}$ in the case of spinning and $f = (\mathcal{V}_x - \omega)\,\omega\,\mathcal{N}$ in the case of skidding. With these definitions the zero point is always approached from the positive side. If this zero is not found before a full rotation is reached, the analysis stops when $\theta = 2\pi$.

Chapter 5

Classification of behavioural patterns of rigid hoops

The main theme of this chapter is the classification of the different behavioural patterns that are obtained for the motion of rigid hoops. These patterns are obtained from the solutions of the equations derived in the previous chapter. In the case of rolling motion the solutions have been obtained analytically; in cases of slipping the solutions are obtained by numerical integration.

The first section contains some general features of the numerical solutions, as well as some new notation.

This is followed by a typical example for which detailed results are given.

In section 5.3 a classification scheme to differentiate between the different behavioural patterns is introduced. Seven types of motion are identified.

Two types of phase diagram are used in section 5.4 to show the regions in a particular parameter space for the different types of motion.

Detailed results are shown in section 5.5 for one example of each of the seven types of motion.

Finally, the "faster than gravity" phenomenon is discussed in section 5.6.

Some of the computer code used to obtain the numerical results is included as Appendix E.

5.1 General features of the numerical results

Simplifying assumptions

The motion of a loaded hoop generally consists of a sequence of rolling and slipping phases. A surprisingly large number of different sequences of these phases is possible, and in order to simplify the subsequent analysis to some extent, four assumptions are made for all examples in this chapter:

a) Initial conditions are such that *initial rolling* occurs; see (4.22).

b) The difference between static and kinetic friction is ignored; i.e. $\mu_k = \mu_s = \mu$.

c) A horizontal plane is used, i.e. $\psi = 0$.

d) A point particle is used; i.e. $\epsilon = 0$.

The effect of these assumptions is investigated in Chapter 6.

Parameters for the numerical results

Using assumptions a, b and d above, the dynamic equations for the rigid hoop simplify to a four-parameter model in which the behaviour depends on the values of the slope ψ, the eccentricity γ, the friction coefficient μ and the initial velocity as defined by ω_0.

It is convenient to define the set of system parameters for this four-parameter problem as

$$\mathcal{P} = \{\psi,\ \gamma,\ \mu,\ \omega_0\}.$$

In the case of a horizontal plane, the three-parameter problem is defined by

$$\mathcal{P}_0 = \{\gamma,\ \mu,\ \omega_0\}.$$

In the remainder of this chapter the influence of these three parameters on various aspects of the behaviour of the hoop is investigated.

Phase labels

The complete motion for any specific example can be summarised conveniently by labelling each of the phases. These labels are the same as the condition codes used in the algorithm in section 4.4. Any motion of the hoop is a sequence of rolling, spinning and skidding phases, which are labelled as:

`R` : Roll, while $|F_f| \leq \mu F_n$, i.e. $|\mathcal{F}| \leq \mu\mathcal{N}$; [1]
`S` : Spin, while $F_f = +\mu F_n$, i.e. $\mathcal{F} = +\mu\mathcal{N}$;
`D` : skiD, while $F_f = -\mu F_n$, i.e. $\mathcal{F} = -\mu\mathcal{N}$.

As shown in section 4.2.1, the analysis ends when the hoop reaches its final condition at position θ_F. This final condition is labelled as:

`Z` : Zero angular velocity, when $\omega_F = \omega(\theta_F) = 0$;
`T` : Top, when $\theta_F = 360^\circ$;
`H` : Hop, when $F_{nF} = F_n(\theta_F) = 0$, i.e. $\mathcal{N}_F = 0$.

[1] Clearly, either notation may be used. In all cases where reference is made to the numerical results and graphs, the non-dimensional notation will be used.

Later results show that a complete description of any particular motion is given by specifying nine phases plus the final condition, i.e. by ten labels. When all nine phases are present, these are `RSRDRSRDR`; when any particular phase is missing, this is indicated by a hyphen; for example, `RSR----DR` implies that the first skidding, second spinning and the associated rolling phases are missing. However, missing phases in the beginning are ignored; i.e. `RD*` indicates that the first spinning phase is missed and that the initial rolling phase changes to skidding. The * is used as a "wild card" to indicate any sequence of phases.

To complete the full pattern of a motion the final phase is added, separated from the rest by a space. Once again a * indicates any of the three final conditions. For example, the case used in the next section to illustrate a typical behavioural pattern is labelled `RDRSR-- T`, indicating that the initial rolling changes to skidding, back to rolling, then to spinning and ending with rolling over the top.

Presentation of results

Results are presented at two levels.

Firstly, detailed results for a number of cases are shown as functions of position (θ), as in Figure 5.2 shown in the next section. These graphs may be used as follows:

- The different rolling, spinning and skidding phases are seen clearly on the graph of the $\mathcal{F}/\mathcal{N}$-ratio. Because of the definitions, $\mathcal{F}/\mathcal{N} = \mu$ indicates a region of spinning, $\mathcal{F}/\mathcal{N} = -\mu$ indicates skidding, and the values in between indicate rolling.
- A zero value on the graph of $\mathcal{N}$ shows where hopping occurs, and a zero value on the graph of ω shows a position where the hoop stops rotating momentarily before starting to rotate backwards.

Secondly, various phase diagrams are used to give a concise description of the overall behavioural patterns.

5.2 A typical example

In this section the results of a typical example are given. Taking a particle mass double the hoop mass so that $\gamma = 2/3$, together with $\mu = 0.3$ and an initial velocity of $\omega_0 = 0.5$, i.e. $\mathcal{P}_0 = \{2/3, 0.3, 0.5\}$, the results shown below in Figure 5.2 are obtained. This case illustrates a typical behavioural pattern and can be used as a "base-line" with which to compare most of the other patterns obtained for other parameter values.

The friction coefficient μ is one of the main factors defining the motion of a hoop, in this and later examples. This effect is seen clearly on the graph of $\mathcal{F}/\mathcal{N}$ as a function of θ, as shown in Figure 5.2(a). In this case the first maximum value is less than the friction coefficient of $\mu = 0.3$, which value is indicated by the horizontal dotted line. The hoop therefore continues rolling up to the position where $\mathcal{F}/\mathcal{N} = -\mu$, and the hoop starts skidding. The skidding lasts for approximately 40° and is followed by rolling, a 40° spinning phase where $\mathcal{F}/\mathcal{N} = \mu$ and a final rolling phase all the way to the top, where the analysis ends with $\theta_F = 360°$. The complete description of the motion for this case in terms of the phase labels is therefore `RDRSR-- T`.

Vertical lines are drawn at $\theta = 180°$ and the angles where the phases change. The different phases are labelled at the top of the figure.

Figure 5.2(b) shows graphs of the normal reaction and friction force, normalised with respect to the weight mg. The upper graph is plotted for scaled values $\mu\mathcal{N}$, and the lower graph shows $\mathcal{F}$; the region of spinning where $\mathcal{F} = \mu\mathcal{N}$ is therefore clearly recognisable.

The normal reaction is essentially symmetric with a maximum value at $\theta = 180°$; the large maximum value is due to the centrifugal effect of the heavy particle, as clearly illustrated by the D'Alembert diagram of the forces as shown in Figure 5.1 for θ approaching 180°.
The graph of $\mathcal{N}$ in Figure 5.2(b) is clearly still positive at the end of the graph; therefore hopping does not occur in this case. The friction force is essentially skew-symmetric.

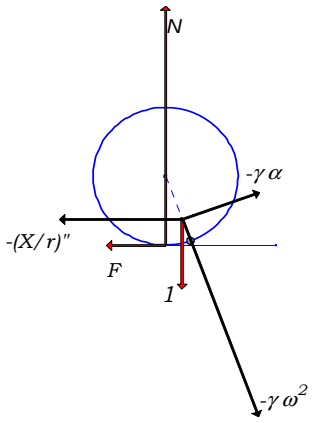

Figure 5.1 : D'Alembert diagram for $\theta \approx 180°$

The dash-dot curve in Figure 5.2(c), labelled a/g, shows the acceleration of the mass centre calculated from (2.18). The maximum value is $a_{max} = 3.5g$, which makes this another example of the "faster than gravity" phenomenon, [15, 16], in which the acceleration is greater than g even though the only active force is the force of gravity. This issue will be discussed in more detail in section 5.6.

In Figure 5.2(c) the angular velocity ω is shown as a solid curve, and the velocity of point O, $\mathcal{V}_x = (X/r)'$, as the dotted curve; at this scale the two graphs are practically identical, although the values do differ slightly during the short skidding and spinning phases when $\omega < \mathcal{V}_x$ and $\omega > \mathcal{V}_x$ respectively. This is shown more clearly by the dash-dot curve showing the difference $\omega - \mathcal{V}_x$, magnified by a factor of ten. The graph also shows that the velocity is still positive when the particle reaches the top.

The fourth graph in Figure 5.2(c) shows the angular acceleration α which is essentially skew-symmetric, being positive while $\theta < 180°$ and the particle is moving downwards and therefore providing a positive torque round the contact point, and being negative when $\theta > 180°$ and the particle is moving upwards. The angular velocity clearly reaches a maximum value at $\theta = 180°$, where the angular acceleration changes from positive to negative.

A notable feature in the graphs is the discontinuity in $\mathcal{F}$ and α at the points where the slipping motion changes back to rolling. In this example rolling resumes after the skidding phase at position $\theta = 108.5°$, at which position a reasonably large discontinuity occurs in the friction force, and consequently also in the angular acceleration and $\mathcal{F}/\mathcal{N}$-graph. The same occurs at the end of the spinning phase. This is similar to the phenomenon that occurs when the motion of a concentric wheel or hoop changes from slipping (skidding or spinning) to rolling, as shown by the analytic results in section 4.3.8.

Detailed analyses of these discontinuities and other features of the results are given in later sections.

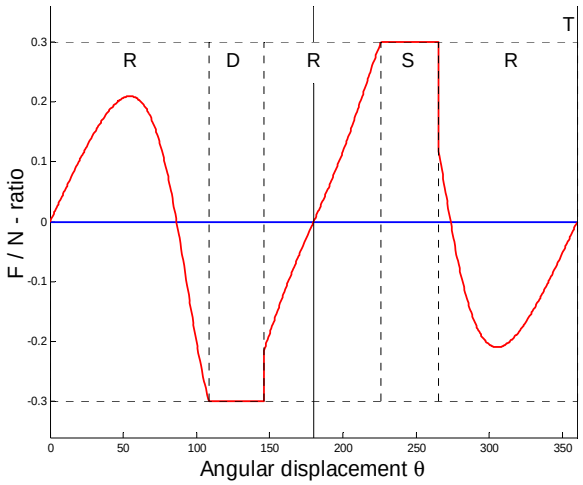

(a) : Ratio of $\mathcal{F}/\mathcal{N}$

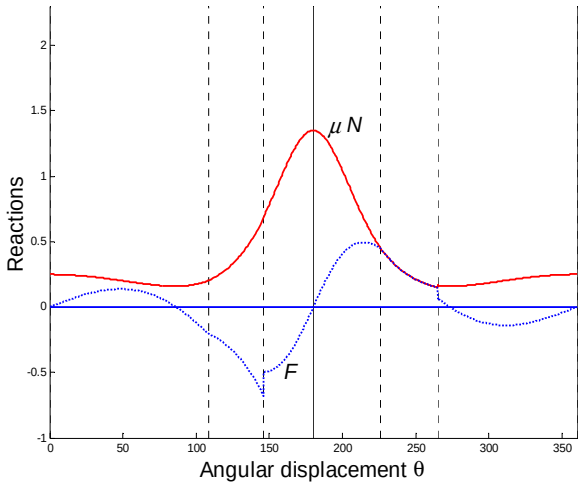

(b) : Reaction forces

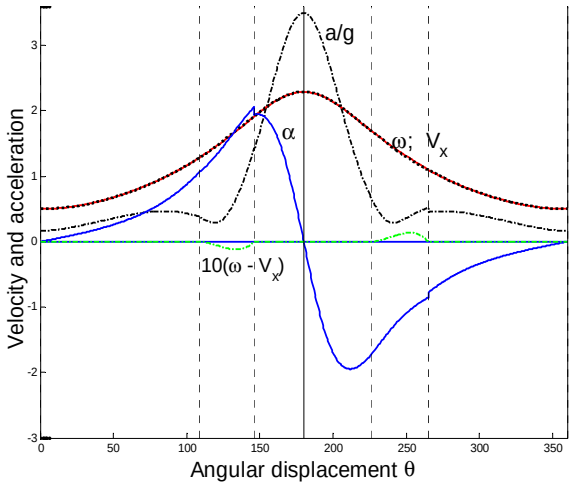

(c) : Kinematic quantities

Figure 5.2 : Detailed results for a typical example of a rigid hoop, using $\mathcal{P}_0 = \{2/3, 0.3, 0.5\}$

5.3 Classification of behavioural patterns

5.3.1 The rolling curve

A fundamental concept in much of the following analysis is the *rolling curve*, defined as the graph of $\mathcal{F}/\mathcal{N}$ as a function of position when the hoop rolls without slipping, as previously discussed in section 4.3.4. Figure 4.5 is repeated here as Figure 5.3.

The normal situation regarding rolling curves is shown in Figure 5.3(a), where four relative maximum and minimum values in one full rotation are shown. These extrema will be referred to as peaks 1, 2, 3 and 4, with peak 1 being the first positive extremum, etc. Also note the skew-symmetry of the curve, as a result of which peaks 1 and 4 have the same magnitude, as do peaks 2 and 3.

The effect of different initial velocities is shown in Figure 5.3(b), which shows only the first two peaks. The case when $\omega_0 = 0.5$ is shown as the solid curve in Figures (a) and (b). Decreasing the initial velocity increases the first maximum and decreases the magnitude of the second peak, as seen in Figure 5.3(b). For $\omega_0 = 0.317$ the magnitudes of all the peaks are the same. For smaller values of ω_0, the first peak is larger than the second.

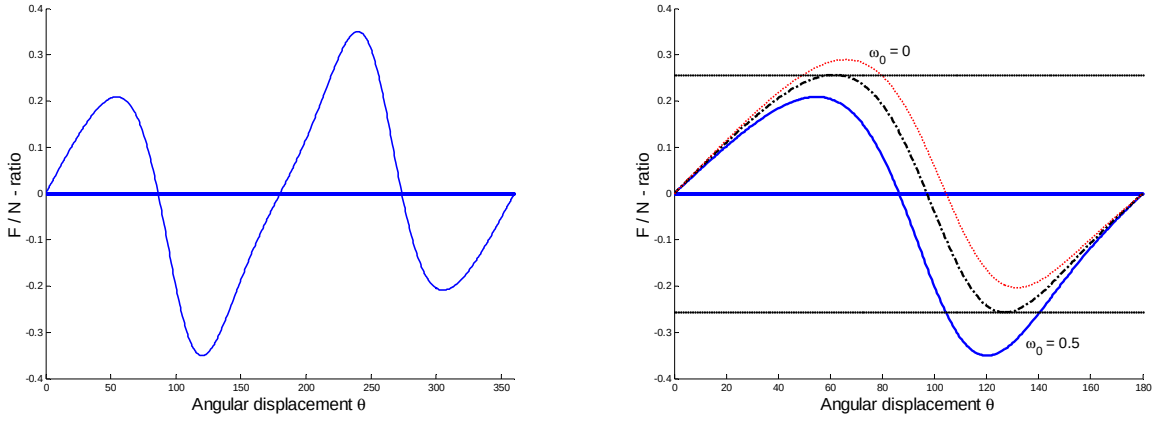

(a) : $\omega_0 = 0.5$ (b) : $\omega_0 = 0.5, 0.317, 0$

Figure 5.3 : Rolling curves for $\gamma = 2/3$

The first two extrema are used in the primary classification introduced in the next section.

5.3.2 Primary classification

It is useful to classify the behaviour of a loaded hoop at two stages. The *primary classification* refers to the first change in phase; i.e. what happens when the hoop stops rolling for the first time. In some cases a secondary classification is also used, based on the second phase change.

In the case of massless hoops, Chapter 3, it was convenient to differentiate between two essentially different situations by defining the critical initial velocity $\bar{\omega}_0$ in equation (3.28) as $\bar{\omega}_0 = \sqrt{(1-\mu^2)/(1+\mu^2)}$, or, equivalently, by defining the critical friction coefficient as

$\bar{\mu} = \sqrt{(1-\omega_0{}^2)/(1+\omega_0{}^2)}$. The behaviour for cases when $\omega_0 < \bar{\omega}_0$, which were classified as cases of low initial velocity, differs from that when $\omega_0 > \bar{\omega}_0$ or high initial velocity. The curve where $\omega_0 = \bar{\omega}_0$ separates the two regions in the (μ, ω_0)-parameter space, Figure 3.2. Alternatively, and equivalent in all respects, the regions can be classified as light friction, with $\mu < \bar{\mu}$, and heavy friction, $\mu > \bar{\mu}$.

In the case of real hoops, Chapters 4 to 7, a similar situation occurs, and it is convenient to define the *primary classification* in terms of the friction coefficient. In this case two critical values for the friction coefficient are identified, denoted by μ_L and μ_H; the subscripts referring to Light and Heavy respectively. These values are determined numerically as functions of ω_0 for a given set of parameters ψ and γ by using the first two extrema of the rolling curve and defining

$$\mu_L = \max(\mathcal{F}/\mathcal{N}), \quad \mu_H = |\min(\mathcal{F}/\mathcal{N})|, \quad \theta < \pi. \tag{5.1}$$

For example, $\mu_L = 0.209$ and $\mu_H = 0.350$ in Figure 5.3(a), for $\gamma = 2/3$ and $\omega_0 = 0.5$.

The implications of the definition for μ_L and μ_H are as follows:

- If $\mu > \max(\mu_L, \mu_H)$, the hoop can never start slipping and will roll through the full revolution. This situation is defined as *heavy friction*. In terms of the labels defined previously, the complete motion is labelled `R T`.
- If $\mu < \mu_L$, the hoop will stop rolling and start slipping while the friction force is positive; i.e. the hoop stops rolling and starts spinning when $\mathcal{F} = \mu\mathcal{N}$. This situation is defined as *light friction*, and the motion is labelled as `RS* *`.
- If $\mu \in [\mu_L,\ \mu_H)$, the hoop will start slipping after the friction force becomes negative; i.e. the hoop stops rolling and starts skidding when $\mathcal{F} = -\mu\mathcal{N}$. This situation is defined as *medium friction* and the motion is labelled as `RD* *`.

Figure 5.3(a) shows that the rolling curves are skew-symmetrical round $\theta = \pi$. Figure 5.3(b) shows the effect of decreasing the initial velocity while keeping the other parameters the same. The graphs shown are for $\omega_0 = 0.5$, 0.317, 0.1 respectively, with μ_L increasing as ω_0 decreases, the values for μ_L being 0.209, 0.257, 0.286 respectively. The corresponding values for μ_H are 0.350, 0.257, 0.208. Note that $\mu_L < \mu_H$ for the larger initial velocity, and that $\mu_L > \mu_H$ for lower initial velocities.

The critical value resulting in $\mu_L = \mu_H = \tilde{\mu}$ is denoted by $\tilde{\omega}_0$; in this case $\tilde{\omega}_0 = 0.317$ and $\tilde{\mu} = 0.257$, which value is shown in Figure 5.3(b) by horizontal lines. Note that medium friction can only occur if $\omega_0 > \tilde{\omega}_0$ (i.e. if $\mu_L < \mu_H$).

5.3.3 Final conditions and motion types

Per definition, the primary classification refers to the first two phases of the motion; in most cases, these are followed by up to seven more phases, ending at a final position denoted by θ_F where the hoop is in one of three possible conditions, as previously defined.

These final conditions are mainly dependent on the initial velocity, and it is convenient to also use the following classification:

A motion is considered to be a motion with *Low initial velocity* or simply *Low velocity* when it ends with zero angular velocity. Later numerical work indicates that this occurs when

$$\omega_0 \in (0, \hat{\omega}_L),$$

where $\hat{\omega}_L$ is determined numerically.

Similarly, motion is deemed to be a motion with *medium velocity* when it rolls to the top; this occurs when

$$\omega_0 \in (\hat{\omega}_L, \hat{\omega}_H),$$

where $\hat{\omega}_H$ is determined numerically.

Finally, a motion starts with *High velocity* when it ends with a hop; this occurs when

$$\omega_0 > \hat{\omega}_H.$$

When these final conditions are superimposed on the primary classification, seven primary types of motion are identified, as shown below in Table 5.1. Either one or two letters can denote the seven types, with the first letter referring to the primary classification in terms of friction, and the second letter referring to the final condition.

Type	Classification	Phase Labels
H	Heavy friction	`RT`
ML	Medium friction, Low velocity	`RD* Z`
MM	Medium friction, Medium velocity	`RD* T`
MH	Medium friction, High velocity	`RD* H`
LL	Light friction, Low velocity	`RS* Z`
LM	Light friction, Medium velocity	`RS* T`
LH	Light friction, High velocity	`RS* H`

Table 5.1 : Classification of primary types of motion

Henceforth any reference to a motion or behaviour as being of type MH for example will indicate the classification given in Table 5.1. Note that all seven types do not necessarily occur for any given eccentricity.

This classification can be shown in a compact form on different types of phase diagram, as shown in later sections.

5.4 Phase diagrams

The regions in a parameter space for which a particular type of motion occurs can be shown clearly and concisely on various types of phase diagram.

Two types of phase diagram are found to be particularly useful. Firstly, phase diagrams in (θ, ω_0)-space for a given (γ, μ)-parameter set give all the information regarding the different phases of a particular motion. Secondly, phase diagrams in (μ, ω_0)-space for a given value of γ give a concise description of the regions resulting in the seven primary types of motion.

5.4.1 Phase diagrams in (θ, ω_0)-space

A phase diagram in (θ, ω_0)-space can be obtained for a fixed (γ, μ)-parameter set by calculating the numerical solution for a range of ω_0-values. For each solution the values of θ where the phase changes are recorded, and these points are plotted on the (θ, ω_0)-plane. The points of a single motion therefore lie on a horizontal line at vertical ordinate ω_0. It becomes clear that these points describe the boundaries of domains in the (θ, ω_0)-plane for each of the possible phases. Besides the interspersing rolling phases, there are four slipping phases, viz. first spinning phase, the first skidding phase, second spinning phase, and second skidding phase. Six examples of such phase diagrams are shown in Figure 5.4. [2]

The domains in which spinning occurs are labelled S_1 and S_2 respectively and are filled with light grey, and the domains where skidding occurs are labelled D_1 and D_2 respectively and are filled with dark grey. The domains where rolling occurs are unlabelled and filled with a diagonal hatch pattern.

The phases S_1 and D_2 form a pair and rise as hump shapes from the bottom of the diagram with decreasing μ. Their maxima have the same value (e.g. Figure 5.4(b)) except in those cases where the point where the maximum would have been is obscured by an earlier phase (e.g. Figure 5.4(d)). Similarly D_1 and S_2 form a pair and drop down from the top with decreasing μ and their minima have the same value (e.g. Figure 5.4(a)) except when obscuration by an earlier phase prevents this (e.g. Figure 5.4(d)).

It is also useful to show the final condition of the motion. The points (θ_F, ω_0) form curves at the right hand boundary of the (θ, ω_0)-plane, viz. the ZERO curve, labelled Z, for lower values of ω_0; the TOP line, which is a vertical line at $\theta = 360^o$; and the HOP curve, labelled H, for higher values of ω_0.

The domain of motion is bounded at the top by the horizontal line $\omega_0 = \hat{\omega}_0$, from (2.30).

In each diagram the pattern for a particular value of ω_0 may be obtained by following a horizontal line from left to right and noting the domains through which this line passes.

For example the case described in section 5.2 is indicated in Figure 5.4(a), case (3), by a dashed horizontal line at $\omega_0 = 0.5$; the label `RDRSR-- T` is easily recognised.

A region where two humps overlap corresponds to cases where the discontinuity in $\mathcal{F}/\mathcal{N}$ needs to be limited to 2μ, thereby eliminating the intermediate rolling phase. Cases (13) to (20) in Figure 5.4(d) all illustrate this phenomenon, which will be discussed in more detail later.

[2] These diagrams were used in [6], and the region filling software used to create them was provided by my co-author.

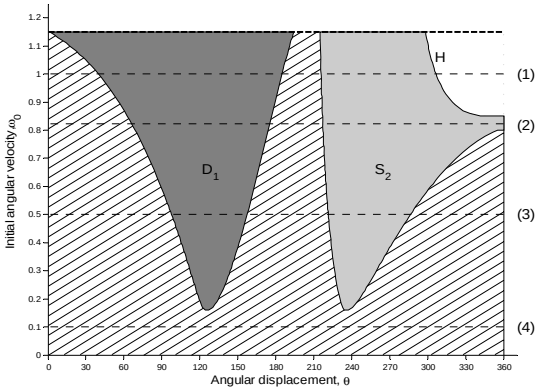

(a) $\gamma = 3/4,\ \mu = 0.4$

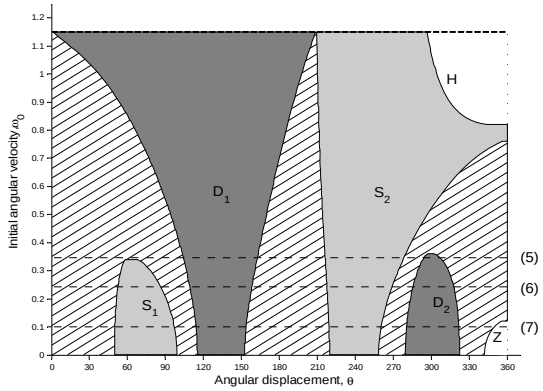

(b) $\gamma = 3/4,\ \mu = 0.3$

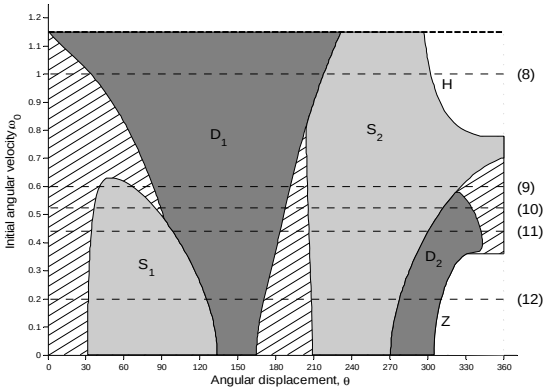

(c) $\gamma = 3/4,\ \mu = 0.2$

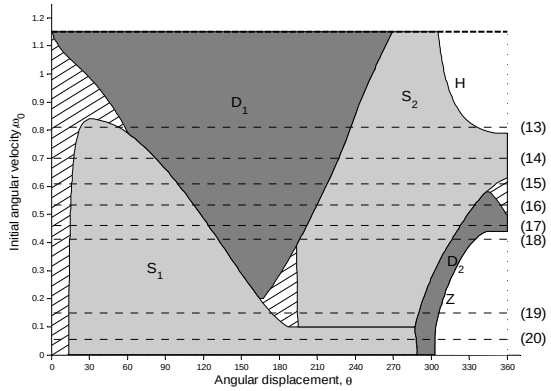

(d) $\gamma = 3/4, \mu = 0.09$

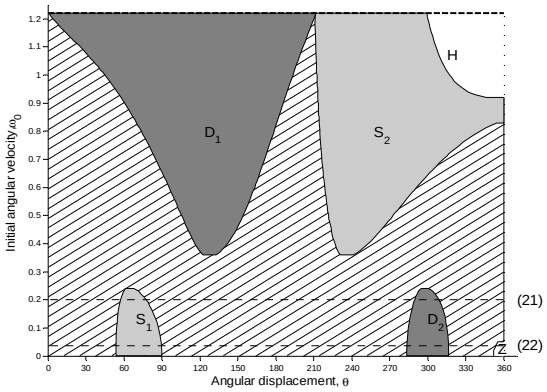

(e) $\gamma = 2/3,\ \mu = 0.27$

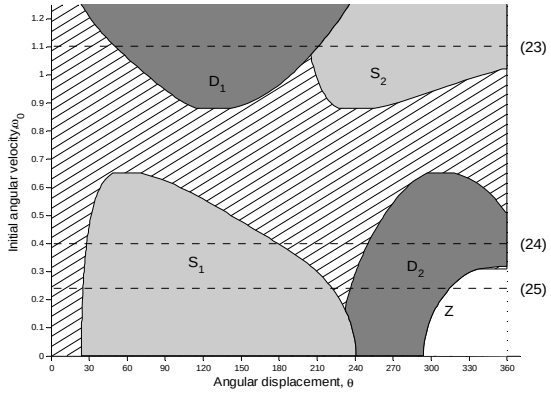

(f) $\gamma = 1/4,\ \mu = 0.05$

Figure 5.4 : Phase diagrams in (θ, ω_0)-space

A total of twenty-five different patterns are shown on the six diagrams in Figure 5.4. Figure 5.4(d) is remarkable in that ten different patterns, of which only the eight new ones are shown, are found for this single (γ, μ) pair.

Figures 5.4(e) and 5.4(f) are for smaller eccentricities and show five new patterns. In these cases there is always a clear gap between the upper and lower humps.

The twenty-five patterns shown in Figure 5.4 are tabulated in Table 5.2. The first column refers to the line number shown in Figure 5.4. Column two contains a reference number, from 1 to 39, used later in Table 6.2 to identify the different patterns. Table 6.2, in section 6.7, contains a list of all the different patterns found to date. The last column refers to the different cases for which detailed results are given in section 5.5.

Fig. 5.4	Table 6.2	Pattern		γ	μ	ω_0-range	# 5.5
5.4a (1)	6	RDRS--- H		3/4	0.4	[0.85, 1.15]	case e
(2)	7	RDRS--- T		3/4	0.4	[0.81, 0.84]	
(3)	4	RDRSR-- T		3/4	0.4	[0.16, 0.80]	case a
(4)	1	R T		3/4	0.4	(0, 0.15]	case b
5.4b (5)	2	RDRSRDR T		3/4	0.3	[0.35, 0.36]	
(6)	11	RSRDRSRDR T		3/4	0.3	[0.13, 0.34]	case c
(7)	12	RSRDRSRDR Z		3/4	0.3	(0, 0.12]	
5.4c (8)	9	RD-S--- H		3/4	0.2	[0.82, 1.15]	
(9)	15	RSRDRSR-- T		3/4	0.2	[0.59, 0.63]	
(10)	16	RSRDRS-DR T		3/4	0.2	[0.49, 0.58]	
(11)	28	RS-DRS-DR T		3/4	0.2	[0.37, 0.48]	
(12)	29	RS-DRS-D- Z		3/4	0.2	(0, 0.36]	
5.4d (13)	18	RSRD-S--- H		3/4	0.09	[0.79, 0.84]	case f
(14)	30	RS-D-S--- T		3/4	0.09	[0.64, 0.78]	
(15)	31	RS-D-SR-- T		3/4	0.09	[0.59, 0.63]	
(16)	32	RS-D-S-DR T		3/4	0.09	[0.50, 0.58]	
(17)	34	RS-D-S-D- T		3/4	0.09	[0.45, 0.49]	
(18)	35	RS-D-S-D- Z		3/4	0.09	[0.39, 0.44]	
(19)	20	RSR--S-D- Z		3/4	0.09	[0.10, 0.19]	
(20)	36	RS-----D- Z		3/4	0.09	(0, 0.09]	
5.4e (21)	21	RSR----DR T		2/3	0.27	[0.06, 0.24]	
(22)	22	RSR----DR Z		2/3	0.27	(0, 0.05]	
5.4f (23)	10	RD-S--- T		1/4	0.05	[1.07, 1.87]	
(24)	23	RSR----D- T		1/4	0.05	[0.32, 0.49]	
(25)	24	RSR----D- Z		1/4	0.05	[0.17, 0.31]	

Table 5.2 : List of twenty-five patterns found in Figure 5.4

Similar diagrams are obtained by plotting the energy instead of the initial velocity on the vertical axis, as shown and discussed later.

5.4.2 Phase diagrams in (μ, ω_0)-space

The values of μ_L and μ_H can be calculated for different values of ω_0, keeping γ fixed, and then plotted on $\mu - \omega_0$-axes. These lines of $\mu = \mu_L$ and $\mu = \mu_H$ then separate the (μ, ω_0)-parameter space into the three regions of light, medium and heavy friction, as shown in Figure 5.5(a) for the case of $\gamma = 2/3$. The three regions are labelled `RS*`, `RD*` and `RT` respectively.

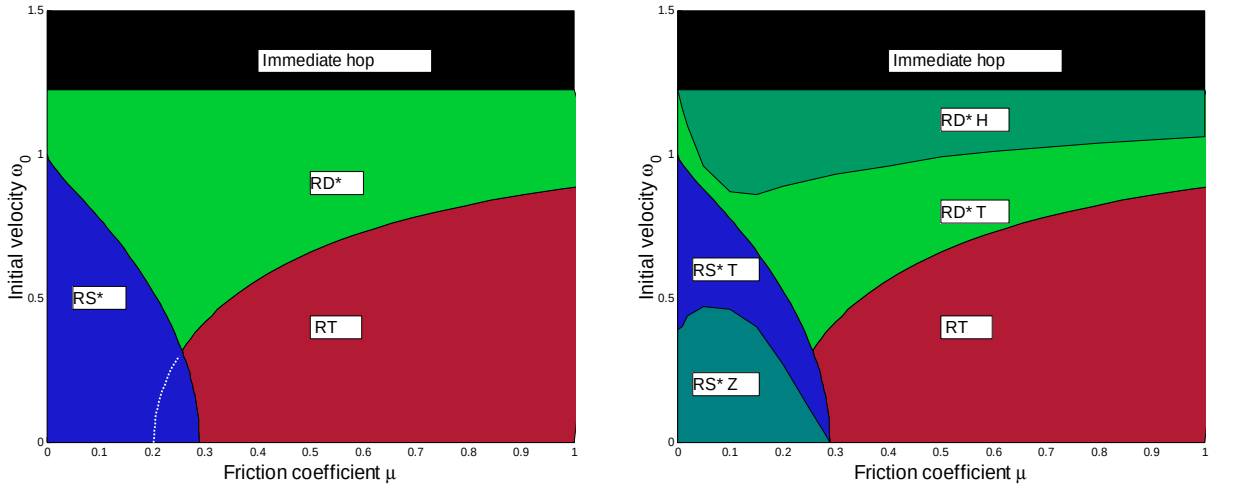

(a) : Primary classification:
regions of light, medium, heavy friction

(b) : Final conditions:
regions of low (Z), medium (T), high (H) velocity

Figure 5.5 : Phase diagrams in (μ, ω_0)-space, for $\gamma = 2/3$

The line $\omega_0 = \hat{\omega}_0 = \sqrt{(1/\gamma)}$, as determined from (2.30), defines an upper limit for the initial velocity. As shown previously, the hoop will hop immediately if ω_0 exceeds this value. In this example, $\hat{\omega}_0 = \sqrt{3/2} \approx 1.2247$.

Figure 5.5(a) clearly shows the overlapping of the light and heavy friction regions when $\omega < \tilde{\omega}_0$ and $\mu_H < \mu_L$; in this range the curve $\mu = \mu_L$ separates the regions of light and heavy friction. As seen in Figure 5.3(b), $\tilde{\mu} = 0.257$ with $\tilde{\omega}_0 = 0.317$. This situation occurs only for $\gamma < 0.74$; for larger eccentricities, μ_L is always less than μ_H and $\tilde{\omega}_0$ is taken as zero.

The diagram also shows that $\mu_L = 0$ when $\omega_0 = 1$. This is true for all values of γ, and follows from the analysis in section 4.3.7, where it was shown that $\mathcal{F} = \frac{1}{2}\gamma\theta(1 - \omega^2)$ for small θ as $\mu \to 0$, implying that rolling changes to spinning if $\omega_0 \in (0, 1)$, and that rolling changes to skidding if $\omega_0 \in (1, \hat{\omega}_0)$, as clearly shown in Figure 5.5.

Figure 5.5(b) shows the phase diagram when the final conditions are super-imposed on the primary classification. In this case only five of the seven primary types are present.

The region labelled `RS* Z` in the bottom left region of the phase diagram shows all the parameter values for which the motion ends with $\omega_F = 0$; i.e. for motions of type LL, classified as light friction with low velocity. Here $\omega_0 < \hat{\omega}_L$, where $\hat{\omega}_L$ is determined numerically by obtaining the complete solution of the motion for a range of values of μ and ω_0.

For $\mu < \mu_L$ and $\omega_0 \geq \hat{\omega}_L$ the region is labelled `RS* T` and shows all the parameter values for which the motion ends with $\theta_F = 360°$; i.e. for motions of type LM, classified as light friction with medium velocity.

The region labelled `RT` shows the region of heavy friction where $\mu > \mu_H$ and the hoop rolls without slipping.

The remaining medium friction region is divided into two. The region labelled `RD* T`, where $\omega_0 < \hat{\omega}_H$, shows all the parameter values for which the motion ends with $\theta_F = 360°$; i.e. for motions of type MM, classified as medium friction with medium velocity.

Finally, the region labelled `RD* H`, where $\omega_0 \geq \hat{\omega}_H$, shows all the parameter values for which the motion ends with a hop where $\mathcal{N}_F = 0$; i.e. for motions of type MH, classified as medium friction with high velocity.

A secondary classification, which divides the medium and light friction regions into "normal" and other sub-regions will be introduced later. For the time being the emphasis is on "normal" situations.

In the next section the effect of γ on the phase diagrams will be shown. The two "missing" types, namely types LH and ML, will be shown to exist if the eccentricity is large enough.

5.4.3 Phase diagrams for different eccentricities

The effect of changing the eccentricity γ is clearly shown in Figure 5.6. Figure 5.6(a) shows the phase diagram for the relatively small eccentricity in the equal mass case, i.e. $m_p = m_h$ and $\gamma = 1/2$. Figure 5.6 (b) is for a heavy particle, $m_p = 3m_h$ and $\gamma = 3/4$, as previously used in Figure 5.4. Figure 5.6 (c) is for a very heavy particle, $m_p = 4m_h$ and $\gamma = 4/5$.

Increasing γ has three main effects on the primary classification:

- The region where immediate hopping occurs becomes larger as γ increases. Values of $\hat{\omega}_0 = \sqrt{(1/\gamma)}$, from (2.30), are shown in the table below. The heavier particle causes immediate hopping at a lower initial velocity because the larger particle mass increases the centrifugal effect.

- The region of light friction increases as γ increases, as clearly shown in Figure 5.6. With zero initial velocity, spinning will occur for friction coefficients less than the values shown for $\mu_L(0)$ in the table below. Note that this is the lower right corner of the light friction region. As mentioned previously, the upper left corner of this region is always at (0, 1), i.e. $\mu = 0$ and $\omega_0 = 1$.

- The region for heavy friction reduces as γ increases, as shown by the values of $\mu_H(0)$ in the table above, this being the lower left corner of this region. The centrifugal effects of the heavier particle causes larger friction forces and slipping at lower velocities, thereby decreasing the region where rolling occurs. The last entry in the table shows that heavy friction requires $\mu > 1$ if $\gamma > 0.846$.

Also shown in the table are the values for $(\tilde{\mu}, \tilde{\omega}_0)$, the point where $\mu_L = \mu_H$ and where the regions of light and heavy friction overlap. It can be shown that there is no overlap between these regions for $\gamma > 0.735$, when $\tilde{\mu} = 0.335$ and $\tilde{\omega}_0 = 0$.

γ	$\hat{\omega}_0$	$\mu_L(0)$	$\mu_H(0)$	$\tilde{\mu}$	$\tilde{\omega}_0$	$\hat{\omega}_{H_{min}}$
1/2	$\sqrt{2} \approx 1.414$	0.204	-	0.129	0.56	1.10
2/3	$\sqrt{3/2} \approx 1.225$	0.290	-	0.258	0.317	0.86
0.735				0.335	0	
3/4	$\sqrt{4/3} \approx 1.155$	0.345	0.377			0.75
4/5	$\sqrt{5/4} \approx 1.118$	0.386	0.585			0.72
0.846			1			

Table 5.3 : Special values of μ and ω_0 for different eccentricities

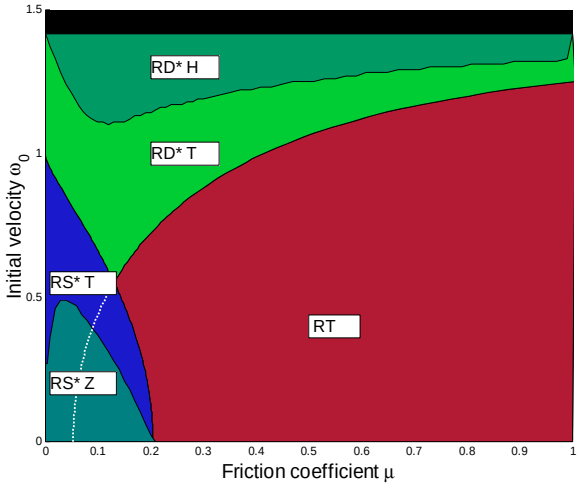

(a) : Phase diagram for $\gamma = 1/2$

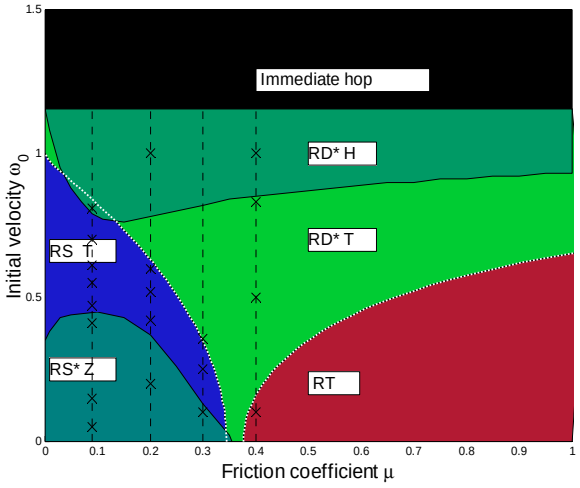

(b) : Phase diagram for $\gamma = 3/4$

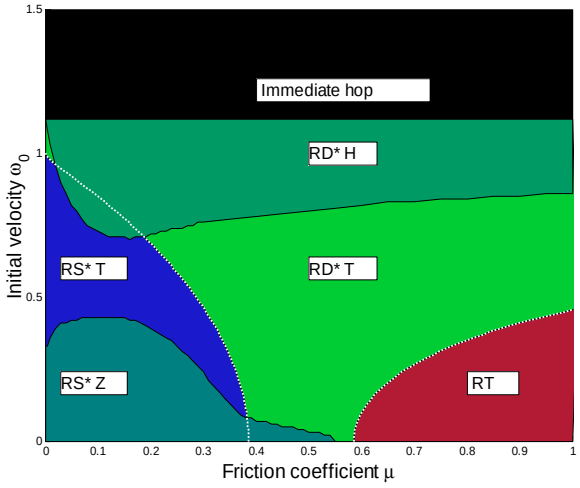

(c) : Phase diagram for $\gamma = 4/5$

Figure 5.6 : Phase diagrams in (μ, ω_0)-space, for different eccentricities

Similar effects are noted for the final conditions. The H-region of high initial velocity that results in hopping increases as γ increases. This is indicated inter alia by the tabulated values of $\hat{\omega}_{H_{min}}$ which is the minimum initial velocity that will cause hopping. Inspection of figures 5.5(b) and 5.6 show that this minimum value occurs in the region of $\mu = 0.11$.

Phase diagrams 5.6(b) and (c) show an overlapping of the H-region and light friction, implying that hopping can occur in cases of light friction if the particle is heavy enough; i.e. motions of type LH, labelled `RS* H` do exist.

A similar overlapping of the Z-region and medium friction can be seen in Figure 5.6(b) and (c), where the Z-region also increases as γ increases. Therefore motions of type ML, labelled `RD* Z`, also exist if the particle is heavy enough.

The vertical lines in Figure 5.6(b) for $\gamma = 3/4$, drawn at $\mu = 0.4,\ 0.3,\ 0.2$ and 0.09, correspond with the $(\theta,\ \omega_0)$-phase diagrams in Figure 5.4 (a) to (d) respectively, and the crosses on these lines show the data points used for cases 1 to 20 shown in Table 5.2.

5.5 Detailed results for examples of the seven types of motion

In this section detailed results are given for seven examples, one for each of the primary types defined in Table 5.1. The parameters for the first five of these examples, for $\gamma = 2/3$, are shown as the points labelled a to e in Figure 5.7.

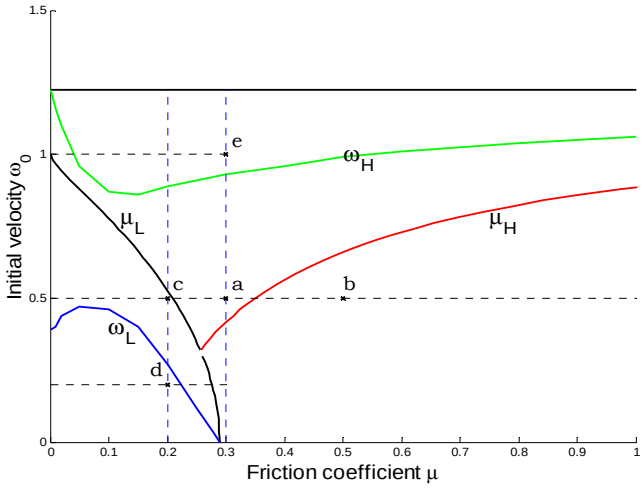

Figure 5.7 : Data points on the (μ, ω_0) phase diagram for $\gamma = 2/3$

The data for the seven examples are summarised in Table 5.4. The first two columns show the case number and type; the next three give the values of the parameters. The sixth column refers to the final phase of the motion, and the last column shows the phase labels for the complete motion for this specific example.

Case	Type	γ	μ	ω_0	Final phase	Phase Labels
a	MM	2/3	0.3	0.5	$\theta_F = 2\pi$	RDRSR-- T
b	H		0.5	0.5	$\theta_F = 2\pi$	R T
c	LM		0.2	0.5	$\theta_F = 2\pi$	RSRDRSRDR T
d	LL		0.2	0.2	$\omega_F = 0$	RSRDRSRD- Z
e	MH		0.3	1.0	$\mathcal{N}_F = 0$	RDRS--- H
f	LH	4/5	0.15	0.75	$\mathcal{N}_F = 0$	RSRD-S--- H
g	ML		0.5	0.02	$\omega_F = 0$	RDRSR-- Z

Table 5.4 : Parameter values for the seven examples

Note that the typical example shown in section 5.2 is case a in Table 5.4. The detailed results for the examples of Table 5.4 will be discussed in the following sections.

In the following sections a numeric subscript refers to the number of the phase change; for example, θ_1 denotes the position where the first rolling phase ends, and ω_2 the angular velocity after the first slipping phase.

5.5.1 Case a, type MM: Medium friction with medium velocity

The example used in section 5.2 is repeated here to illustrate the behaviour of a hoop in the medium friction, medium velocity region. Using $\gamma = 2/3$, $\mu = 0.3$ and $\omega_0 = 0.5$, i.e. $\mathcal{P}_0 = \{2/3, 0.3, 0.5\}$, this specifies the point marked a in Figure 5.7. This point is in the medium friction region because $\mu \in (\mu_L, \mu_H)$, and also in the medium velocity region, as $\omega_0 < \hat{\omega}_H$.

Figure 5.1 is repeated here as Figure 5.8 to show the graphs for case a.

As discussed in section 5.2, the description of this motion in terms of the phase labels is `RDRSR-- T`, as seen in Figure 5.8(a). The same pattern (with different parameters) is shown in Figure 5.4(a), case (3), where the two slipping phases can be seen clearly.

The main feature of the graphs in Figure 5.8(b) and (c) is that $\mathcal{N}$, a/g, $\mathcal{V}_x$ and ω are basically symmetrical, and $\mathcal{F}$ and α skew-symmetrical, with slight distortions due to the loss of energy during the slipping phases.

The region of spinning where $\mathcal{F} = \mu\mathcal{N}$ is clearly recognisable in Figure 5.8(b).

This is not the only pattern obtainable for type MM motion. In Figure 5.4 and Table 5.2 there are three more patterns with the label `RD* T`, namely `RDRS--- T`, `RDRSRDR T` and `RD-S--- T`. Two more patterns of type MM are found later, and all six patterns are listed in Table 6.2.

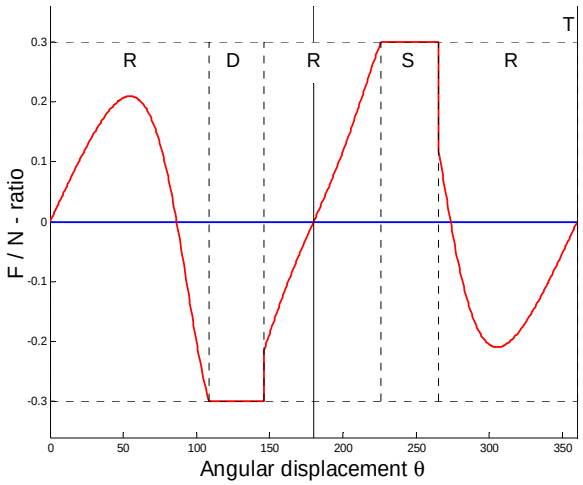

(a) : Ratio of $\mathcal{F}/\mathcal{N}$

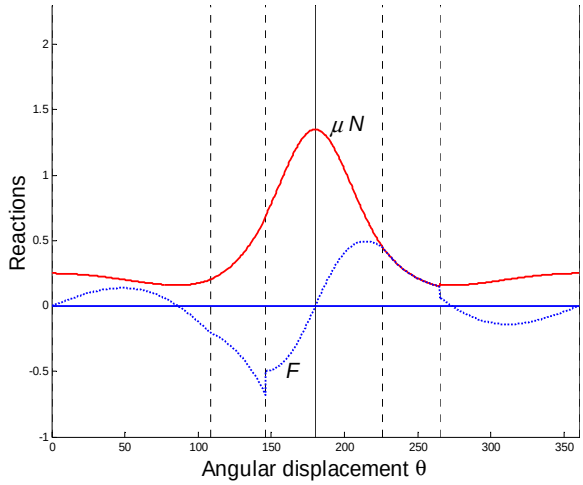

(b) : $\mu\mathcal{N}$ and $\mathcal{F}$

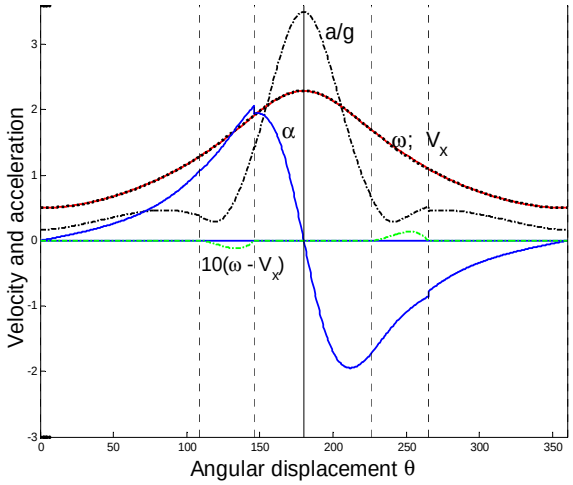

(c) : ω, α, $\mathcal{V}_x$ and a/g

Figure 5.8 : Case a, type MM - Medium friction, medium velocity, $\mathcal{P}_0 = \{2/3,\ 0.3,\ 0.5\}$

5.5.2 Case b, type H: an example of heavy friction

The case of heavy friction is considered as a second example. If the friction coefficient is set at $\mu = 0.5$ and the other parameters are the same as for case a, Figure 5.7 shows that the point marked b falls within the region of heavy friction. The results are shown in the graphs in Figure 5.9, using $\mathcal{P}_0 = \{2/3,\ 0.5,\ 0.5\}$.

The defining characteristic for heavy friction is that the hoop rolls through one complete rotation without any loss of energy. Figure 5.9(a) clearly shows that the $\mathcal{F}/\mathcal{N}$-ratio is less than μ throughout. This motion is therefore labelled `R T`, and is also shown as example (4) in Figure 5.4(a). Note that this is the rolling curve as defined in section 5.3.1 and shown in Figure 5.3(a).

The graphs in Figure 5.9(b) and (c) are fundamentally the same as in case a, except that here the symmetries are not distorted. This can be shown by considering the equations derived in section 4.3.2 for the analysis of rolling motion on a horizontal plane. In this case

$$\mathcal{F} = \tfrac{1}{2}\gamma \sin\theta\,(1 - \omega^2),$$

as shown in (4.24). The friction force is therefore zero initially and is positive while $\omega < 1$. It reaches a maximum positive value, which in this case is less than $\mu\mathcal{N}$ as clearly seen in Figure 5.9(b). It then changes to negative when $\omega > 1$ and back to positive at $\theta = \pi$, with further zero's when $\omega = 1$ and finally when $\theta = 2\pi$. The skew-symmetry in the graph is clear from (4.24), taking into account that ω^2 is symmetric as will be shown below.

It was also shown in section 4.3.2 for rolling on a horizontal plane that

$$\omega^2 = \frac{C - \gamma\cos\theta}{1 + \gamma\cos\theta}.$$

This is clearly a symmetric function in θ, as confirmed by the solid curve showing the angular velocity ω in Figure 5.9(c).

The dotted curve in Figure 5.9(c) shows the angular acceleration α. It was also shown in section 4.3.2 that

$$\alpha = \tfrac{1}{2}(C + 1)\frac{\gamma\sin\theta}{(1 + \gamma\cos\theta)^2};$$

this is clearly a skew-symmetric function in θ. This is in agreement with a result noted previously for the typical example, where it was shown that α is positive while the particle is moving downwards ($\theta < \pi$) and negative while the particle is moving upwards.

The maximum values of $\mathcal{N}$, ω and a/g at $\theta = \pi$ can be calculated analytically, using (4.32). In this example $\omega(\pi) = \sqrt{21/4} = 2.29$, $a(\pi)/g = 3.5$ and $\mathcal{N}(\pi) = 4.5$. These values are confirmed in Figure 5.9(b) and (c) after scaling as shown.

Note that the value of μ has no effect on the results, on condition that it is large enough to ensure heavy friction; for the case under consideration, with $\omega_0 = 0.5$, this implies $\mu > \mu_H(0.5) = 0.35$ as found previously in Figure 5.3(a).

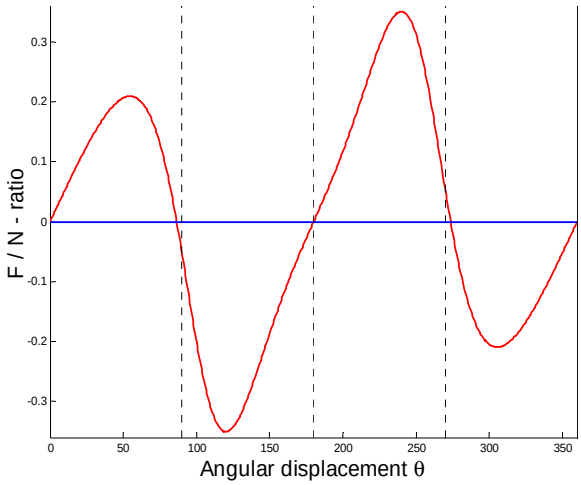

(a) : Ratio of $\mathcal{F}/\mathcal{N}$

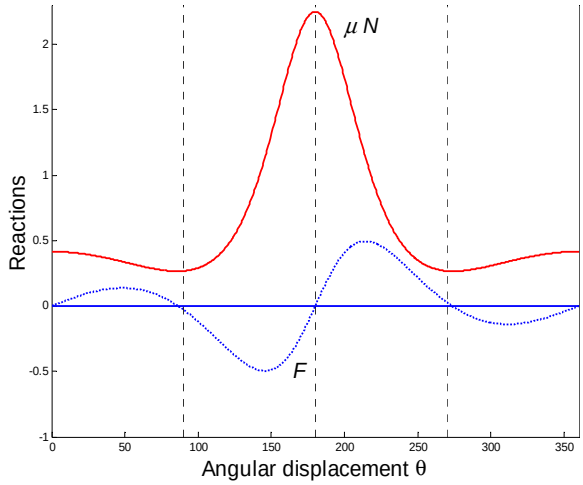

(b) : $\mu\mathcal{N}$ and $\mathcal{F}$

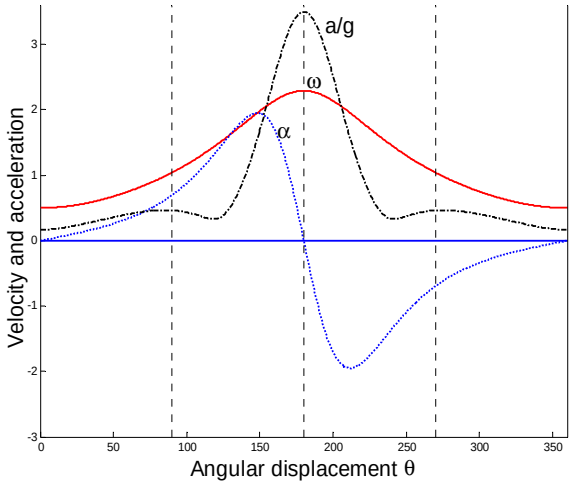

(c) : ω, α, $\mathcal{V}_x$ and a/g

Figure 5.9 : Case b - Heavy friction, $\mathcal{P}_0 = \{2/3, 0.5, 0.5\}$

5.5.3 Case c, type LM: Light friction with medium velocity

Still keeping $\gamma = 2/3$ and $\omega_0 = 0.5$, but taking the friction coefficient as $\mu = 0.2$, Figure 5.7 shows that case c specifies a point in the light friction with medium velocity region, i.e. motions labeled as `RS* T`. This is case c in Table 5.2, with parameters $\mathcal{P}_0 = \{2/3, 0.2, 0.5\}$, and the results are shown in Figure 5.10.

The fundamental difference between this and the first two examples is that here the friction coefficient is reduced to less than μ_L, which means that spinning occurs at the first peak of the rolling curve after a small rotation; this is the defining characteristic of light friction. Figure 5.10 (a) shows that all four peaks exceed the value of μ in this case; also Figure 5.10 (b) and (c) show that $\mathcal{N}$ and ω are still positive after a rotation through 360°. Therefore this is medium velocity case, and the full description of the motion is `RSRDRSRDR T`; nine phases in all, the maximum number that is possible. Another example of this pattern is given in Figure 5.4(b), case (6), where all four slipping phases are easily identified.

Figure 5.10 (b) again clearly shows the two spinning phases where $\mathcal{F} = \mu\mathcal{N}$, and the maximum value for $\mathcal{N}$ when it rolls through $\theta = \pi$. Compared to case a, the discontinuities in $\mathcal{F}$ at the end of the slipping phases are larger for case c.

The graphs of ω, $\mathcal{V}_x$, α and a/g are very similar to case a, except that the difference between ω and $\mathcal{V}_x$ is much larger in case c and can be seen on the graphs.

Figure 5.10(a) shows that the discontinuity at the end of the second slipping phase is just less than 2μ, which results in an extremely short rolling phase at $\theta = 280°$. It is found that a further reduction in μ causes this rolling phase to disappear completely; this phenomenon is shown in later examples and is discussed in more detail in section 6.5.2. This phenomenon, where one or more of the discontinuities needs to be limited to 2μ and the corresponding rolling phase does not exist, causes most of the twelve additional patterns of type LM that are listed in Table 6.2; nine of these are found in Table 5.2.

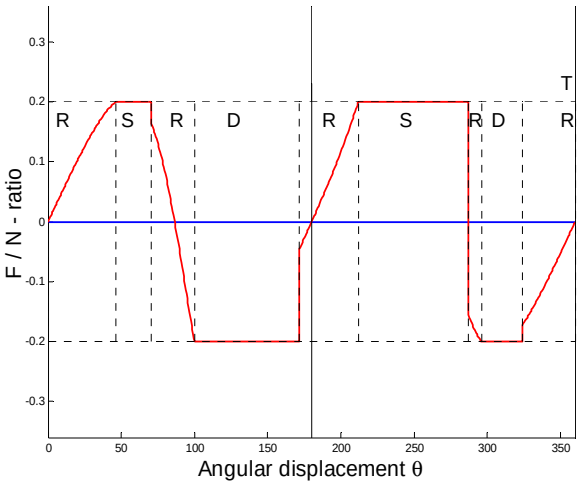

(a) : Ratio of $\mathcal{F}/\mathcal{N}$

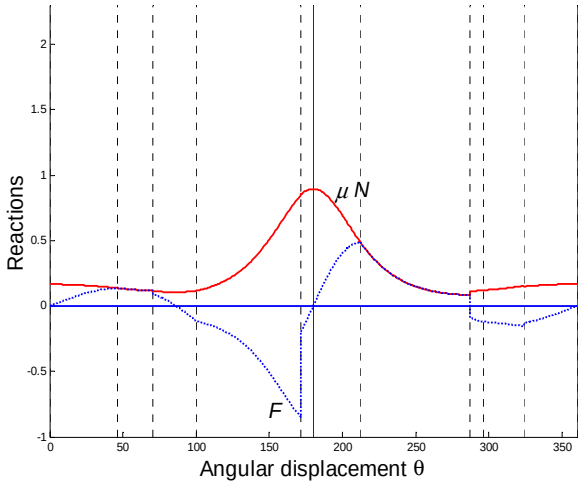

(b) : $\mu\mathcal{N}$ and $\mathcal{F}$

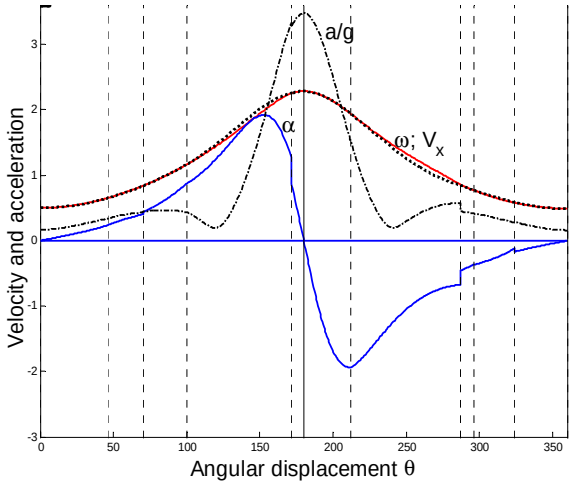

(c) : ω, α, $\mathcal{V}_x$ and a/g

Figure 5.10 : Case c, type LM - Light friction, medium velocity, $\mathcal{P}_0 = \{2/3,\ 0.2,\ 0.5\}$

5.5.4 Case d, type LL: Light friction with low velocity

In this case the initial velocity is reduced to $\omega_0 = 0.2$, keeping $\mu = 0.2$; as shown in Figure 5.7, this is in the light friction, low velocity region with general label `RS* Z`.

This is case d in Table 5.2, with parameters $\mathcal{P}_0 = \{2/3,\ 0.2,\ 0.2\}$, and the results are shown in Figure 5.11.

The fundamental difference between this and the previous case is that here the angular velocity becomes zero before the particle reaches the top.

Figures 5.11(a) and (c) show that the full description of this motion in terms of phase labels is `RSRDRSRD- Z`. Note the extremely short rolling phase following the first spin; this is the result of the very large discontinuity, which is slightly smaller than the maximum value of 2μ. This specific case does not appear in Table 5.2 or Figure 5.4.

Figure 5.11(b) shows basically the same behaviour for the reactions, compared to previous cases. The discontinuity in $\mathcal{F}$ at the end of the first slipping phase is very large, and results in a discontinuity that *increases* a positive value of α. This is in contrast to all the previously noted discontinuities; as mentioned before, this issue will be discussed in section 6.5.2.

Figure 5.11(c) shows that $\mathcal{V}_x > 0$ when $\omega = 0$ at position $\theta_F = 313°$. The hoop is therefore skidding forward at this point, with zero angular velocity. If the analysis were to be continued, we would find that the angular velocity becomes negative and the particle starts moving downwards while the centre of the hoop continues moving forward. The figure shows that the slope of the $\omega - \theta$-graph is vertical at this point; this is in agreement with the definitions that $\alpha = \frac{\mathrm{d}\omega}{\mathrm{d}\theta}\frac{\mathrm{d}\theta}{\mathrm{d}\tau}$, i.e. $\frac{\mathrm{d}\omega}{\mathrm{d}\theta} = \alpha/\omega$.

Twelve more patterns of type LL are listed in Table 6.2.

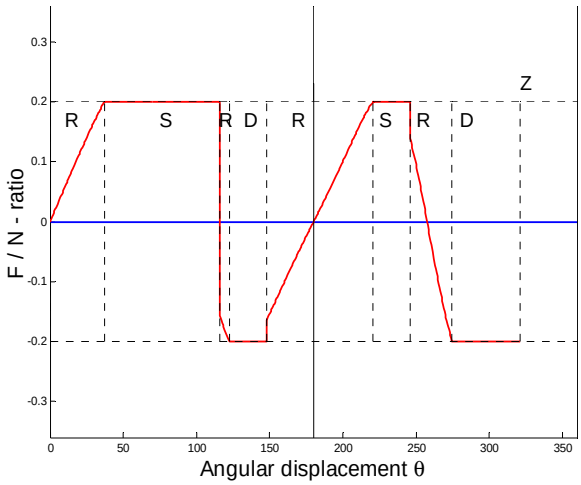

(a) : Ratio of $\mathcal{F}/\mathcal{N}$

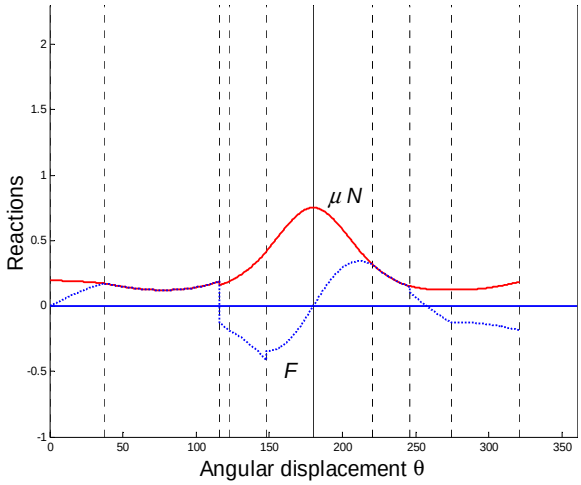

(b) : $\mu\mathcal{N}$ and $\mathcal{F}$

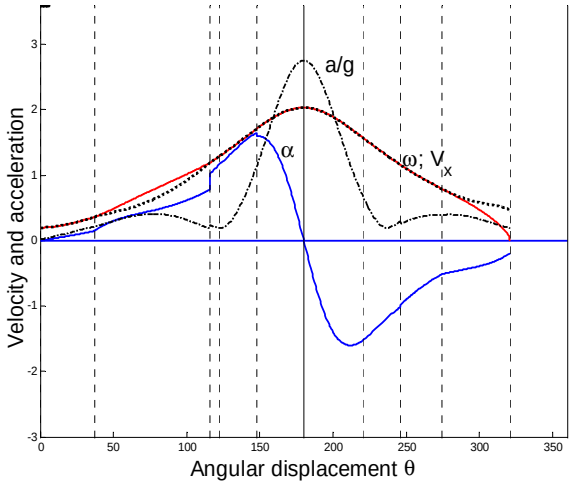

(c) : ω, α, $\mathcal{V}_x$ and a/g

Figure 5.11 : Case d, type LL - Light friction, low velocity,
$\mathcal{P}_0 = \{2/3,\ 0.2,\ 0.2\}$

5.5.5 Case e, type MH: Medium friction with high velocity

In the next example we return to case a with $\mu = 0.3$, but double the initial velocity to $\omega_0 = 1$; as shown in Figure 5.7, this is in the medium friction, high velocity region, because $\omega_0 > \hat{\omega}_H$. This is case e in Table 5.2, with parameters $\mathcal{P}_0 = \{2/3,\ 0.3,\ 1.0\}$, and the results are shown in Figure 5.12.

The fundamental difference between this and the previous cases is that here the normal reaction becomes zero before the particle reaches the top. This occurs at position $\theta_F = 319°$, as seen in Figure 5.12(b) which clearly shows that $\mathcal{F}$ and $\mathcal{N}$ tend to zero at the same rate while spinning. Also, as seen in Figure 5.12(c), the angular velocity at this point has a large positive value; therefore the criterion for hopping, equation (4.19), is satisfied and the hoop hops at position θ_F, due to the large centrifugal effect as illustrated by the D'Alembert diagram.

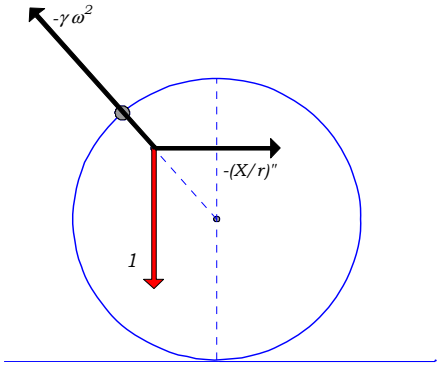

D'Alembert diagram for $\theta > 3\pi/2$

Figure 5.12(a) shows that the full description of the motion in terms of labels is `RDRS--- H`, the same as case (1) in Figure 5.4(a) for other parameters.

As previously noted, an increase in initial velocity has the effect that peak 1 of the rolling curve is reduced, in this case to zero. Therefore $\mu_L = 0$ when $\omega_0 = 1$, as previously noted. Also the friction force becomes negative immediately for $\omega_0 > 1$, as seen from (4.24),
$\mathcal{F} = \frac{1}{2}\gamma \sin\theta\,(1 - \omega^2)$. Therefore peak 1 disappears if $\omega_0 > 1$.

As also noted before, the centrifugal effects due to the large angular velocity result in a smaller normal reaction for $\theta < 90°$, as illustrated by the D'Alembert diagram. The initial value, using (4.6) as shown in section 4.3.1, is

$$\mathcal{N}(0) = 1 - \gamma\omega_0^2;$$

in this case $\mathcal{N}(0) = 1/3$, compared to 5/6 in case a. The graph for $\mathcal{N}$ shows that the value remains almost constant up to $\theta = 90°$. One result of this is that the skidding phase starts sooner than before; now $\theta_1 = 46°$ compared to 108° for case a.

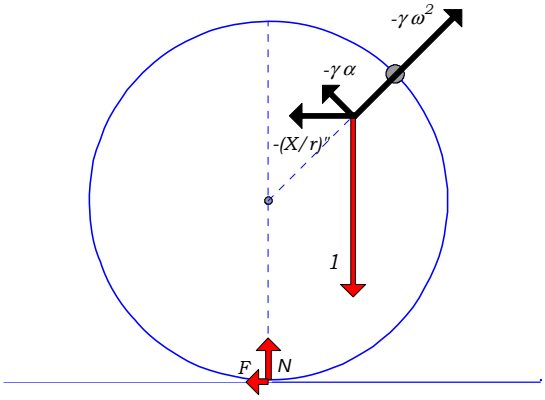

D'Alembert diagram for $\theta < \pi/2$

The graphs in Figure 5.12(c) show that $\mathcal{V}_x$ remains larger than ω past the 180° position. This means that the spinning phase continues past the lowest position of the particle and the hoop does not roll through this position, in contrast to all the previous examples. Therefore $\mathcal{N}(\pi)$ is not the maximum value as before; now the maximum occurs at $\theta_2 = 188°$. The resultant friction force is therefore also large, with the largest being calculated as $\mathcal{F}(\theta_2) = -\mu\mathcal{N}(\theta_2) = -1.96$ at the position where the skidding ends.

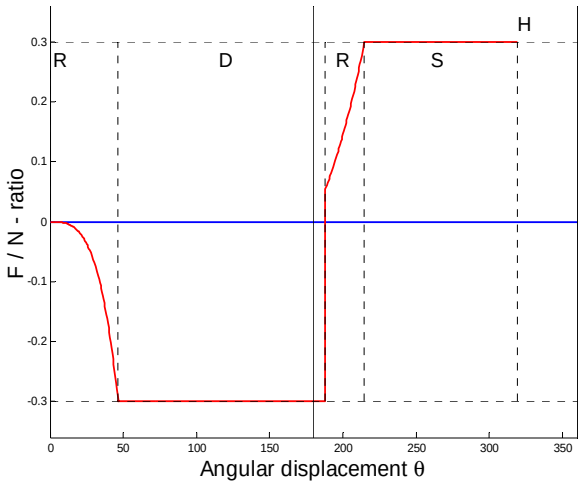

(a) : Ratio of $\mathcal{F}/\mathcal{N}$

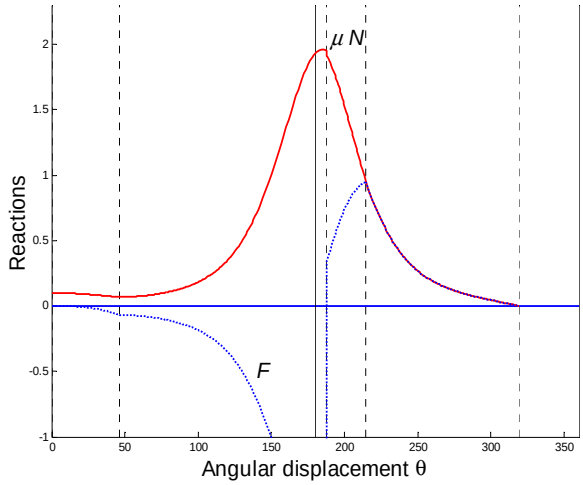

(b) : $\mu\mathcal{N}$ and $\mathcal{F}$

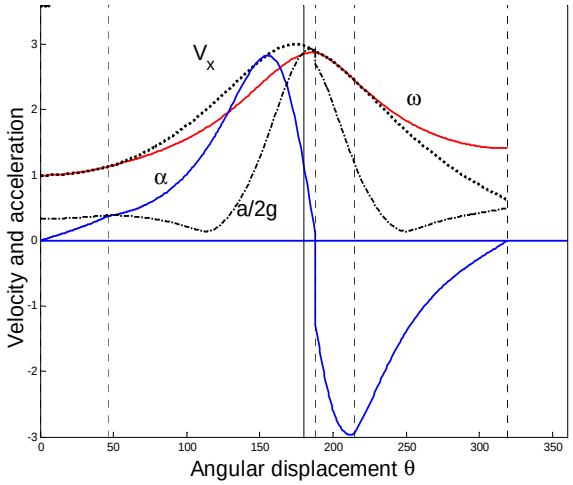

(c) : ω, α, $\mathcal{V}_x$ and a/g

Figure 5.12 : Case e, type MH - Medium friction, high velocity, $\mathcal{P}_0 = \{2/3,\ 0.3,\ 1.0\}$

5.5.6 Case f, type LH: Light friction with high velocity

Figure 5.5(b) shows that motion of type LH is not possible for $\gamma = 2/3$. However, a sufficient increase of the particle mass, and hence the eccentricity, does make this type of motion possible, as seen in Figures 5.6(b) and (c).

In the next example therefore the mass of the particle is increased to four times the hoop mass, giving $\gamma = 4/5$. Using a light friction and reasonably high initial velocity, case f in Table 5.2 is obtained, with parameters $\mathcal{P}_0 = \{4/5,\ 0.15,\ 0.75\}$, and the results are shown in Figure 5.13.

Figure 5.13(a) shows that the smaller initial velocity (compared to case e) results in peak 1 exceeding the value of μ so that both spinning phases occur in case f. The long skidding phase through the lowest point is very similar in the two cases; however, in case f the discontinuity at the end of the skidding phase needs to be limited to 2μ and the skidding changes to spinning without the intermediate rolling phase at position $\theta_4 = 217^\circ$. This issue will be explored in section 6.5.2. The total motion is labelled as `RSRD-S--- H`. This is also the pattern of case (13) in Figure 5.4(d), where the overlapping of the D1 and S2 regions corresponds with the instantaneous change from spin to skid. The extremely short rolling phase between the S1 and D1 regions is also noticeable.

Figure 5.13(b) shows a discontinuity in $\mathcal{N}$ as well as $\mathcal{F}$ at position θ_4; this is the first example where the discontinuity in $\mathcal{N}$ is noticeable in the scale being used.

Figure 5.13(c) shows very clearly how $\mathcal{V}_x$ changes from greater than ω to less than ω at position θ_4. Also note that the discontinuity in α is "outwards", in contrast to most other examples.

Note finally that the scales in Figure 5.13 (b) and (c) are different to those used in previous figures, in order to show the complete graphs for the large friction force and angular acceleration.

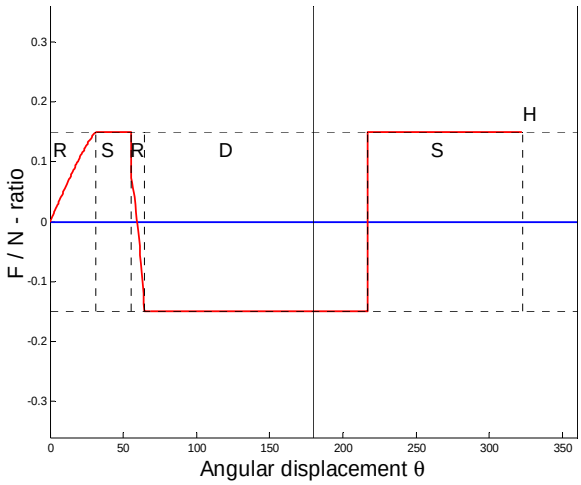

(a) : Ratio of $\mathcal{F}/\mathcal{N}$

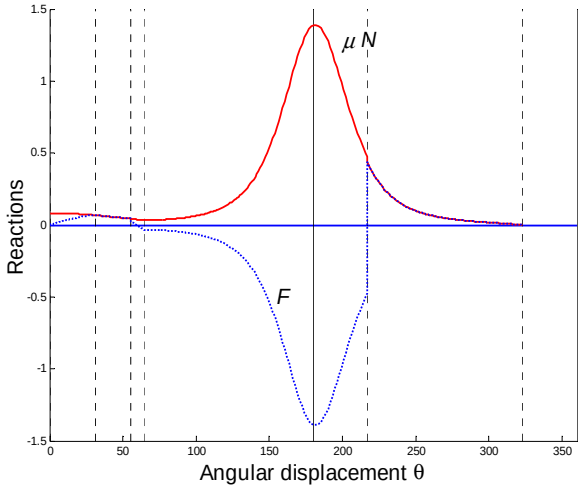

(b) : $\mu\mathcal{N}$ and $\mathcal{F}$

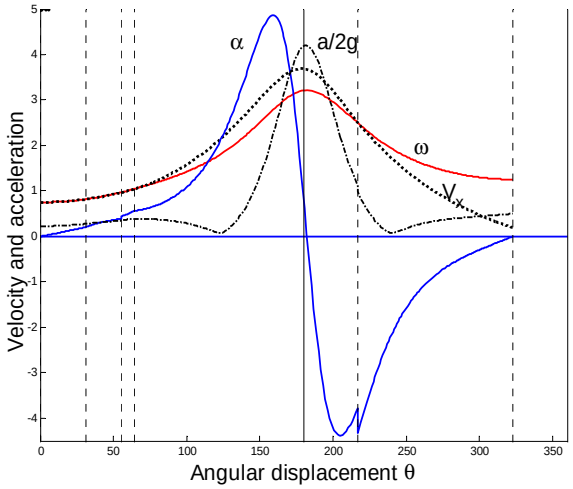

(c) : ω, α, $\mathcal{V}_x$ and a/g

Figure 5.13 : Case f, type LH - Light friction, high velocity,
$\mathcal{P}_0 = \{4/5,\ 0.15,\ 0.75\}$

5.5.7 Case g, type ML: Medium friction with low velocity

Finally, to complete the set of possible types of motion, we consider an example of type ML; as seen on Figure 5.6, this is again only found for heavy particles.

Keeping $\gamma = 4/5$, and selecting medium friction and very low initial velocity, case g in Table 5.2 is specified with parameters $\mathcal{P}_0 = \{4/5,\ 0.5,\ 0.02\}$; the results are shown in Figure 5.14.

Comparison between this case and case a, Figure 5.8, show that the behaviour in the two cases is basically the same. The only significant difference is that in case g the angular velocity becomes zero just before the particle reaches the top; $\omega_F = 0$ at $\theta_F = 357°$. In this case the total motion is labelled as `RDRSR-- Z`, which is not included in Table 5.2.

Note that the scales in Figure 5.14 are different to those used in previous figures.

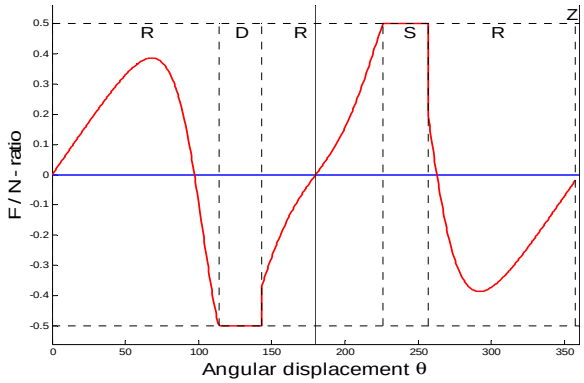

(a) : Ratio of $\mathcal{F}/\mathcal{N}$

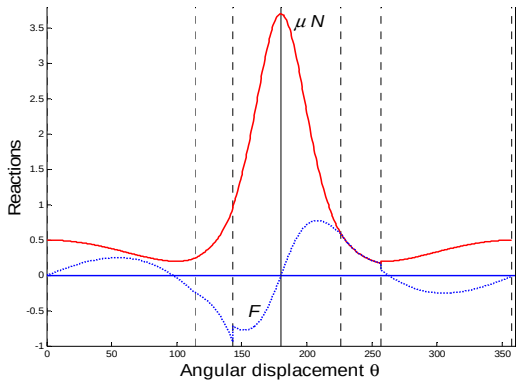

(b) : $\mu\mathcal{N}$ and $\mathcal{F}$

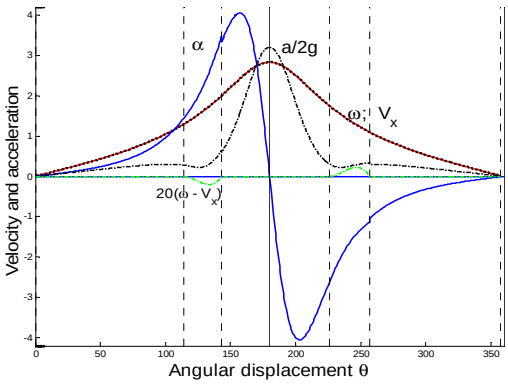

(c) : ω, α , $\mathcal{V}_x$ and a/g

Figure 5.14 : Case g, type ML - Medium friction, low velocity, $\mathcal{P}_0 = \{4/5,\ 0.5,\ 0.02\}$

5.6 Acceleration of the centre of gravity

Another interesting facet of a loaded hoop with large eccentricity is that extremely large accelerations occur in the vicinity of $\theta = \pi$. This phenomenon can be explained by noting that the moment of inertia about the contact point C is extremely small in this position in cases where $\gamma \to 1$; from (4.1) with $\theta = \pi$, $\kappa_C(\pi) = 2(1-\gamma)$. Division by this small value in equations (4.11) and (4.12) for rolling leads to very large velocities and accelerations, as also seen in all the examples shown in Figures 5.8 to 5.14.

The maximum value of a is obtained analytically in cases where the hoop *rolls* through position $\theta = \pi$ on a horizontal plane, as was shown in section 4.3.6. Three situations can be identified:

- In cases of heavy friction, as discussed in section 5.5.2 and shown in Figure 5.9, the maximum acceleration is found from (4.32) as

$$a_{max} = a(\pi) = g\,\gamma\left(\omega_0^2 + 2\gamma(1+\omega_0^2)/(1-\gamma)\right). \tag{5.2}$$

- In some cases of light and medium friction the hoop rolls through position $\theta = \pi$ and $a(\pi)$ is the maximum. In such cases the constant C is calculated from the numerical solution, and using (4.31)

$$a_{max} = a(\pi) = g\,\gamma(C+\gamma)/(1-\gamma).$$

  Figures 5.8 and 5.10, 5.11 and 5.14 illustrate this case.

- In other cases, the hoop can spin or skid through this position, and the maximum acceleration is found at an angle slightly larger than 180°. This maximum can still be extremely large, as can be seen on the graphs of a/g in Figures 5.12 and 5.13.

In Figure 5.15 the values of a_{max}/g are calculated numerically from the complete solution of the motion for all cases, and contours are drawn on the phase diagrams.

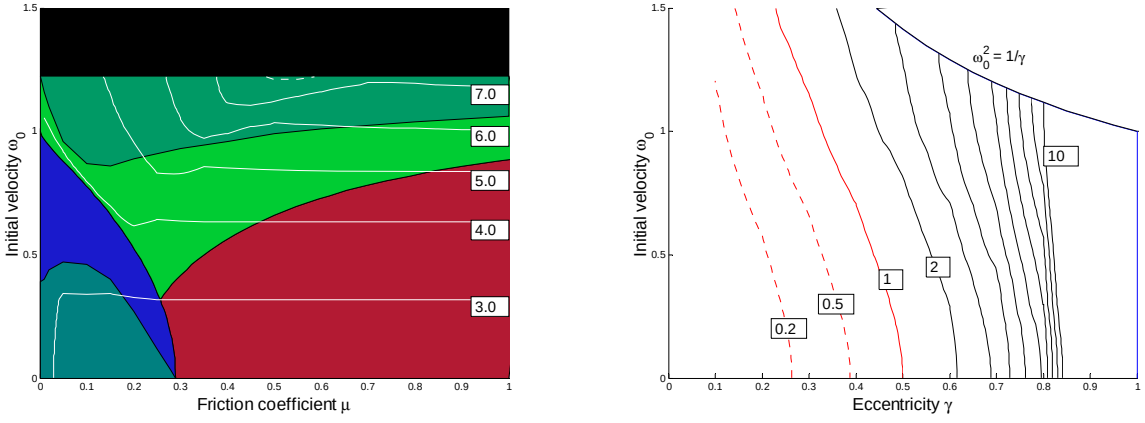

(a) (μ, ω_0)-plane for $\gamma = 2/3$ (b) (γ, ω_0)-plane for $\mu = 0.2$

Figure 5.15 : Phase diagrams showing contours of maximum a/g

Figure 5.15(a) shows the (μ, ω_0)-phase diagram for $\gamma = 2/3$, with contours for $a_{max}/g = 3,\ 4,\ \ldots\ 7$. For $\gamma = 2/3$, (5.2) reduces to $a_{max} = \frac{8}{3}(1 + \omega_0^2)$ g; in the heavy friction region the value of a_{max} is therefore independent of μ and the minimum value of a_{max} is $(8/3)\,g$, using $\omega_0 = 0$. This equation also shows the sensitivity of a_{max} to the initial velocity. These characteristics are clearly confirmed by Figure 5.15(a).

Similarly, the sensitivity of a_{max} to the eccentricity is clearly shown in Figure 5.15(b), which shows contours of a_{max}/g on the (γ, ω_0)-parameter space for $\mu = 0.2$. The values increase rapidly for large eccentricities, as seen from the contours for the values 1 to 10. Extremely large accelerations occur for $\gamma > 0.85$; for example, the numerical solution for $\omega_0 = 0$ and $\gamma = 0.9$ results in $a_{max} = 16.2\,g$. For $\gamma = 0.99$, a_{max} increases from $191\,g$ at $\omega_0 = 0$ to $208\,g$ at $\omega_0 = 1$.

Equation (5.2) and Figure 5.15(b) show that $a_{max} > g$ if $\gamma > 0.5$ for all positive initial velocities; i.e. the acceleration of the centre of mass exceeds g if the mass of the particle exceeds the mass of the hoop, provided that $\mu_s \geq 0.2$. For smaller eccentricities, $a_{max} > g$ if the initial velocity is large enough, as shown by the a/g-contour labelled 1 in Figure 5.15(b).

5.7 Summary and Conclusions

In the previous two chapters the dynamic behaviour of a rigid hoop rolling on a rough horizontal surface while loaded by a heavy particle on its rim has been analysed in great detail. A simplified model, in which the moment of inertia of the particle round its own axis is ignored, is used for all the numerical results. The results are for motion on a horizontal plane and for cases where the distinction between static and kinetic friction is ignored. In all cases the initial conditions are chosen so that the motion starts with a rolling phase. This results in a model for which the motion is defined by only three parameters, namely the eccentricity γ, the friction coefficient μ and the initial angular velocity ω_0.

Analytical solutions are obtained for the equations for rolling, and numerical solutions based on MATLAB's ODE45 function are obtained for the slipping phases.

The motion consists of a sequence of a maximum of five rolling phases alternating with spinning and skidding phases. The different phases are clearly recognised on graphs of the $\mathcal{F}/\mathcal{N}$-ratio plotted against position θ. These phases are labelled `R`, `S` and `D` respectively, and together with the labels `H`, `T` and `Z` for the possible final conditions a convenient method for describing the different patterns of motion is defined.

Phase diagrams in the (θ, ω_0)-parameter space are particularly useful in identifying the different patterns. Twenty-five different patterns are identified and listed in Table 5.2.

A primary classification scheme is introduced to differentiate between different types of motion. This scheme defines motion with light, medium or heavy friction, depending on whether the first rolling phase changes to spinning, to skidding or continues through one full rotation. This classification is clearly shown on phase diagrams in the (μ, ω_0)-parameter space.

These phase diagrams clearly show that an increase in the friction coefficient or a decrease in the eccentricity causes an increase in the region of heavy friction and a decrease in the region of light friction.

When this classification is combined with the three possible final conditions, seven different primary types of motion are identified. Detailed results are given in graphical form for one example of each type.

A few results are shown to illustrate that this is a "faster than gravity" model. For $\mu_s \geq 0.2$ the acceleration of the centre of mass exceeds g if the mass of the particle exceeds the mass of the hoop.

Chapter 6

Additional results for rigid hoops

Further insight into the behaviour of rigid hoops is obtained in this chapter, with some emphasis on identifying new patterns of motion.

The effect of the eccentricity is shown in a new type of phase diagram, and the effect of lifting the simplifying assumptions that were used in chapter 5 is shown in sections 6.2 to 6.4 .

A number of aspects affecting the patterns are discussed, and new insights are gained by considering the total energy of the system.

In this chapter all references to the list of patterns will be to Table 6.2 in section 6.7. This includes all the patterns previously listed in Table 5.2, plus a number of additional patterns identified in Chapter 6.

6.1 Effect of the eccentricity - Phase diagrams in (γ, ω_0)-space

The effect of the eccentricity has been shown to some degree in the previous work, inter alia in Figures 5.5 and 5.6, where phase diagrams in (μ, ω_0)-space are shown for four different eccentricities. This aspect is shown more completely in Figure 6.1 below, where phase diagrams showing the primary classification of the types of motion in (γ, ω_0)-space are shown for the full range of $\gamma \in [0, 1)$ for two values of the friction coefficient and a horizontal surface.

In Figure 6.1(a) the value $\mu = 0.2$ is used, and six of the seven primary regions are identified. These regions clearly correspond to previous results; for example, heavy friction only occurs for small eccentricities and light friction for larger eccentricities.

The region where the hoop hops immediately for large velocities is now demarcated by the curve $\omega_0 = \sqrt{1/\gamma}$, between the points $(4/9, 1.5)$ and $(1, 1)$.

In Figure 6.1(b) the value $\mu = 0.4$ is used. In this case there is no overlapping between the heavy friction and light friction regions, and the medium friction region extends down to the zero velocity line. The missing primary type, namely type ML labelled `RD* Z`, is now present.

An aspect that has not been noticeable previously is that the region of type LH, labelled `RS* H`, extends down to zero initial velocity when the eccentricity is close to the limit of 1, i.e. as $m_h \to 0$. Numerical solutions show that for $\gamma \geq 0.981$ and $\omega_0 = 0$, a motion not found previously, labelled `RS-DRS-- H` is obtained. For larger initial velocities a motion labelled

`RS-D-S-- H` is obtained. These patterns are listed in Table 6.2.

Also note that heavy friction occurs for very large initial velocities if the eccentricity is small, as is to be expected on physical grounds.

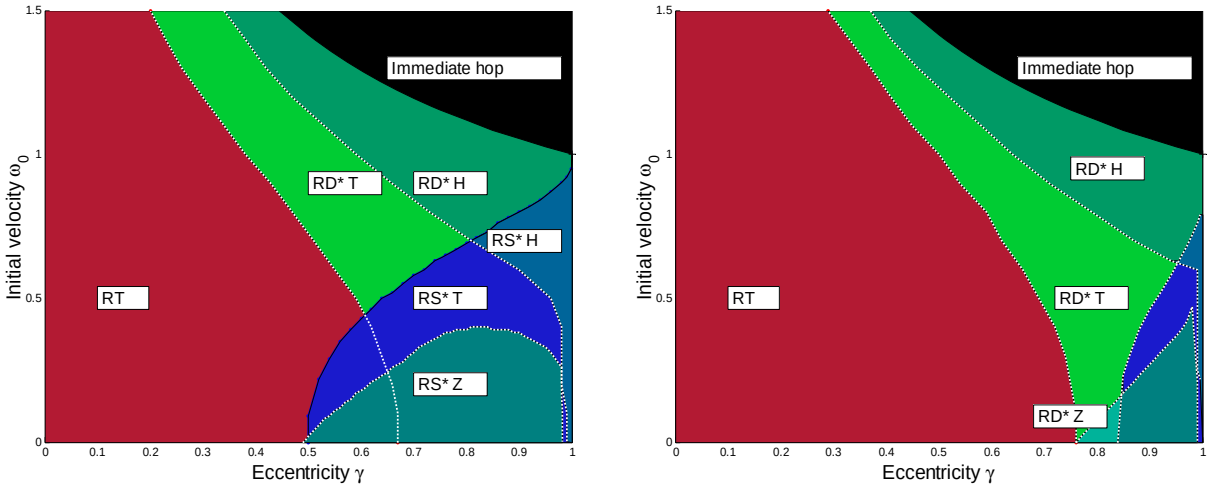

(a) $\mu = 0.2$ (b) $\mu = 0.4$

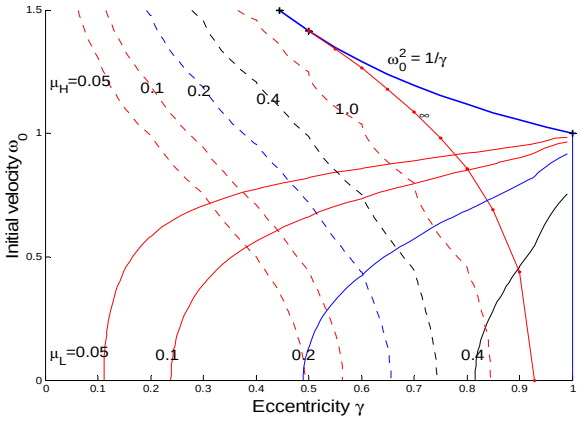

(c) Contours of μ_H and μ_L

Figure 6.1 : Phase diagrams in (γ, ω_0)-space.

Figure 6.1(c) shows contours of μ_H and μ_L on the (γ, ω_0)-plane. Note that these contours are used to define the three primary regions of heavy, medium and light friction.

The dotted curves show $\mu_H = 0.05, 0.1, 0.2, 0.4, 1$. Note that the curves for $\mu_H = 0.2$ and 0.4 correspond to the boundary of the heavy friction region in Figures (a) and (b) respectively. The value of μ_H tends to infinity on the curve marked ∞, which is the curve where the first minimum of $\mathcal{N}$ equals zero, as previously seen in Figure 4.4.

The solid curves in Figure 6.1(c) show $\mu_L = 0.05, 0.1, 0.2, 0.4$. The maximum value is obtained at point $(0.99, 0)$, where $\mu_L = 0.779$; the implication being that the region for light friction does not exist for larger values of the friction coefficient. The curves for $\mu_L = 0.2$ and 0.4 correspond to the boundary of the light friction region in Figures (a) and (b) respectively.

6.2 Effect of kinetic friction

No distinction was made between the static and kinetic friction coefficients in all the previous numerical results. The effect of making this distinction is investigated in this section. Two medium velocity examples, cases b and c, are repeated here, but with $\mu_k = 0.9\mu_s$.

Figure 6.2(a) shows the $\mathcal{F}/\mathcal{N}$-curve for case a, type MM, previously shown in Figure 5.8. The only real effect in this case is the discontinuity in $\mathcal{F}$, as shown on the $\mathcal{F}/\mathcal{N}$-curve, at the positions where rolling changes to skid or spin. The smaller loss in energy during the slipping phases does affect the numerical values, but not the pattern of the motion. This is the normal situation for almost all cases.

However, in cases with large discontinuities such as Δ_3 in case c, Figure 5.10, the effect of the smaller kinetic friction may result in the loss of a rolling phase, as seen by comparing Figures 5.10(a) and 6.2(b), where the pattern changes from `RSRDRSRDR T` to `RSRDRS-DR T`. This will occur at all discontinuities where the rolling curve passes between the values of μ_s and μ_k.

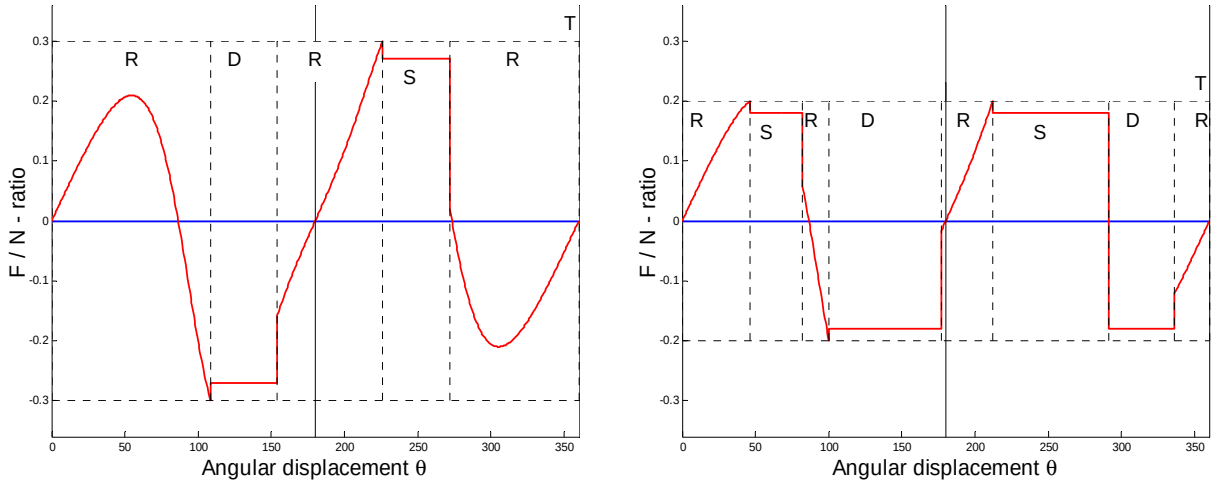

(a) Case a, type MM

(b) Case c, type LM

Figure 6.2 : $\mathcal{F}/\mathcal{N}$-diagrams showing the effect of kinetic friction.

6.3 Effect of the slope

Some results showing the effect of increasing the slope to 10° are shown in Figure 6.3, for the case $\gamma = 2/3$ and keeping $\mu_k = \mu_s$ and $\epsilon = 0$.

Figure 6.3(a) shows the (μ, ω_0)-phase diagram.The corresponding regions of the primary classification for the horizontal plane, Figure 5.5, are shown by the white dotted lines. The most noticeable effect of the slope is the increase in the region of medium friction, with both the regions of light and heavy friction being reduced. Comparison of Figures 6.3(a) and 5.5 also show that when $\psi = 10°$ the region for high velocity is larger than the corresponding region for the horizontal plane. This is explained by the fact that the increase in kinetic energy as the hoop rolls down the slope makes it "easier" to hop and that hopping therefore occurs with lower initial velocities.

The white region in Figure 6.3(a) indicates parameter values for which it is impossible for the hoop to start with a rolling motion if $\mathcal{V}_{x0} = \omega_0$, but will start slipping immediately. It was previously shown in section 4.3.1 that the initial condition $\mathcal{V}_{x0} = \omega_0$ ensures rolling provided that $\mu_s \geq \hat{\mu}$ as defined in equation (4.21). This definition is repeated here:

$$\hat{\mu} = \frac{(1-\gamma)\,\sin\psi}{2(\cos\psi - \gamma\,\omega_0^2)}. \tag{6.1}$$

To reiterate, $\hat{\mu}$ is the *minimum friction coefficient* required to ensure initial rolling for given ψ, γ and ω_0, assuming $\mathcal{V}_{x0} = \omega_0$ and $\epsilon = 0$.

Using (6.1), the curve given by

$$\omega_0 = \sqrt{(2\mu_s\,\cos\psi - (1-\gamma)\sin\psi)/(2\mu_s\,\gamma)}$$

separates the region where initial rolling occurs from the region of initial slipping. The region of initial slipping is shown by the white region in Figure 6.3(a).

For $\omega_0 = 0$, limits for the slope and friction coefficient are obtained by simplifying (6.1) to

$$\tan\psi \leq 2\mu_s\,/(1-\gamma) \quad \text{or} \quad \mu_s \geq \tfrac{1}{2}(1-\gamma)\,\tan\psi. \tag{6.2}$$

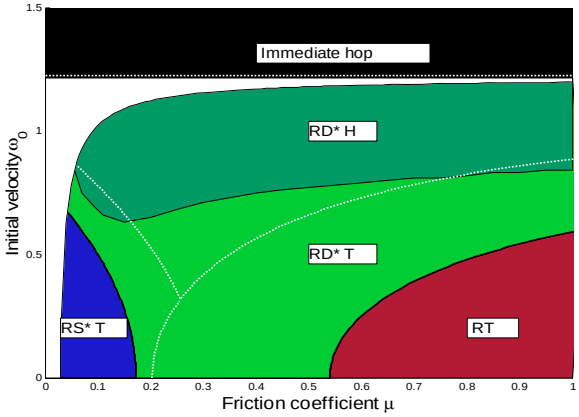

(a) : (μ, ω_0)-space, for $\gamma = 2/3$ and $\psi = 10°$

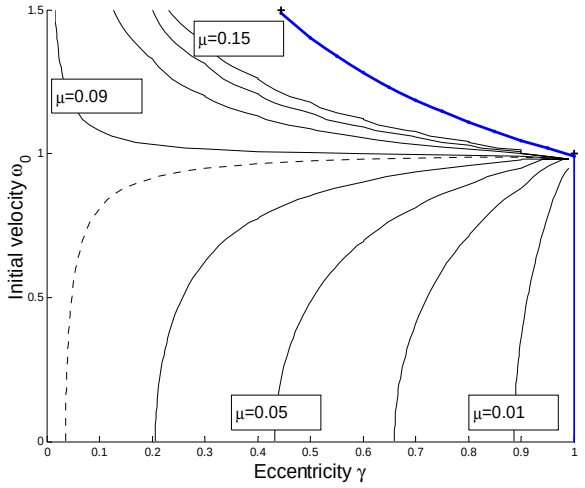

(b) : Contours of $\hat{\mu}$ on (γ, ω_0)-space for $\psi = 10°$

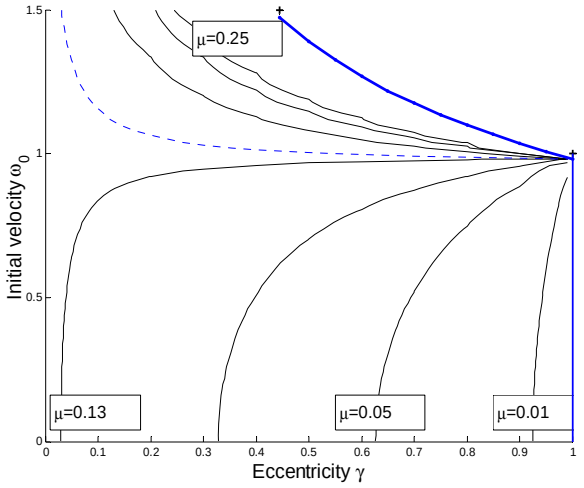

(c) : Contours of $\hat{\mu}$ on (γ, ω_0)-space, for $\psi = 15°$

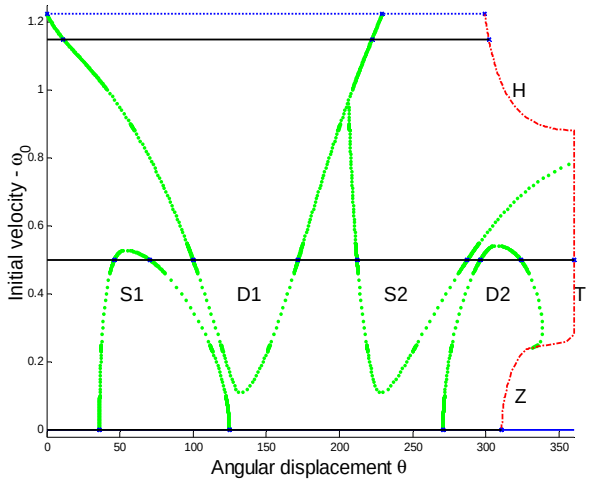

(d) : (θ, ω_0)-space for $\gamma = 2/3$, $\mu = 0.2$ and $\psi = 0°$

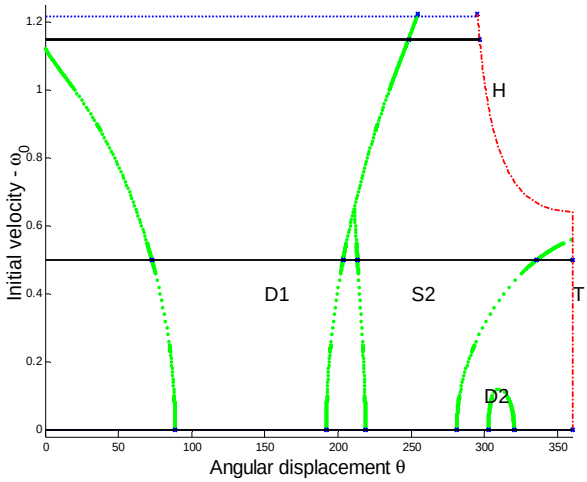

(e) : (θ, ω_0)-space for $\psi = 10°$

Figure 6.3 : Phase diagrams illustrating the effect of increasing the slope ψ.

Figure 6.3(b) shows contours of $\hat{\mu}$ on the (γ, ω_0) parameter space for a slope of $\psi = 10°$, using (6.1). Contours are shown by light solid curves for $\hat{\mu} = 0.01, 0.03, ...0.15$. The heavy curve between the points (4/9, 1.5) and (1, 1) is the curve for $\hat{\omega}_0$, demarcating the region of immediate hopping as before.

Clearly, $\hat{\mu} = 0$ for $\gamma = 1$ and/or $\psi = 0$, provided that $\omega_0 < \hat{\omega}_0$. Also, for $\gamma = 0$, $\hat{\mu}(0) = \frac{1}{2}\tan(\psi) = 0.08816$. This value separates the cases which are defined for $\omega_0 = 0$ from those that

are not. This is illustrated in Figure 6.3(b) by the dotted curve for the contour $\hat{\mu} = 0.085 < \hat{\mu}(0)$ and the solid curve for $0.09 > \hat{\mu}(0)$.

Figure 6.3(c) shows similar contours, with intervals of 0.04, for a slope of $\psi = 15°$. The values of $\hat{\mu}$ are significantly larger than for $10°$, as could be expected because preventing slipping now requires larger friction coefficients. Now $\hat{\mu}(0) = 0.134$, as illustrated by the solid curve for $\hat{\mu} = 0.13$ and the dotted curve for 0.14.

The effect of ψ on the (θ, ω_0)-phase diagrams is shown in Figures 6.3(d) and (e), drawn for $\mu = 0.2$ and $\gamma = 2/3$. Figure (d), for $\psi = 0°$, is similar to the previously shown diagrams in Figure 5.4. Comparing Figure 6.3(e), for $\psi = 10°$, with (d), it is clear that all the humps have shifted downwards and that the S1 hump has disappeared. Therefore no cases of light friction are possible for these parameter values, and the patterns listed in Table 6.2 as patterns 2 and 4 are obtained for $\omega_0 = 0$ and 0.5. Also, the Z-curve has disappeared.

Two interesting *new* patterns falling outside the previous classification scheme are found for high velocities. Figure 6.3(e) shows that the initial rolling phase does not exist for $\omega_0 \geq 1.13$, assuming the previous initial condition that $\mathcal{V}_{x0} = \omega_0$. The horizontal line for $\omega_0 = 1.15$ shows a new pattern labelled `-D-S--- H`; i.e. the hoop skids from the start. By increasing the friction coefficient to 0.4 the rolling phase between the D1 and S2 humps reaches to the top of the diagram and pattern `-DRS--- H` is obtained.

An additional feature of motion down a slope is that low velocity cases ending with zero angular velocity (Z-curve) do not exist for $\psi > 4.5°$. This was found by numerical experimentation, using the extreme values of $\gamma = 0.99$, $\mu = 1$ and $\omega_0 = 0$.

6.4 Massless hoops

In this section we return to the problem analysed in Chapter 3, namely a massless hoop, $\gamma = 1$, loaded with a particle and rolling on a horizontal plane, $\psi = 0$, and consider the problem in the context of the solutions developed in the chapters on rigid hoops. The main question is whether the hoop can hop while the particle is moving downwards.

6.4.1 Analytic results for Littlewood's hoop

Littlewood's hoop is characterised by the condition that $I_G = 0$. This is the case for a massless hoop loaded with a point particle with centre on the rim of the hoop and zero dimension; i.e. $\gamma = 1$ and $\epsilon = 0$. The geometric factors in (4.1) now become

$$\mathcal{H} = 1 + \cos\theta\,; \quad \kappa_G = 0\,; \quad \kappa_C = 2\mathcal{H} = 2(1 + \cos\theta). \tag{6.3}$$

Now $\kappa_C(\pi) = 0$ and, very significantly, $I_G = 0$. Therefore Newton's second law requires that the torque around G always be zero, but provides no information whatsoever about the angular acceleration.

The previous solution for rolling motion of a rigid hoop also applies for the massless case, so that (4.12) and (4.11) simplify to

$$\omega^2 = 2\,(C_0 - \cos\theta)\,/\,\kappa_c = (C_0 - \cos\theta)\,/\,(1 + \cos\theta); \qquad \alpha = (\omega^2 + 1)\,\sin\theta\,/\,\kappa_c.$$

Using $C_0 = 2\omega_0^2 + 1$ in (4.24) and (4.26) from section 4.3.2, the expressions for the reactions simplify to

$$\mathcal{F} = \tfrac{1}{2}\,\sin\theta\,(1-\omega^2) = (\cos\theta - \omega_0^2)\,\tan(\theta/2); \qquad \mathcal{N} = \mathcal{H} - \tfrac{1}{2}(C_0+1) = \cos\theta - \omega_0^2.$$

These equations are exactly the same as the corresponding equations (3.11) to (3.14) in Chapter 3. Also note that $\mathcal{F}/\mathcal{N} = \tan(\theta/2)$, thus satisfying the requirement of zero torque around G for $\theta < \pi$.

In Littlewood's original problem $\omega_0 = 0$, so that the normal reaction becomes zero at $\theta_* = \pi/2$, provided that $\mu > \tan(\theta_*/2) = 1$ to prevent slipping.

If $\mu < 1$ the hoop will slip at a position $\theta_s < \pi/2$. Using $\gamma = 1$, $\epsilon = 0$ and $\psi = 0$ in (4.13), the differential equation governing slipping motion of a rigid hoop, we obtain

$$\frac{\mathrm{d}\omega^2}{\mathrm{d}\theta} = \frac{2S\,(1-\omega^2\,\cos\theta)}{S\,\sin\theta} = \frac{2\,(1-\omega^2\,\cos\theta)}{\sin\theta} = 2\,\csc\theta - 2\omega^2\,\cot\theta.$$

This is precisely the same as the differential equation (3.22) for skimming motion obtained in Chapter 3. As before, this equation is only valid for $\theta < \pi$. Note that $\kappa_G = 0$ results in the cancellation of the slip factor $S = \sin\theta - \mu\,(1+\cos\theta)$, provided that $\theta \neq \pi$.

We therefore conclude that for $\theta < \pi$, the equations governing the motion of a rigid hoop are also applicable to Littlewood's hoop. The solution algorithm for the rigid hoop must be adapted to account for the case when rolling changes to skimming at the point where $\mathcal{N}$ becomes zero. However, as discussed in Chapter 3, this is not a proof that Littlewood's hoop cannot hop.

6.4.2 Numerical results for Pritchett's hoop

In this section the previously used algorithm for rigid hoops will be used to obtain results for Pritchett hoops; i.e. for hoops loaded with small bodies for which the parameter ϵ is *not* zero. Now the restriction that $\theta < \pi$ can be lifted.

Using the parameters $\gamma = 1$, $\mu_s = 1$ and $\psi = 0$, with initial angular velocity $\omega_0 = 0$, the effect of different values of ϵ is investigated.

In Figure 6.4(a) the angular velocity ω is shown as a function of θ. The solid curve shows the values obtained for Littlewood's hoop with $\epsilon = 0$, from the analytic solution using (3.12) and (3.23) to calculate ω. The heavy dotted curve is the numerical solution for $\epsilon = 0.1$, and the lightly dotted curves show the values obtained for $\epsilon = 0.01$, 10^{-3} and 10^{-6}.

The angular velocity obtained from the numerical solution for $\epsilon \leq 0.01$ is barely distinguishable from that obtained for Littlewood's hoop. This value tends to ∞ for $\theta = \pi$ and $\epsilon = 0$, as seen from the analysis in the previous section.

Figures 6.4(b) and (c) are graphs of the numerical solutions for $\mathcal{N}$. The solid curve shows the values obtained from the analytic solution above for Littlewood's hoop, becoming zero at $\theta_* = 90^\circ$, and remaining zero till $\theta = 180^\circ$. As shown in Chapter 3, the particle hits the surface at this point, resulting in a large impulse in the reaction force. Figures (b) and (c) show that this impulse is modelled by the dotted curves obtained from the numerical solutions using $\epsilon = 0.1$, 0.01, 10^{-3} and 10^{-6}. The maximum value of $\mathcal{N} \to \infty$ as $\epsilon \to 0$; for example, with $\epsilon = 10^{-6}$, $(\mathcal{N})_{max} = 2.03 * 10^6$. We therefore conclude that the numerical solution for sliding of a Pritchett hoop tends to the analytic solution for skimming as $\epsilon \to 0$.

Figures (b) and (c) also show that the reaction never becomes zero and that a Pritchett hoop *cannot hop* for $\theta < 180°$.

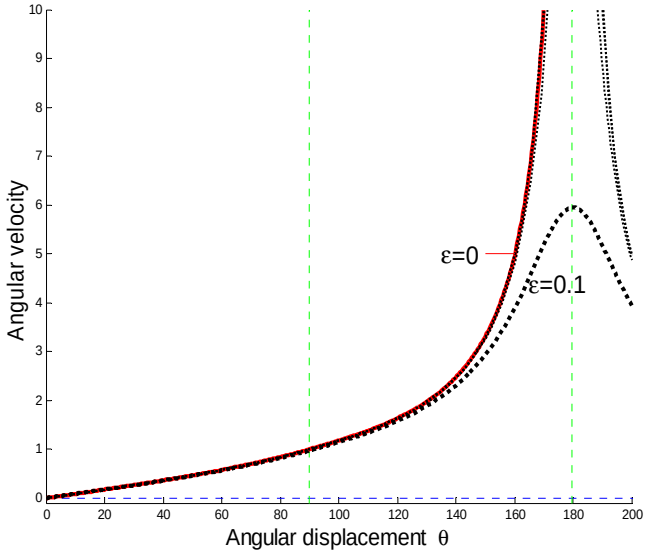

(a) Angular velocity ω

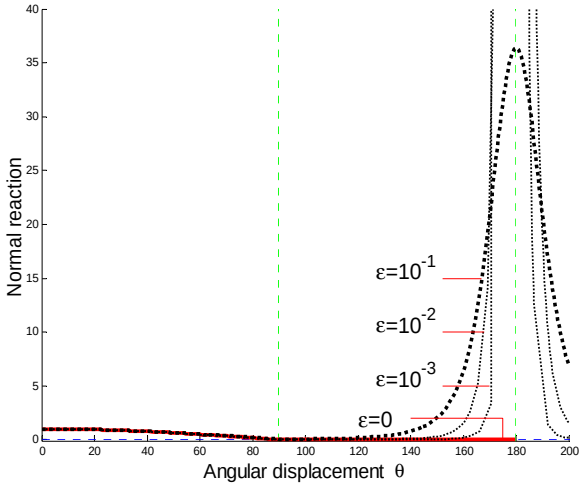

(b) Normal reaction $\mathcal{N}$

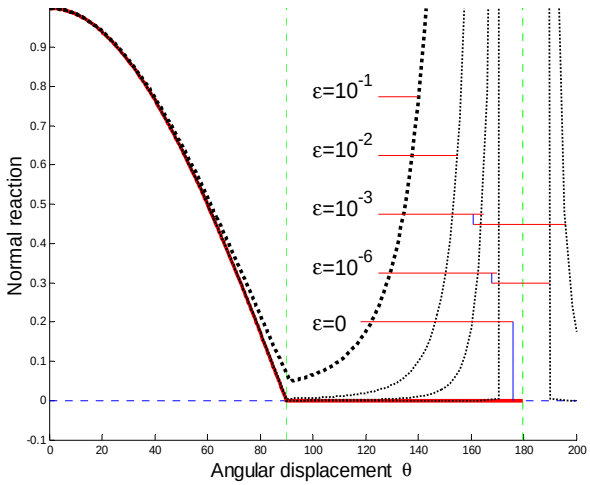

(c) Normal reaction $\mathcal{N}$ (larger scale)

Figure 6.4 : Graphs for $\gamma = 1$ and $\epsilon = 0,\ 10^{-1},\ 10^{-2},\ 10^{-3},\ 10^{-6}$.

6.5 Aspects affecting the patterns

In the previous chapter one example was given for each of the seven primary types of motion. For most of these types there are a number of different patterns for the intermediate phases; two aspects affecting these intermediate phases are discussed in the next two sections.

6.5.1 Symmetry - normal and unusual patterns

Careful consideration of the seven examples on a horizontal surface shown in the previous chapter show that the different patterns of motion are determined mainly by the friction coefficient, in the sense that whether the friction coefficient is smaller or greater than the values of the four peaks in the rolling curve determines whether a slipping phase occurs or not.

As discussed previously, the magnitude of these peaks have the property that they are skew-symmetric; in cases of heavy friction, peaks 1 and 4 have the same magnitude, as do peaks 2 and 3; in other cases the magnitudes differ slightly, due to loss of energy during the slipping phases. This skew-symmetry implies that in most cases the rolling curve has the following characteristics:
. if peak 1 is greater (less) than μ, then peak 4 is greater (less) than μ;
. if peak 2 is greater (less) than μ, then peak 3 is greater (less) than μ.

In terms of the humps in Figure 5.4, this implies that if a line representing a motion hits (misses) the S1 hump, it will also hit (miss) the D2 hump; similarly, the middle humps (D1 and S2) will normally both be hit or both be missed.

Patterns, that have these characteristics, will be termed *normal patterns*, with the implication that in these cases spinning and skidding phases alternate. Patterns that are exceptions to the above will be termed *unusual*. Patterns 2 and 3 in Table 6.2 are unusual in that the S1 phase is missed, but not the D2. Patterns 20 and 21 in Table 6.2 are unusual in that the D1 phase is missed, resulting in consecutive spinning phases. No cases of consecutive skidding phases have been found.

Figure 6.3(e) for $\psi = 10^\circ$ shows that unusual patterns occur for low velocities because the S1-hump is missing, similar to pattern 2 in Table 6.2.

6.5.2 The discontinuities in the rolling curve

As seen in the examples above, the graph of the $\mathcal{F}/\mathcal{N}$-ratio contains a discontinuity at each point where a slipping phase comes to an end; these will henceforth be referred to as Δ_1, Δ_2, Δ_3 and Δ_4 for the discontinuity at the end of the first spin, first skid, second spin and second skid respectively.

The magnitude of these discontinuities determines whether a rolling phase separates two slipping phases or not. The normal situation here is that the magnitude of the discontinuity is smaller than 2μ, in which situation the rolling phase exists; in extreme cases $\Delta_* > 2\mu$ in which situation spin changes to skid instantaneously without the intermediate rolling phase, or vice versa. The presence or absence of these intermediate rolling phases gives rise to a great number of different motions, as will be shown later.

In terms of the (θ, ω_0)-phase diagrams in Figure 5.4, the overlapping of two humps shows that the intermediate rolling phase does not exist; i.e. the overlapping occurs where the discontinuity exceeds 2μ.

In section 4.3.8 some results for a concentric hoop were obtained. On a horizontal plane $\mathcal{N}$ now equals unity for the complete motion. If $\mathcal{V}_x(0)$ is taken as zero and the motion starts with initial spinning, the analysis shows that a discontinuity of magnitude $\mu_k mg$ occurs in the friction force at the point where spinning changes to rolling, namely at position $\theta_1 = \frac{3}{8}\omega_0^2/\mu$. In this case therefore the graphs of $\mathcal{F}$ and $\mathcal{F}/\mathcal{N}$ are identical, and equal to zero during the rolling phase.
Figure 6.5 was obtained by using the initial condition $\mathcal{V}_x(0) = 0$ in the standard program for rigid hoops with $\mathcal{P}_0 = \{0,\ 0.1,\ 0.5\}$. The graph for $\mathcal{F}/\mathcal{N}$ clearly shows that $\Delta_1 = -\mu$ at position $\theta_1 = 53.7°$, in agreement with the analytical results mentioned above.

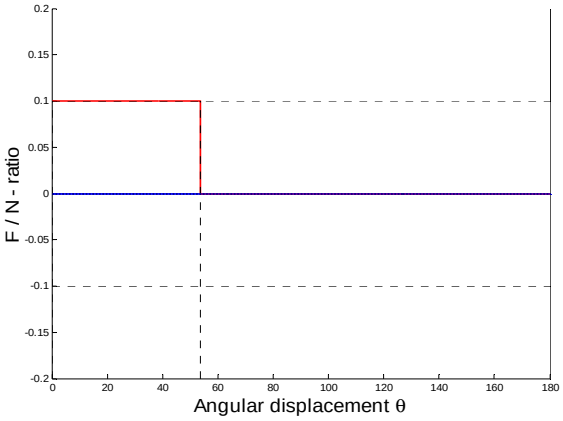

Figure 6.5 : $\mathcal{F}/\mathcal{N}$-ratio for a concentric hoop

This is the only result given in this dissertation for a rigid hoop with an initial condition other than $\mathcal{V}_x(0) = \omega_0$. Increasing μ decreases the length of the spinning phase; increasing ω_0 lengthens this phase.

With loaded hoops the magnitude of Δ_1 can vary between almost zero to greater than 2μ, as seen in the graphs of the $\mathcal{F}/\mathcal{N}$-ratio in all the previous examples. In Figure 6.6 below the different facets of this phenomenon are illustrated with four examples.

Firstly, Figure 6.6(a) shows the graph of the $\mathcal{F}/\mathcal{N}$-ratio for case c, $\mathcal{P}_0 = \{2/3,\ 0.2,\ 0.5\}$; in this case Δ_1 is small. Super-imposed on this graph is a dotted curve representing the rolling curve with the same initial conditions; this will be referred to as the *initial rolling curve*. Note that the true $\mathcal{F}/\mathcal{N}$-ratio seems to drop down to the rolling curve and then follows it for the second rolling phase.

In Figure 6.6(b) the graphs are drawn for a smaller initial velocity, $\mathcal{P}_0 = \{2/3,\ 0.2,\ 0.2\}$, which is the previous case d. This results in a much larger discontinuity with Δ_1 almost equal to 2μ. Note that the true $\mathcal{F}/\mathcal{N}$-ratio drops down to very near the initial rolling curve; however, due to the loss of energy during the spinning phase, the graph for the second rolling phase is as shown by the thin solid curve. The true $\mathcal{F}/\mathcal{N}$-graph then follows this new rolling curve for a short rolling phase until skidding commences at peak 2.

Figure 6.6(c) shows an example similar to case d, but the initial velocity is reduced to 0.1; i.e. $\mathcal{P}_0 = \{2/3,\ 0.2,\ 0.1\}$. The second rolling curve now misses peaks 2 and 3, and skidding only commences at peak 4, giving a motion labelled `RSR----D- Z` which will be discussed again later.

Figure 6.6(d) is for a smaller friction coefficient, with the same initial velocity as in Figure 6.6(b), i.e. for $\mathcal{P}_0 = \{2/3,\ 0.18,\ 0.2\}$. This results in a discontinuity where $\Delta_1 > 2\mu$; as this is not possible on physical grounds, the hoop starts skidding immediately, without the intermediate rolling phase. The first phases are therefore labelled `RS-D*`; a number of examples are listed in

Table 6.2 as reference numbers 26 to 35; these include all those cases in Figures 5.4(c) and (d) where the S1 and D1 humps overlap.

Figures (a), (b) and (d) show that a discontinuity Δ_2 occurs at the end of the skid, where the $\mathcal{F}/\mathcal{N}$-ratio "jumps up" to a third rolling curve, corresponding to the energy after the end of the skidding phase. This third curve is however not shown here, as it is barely distinguishable from the first two rolling curves with the scale being used. Similar arguments hold for the third and fourth discontinuities Δ_3 and Δ_4.

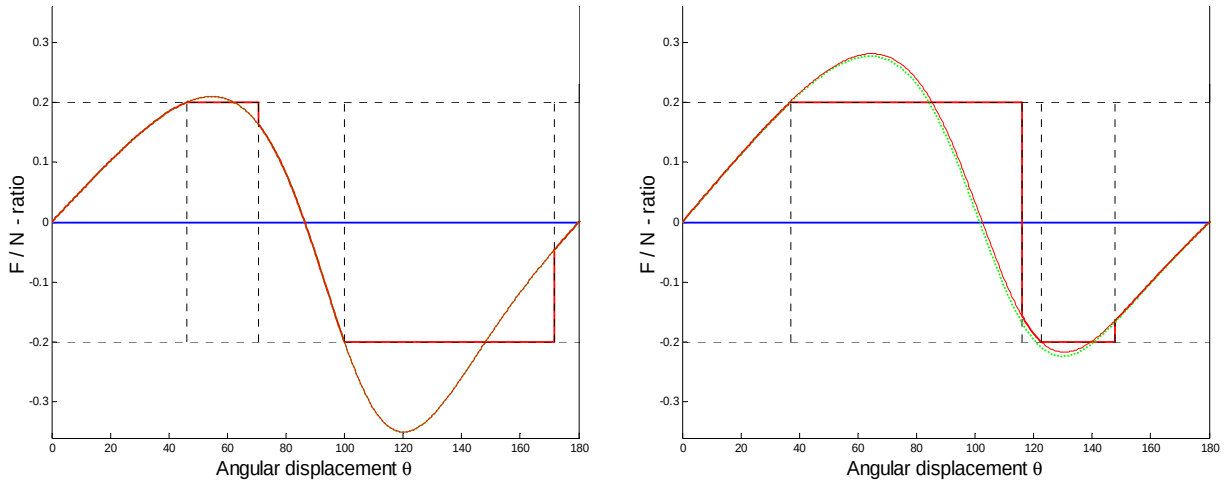

(a) : $\mathcal{P}_0 = \{2/3,\ 0.2,\ 0.5\}$

(b) : $\mathcal{P}_0 = \{2/3,\ 0.2,\ 0.2\}$

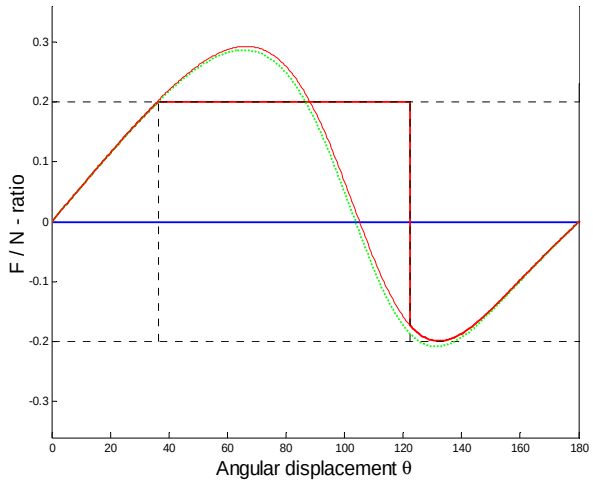

(c) : $\mathcal{P}_0 = \{2/3,\ 0.2,\ 0.1\}$

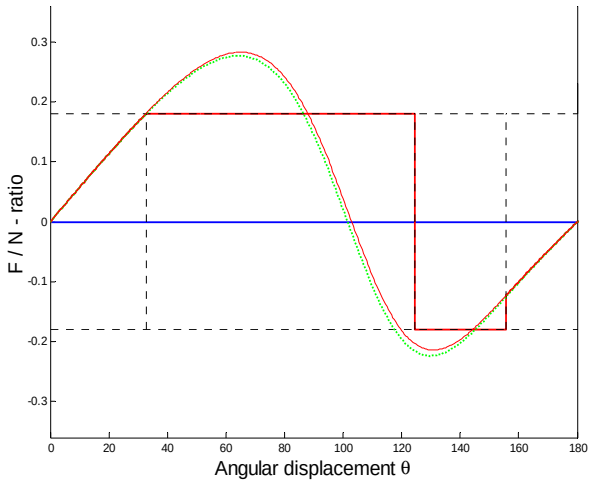

(d) : $\mathcal{P}_0 = \{2/3,\ 0.18,\ 0.2\}$

Figure 6.6 : Four examples of Δ_1, the first discontinuity in $\mathcal{F}/\mathcal{N}$

6.5.3 Energy associated with the discontinuities

The second, third and fourth rolling curves are computed in terms of the total energy of the hoop at the start of that rolling phase. The total energy is given by (4.8) and (4.9); in the case of the simplified model with a rolling start these simplify to

$$\mathcal{E}_1 = (1+\gamma)(\cos\psi + \omega_0^2); \quad \mathcal{E} = (1+\gamma\cos\theta)(\cos\psi+\omega^2) - \mathcal{X}\sin\psi. \tag{6.4}$$

Here $\mathcal{E}_1$ is the initial energy, which is the total energy (potential plus kinetic) during the first rolling phase, and $\mathcal{E}$ is the total energy at a position θ.

In the case of the horizontal plane, and defining $\mathcal{E}_0$ as the initial potential energy, this simplifies further to

$$\mathcal{E}_0 = (1+\gamma); \quad \mathcal{E}_1 = (1+\gamma)(1+\omega_0^2); \quad \mathcal{E} = (1+\gamma\cos\theta)(1+\omega^2). \tag{6.5}$$

The initial angular velocity which is required to produce the second rolling curve, ω_{02}, can now be calculated from the total energy at the position where the spinning phase ends, which is

$$\mathcal{E}_2 = (1+\gamma\cos\theta_r)(1+\omega_2^2).$$

Then

$$\omega_{02}^2 = (\mathcal{E}_2/\mathcal{E}_0) - 1.$$

In cases where $\mathcal{E}_2 < \mathcal{E}_0$ this implies negative kinetic energy, as discussed below for case (c).

These values are shown below in Table 6.1, together with other values calculated from the above equations. The tabulated values of θ_1, θ_2 and ω_2 are obtained from the numerical solution for the different cases. The last column shows the value of $\Delta_1 = \mu - (\mathcal{F}/\mathcal{N})_2$, where $(\mathcal{F}/\mathcal{N})_2$ is the value of the second rolling curve at position θ_2.

The initial potential energy is the same for all four cases and is not shown in the table; the value is $\mathcal{E}_0/mgr = 1+\gamma = 5/3$.

Fig.	μ	ω_0	ω_{02}	$\mathcal{E}_1$	$\mathcal{E}_2$	ω_2	$\theta_1(^\circ)$	$\theta_2(^\circ)$	$\theta_2-\theta_1$	Δ_1
a	0.2	0.5	0.499	2.0833	2.0831	0.84	46.2	70.6	24.4	0.0368
b	0.2	0.2	0.163	1.7333	1.7112	1.19	37.0	116.0	79.0	0.3563
c	0.2	0.1	-	1.6833	1.6521	1.25	36.3	122.4	86.1	0.373
d	0.18	0.2	0.145	1.7333	1.7019	1.32	32.8	124.4	91.6	0.383

Table 6.1 : Energies associated with Δ_1, for $\gamma = 2/3$

Note that in case (c) the loss in energy due to the spin reduces the total energy to *less than the initial potential energy*, implying that negative kinetic energy must be used initially to obtain the correct rolling curve. Although this is impossible in practice, this causes no problem when computing the second rolling curve.

The values in the table show that in the first case the loss of energy is extremely small, being $E_1 - E_2 = 0.0002mgr$. This is due to the short spinning phase of 24.4°, and has the result that the second rolling curve is indistinguishable from the first, as also shown by the small difference between ω_0 and ω_{02} in columns 3 and 4. The short slipping phase also results in the small value of the discontinuity, being only 0.184μ.

The remaining three examples have much longer spinning phases, resulting in greater loss of energy, distinguishable second rolling curves and larger discontinuities. As already mentioned, in the third case $\mathcal{E}_2 < \mathcal{E}_0$, and in the last case $\Delta_1 > 2\mu$.

The table shows that ω_2, θ_2, the length of the spin and Δ_1 all become progressively larger as the initial energy is reduced.

Note again that while the hoop spins, $\omega > \mathcal{V}_x$ as can be seen on Figure 5.11(c) for case d. The angular acceleration is positive, therefore ω increases during the spin; however, due to the combination of forces and accelerations, the large horizontal acceleration of the centre of the hoop causes the horizontal velocity $\mathcal{V}_x$ to "catch up" with ω and the spin phase ends when the two become equal.

6.5.4 Secondary classification : extremely light friction

As seen in Figure 6.6 and elsewhere, large discontinuities in the $\mathcal{F}/\mathcal{N}$-curve can occur when the slipping phases end and rolling resumes, and that in some cases these discontinuities can be so large that the rolling phase does not occur, and that the motion changes instantaneously from spin to skid or vice versa.

All cases where the first discontinuity has this characteristic, namely that $\Delta_1 = 2\mu$, are classified as *extremely light friction*, abbreviated as type eLF. These are therefore all cases with label `RS-D* *`, with the property that the first spin phase changes from spin to skid instantaneously, without the intermediate rolling phase. These cases can be recognised on the phase diagrams in Figure 5.4 as all cases where the S1 hump and the D1 hump overlap. The last fourteen examples in Table 6.2 are of type eLF.

In phase diagrams for the (μ, ω_0)-space, the region for type eLF occurs as a sub-region of the light friction region, for small values of μ and low velocities. This sub-region is to the left of the heavy dotted curve that ends at point (0.26, 0) as shown in Figure 6.7. This includes cases of low and medium velocity, labelled as `RS-D* Z` and `RS-D* T` respectively.
A similar sub-region of medium friction, in which skidding changes to spinning instantaneously, occurs to the left of the heavy dotted curve ending at point $(0.3, \hat{\omega}_0)$ in Figure 6.7. Motions in this region are labelled as `RD-S* *`; three patterns are listed in Table 6.2. These cases can be recognised on the phase diagrams in Figure 5.4 as cases where the S1 hump is missed and the D1 hump overlaps with the S2 hump.
Not shown here is the section of this curve that extends into the light friction region, separating the `RSRD-S* *` patterns from `RSRDRS* *`.

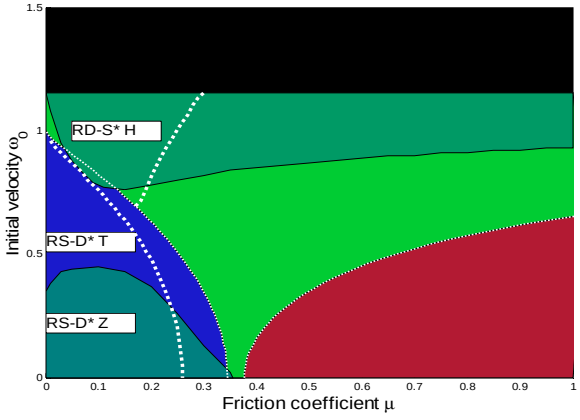

Figure 6.7 : Phase diagram in (μ, ω_0)-space for $\gamma = 3/4$ showing sub-regions of light and medium friction

6.6 Analysis in terms of Energy

Additional insight into the behaviour of the hoop can be obtained by considering the loss in the total energy during the slipping phases of a motion.

6.6.1 Energy expressions

For a rigid hoop, the expressions for the total energy are given by (4.8) and (4.9), repeated here for ease of reference:

$$\mathcal{E}_1 = (1+\gamma)\cos\psi + \tfrac{1}{2}(\mathcal{V}_{x0} + \gamma\omega_0)^2 + \tfrac{1}{2}\mathcal{K}_G\omega_0^2;$$

$$\mathcal{E} = (1+\gamma\cos\theta)\cos\psi - \mathcal{X}\sin\psi + \tfrac{1}{2}\mathcal{V}_x^2 + \mathcal{V}_x\gamma\omega\cos\theta + \tfrac{1}{2}(1+\epsilon)\omega^2.$$

In the case of the simplified model with a rolling start on a horizontal plane, this simplifies to (6.5):

$$\mathcal{E}_0 = (1+\gamma); \quad \mathcal{E}_1 = (1+\gamma)(1+\omega_0^2); \quad \mathcal{E} = (1+\gamma\cos\theta)(1+\omega^2).$$

As before, $\mathcal{E}_0$ denotes the (n-d) initial potential energy, $\mathcal{E}_1$ the total initial energy and $\mathcal{E}$ the total energy during rolling.

Note that for a given eccentricity, $\mathcal{E}_1 = \mathcal{E}_1(\omega_0)$. The upper limit for the initial energy is calculated as $\hat{\mathcal{E}}_1 = \mathcal{E}_1(\hat{\omega}_0)$; once again the implication is that the hoop hops immediately if the initial energy exceeds this value. Using (6.5) and $\hat{\omega}_0^2 = 1/\gamma$ from (2.30), this value is

$$\hat{\mathcal{E}}_1 = (1+\gamma)(1+1/\gamma); \tag{6.6}$$

clearly $\hat{\mathcal{E}}_1 \to \infty$ as $\gamma \to 0$, and $\hat{\mathcal{E}}_1 \to 4$ as $\gamma \to 1$.

6.6.2 Energy diagrams

An alternative to the phase diagrams in (θ, ω_0)-space in Figure 5.4 are *energy diagrams*, where an energy diagram is a phase diagram in $(\theta, \mathcal{E})$-space, as shown below in Figure 6.8. Now any motion of the hoop is a curve showing the total energy as a function of position; these will be referred to as *energy curves*.

The humps indicating the regions of spinning and skidding are obtained as before by marking the total energy at each of the positions where a phase change occurs, for given values of ψ, γ and μ. As before, these points describe the boundaries of domains in the $(\theta, \mathcal{E})$-plane for each of the possible phases. These domains appear as humps showing the S1, D1, S2, and D2 slipping phases, similar to Figure 5.4.

The energy curves end on curves indicating the final conditions as before. With low initial energy, the curves end on the curve marked Z, indicating zero angular velocity. With medium initial energy, the curves end on the vertical line at 360°, indicating rotation to the top. With high initial energy, the curves end on the curve marked H, indicating a hop.

The difference between the energy diagrams and the previous phase diagrams in Figure 5.4 is that the energy curves are no longer straight lines parallel to the horizontal axis, and that the humps become distorted because of this. This is because the loss in energy during slipping is

now shown, with the advantage that certain unusual patterns of motion can be recognised and explained more easily.

An example of an energy diagram is shown in Figure 6.8, for $\gamma = 2/3$ and $\mu = 0.2$. The vertical scale from 1.5 to 4 shows the total energy in non-dimensional form, $\mathcal{E}$, as given by (4.9). The value $\hat{\mathcal{E}}_1$ is shown as the dotted horizontal line at the top of the diagram, using (6.6). The dotted horizontal line at the bottom represents the initial potential energy $\mathcal{E}_0 = 1 + \gamma$. For $\gamma = 2/3$, $\mathcal{E}_0 = 5/3$ and $\hat{\mathcal{E}}_1 = 25/6$.

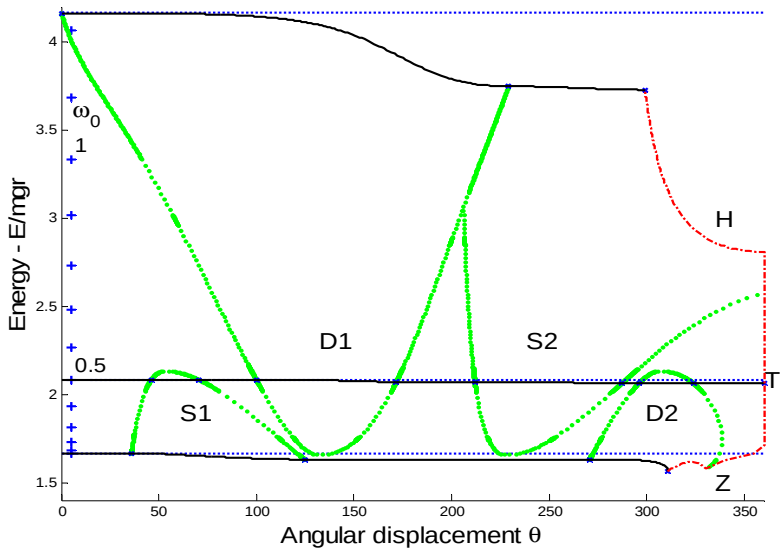

Figure 6.8 : Energy diagram for $\mathcal{P}_0 = \{2/3,\ 0.2,\ *\}$

A second (quadratic) vertical scale shows the initial angular velocity, ω_0, corresponding to the initial energy, and is marked by +-signs, from 0 to 1.1 in steps of 0.1.

Any particular motion, starting with a given initial ω_0, i.e. with initial energy $\mathcal{E}_1$, is shown as an energy curve on which all the phases of the motion can be identified. Three examples are shown in Figure 6.8:

- For $\omega_0 = 0$ pattern 25, `RSR----D-  Z`, is obtained.
- The curve starting at $\omega_0 = 0.5$ is the energy curve for case c, results of which are shown in Figure 5.10. The dotted horizontal line represents the initial energy $\mathcal{E}_1(0.5)$.
- The uppermost curve is drawn for $\omega_0 = 1.224$, which is fractionally less than $\hat{\omega}_0 = \sqrt{3/2}$ and provides the upper limit for our analysis.

6.6.3 The influence of the friction coefficient on energy diagrams

Figure 6.9 shows the energy diagrams for three different friction coefficients, all for $\gamma = 2/3$. The middle diagram, Figure 6.9(b), which is the same as the previous Figure 6.8 for the case $\mu = 0.2$, is used as a reference.

If the friction coefficient is reduced to $\mu = 0.15$, the energy diagram shown in Figure 6.9(a) is obtained. The shapes of the humps are basically the same, but their sizes and positions have changed. The lower humps are raised, thereby increasing the region of the first spinning phase (i.e. region of light friction). This clearly corresponds to the correct interpretation of the phase diagrams in (μ, ω_0) space, for example Figure 5.5, which clearly shows that light friction is defined for a larger range of initial velocities for $\mu = 0.15$ compared to $\mu = 0.2$. Note that one energy diagram such as Figure 6.9(a) corresponds to a vertical line for constant μ on a phase diagram such as Figure 5.5.

The inverted humps are lowered, and the regions of overlapping between the different humps is much larger for the smaller friction coefficient.

An increase in the friction coefficient to $\mu = 0.27$ is shown in Figure 6.9(c); this increase causes the lower humps to drop, and light friction is found only for small initial velocity. This is in agreement with Figure 5.5, which also shows that light friction is not found at all for $\mu > 0.29$, in which case the lower humps disappear altogether.

The inverted humps also retain their shapes as μ increases, but lift upwards, away from the zero line. The region of heavy friction now appears as the gap between the top of the lower humps and the bottom of the inverted humps; an example is shown in Figure 6.9(b) for $\omega_0 = 0.3$ with pattern `RT`.

Figure 6.9(c) is drawn for the same parameters as those used to draw the phase diagram Figure 5.4(e). The humps have similar shapes, but the difference between the energy curves and the previously used horizontal lines for ω_0 become apparent by comparing the two diagrams.

To summarise, we note that for small values of μ there is very little rolling and large overlapping between the different slipping regions; this can of course be expected on physical grounds, namely that the hoop cannot roll when the friction coefficient is very small. As μ increases, the rolling regions which separate the different slipping regions become larger, and the individual humps no longer overlap.

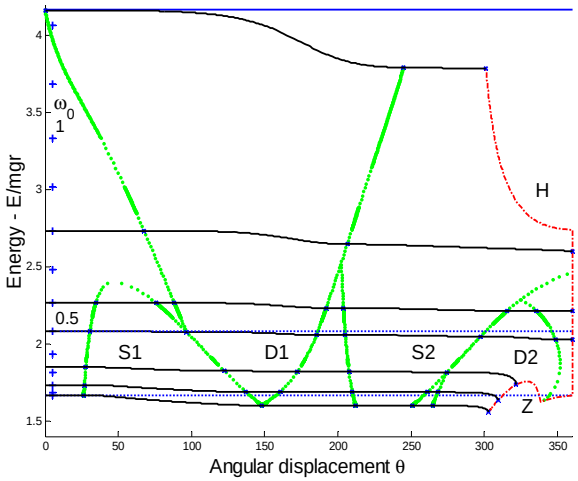

(a) : $\mu = 0.15$

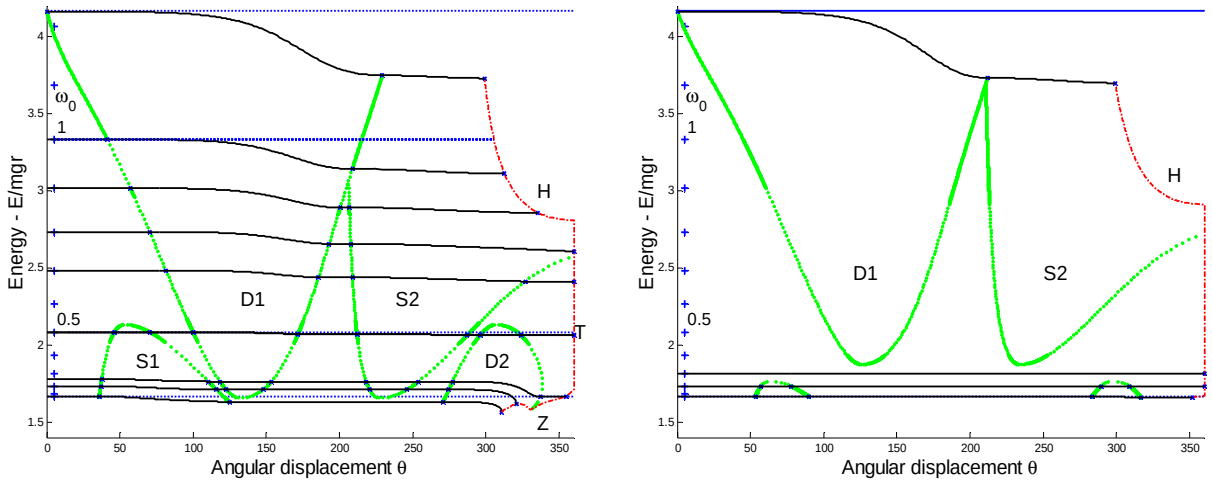

(b) : $\mu = 0.2$ (c) : $\mu = 0.27$

Figure 6.9 : Energy diagrams for $\gamma = 2/3$ and three friction coefficients

With large enough μ the lower humps disappear from the bottom of the scale and the inverted humps rise to the top of the region, and can disappear altogether for smaller eccentricities.

Eighteen different patterns are identified by the curves in Figure 6.9, and are referred to in the last column of Table 6.2. Most of these have been discussed previously with reference to Figure 5.4; one pattern only is singled out for discussion below.

The zero initial velocity curve in Figure 6.9(a) is labelled `RSR--SRD- Z`, with reference number 20 in Table 6.2. This is an example of the unusual situation described in section 6.5, where the second peak is missed, but not the third. The energy diagram shows that the lower part of the D1 hump is obscured by the S1 hump, causing the energy curve to miss the D1 hump.

The reason for this can be seen in Figure 6.10, which shows the $\mathcal{F}/\mathcal{N}$-graph for this case. Also shown are the initial rolling curve shown as the dotted curve, and the second rolling curve shown by the solid curve. The first spinning phase continues past the position where the rolling curves reach the first minimum; this is reflected in the energy diagram by the obscuration of the D1 minimum by the S1 hump, and is in contrast to the examples of similar graphs in Figure 6.6. In this case the first discontinuity in Figure 6.10 drops on to the second rolling curve *after* the minimum point and no skidding occurs. Note that the initial kinetic energy for the second rolling curve is negative, as seen in Figure 6.9(a) and previously discussed in section 6.5.3.

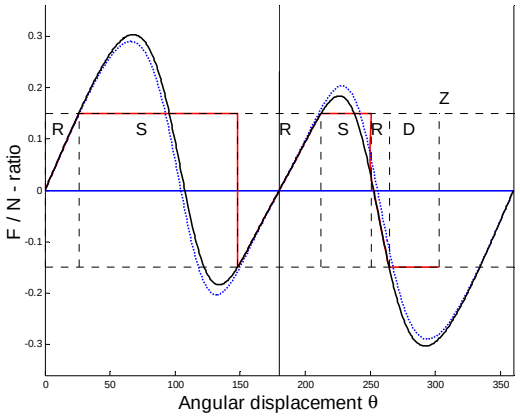

Figure 6.10 : $\mathcal{F}/\mathcal{N}$ for $\mathcal{P}_0 = \{2/3, 0.15, 0\}$

These examples illustrate the remarkable variety of patterns that are obtained with small variations in the parameters. To illustrate this further, all the examples from Figure 6.9 are shown as data points marked by crosses on the (μ, ω_0) phase diagram in Figure 6.11. The dotted curves are similar to those in Figure 6.7 to show the sub-regions for type eLF and `RD-S* *`.

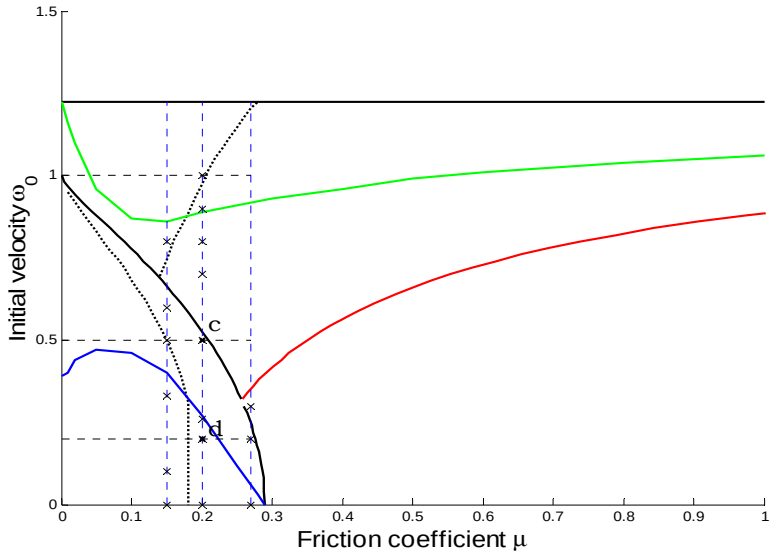

Figure 6.11 : Data points on the (μ, ω_0)-phase diagram for $\gamma = 2/3$ and $\psi = 0$

6.6.4 The influence of the eccentricity on energy diagrams

Figure 6.12 shows the energy diagrams for a smaller and larger eccentricity, using Figure 6.9(b), $\gamma = 2/3$, as reference and keeping $\mu = 0.2$.

A reduction in eccentricity has the same effect as increasing the friction coefficient, as can be seen by comparing Figure 6.12(a), $\gamma = 1/2$, with 6.9(c).

Vice versa, increasing the eccentricity to $\gamma = 4/5$ as shown in Figure 6.12(b) is very similar to 6.9(a). The only new pattern on 6.12(b) is for $\omega_0 = 0.6$, resulting in pattern nr. 15, `RSRDRSR-- T`.

Note that the values of $\hat{\mathcal{E}}_1 = (1+\gamma)(1+1/\gamma)$, from (6.6), confirm the result shown earlier, namely that $\hat{\mathcal{E}}_1$ is large for small γ and tends to 4 from above as γ increases. The examples above have $\hat{\mathcal{E}}_1 = 9/2,\ 25/6$ and $81/20$ for $\gamma = 1/2,\ 2/3$ and $4/5$ respectively.

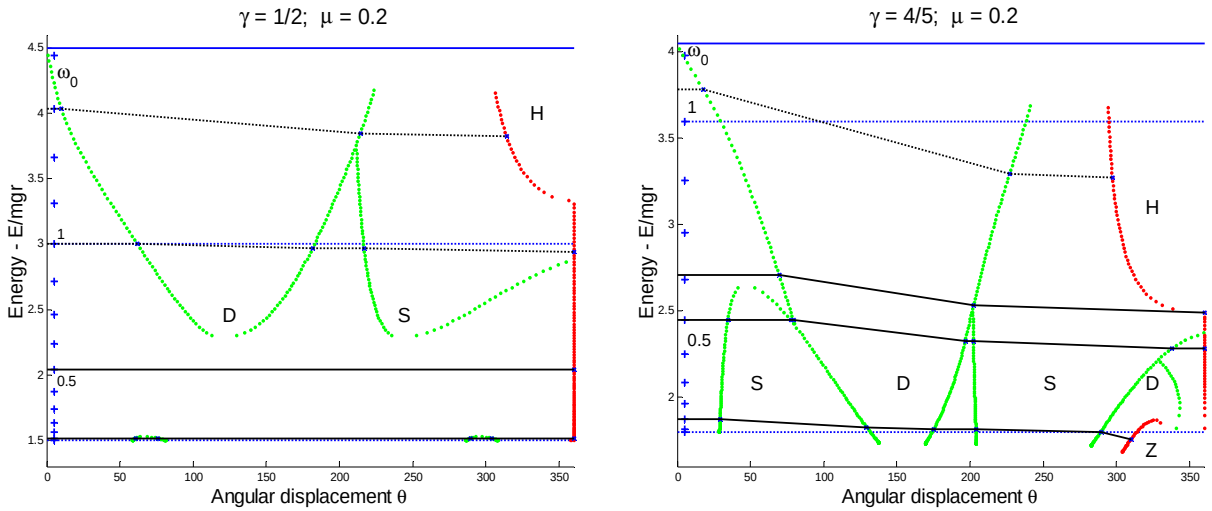

(a) $\gamma = 1/2$ (b) $\gamma = 4/5$

Figure 6.12 : Energy diagrams for two eccentricities, with $\mu = 0.2$

6.6.5 Cusp in the Z-curve

Figures 6.9(a) and (b) show that the Z-curve forms a cusp where it meets the D2 hump. This is caused by the very sharp dip in the energy curve towards the end of the motion, and results in the solutions in this region being extremely sensitive to the initial velocity.

This phenomenon provides the motivation for using energy diagrams, as opposed to the simpler (θ, ω_0)-phase diagrams of Figure 5.4, which cannot provide an explanation for this type of behaviour.

This region of Figure 6.9(a) is shown with an enlarged vertical scale in Figure 6.13(a), with the energy curves for six initial velocities. The zero velocity curve, `RSR--SRD- Z`, has been discussed above. The curve for $\omega_0 = 0.38$ has pattern nr. 32, `RS-DRS-D- Z`, and has been found before; note the sharp dip in the curve at the end. For slightly larger velocities this dip in the curve is accentuated, and for $\omega_0 = 0.39028$ this same pattern is found for the curve reaching the lowest point in the cusp, as shown in Figure 6.13(b) which shows the region of the cusp in a greatly enlarged scale. For slightly larger velocities a short rolling phase is encountered, as seen in the next curve, shown for $\omega_0 = 0.391$ with pattern `RS-DRS-DR Z`, pattern nr. 27. The extreme sensitivity to the value of ω_0 is illustrated by the fact that this pattern is found for $\omega_0 \in (0.3903, 0.3914)$. Finally, a curve with the pattern nr. 28, `RS-DRS-DR T` is shown for $\omega_0 = 0.392$. In Figure 6.13(a) this pattern is also shown for the uppermost curve, for $\omega_0 = 0.45$.

The same phenomenon is shown in Figure 6.14 for $\gamma = 4/5$ and $\mu = 0.2$. The larger eccentricity has the effect that the humps overlap almost completely, so that the middle rolling phase is also missing, resulting in three new patterns. The zero velocity curve shows pattern nr. 21, `RS--RS-D- Z`, seen previously. As in Figure 6.13, the next three curves are very close together, and are only distinguishable in the very large scale in Figure 6.14(b). The three patterns are: `RS-D-S-D- Z` for $\omega_0 = 0.42$, included in Table 6.2 as pattern nr. 34;

`RS-D-S-DR Z` for $\omega_0 = 0.426554$, pattern nr 30;
`RS-D-S-DR T` for $\omega_0 = 0.43$, pattern nr. 29.

Pattern 30 is found only for $\omega_0 \in (0.426552,\ 0.426554)$, an extremely narrow range.

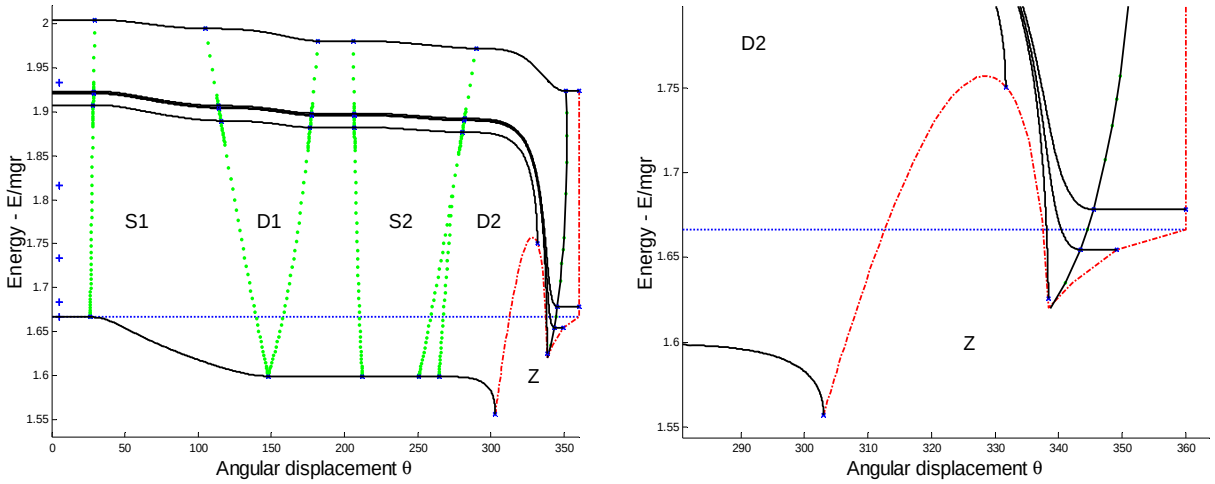

(a) (b) : Enlarged scale showing the cusp

Figure 6.13 : Energy diagram for $\gamma = 2/3$ and $\mu = 0.15$

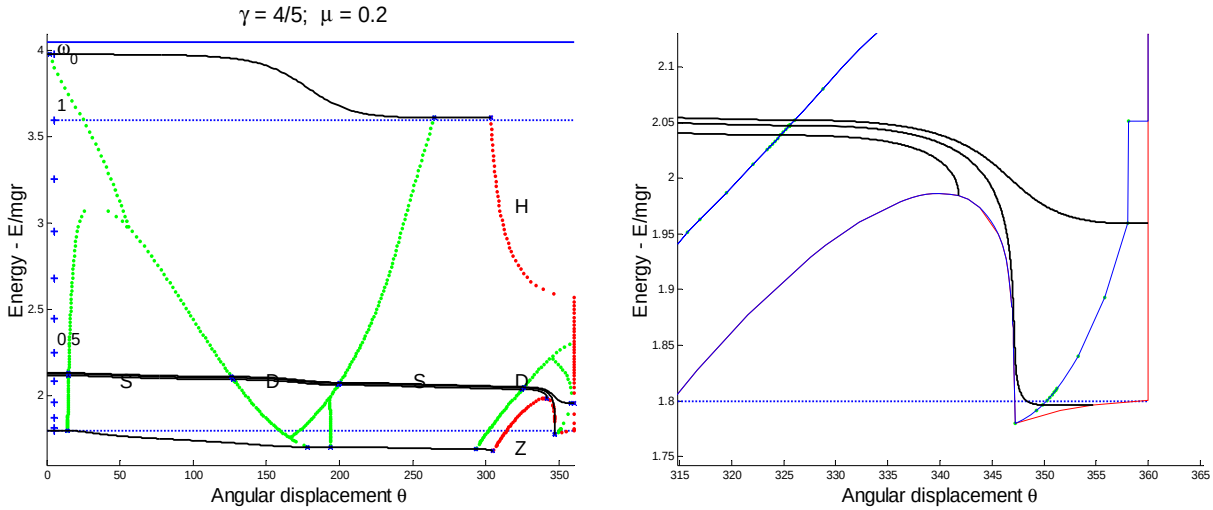

(a) (b) Enlarged scale showing the cusp

Figure 6.14 : Energy diagrams for $\gamma = 4/5$ and $\mu = 0.2$.

The motions ending with ***DR Z** and ***DR T** exhibit the further peculiarity that the angular velocity *increases* during the final part of the last skid, even though the potential energy is increasing but the system is losing energy. For example, detailed results for the case of pattern nr. 27 are shown in Figure 6.15, and the increase in ω just before the last rolling phase is visiblae in Figure 6.15(b). The corresponding large decrease in $\mathcal{V}_x$ results in the loss in total energy, as shown in the graphs of Figure 6.15(b). The upper graph shows the total energy, which remains almost constant until the sharp drop at the end of the second skid.

The horizontal dotted line at 1.67 on the vertical scale represents the initial potential energy, $\mathcal{E}_0 = (1 + \gamma)$.

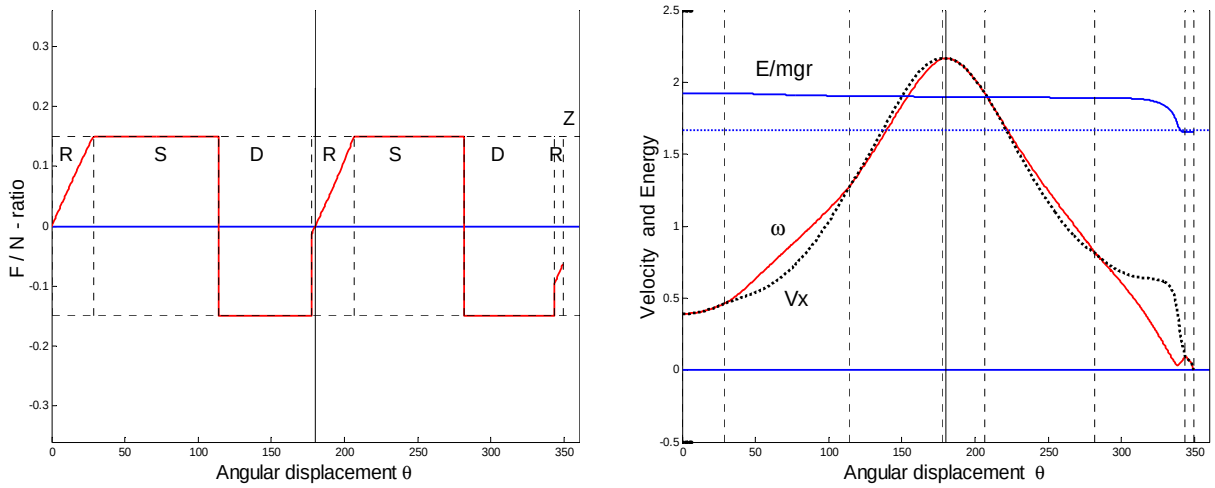

(a) : Ratio of $\mathcal{F}/\mathcal{N}$

(b) : Velocities and Energy

Figure 6.15 : An example of type eLF, with $\mathcal{P}_0 = \{2/3,\ 0.15,\ 0.391\}$

6.7 Complete list of possible motions

Table 6.2 below contains a complete list of all the different patterns of motion that have been found for a loaded hoop on a horizontal surface and starting with a rolling phase. This rather amazing variety of motions is the subject of a recent article [6].

The twenty-five patterns listed in Table 5.2 are repeated here. However, the parameters for which these patterns are found now refer to the energy diagrams in Figures 6.8 to 6.14, and are therefore different to those in Table 5.2 in most cases. Fourteen patterns not seen in the phase diagrams of Figure 5.4 have now been included, and can be recognised by the lack of a case number in the column referring to Figure 5.4.

The order in which the patterns are listed is as follows. Phase number j is given a weight 2^{j-1}. Therefore the first rolling phase has weight 1, and the last rolling phase has weight $2^8 = 256$. Zero weight is attached to all missing phases. The weight of a pattern is the sum of the weights of the phases; for example, pattern 2 has weight 508, pattern 3 is 444 and pattern 4 is 124, etcetera. For each primary type the patterns are then listed in decreasing order of their weights.

In cases where more than one final condition is found, the order is `* H`, `* T`, `* Z`. In such cases only the first pattern is shown completely. Inspection of Table 6.2 shows twelve patterns for which two different final conditions are found.

Note that patterns 20 and 21 are unusual in that they have two spinning phases without a skidding phase in between; see the comments in section 6.5.

The patterns 26 to 39 are listed separately as being of type eLF, extremely light friction. These include the patterns found in Figures 6.14 and 6.15 showing the cusp in the Z-curve and are found for only an extremely small range of velocities.

Pattern 37 is exceptional in that hopping occurs due to the extremely large eccentricity *even with zero initial velocity.*

Type	Ref.	Pattern	γ	μ	ω_0-range	Fig. 5.4	# 5.5	Figure
H	1	R T	2/3	0.27	0.3	5.4a(4)	case a	6.9(c)
M*	2	RDRSRDR T	3/4	0.3	[0.35 , 0.36]	5.4b(5)		
	3	RDRS-DR T	3/4	0.24	[0.54 , 0.55]			
	4	RDRSR-- T	2/3	0.2	[0.70]	5.4a(3)	case b	6.9(b)
	5	Z	4/5	0.5	(0 , ??]		case g	
	6	RD-SR-- T	2/3	0.15	[0.70 , 0.72]			
	7	RDRS--- H	2/3	0.2	[0.9]	5.4a(1)	case e	6.9(b)
	8	T	2/3	0.2	[0.8]	5.4a(2)		6.9(b)
	9	RD-S--- H	2/3	0.2	[1.0]	5.4c(8)		6.9(b)
	10	T	2/3	0.15	[0.8]	5.4f(23)		6.9(a)
L*	11	RSRDRSRDR T	2/3	0.2	[0.5]	5.4b(6)	case c	6.9(b)
	12	Z	2/3	0.2	(0.26]	5.4b(7)		6.9(b)
	13	RSRDRSRD- T	1/2	0.09	[0.46 , 0.52]			
	14	Z	2/3	0.2	[0.11 , 0.24]		case d	6.9(b)
	15	RSRDRSR-- T	4/5	0.2	[0.6]	5.4c(9)		6.12(b)
	16	RSRDRS-DR T	2/3	0.15	[0.6]	5.4c(10)		6.9(a)
	17	RSRDRS--- T	4/5	0.2	[0.66 , 0.68]			
	18	RSRD-S--- H	3/4	0.09	[0.79 , 0.84]	5.4d(13)	case f	
	19	T	3/4	0.1	0.77			
	20	RSR--SRD- Z	2/3	0.15	0.001			6.9(a)
	21	RSR--S-D- Z	3/4	0.09	[0.10 , 0.19]	5.4d(19)		
	22	RSR----DR T	2/3	0.27	[0.06 , 0.24]	5.4e(21)		6.9(c)
	23	Z	2/3	0.27	(0 , 0.05]	5.4e(22)		6.9(c)
	24	RSR----D- T	1/4	0.05	[0.32 , 0.49]	5.4f(24)		
	25	Z	1/4	0.05	[0.17 , 0.31]	5.4f(25)		
eLF	26	RS-DRSRDR Z	3/4	0.24	0.27			
	27	RS-DRS-DR Z	2/3	0.15	0.391			6.13(b)
	28	T	2/3	0.15	[0.5]	5.4c(11)		6.9(a)
	29	RS-D-S-DR T	4/5	0.2	[0.43]	5.4d(16)		6.14(b)
	30	Z	4/5	0.2	0.426554			6.14(b)
	31	RS-DRSRD- Z	3/4	0.24	[0 , 0.26]			
	32	RS-DRS-D- Z	2/3	0.15	(0.33]	5.4c(12)		6.9(a)
	33	RS-D-S-D- T	3/4	0.09	[0.45 , 0.49]	5.4d(17)		
	34	Z	4/5	0.2	[0.42]	5.4d(18)		6.14(b)
	35	RS-----D- Z	3/4	0.09	[0 , 0.09]	5.4d(20)		
	36	RS-D-SR-- T	3/4	0.09	[0.59 , 0.63]	5.4d(15)		
	37	RS-DRS--- H	0.99	0.2	[0 , 0.4]			6.1(a)
	38	RS-D-S--- H	0.99	0.2	[0.41 , 0.89]			6.1(a)
	39	T	3/4	0.09	[0.64 , 0.78]	5.4d(14)		

Table 6.2 : List of identifiable patterns for $\psi = 0$, ordered by weight

Table 6.3 contains the same patterns, but ordered according to the parameters, with increasing eccentricity, followed by increasing friction, followed by decreasing initial velocity.

Ref.	Pattern	γ	μ	ω_0	Fig. 5.4	# 5.5	Figure
24	RSR----D- T	1/4	0.05	0.4	5.4f(24)		
25	Z			0.2	5.4f(25)		
13	RSRDRSRD- T	1/2	0.09	0.5			
10	RD-S--- T	2/3	0.15	0.8	5.4f(23)		6.9(a)
6	RD-SR-- T			0.7			
16	RSRDRS-DR T			0.6	5.4c(10)		6.9(a)
28	RS-DRS-DR T			0.5	5.4c(11)		6.9(a)
27	Z			0.391			6.13(b)
32	RS-DRS-D- Z			0.33	5.4c(12)		6.9(a)
20	RSR--SRD- Z			0			6.9(a)
9	RD-S--- H		0.2	1.0	5.4c(8)		6.9(b)
7	RDRS--- H			0.9	5.4a(1)	case e	6.9(b)
8	RDRS--- T			0.8	5.4a(2)		6.9(b)
4	RDRSR-- T			0.70	5.4a(3)	case b	6.9(b)
11	RSRDRSRDR T			0.5	5.4b(6)	case c	6.9(b)
12	RSRDRSRDR Z			0.26	5.4b(7)		6.9(b)
14	RSRDRSRD- Z			0.2		case d	6.9(b)
1	R T		0.27	0.3	5.4a(4)	case a	6.9(c)
22	RSR----DR T			0.1	5.4e(21)		6.9(c)
23	RSR----DR Z			0	5.4e(22)		6.9(c)
18	RSRD-S--- H	3/4	0.09	0.8	5.4d(13)	case f	
39	RS-D-S--- T			0.7	5.4d(14)		
36	RS-D-SR-- T			0.6	5.4d(15)		
33	RS-D-S-D- T			0.47	5.4d(17)		
21	RSR--S-D- Z			0.15	5.4d(19)		
35	RS-----D- Z			0	5.4d(20)		
19	RSRD-S--- T		0.1	0.77			
3	RDRS-DR T		0.24	0.54			
26	RS-DRSRDR Z			0.27			
31	RS-DRSRD- Z			0			
2	RDRSRDR T		0.3	0.34	4.6b(5)		
17	RSRDRS--- T	4/5	0.2	0.67			
15	RSRDRSR-- T			0.6	5.4c(9)		6.12(b)
29	RS-D-S-DR T			0.43	5.4d(16)		6.14(b)
30	RS-D-S-DR Z			0.426554			6.14(b)
34	RS-D-S-D- Z			0.42	5.4d(18)		6.14(b)
5	RDRSR-- Z		0.5	0		case g	
38	RS-D-S--- H	0.99	0.2	0.5			6.1(a)
37	RS-DRS--- H			0			6.1(a)

Table 6.3 : List of identifiable patterns for $\psi = 0$, ordered by parameters

6.8 Summary and Conclusions

In this chapter some additional results have been obtained for a rigid loaded hoop rolling on a rough surface.

The effect of the eccentricity on the types of motion is clearly shown in phase diagrams in the (γ, ω_0)-parameter space for given values of μ and ψ. These diagrams led to the "discovery" of two patterns not found previously, listed as patterns 37 and 38 in Table 6.2.

The effect of distinguishing between static and dynamic friction coefficients is shown to be negligible.

Two effects of increasing the slope to $\psi > 0$ are that hopping occurs at lower initial velocities, and that the zero curve is only present for slopes with $\psi < 4.5°$. Also, initial rolling is not always possible when using the initial condition that $\mathcal{V}_{x0} = \omega_0$. A minimum friction coefficient, $\hat{\mu}$, is defined as a function of ψ, γ and ω. Two new patterns are found for motion on a slope when $\mu < \hat{\mu}$, resulting in initial skidding. (These are not included in Table 6.2).

The behaviour of a massless hoop, previously analysed in Chapter 3, is considered here in the context of the solutions developed in the chapters on rigid hoops. It is found that:

- The equations governing the motion of a rigid hoop are also applicable to Littlewood's hoop, i.e. a hoop for which $\gamma = 1$ and $\epsilon = 0$, but limited to $\theta < \pi$.
- In the case of a Pritchett hoop, i.e. a hoop for which $\gamma = 1$ and $\epsilon > 0$, the numerical solution for sliding tends to the analytic solution for skimming as $\epsilon \to 0$. This solution precludes hopping for $\theta < \pi$.

Two additional aspects regarding the patterns of motion are identified. Patterns are termed *unusual* in cases where the spinning and skidding phases do not alternate. A sub-type of light friction, termed *extremely light friction* or type eLF, is identified; Table 6.2 lists fourteen patterns of type eLF.

Finally, the total energy, E, of the system is considered. Phase diagrams in $(\theta, \mathcal{E})$-space result in diagrams very similar to Figure 5.4. These are termed energy diagrams and make it possible to identify new patterns for a few extreme cases.

Some unexpected behaviour is observed. In some cases both the potential energy and the rotational kinetic energy are *increasing* simultaneously even though the total energy is decreasing.

Thirty-nine different patterns are identified and listed in Table 6.2.

Chapter 7

Dynamics of an elastic hopping hoop

7.1 Introduction

As discussed in the Introduction, Chapter 1.2, hoops that have actually hopped have been observed and photographed [11, 13]. In both cases a hula-hoop was loaded with a heavy "particle" and hopped as predicted by Littlewood, namely when the radius to the particle is horizontal and the particle is moving downwards.

It was shown in Chapters 4 to 6 that rigid hoops cannot hop in this position. The purpose of this chapter, and the corresponding article [3], is an attempt at explaining this observed phenomenon by taking elasticity into account. *This is the main purpose of this Chapter* - no attempt is made to achieve the complete description of all possible motions as was done for rigid hoops.

Two extremely simple elastic models are considered. The general model which was developed in Chapter 2 is based on the assumption that the hoop is rigid and the surface on which it rolls is deformable. This will henceforth be referred to as the *external* elastic model. In the second model, henceforth referred to as the *internal* elastic model, it is assumed that radius OC, as shown in Figure 7.2, deforms elastically, and that the remainder of the hoop is rigid. This is the model used in [3] and is developed in section 7.3.

In spite of their simplicity these models yield the desired result, namely to define the conditions under which a hoop can hop as shown in Pritchett's photograph.

7.2 The mathematical model for the external elastic model

The general model that was developed in Chapter 2 consists of a rigid hoop rolling on a deformable surface. In this chapter the solution of this model is obtained for motion on a horizontal surface, i.e. $\psi = 0$, for a load consisting of a point particle (i.e. $\epsilon = 0$).

7.2.1 Kinematic and kinetic equations

When these simplifications are introduced the model shown in Figure 7.1 is obtained based on the elastic model where the surface is compressed by an amount $d(t)$ as given in (2.5) and (2.14):

$$Y = r - d(t)\ ; \quad Y/r = 1 - \delta(\tau).$$

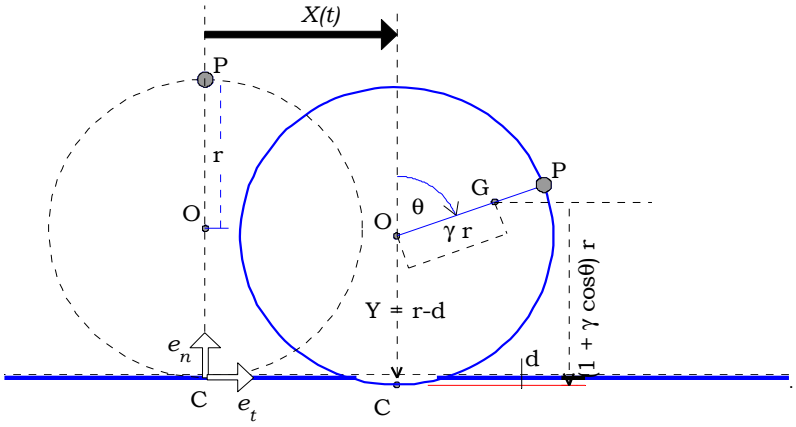

(a) : Geometry

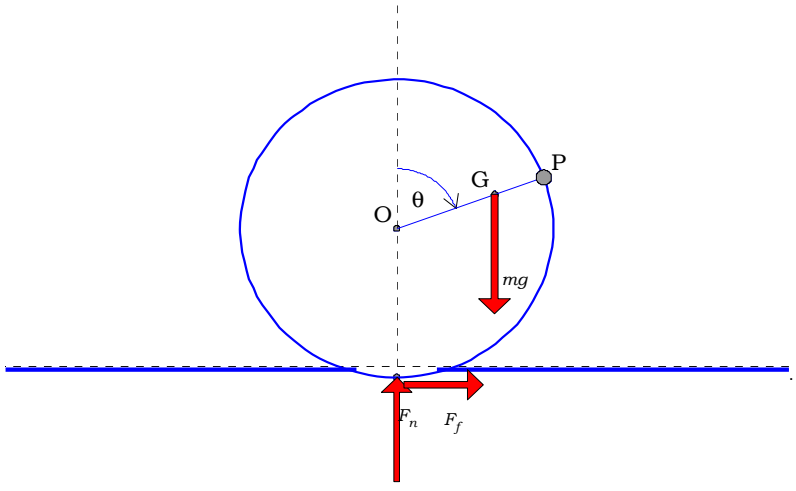

(b) : Forces

Figure 7.1 : The external elastic model

The geometry of this model is summarised by

$$\mathcal{H} = 1 + \gamma \cos\theta; \quad \kappa_G = 1 - \gamma^2; \quad \kappa_C = 2\mathcal{H}, \tag{7.1}$$

remembering that $\mathcal{H}$ denotes the non-dimensional height of point G. It is found useful at a later stage to define the non-dimensional height of point O as

$$\mathcal{H}_O = Y/r - 1.$$

While the hoop is in contact with the surface $\mathcal{H}_O = -\delta$; during the hop, $\mathcal{H}_O > 0$ describes the path of the centre of the hoop.

The rigidity constraint and kinematic equations (2.15) to (2.17) are repeated below for ease of reference:

$$x/r = \mathcal{X} + \gamma \sin\theta; \qquad y/r = 1 - \delta + \gamma \cos\theta.$$

$$\mathcal{V}_x = (X/r)'; \qquad (x/r)' = \mathcal{V}_x + \gamma\,\omega \cos\theta; \qquad (y/r)' = -\delta' - \gamma\,\omega \sin\theta.$$

$$(x/r)'' = \mathcal{X}'' + \gamma\,\theta'' \cos\theta - \gamma\,\omega^2 \sin\theta; \qquad (y/r)'' = -\delta'' - \gamma\,\theta'' \sin\theta - \gamma\,\omega^2 \cos\theta.$$

The non-dimensional form of the kinetic equations (2.19) to (2.21) of Chapter 2 simplify to:

$$\mathcal{F} = \mathcal{X}'' + \gamma\,\theta'' \cos\theta - \gamma\,\omega^2 \sin\theta; \tag{7.2}$$

$$\mathcal{N} = -\delta'' - \gamma\,\theta'' \sin\theta - \gamma\,\omega^2 \cos\theta + 1; \tag{7.3}$$

$$(\mathcal{N})\,\gamma \sin\theta - (\mathcal{F})\,\mathcal{H} = \kappa_G\,\theta''. \tag{7.4}$$

The only additional modelling assumption that is now needed is the relationship between the normal reaction and the deformation of the surface. Here the simplest linear relationship is used, namely Hooke's law in the form

$$F_n = kd.$$

To obtain the non-dimensional form we define the *static deformation*

$$d_s = mg/k,$$

and the non-dimensional *elastic constant* as the ratio

$$e = r/d_s = rk/mg. \tag{7.5}$$

Then the non-dimensional form of Hooke's law is

$$\mathcal{N} = e\,\delta, \quad \delta \geq 0. \tag{7.6}$$

For example, if a hoop with 1 meter diameter causes a large static deformation of 25 mm when loaded, then $d_s = 0.05\ r$, i.e. $e = 20$ and this could be considered to be a "soft" surface. Similarly, a deformation of 1 mm, or $e = 500$, could be considered stiff. Clearly, the rigid model is approximated by $e \to \infty$.

7.2.2 Initial conditions

As before, we assume that the motion always starts with the particle at the highest point; therefore $\theta(0) = 0$ and $X(0) = 0$; that the initial angular velocity ω_0 is given; that the initial velocity is horizontal, so that $\delta'(0) = 0$; and that the hoop always starts in rolling mode, so that $\mathcal{V}_{x0} = \omega_0$.

This leaves the initial elastic deformation, $d(0)/r = \delta_0$ still undefined, and for this an additional simplifying assumption is required. In this model we make the physically reasonable assumption that the initial displacement equals the static deformation; i.e $d(0) = d_s$, or in non-dimensional terms,

$$\delta_0 = d_s/r = 1/e. \tag{7.7}$$

The centrifugal effect of the angular velocity causes an initial impulse in $\mathcal{N}$, thus causing initial oscillations in the vertical direction. Later numerical results show that these oscillations can be significant in cases of a soft surface combined with large initial velocities. In the original article [1] these initial oscillations were avoided by assuming that the initial elastic deformation is chosen in such a manner that it does not cause an impulse. To achieve this, $\delta''(0)$ is assumed to be zero so that the initial normal reaction from (7.3) is $\mathcal{N}(0) = 1 - \gamma\,\omega_0^2$. Equating this to Hooke's law, (7.6), results in $\delta_0 = (1 - \gamma\,\omega_0^2)/e$. This form will not be used in this dissertation.

7.2.3 Rolling motion

It was shown in Chapter 2 that the non-dimensional specification for rolling motion is (2.24),

$$\mathcal{V}_{x0} = \omega_0; \quad \mathcal{V}_x = \omega; \quad \mathcal{X}'' = \theta''. \tag{7.8}$$

In the present model the torque equation (2.25) simplifies to

$$\kappa_C\,\theta'' + \gamma\,\sin\theta\,\delta'' = \gamma\,\sin\theta\,\omega^2 + \gamma\,\sin\theta. \tag{7.9}$$

Note that this is fundamentally different compared to the equations of the previous two chapters, in that we now have an equation in two independent variables.

A second equation is obtained by equating (7.6) to (7.3) to obtain $e\,\delta = 1 - \delta'' - \gamma\,\theta''\,\sin\theta - \gamma\,\omega^2\,\cos\theta$, or

$$\delta'' + \gamma\,\sin\theta\,\theta'' = 1 - e\,\delta - \gamma\,\omega^2\,\cos\theta. \tag{7.10}$$

Equations (7.9) and (7.10) can be written as the simultaneous equations

$$\begin{bmatrix} \kappa_C & \gamma\,\sin\theta \\ \gamma\,\sin\theta & 1 \end{bmatrix} \begin{bmatrix} \theta'' \\ \delta'' \end{bmatrix} = \omega^2 \begin{bmatrix} \gamma\,\sin\theta \\ -\gamma\,\cos\theta \end{bmatrix} + \begin{bmatrix} 0 \\ -e\,\delta \end{bmatrix} + \begin{bmatrix} \gamma\,\sin\theta \\ 1 \end{bmatrix}.$$

These equations are easily decoupled by pre-multiplying with the inverse of the coefficient matrix to obtain the first equation as

$$\theta'' = \Big[\,(\omega^2\,(1 + \gamma\,\cos\theta) + e\,\delta\Big]\;\gamma\,\sin\theta/D_1, \tag{7.11}$$

where the determinant of the coefficient matrix simplifies to

$$D_1 = \kappa_C - (\gamma\,\sin\theta)^2 \quad \text{or} \quad D_1 = \kappa_G + \mathcal{H}^2.$$

The second equation is not easily simplified, and it is more convenient to use the expression for θ'' from (7.11) in the second equation to obtain

$$\delta'' = -\omega^2\,\gamma\,\cos\theta - e\,\delta + 1 - (\gamma\sin\theta)\theta''. \tag{7.12}$$

This system of second order equations can be solved numerically in the standard manner by writing them as a system of first order equations. In the MATLAB implementation the function ODE45 is used. The vector of unknown variables includes the horizontal displacement X, and is defined as

$$Z = [\theta,\, \omega,\, \mathcal{X},\, \mathcal{V}_{x0},\, \delta,\, \delta'].$$

The first derivative is given by

$$Z' = [\omega,\, \theta'',\, \mathcal{V}_{x0},\, \mathcal{X}'',\, \delta',\, \delta''],$$

with θ'', $\mathcal{X}''$ and δ'' being calculated from (7.11), (7.8) and (7.12) respectively.

From this solution, the friction force is found from (7.2) and the normal reaction from (7.6), giving the reaction forces as

$$\mathcal{F} = \mathcal{X}'' + \theta''\,\gamma\,\cos\theta - \omega^2\,\gamma\,\sin\theta; \quad \mathcal{N} = e\,\delta.$$

The rolling motion will continue as long as both the following criteria are met:

- the hoop remains in contact with the surface, which implies $\mathcal{N} > 0$, i.e. $\delta > 0$;
- the hoop does not start slipping, which implies $|\mathcal{F}| < \mu_s\mathcal{N}$.

As discussed previously, the first criterion can never be broken, because the hoop will always start slipping before the normal reaction becomes zero. Therefore the rolling phase will either continue until the maximum angle specified for the analysis is reached, or the hoop will start slipping at the point where $|\mathcal{F}| = \mu_s\mathcal{N}$. The angular displacement at the point where the hoop stops rolling and starts slipping is denoted by θ_s, and the remaining initial values for the subsequent motion by ω_s, $\mathcal{X}_s$, $\mathcal{V}_{xs}$, δ_s and δ'_s.

7.2.4 Spinning or skidding

Depending on the values of the parameters, the rolling motion will end with the friction force being either positive or negative, resulting in the corresponding spinning or skidding motions. Using the same definitions as in chapters 2 and 4, namely $\mu = +\mu_k$ in the case of spinning, $\mu = -\mu_k$ in the case of skidding, and the slip factor from (2.27)

$$S(\theta) = \gamma\sin\theta - \mu\,\mathcal{H},$$

the torque equation (7.4) becomes

$$\kappa_G\,\theta'' = \mathcal{N}\,S,$$

and with Hooke's equation (7.6), $\mathcal{N} = e\,\delta$,

$$\theta'' = (S/\kappa_G)\,e\,\delta. \tag{7.13}$$

Also, from (7.3), $(\kappa_G/S + \gamma \sin\theta)\,\theta'' + \delta'' = 1 - \gamma\,\omega^2 \cos\theta$, or

$$\delta'' = 1 - \gamma\,\omega^2 \cos\theta - e\,\delta(1 + (S/\kappa_G)\,\gamma \sin\theta). \tag{7.14}$$

The numerical solution is once again found in terms of the six non-dimensional variables

$$Z = [\theta, \omega, \mathcal{X}, \mathcal{V}_x, \delta, \delta'],$$

with first derivatives

$$Z' = [\omega, \theta'', \mathcal{V}_x, \mathcal{X}'', \delta', \delta''],$$

where θ'' is calculated from (7.13), δ'' from (7.14) and

$$\mathcal{X}'' = \mu\,e\,\delta - \gamma\,\theta'' \cos\theta + \gamma\,\omega^2 \sin\theta,$$

using (7.2) with Coulomb and Hooke's laws.

From this solution, the reactions are

$$\mathcal{N} = e\,\delta \quad \text{and} \quad \mathcal{F} = \mu\mathcal{N}.$$

The slipping motion will continue as long as both the following criteria are met:

- the hoop remains in contact with the surface, which implies $\mathcal{N} > 0$, i.e. $\delta > 0$;
- the hoop does not start rolling again. In the case of spinning, this implies $r\,\dot\theta > \dot X$, i.e. as long as $\omega > \mathcal{V}_x$, and skidding continues as long as $\omega < \mathcal{V}_x$.

The case when the angular velocity becomes zero is discussed later in section 7.7.2.

7.3 The mathematical model for the internal elastic model

As mentioned in the Introduction, the main purpose of this chapter is to find a model that produces hopping as shown in Pritchett's photograph [13]. The model developed in the previous sections can produce hops similar to those in the photo, but is not a good physical representation of a hula-hoop rolling on a rigid surface. The internal elastic model developed below is a reasonable representation of the physical model in the photo. In this internal model the hoop rolls on a rigid surface and the hoop is assumed to deform elastically, as shown in Figure 7.2.

7.3.1 Modelling assumptions

Figure 7.2(a) shows the geometry of an elastic hoop rolling on a rigid horizontal surface. Point O is the centre of the un-deformed hoop, which is loaded with a particle at point P on the rim, and point C is the point of contact, assumed to be at the midpoint of the deformed part of the hoop.

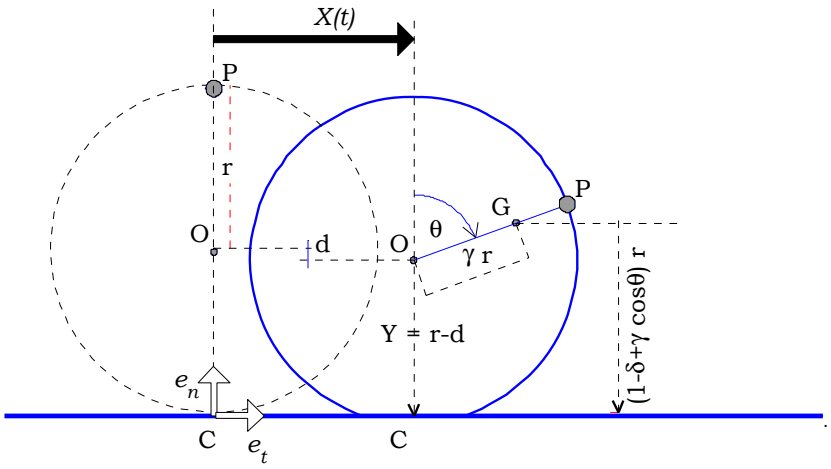

(a) Geometry

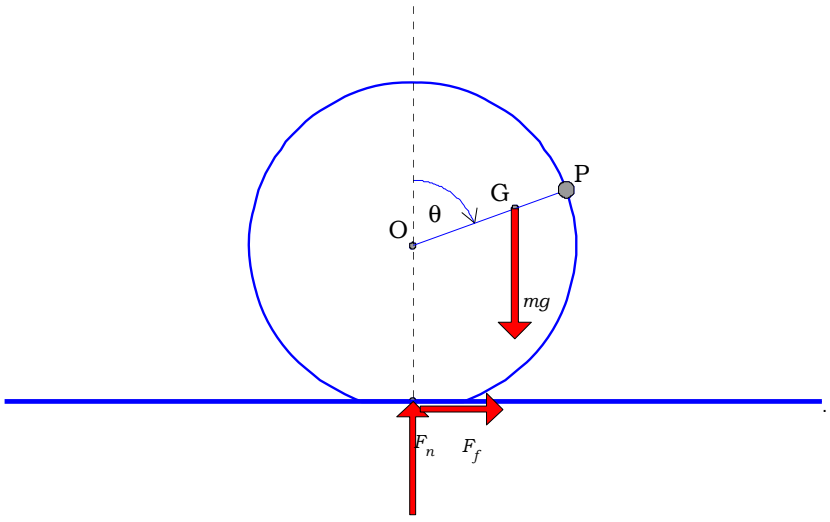

(b) Forces

Figure 7.2 : The internal elastic model

The first and fundamental assumption in this model is:

1. The radius to the contact point, OC, deforms elastically.
This is modelled by defining $Y(t) = r - d(t)$, and the elastic deformation as the non-dimensional ratio $\delta = d/r$. Then the non-dimensional height of G is

$$\mathcal{H} = 1 - \delta + \gamma \cos\theta.$$

Note that, in contrast to the external model, $\mathcal{H}$ is now a function of δ and also that now $\mathcal{H} = y/r$.

Two further assumptions regarding the geometry of the elastic hoop are made in order to simplify the model. These are

2. The eccentricity γ is constant, which is true if the radius to the particle is constant.
In other words, it is assumed that OP $= r$. If this assumption is not made, a fourth degree of freedom is introduced which greatly increases the complexity of the problem.

3. The moment of inertia around G, I_G, is not affected by the deformation of the hoop.
This implies that $\kappa_G = 1 - \gamma^2$, which is true for rigid hoops, may be used for elastic hoops as well, on the assumption that the deformation of the elastic hoop will not have a significant influence on the moment of inertia. It is shown in Appendix D that this is a very reasonable assumption, except when very large values of δ occur for $\theta \approx 180°$.

By making these assumptions, the complexity of the model is comparable to that of a rigid hoop and very similar to that of the external elastic model. If these assumptions are not made, the complexity of the mathematical model is greatly increased.

Based on these assumptions, the moment of inertia around point C is

$$I_C = I_G + m(GC)^2 = I_G + m\,(\,(\gamma r \sin\theta)^2 + (\mathcal{H}r)^2\,) = mr^2\,(1 + (1-\delta)^2 + 2(1-\delta)\gamma\cos\theta).$$

The geometry of this model is therefore summarised as

$$\mathcal{H} = 1 - \delta + \gamma\,\cos\theta; \quad \kappa_G = 1 - \gamma^2; \quad \kappa_C = 1 + (1-\delta)^2 + 2(1-\delta)\,\gamma\,\cos\theta. \tag{7.15}$$

The relationship between the normal force and the elastic deformation is defined by Hooke's law as for the external model in (7.5) and (7.6), namely

$$F_n = kd \quad \text{or} \quad \mathcal{N} = e\,\delta, \quad \delta \geq 0.$$

As before, $e = r/d_s$ and for example a plastic hula hoop with 1 meter diameter and static deformation of 10 mm when loaded results in $e = 50$.

Rolling motion is characterised by the condition that the contact point C is momentarily at rest, which now implies the relationship $\dot{X} = (r-d)\dot{\theta}$ or

$$\mathcal{V}_x = (1-\delta)\omega \quad \text{and} \quad \mathcal{V}_{x0} = (1-\delta_0)\omega_0. \tag{7.16}$$

The remaining initial conditions are the same as for the external model.

7.3.2 Rolling motion

Differentiating (7.16), the acceleration for rolling motion is now

$$\mathcal{X}'' = (1-\delta)\theta'' \ - \delta'\,\omega. \tag{7.17}$$

Using this and the other simplifications in the kinetic equations (2.19) and (2.20), these become,

$$\mathcal{F} = (1-\delta+\gamma\,\cos\theta)\theta'' \ - \delta'\,\omega - \gamma\,\omega^2\,\sin\theta; \tag{7.18}$$

$$\mathcal{N} = 1 - \delta'' - \gamma\,\theta''\,\sin\theta - \gamma\,\omega^2\,\cos\theta. \tag{7.19}$$

The torque equation for rolling of an elastic hoop, (2.25), now becomes

$$\kappa_C\,\theta'' + \gamma\,\sin\theta\,\delta'' = \gamma\,\sin\theta(1-\delta)\,\omega^2 + \mathcal{H}\,\delta'\,\omega + \gamma\,\sin\theta. \tag{7.20}$$

The second equation is obtained as before by equating (7.6) to (7.19), to give the simultaneous equations [1]

$$\begin{bmatrix} \kappa_C & +\gamma\,\sin\theta \\ +\gamma\,\sin\theta & 1 \end{bmatrix} \begin{bmatrix} \theta'' \\ \delta'' \end{bmatrix} = \omega^2 \begin{bmatrix} \gamma\,\sin\theta(1-\delta) \\ -\gamma\,\cos\theta \end{bmatrix} + \begin{bmatrix} \delta'\,\omega\,\mathcal{H} \\ -e\,\delta \end{bmatrix} + \begin{bmatrix} \gamma\,\sin\theta \\ 1 \end{bmatrix}.$$

Note that this is essentially the same as the equations for the external model, and can be solved in the same manner by pre-multiplying with the inverse of the coefficient matrix to obtain the first equation as

$$\theta'' = \Big[\,(\omega^2\,\mathcal{H} + e\,\delta)\,\gamma\,\sin\theta + \delta'\,\omega\,\mathcal{H}\Big]\,/(\kappa_G + \mathcal{H}^2), \tag{7.21}$$

where the determinant of the coefficient matrix in this case simplifies to $(\kappa_G + \mathcal{H}^2)$.

The second equation is again written as

$$\delta'' = 1 - e\,\delta - \omega^2\,\gamma\,\cos\theta - \gamma\sin\theta\,\theta''. \tag{7.22}$$

As before, this system of second order equations is solved numerically by writing them as a system of first order equations, using $Z = [\theta,\, \omega,\, \mathcal{X},\, Vx,\, \delta,\, \delta']$ and

$$Z' = [\omega,\, \theta'',\, Vx,\, \mathcal{X}'',\, \delta',\, \delta''],$$

with θ'', $\mathcal{X}''$ and δ'' being calculated from (7.21), (7.17) and (7.22) respectively.

From this solution, the friction force is found from (7.18) and the normal reaction from (7.6). The remaining detail of the solution algorithm is the same as for the external model.

7.3.3 Spinning or skidding

The slip factor S differs slightly from the factor for the external model, and is now

$$S(\theta) = \gamma\sin\theta - \mu\,\mathcal{H} = \gamma\sin\theta - \mu\,(1-\delta+\gamma\,\cos\theta).$$

Using this in (7.13) and (7.14), the solution is obtained by using the method as for the external model.

[1] There are some typing errors in the corresponding equation in the original article [3].

7.4 Hopping

It is of some interest to derive the equations of the motion while the hoop is airborne, inter alia so that the calculated values can be compared to measurable values on a photo such as that published by Pritchett [13]. These measurable values are the following:

- the rotation at the start of the hop, denoted by θ_*,
- the rotation at the end of the hop, denoted by θ_+,
- the maximum height of the centre of the hoop, denoted by $\mathcal{H}_{O_{max}}$,
- the horizontal span of the hop, denoted by $\mathcal{S}_h = \mathcal{X}_+ - \mathcal{X}_*$.

The equations to calculate these values are derived as functions of (dimensionless) time, and are valid for both elastic models, depending only on the position and velocity at the point where the hop starts.

The angular displacement at the point where hopping occurs is denoted by θ_*, with $\mathcal{N}(\theta_*) = e\,\delta(\theta_*) = 0$ at time τ_*. The initial conditions for the subsequent motion are therefore $\omega_* = \omega(\theta_*)$, $X_* = X(\theta_*)$, $\mathcal{V}_{x*} = \mathcal{V}_x(\theta_*)$ and $\delta'_* = \delta'(\theta_*)$, the values being known from the solution of the previous phase.

Note that $\delta'_* < 0$, is a sufficient condition for hopping.

For $\tau > \tau_*$, there is no elastic deformation and the rigidity condition (2.15) becomes

$$x/r = X/r + \gamma\,\sin\theta, \qquad y/r = Y/r + \gamma\,\cos\theta.$$

The subsequent motion of the hoop is controlled by the fact that the torque around G is zero and therefore, since $\kappa_G > 0$, the angular acceleration is zero and the hoop rotates with constant angular velocity ω_*, so that

$$\theta(\tau) = \theta_* + (\tau - \tau_*)\,\omega_*. \tag{7.23}$$

Also, with zero reaction force, the weight is the only force and the centre of mass G follows a parabolic path with acceleration $\mathbf{a} = -g\mathbf{e}_n$ or $(y/r)'' = -1$.

It is convenient to re-define the non-dimensional height of G for both models as $\mathcal{H} = y/r$ for $\tau \geq \tau_*$, in which case the initial values of the vertical components are

$$\mathcal{H}_* = 1 + \gamma\,\cos\theta_*, \quad \mathcal{H}'_* = -\delta'_* - \omega_*\,\gamma\,\sin\theta_*.$$

Then

$$\mathcal{H}(\tau) = \mathcal{H}_* + \mathcal{H}'_*\,(\tau - \tau_*) - \tfrac{1}{2}\,(\tau - \tau_*)^2.$$

For point O, the centre of the hoop, $Y = y - r\,\gamma\,\cos\theta$, therefore

$$Y/r = \mathcal{H}_* + \mathcal{H}'_*\,(\tau - \tau_*) - \tfrac{1}{2}\,(\tau - \tau_*)^2 - \gamma\,\cos\theta(\tau),$$

where $\theta(\tau)$ is found from (7.23).

At the beginning of this chapter the non-dimensional height of point O, $\mathcal{H}_O$, was defined as $\mathcal{H}_O = Y/r - 1$. While the hoop is in contact with the surface, $\mathcal{H}_O = -\delta$; during the hop, $\mathcal{H}_O > 0$ describes the path of the centre of the hoop. From the above therefore,

$$\mathcal{H}_O = -\delta \quad \text{or} \quad \mathcal{H}_O = \gamma\,\cos\theta_* + \mathcal{H}'_*\,(\tau - \tau_*) - \tfrac{1}{2}\,(\tau - \tau_*)^2 - \gamma\,\cos\theta(\tau). \tag{7.24}$$

This motion continues as long as $\mathcal{H}_O > 0$. Denoting the time at the end of the hop by τ_+, i.e. $\mathcal{H}_O(\tau_+) = 0$, then $\theta_+ = \theta_* + (\tau_+ - \tau_*)\,\omega_*$. The values of $\mathcal{H}_{O_{max}}$ and τ_+ are found by calculating $\mathcal{H}_O$ from (7.24).

The horizontal displacement of point O can be found in a similar manner. Noting that $(x/r)_* = \mathcal{X}_* + \gamma \sin\theta_*$, $(x/r)'_* = \mathcal{V}_{x*} + \omega_* \gamma \cos\theta_*$, and $(x/r) = (x/r)_* + (x/r)'_* (\tau - \tau_*)$, the horizontal displacement of the centre of the hoop during the hop is

$$X/r = \mathcal{X}_* + \gamma \sin\theta_* + (\mathcal{V}_{x*} + \omega_* \gamma \cos\theta_*)(\tau - \tau_*) - \gamma \sin\theta(\tau).$$

The horizontal span of the hop, $\mathcal{S}_h = \mathcal{X}_+ - \mathcal{X}_*$, is then given by

$$\mathcal{S}_h = +\gamma \sin\theta_* + (\mathcal{V}_{x*} + \omega_* \gamma \cos\theta_*)(\tau_+ - \tau_*) - \gamma \sin\theta_+. \tag{7.25}$$

7.5 Behavioural patterns of the elastic models

A few numerical results for the elastic models are shown on graphs and phase diagrams similar to those used for rigid hoops. There is however no attempt at repeating the detailed analysis of the previous chapters, and the emphasis is almost completely on aspects relating to hopping. Except where specifically mentioned, the results shown are for the external elastic model.

7.5.1 Rolling curves

Once again the rolling curves can be used as an aid in understanding the motion, where a rolling curve is the graph of $\mathcal{F}/\mathcal{N}$ as a function of θ during rolling. In the case of elastic hoops these rolling curves are often characterised by oscillations caused by the initial impulse of the centrifugal effect of the initial angular velocity.

The relative maximum and minimum values of this curve define the critical friction coefficients μ_L and μ_H as before; in this case however the precise definition is more complicated than that for the rigid model because of the oscillations. The curves are no longer skew-symmetric, and only the the first half, for $\theta \leq \pi$, is used.

In Figure 7.3(a) the rolling curves for four values of the elastic constant are shown, for the case $\gamma = 2/3$ and $\omega_0 = 0.2$. The upper curve, shown as a heavy solid curve, with values of $\mu_L = 0.276$ and $\mu_H = 0.224$, is the curve for a rigid hoop on a rigid surface. It is convenient to refer to this as the *rigid rolling curve*, abbreviated as the RRC.

The lower curve, shown as a light dotted curve, with values of $\mu_L = 0.278$ and $\mu_H = 0.512$, is the curve obtained when $e = 10$, i.e. for a very soft surface. The elasticity clearly has very little influence on the value of μ_L, but causes a large increase in the value of μ_H.

The heavy dotted curve is for $e = 20$ and the light solid curve for $e = 200$; clearly the curves tend to the RRC as e tends to infinity.

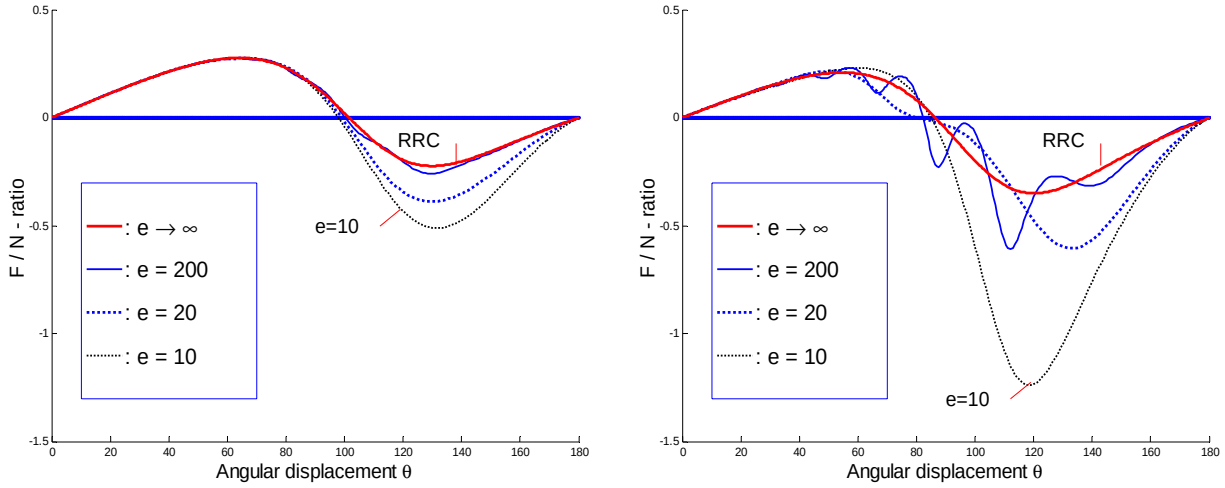

(a) : $\omega_0 = 0.2$ (b) : $\omega_0 = 0.5$

Figure 7.3 : Examples of Rolling curves for $\gamma = 2/3$

Figure 7.3(b) shows the effect of increasing the initial velocity to 0.5, keeping the other parameters the same. For the very soft surface, $e = 10$, the main effect is to increase the magnitude of the minimum point to $\mu_H = 1.24$; very little oscillation is discernable. The curve for $e = 20$ shows slight oscillations, and the stiffer surface with $e = 200$ shows five oscillations around the curve for the rigid surface. The values of μ_L and μ_H are shown in the last two columns of Table 7.1.

These oscillations are illustrated best on the graphs of δ, as shown in Figure 7.4, where δ is now shown as a function of dimensionless time τ. In Figure 7.4(a) the initial velocity is $\omega_0 = 0.5$ and the curves are shown for $e = 20$ and 200. Note the initial displacements of $\delta_0 = 1/e$. As could be expected on physical grounds, the stiffer surface with the large e-value oscillates at a higher frequency and smaller amplitude.

Figure 7.4(b) shows the effect of increasing ω_0 to 0.8. The value of θ is also shown as a second horizontal axis. The larger initial impulse and centrifugal effect cause greater amplitudes in the oscillation, and the second minimum point is almost zero. This suggests that a further increase in the initial velocity may cause hopping; this aspect will be explored later.

It is also of some interest to compare the period of these oscillations with the period of the free oscillations of a simple oscillator. A simple oscillator with mass m and stiffness k oscillates with a natural period of $2\pi\sqrt{m/k}$. In terms of non-dimensional time this becomes

$$\tau_n = 2\pi \sqrt{g/r}\,\sqrt{m/k} = 2\pi/\sqrt{e}.$$

For large values of e, this correlates reasonably well with the period of the early oscillations during rolling, as measured in for example Figure 7.4. These results are summarised in Table 7.1, where τ_1 is the period measured between the start and the first relative maximum, and

τ_2 is the period between the first two relative minima, for different values of e. Clearly the correlation is better for the stiffer surfaces.

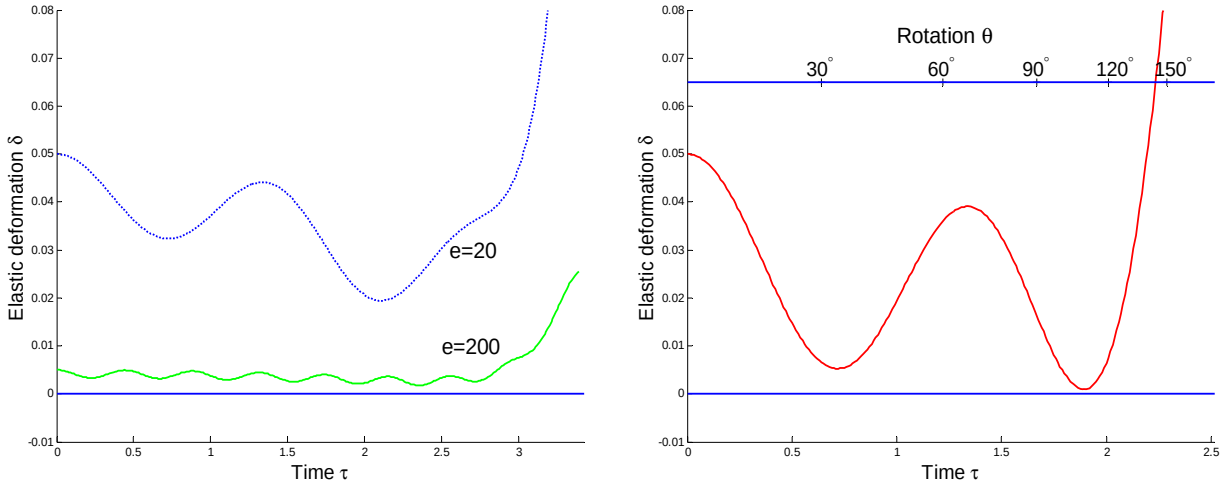

(a) : $\omega_0 = 0.5$. (b) : $\omega_0 = 0.8$, $e = 20$.

Figure 7.4 : Examples of the oscillations during rolling, for $\gamma = 2/3$

e	τ_n	τ_1	τ_2	μ_L	μ_H
10	1.99	1.79	1.62	0.23	1.24
20	1.40	1.33	1.38	0.22	0.61
200	0.44	0.44	0.45	0.27	0.61
∞	-	-	-	0.21	0.35

Table 7.1 : Values of the oscillation periods and critical friction coefficients for $\gamma = 2/3$ and $\omega_0 = 0.5$ with different elasticities

In terms of real time, these periods are $\sqrt{r/g}\,\tau_n$. For example, taking a large hoop with 1 meter diameter on a soft surface with $e = 10$, $\tau_n = 1.99$ converts to 0.45 seconds; for a stiff surface and hoop with radius 0.1 meter, $\tau_n = 0.44$ converts to 0.044 seconds.

The last two columns in Table 7.1 show the values of the critical friction coefficients μ_L and μ_H from the rolling curves in Figure 7.3, confirming the earlier remarks that μ_L is not really affected by the elasticity at this initial velocity, but that μ_H is significantly affected.

This section is concluded with a comparison of the rolling curves for the two elastic models. Figure 7.5 shows the rolling curves for the rigid model, for the external elastic model, and for the internal elastic model, using medium soft elasticity of $e = 50$ and keeping $\gamma = 2/3$.

The graphs show that the curves for the two models are almost indistinguishable during the first half of the motion, so that the values of μ_L are essentially the same for the two models. However,

for θ approximately $> 90°$, the curves for the two models differ substantially, as reflected inter alia by the values for μ_H. In figure (a) μ_H is larger for the internal model, but the reverse is true for the higher velocity of $\omega_0 = 0.6$ in figure (b).

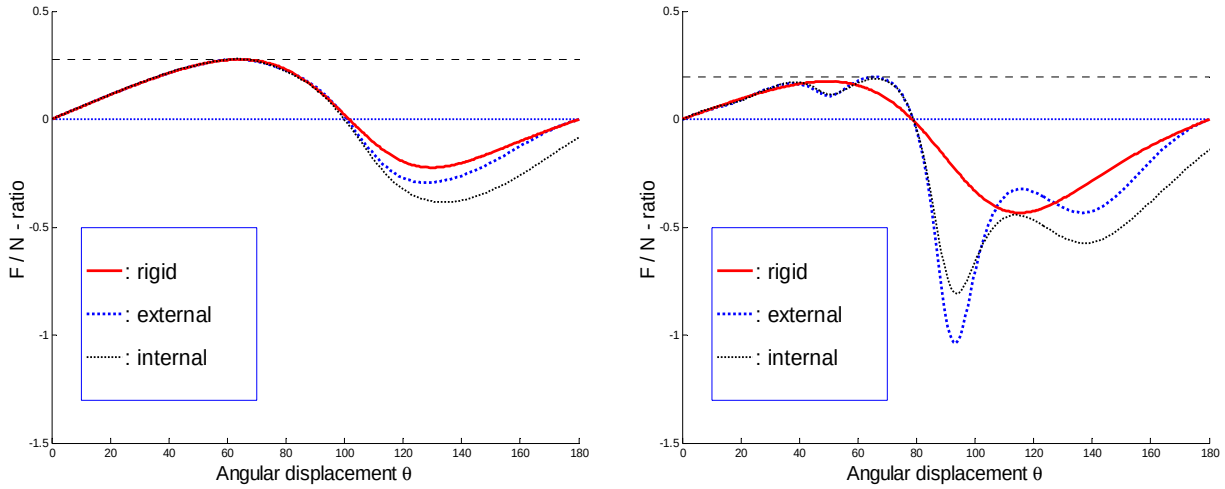

(a) : $\omega_0 = 0.2$ (b) : $\omega_0 = 0.6$

Figure 7.5 : Rolling curves for $\gamma = 2/3$ and $e = 50$ for both elastic models

7.5.2 Primary classification of the behaviour

The behavioural patterns of rigid hoops are also found for elastic hoops. In particular, the primary classification based on the first phase change is still valid. However, because of the initial oscillations, the previous definitions of, and algorithm for finding, the critical friction coefficients μ_L and μ_H are no longer valid for all cases and need to be modified as follows:

Heavy friction occurs when $\mu_s > \max(\mu_L, \mu_H)$, and implies rolling past $\theta = \pi$, or the bottom, and is therefore labelled `RB`. In this case heavy friction does not imply rolling through one complete revolution, and may include slipping phases and any final condition for $\theta > \pi$.

Medium friction is defined as cases where the first rolling phase changes to skidding with $\theta < \pi$, and is therefore labelled `RD*` as before. This occurs when $\mu_s \in (\mu_L, \mu_H]$.

Light friction is defined as cases where the first rolling phase changes to spinning with $\theta < \pi$, and is therefore labelled `RS*` as before. This occurs when $\mu_s \leq \mu_L$.

A precise algorithm for determining the numerical values of μ_L and μ_H is given below and is illustrated by the examples shown in Figure 7.6.

Algorithm 7.1 : Algorithm to determine μ_L and μ_H

- Draw the rolling curve for given values of parameters e, γ and ω_0.
- Specify a maximum value μ_{max}.
- Find $\mu_2 = \min(\mathcal{F}/\mathcal{N})$, occurring at position $\theta_H \leq \pi$; $\mu_H = \|\mu_2\|$.
- If $\mu_H > \mu_{max}$, find θ_H as the smallest θ where $\mathcal{F}/\mathcal{N} = -\mu_{max}$.
- REPEAT
  - Find $\mu_L = \max(\mathcal{F}/\mathcal{N})$, for $\theta \in (0, \theta_H)$, occurring at position θ_L.
  - Find $\mu_2 = \min(\mathcal{F}/\mathcal{N})$, for $\theta \in (0, \theta_L)$, occurring at position θ_H.

  UNTIL $\mu_L > \|\mu_2\|$.

Figure 7.6 illustrates the different situations that can now occur due to the initial oscillations. A value of $e = 50$ is used with $\gamma = 2/3$ and $\mu_{max} = 1.5$.

In case (a), $\omega_0 = 0.5$, there is a clear maximum and minimum and determining $\mu_L = 0.231$ and $\mu_H = 0.663$ is straight forward.

In case (b), $\omega_0 = 0.8$, the value of μ_H exceeds the maximum allowable value of 1.5 at approximately $\theta_H = 60°$. The maximum value before this point occurs at the second peak, $\mu_L = 0.158$, and this is clearly greater than the absolute value of the first minimum point at approximately $25°$, as shown in Figure 7.6(b).

In case (c), the slight increase in velocity to $\omega_0 = 0.82$ causes the first trough to drop below the value of the second peak, as shown by the horizontal dotted lines. Now the loop in the algorithm has to be repeated once, and $\mu_L = 0.035$ is measured at the first peak. This causes a sharp drop in the value of μ_L.

In case (d), $\omega_0 = 0.85$ the first trough drops below $-\mu_{max}$, and $\mu_L = 0.033$ is again measured at the first peak.

These examples illustrate the extreme sensitivity of the rolling curve to the initial velocity.

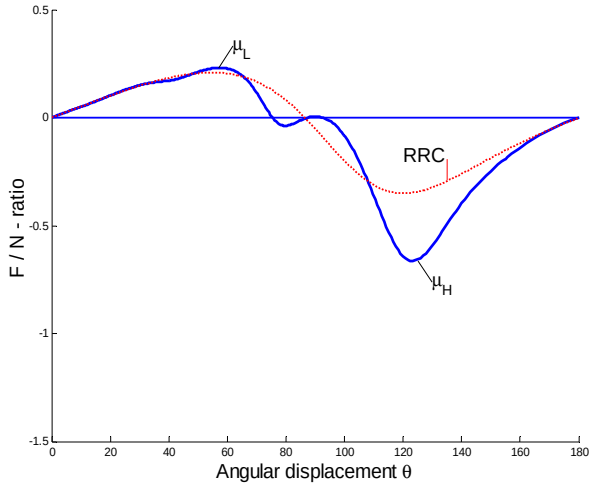

(a) : $\omega_0 = 0.5$.

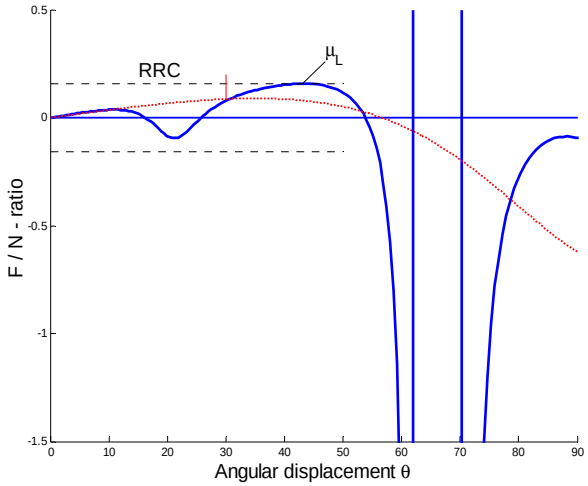

(b) : $\omega_0 = 0.8$.

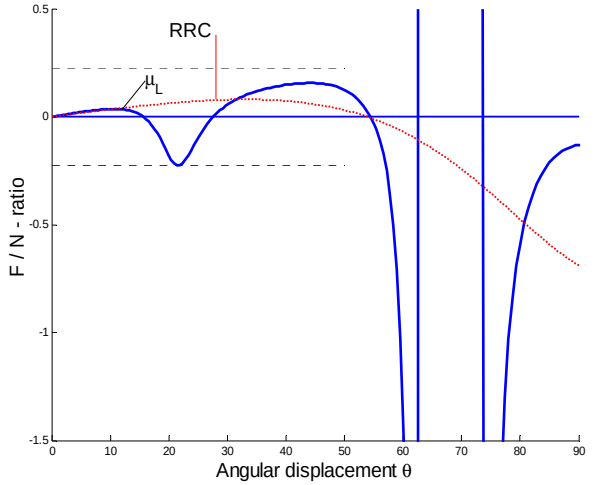

(c) : $\omega_0 = 0.82$.

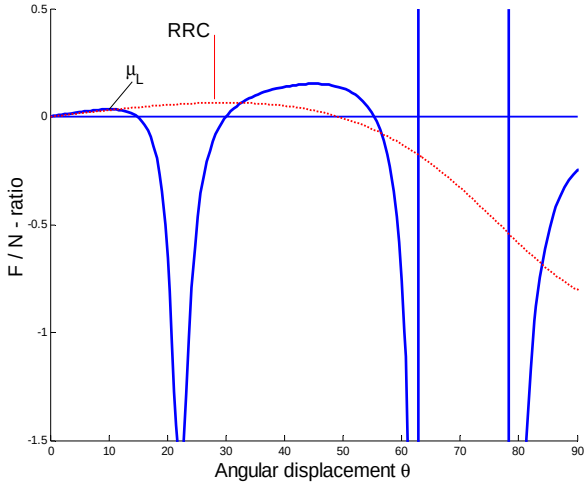

(d) : $\omega_0 = 0.85$.

Figure 7.6 : Examples of rolling curves used to find μ_L and μ_H, for $\gamma = 2/3$ and $e = 50$

7.5.3 Phase diagrams in (μ, ω_0)-space

The primary classification can again be shown on (μ, ω_0)- phase diagrams, for specific values of γ and e. An example is shown in Figure 7.7 for $\gamma = 2/3$ and $e = 50$.

The results for the external model are shown in Figure 7.7(a), and as could be expected from the results in the previous section, the oscillations have the effect that the curves are no longer smooth. The large step in this curve when $\omega_0 = 0.82$ is due to the sudden change when the value of μ_L jumps from the second to the first peak on the rolling curve, as discussed in the previous section. The solid white curves are the corresponding curves for a rigid hoop. The region of light friction is approximately the same for the two cases, but the region of heavy friction is much smaller in the case of the elastic model. The solid white line at $\omega_0 = \sqrt{3/2} = 1.22$ is the line for $\hat{\omega}_0$ for the rigid case. In the elastic model no such limit on ω_0 exists.

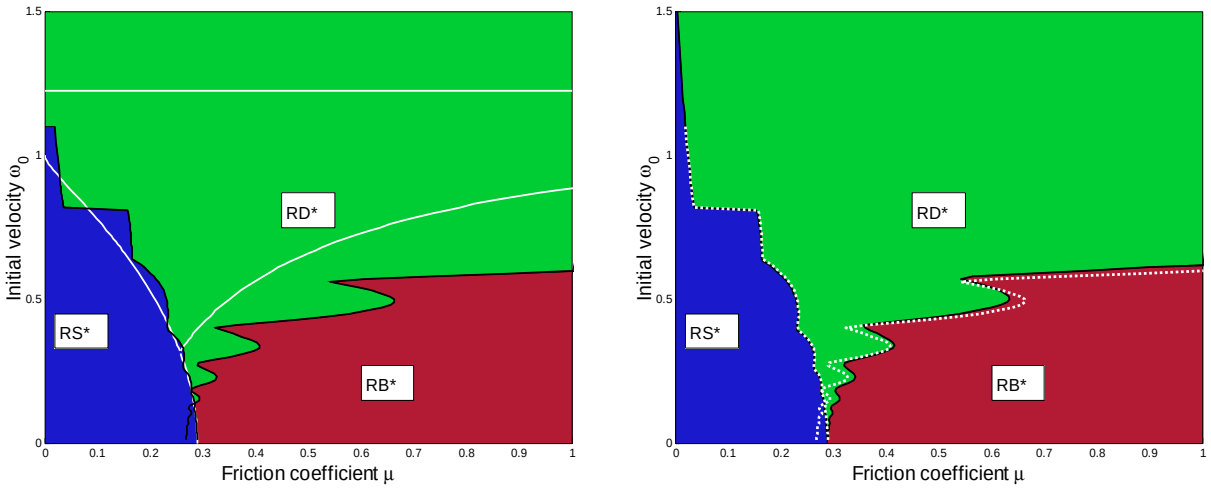

a: External model

b: Internal model

Figure 7.7 : Phase diagrams showing the primary classification in (μ, ω_0)-space for $\gamma = 2/3$ and $e = 50$

The regions for the internal model are shown in Figure 7.7(b), with the dotted white lines demarcating the regions for the external model. At this scale the curves for μ_L for the two elastic models are indistinguishable, and the difference in μ_H between the two models is noticeable, but not significant.

7.6 Classification of different types of hopping

In chapters 4 to 6 it was shown that rigid hoops could hop in two situations:

- If $\omega_0 > \hat{\omega}_0$, hopping occurs at $\theta_* = 0$; this is termed immediate hopping for a rigid hoop.
- If $\omega_0 \in (\hat{\omega}_H, \hat{\omega}_0)$, hopping occurs at $\theta_* > \pi$, i.e. while the particle is moving *upwards*.

The latter type of hopping will henceforth be termed *normal hopping*, and it also occurs in the case of both elastic models. However, θ_* is usually smaller than in the case of the rigid model.

With the elastic models we find that the hoop can also hop while the particle is moving *downwards* and $\theta_* < \pi$; later results show that in fact this occurs with $\theta_* < \pi/2$. Two situations are found:

- In the case of the elastic models, *immediate hopping* is characterised by the property that no oscillation occurs before the hop; i.e. the hop commences before the first minimum in δ, with $\theta_* > 0$. This immediate hopping region on phase diagrams is similar to, but larger than, the corresponding region of immediate hopping of rigid hoops. Immediate hopping is due to a large initial centrifugal effect, similar to that seen in the case of rigid hoops, section 4.2.5.
- Hopping can also occur as a result of the initial oscillations combined with the centrifugal effect of the particle, with $\theta_* < 90°$; this type of hopping will be termed *early hopping*.

Finally, a sub-class of normal hopping occurs with very large eccentricities. In these cases the angular velocity becomes zero just before the hop occurs, and the hoop has a *negative angular velocity* during the hop. This will be referred to as *backspin hopping*. Henceforth all references to normal hopping will imply exclusion of backspin hopping.

When labels are used to described the different phases of the motion, the four different types of hop are indicated by subscripts.

To summarise, hops are classified as follows:

- Normal hopping occurs at $\theta_* > \pi$ and with $\omega_* > 0$. This is denoted by `R* H`$_n$.
- Backspin hopping occurs at $\theta_* > \pi$ with $\omega_* < 0$ and is denoted by `R* H`$_b$.
- Immediate hopping occurs without any oscillation and is denoted by `R* H`$_i$.
- Early hopping occurs at $\theta_* < \pi/2$ after one or more oscillations and is denoted by `R* H`$_e$.

7.6.1 Normal Hopping

Normal hopping constitutes the case where the behaviour of the hoop is similar to that of the rigid hoop, in that hopping occurs after the particle has passed its lowest position. Because of the large centrifugal effect of the high angular velocity in the region of $\theta = \pi$, the compression at the lowest point is large, corresponding to the large normal reaction in this position. As the particle starts moving upwards, with $\theta > \pi$, the "spring" tends to push upwards and the effect

is that the normal reaction reduces to zero very rapidly in most cases, resulting in a hop shortly after the particle passes the lowest point, usually at angles which are smaller than those found previously for the rigid case.

This is illustrated in Figure 7.8 for two cases, in which a reasonably soft surface with $e = 50$ is used, together with $\gamma = 2/3$ and $\mu = 0.3$. The curves show the $\mathcal{F}/\mathcal{N}$-ratio and the height of point O as defined by $\mathcal{H}_O$, as calculated from (7.24).

In Figure 7.8(a) a low initial velocity, $\omega_0 = 0.2$, is used; this does not cause significant initial oscillations. The friction coefficient is large enough to ensure rolling past 180°, making this a case of heavy friction. However, as is clear from the graph in Figure 7.8 (a), a slight increase in initial velocity or a slight decrease in the friction coefficient will change the motion to that of medium friction.

In contrast to the rigid hoop, the elasticity causes a sharp drop in the normal reaction when $\theta > 180°$, resulting in a very short spinning phase and a hop at $\theta_* = 225°$, marked by the second vertical dotted line. The phase labels are `R----S` $\mathtt{H}_n$. By reducing the friction coefficient to $\mu_s = 0.28$ the motion changes to one of medium friction, labelled `RDRS` $\mathtt{H}_n$. A further reduction to $\mu_s = 0.25$ results in a case of light friction, labelled `RSRDRS` $\mathtt{H}_n$, with very little change in the value of θ_*.

In Figure 7.8(b) a higher initial velocity, $\omega_0 = 0.6$, is used; this causes initial oscillations and a higher value of μ_H, taking the motion out of the heavy friction and into the medium friction region, labelled `RDRS` $\mathtt{H}_n$. The larger velocity also causes a larger hop; in this case $\mathcal{H}_{O_{max}} = 0.118$.

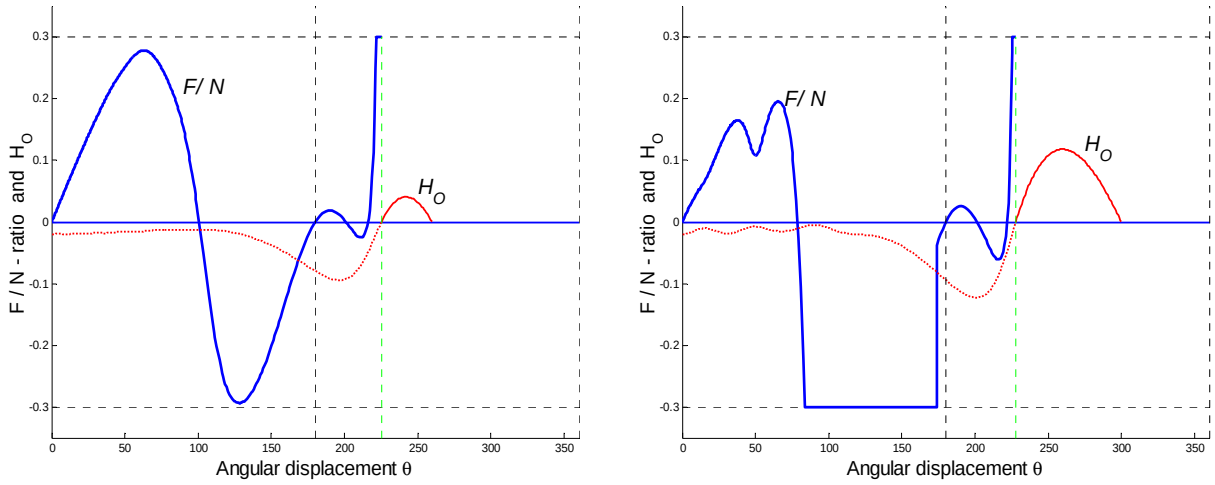

(a) : $\mathcal{P}_0 = \{2/3,\ 0.3,\ 0.2\}$ (b) : $\mathcal{P}_0 = \{2/3,\ 0.3,\ 0.6\}$

Figure 7.8 : Examples of Normal hopping for $e = 50$

7.6.2 Early Hopping

Early hopping is defined as hopping when $\theta_* < 90°$, i.e. hopping while the particle is moving *downward*, but excluding cases of immediate hopping. Hopping therefore occurs at the second or later maxima of the $\mathcal{H}_O$-curve. Note that $\mathcal{H}_O = -\delta$ while $\theta < \theta_*$, and therefore the maxima on the $\mathcal{H}_O$-curve correspond to the minima on the δ-curve.

Two examples are shown in Figure 7.9; in this case the $\mathcal{H}_O$-curve is magnified by a factor of 10.

In the first case the parameters are the same as in Figure 7.8, but the initial velocity is increased to $\omega_0 = 0.8$. Now a minute hop occurs at $\theta_* = 62.4°$, with $\mathcal{H}_{O_{max}} = 0.0003$. The pattern of the motion is `RD` $\mathtt{H}_e$; this is therefore an example of medium friction and early hopping.

In the second case a heavier particle is used, with eccentricity $\gamma = 4/5$. If the initial velocity is reduced to 0.7, and the friction coefficient to 0.21, the pattern changes to `RSRD` $\mathtt{H}_e$, with $\theta_* = 54.1°$, i.e. early hopping and light friction.

In both cases the initial value of $\mathcal{H}_O(0) = -1/e = 0.02$ is clearly recognisable.

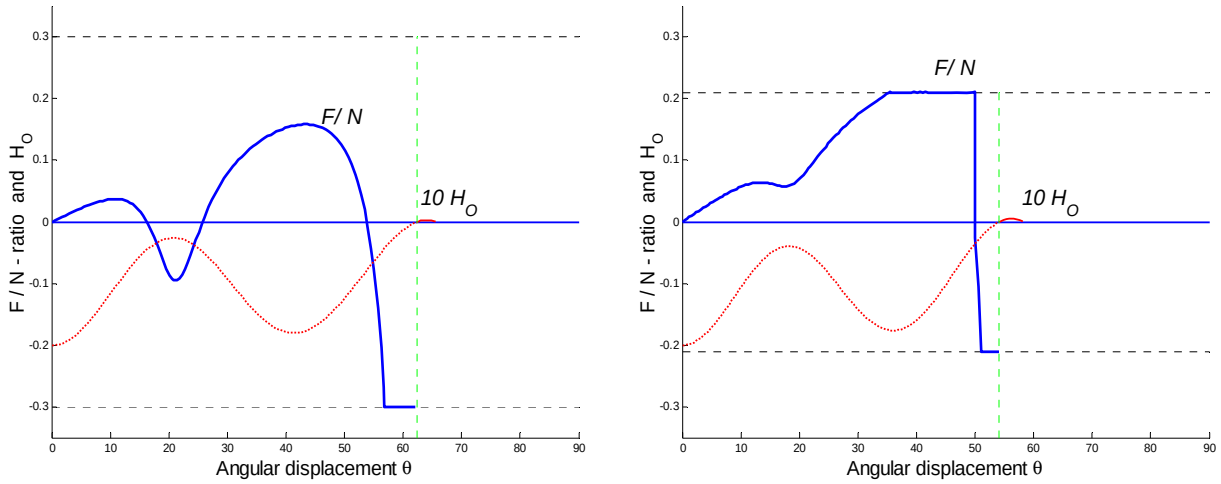

(a) : $\mathcal{P}_0 = \{2/3,\ 0.3,\ 0.8\}$ (b) : $\mathcal{P}_0 = \{4/5,\ 0.21,\ 0.7\}$

Figure 7.9 : Examples of Early hopping for $e = 50$

7.6.3 Immediate Hopping

In the context of elastic models, immediate hopping is characterised by the property that hopping occurs without any prior oscillations; i.e. the original compression combined with the centrifugal effect of a high initial velocity "shoots" the hoop away from the surface after rotating through a relatively small angle. This implies that hopping corresponds to the first minimum in the δ-curve.

Figure 7.10 shows the graphs for two examples of immediate hopping. As before, the solid curves show the $\mathcal{F}/\mathcal{N}$-ratio, showing the different phases of the motion, and the dotted curves show $\mathcal{H}_O$, magnified by a factor 2.

In case (a) the parameters are $e = 50$, $\gamma = 2/3$ and $\mu_s = 0.3$, as used in figures 7.8 and 7.9(a), and the initial velocity is increased to $\omega_0 = 1.0$. This results in a very short roll and skid before the hop occurs at $\theta_* = 17^\circ$, with $\mathcal{H}_{O_{max}} = 0.01$.

The corresponding graphs in Figure 7.10(b) are for a softer surface with $e = 20$, resulting in a longer motion with $\theta_* = 26.9^\circ$ and larger hop with $\mathcal{H}_{O_{max}} = 0.023$.

Once again the initial value of $\mathcal{H}_O(0) = -1/e$ is clearly recognisable, as is the medium friction pattern of `RD` $\mathtt{H}_i$.

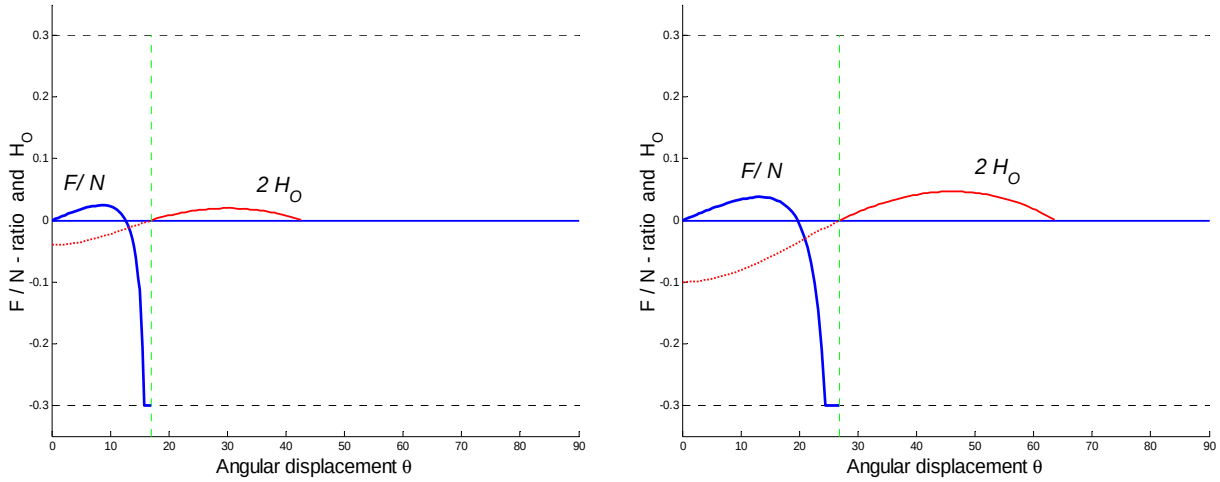

(a) : $e = 50$ (b) : $e = 20$

Figure 7.10 : Examples of Immediate hopping for $\mathcal{P}_0 = \{2/3,\ 0.3,\ 1.0\}$

In Figure 7.11 the hop produced by the two elastic models is compared, in case (a) for a medium stiff elasticity and case (b) for a very soft case. For $e = 50$ there is no discernable difference in the hop of the two models, and for $e = 10$ the external model produces a slightly larger hop than the internal model.

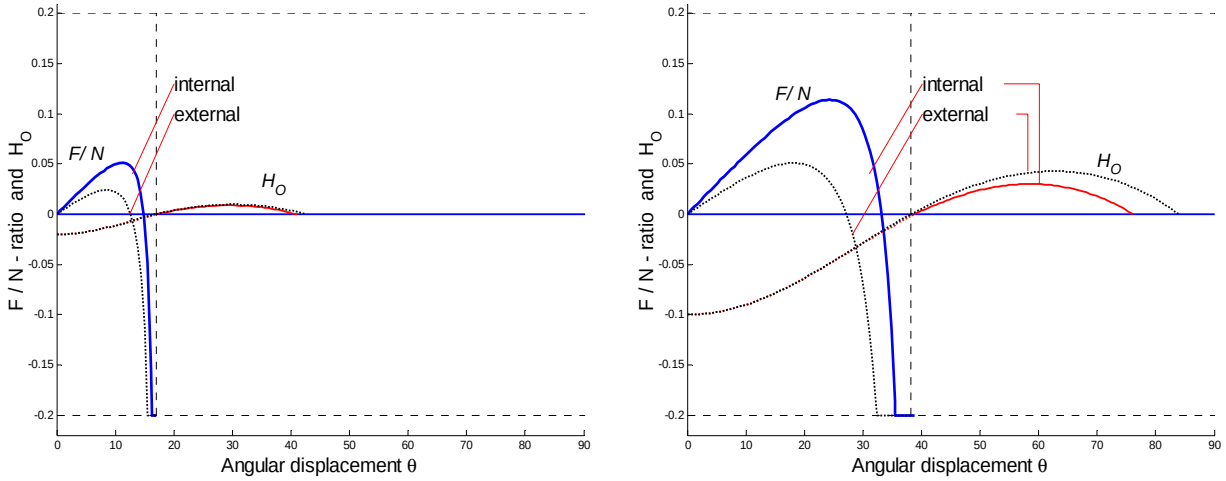

(a) : $e = 200$ (b) : $e = 10$

Figure 7.11 : Examples of Immediate hopping for $\mathcal{P}_0 = \{2/3,\ 0.2,\ 1.0\}$, showing the curves for external (dotted) and internal (solid) elastic models

This immediate hop is mainly due to the centrifugal effects of the initial angular velocity. Therefore increasing ω_0 and/or γ will enlarge this effect, resulting in smaller values of θ_*. The examples in Table 7.2 illustrate the extremes; in the first case, a small value of θ_* is obtained with a stiff surface and very heavy particle; in the second, a large value of θ_* is obtained with a soft surface and small γ. In both cases the pattern is once again medium friction, RD H_i.

Also shown in Table 7.2 are the values for $\mathcal{H}_{O_{max}}$ for each case. In the first case this value is very large due to the very high initial velocity. In the second case the hop is extremely small, because the value of ω_0 is the minimum required to cause initial hopping.

Shown in the last column are the values of the minimum initial velocity required to cause immediate hopping, denoted by $\hat{\omega}_0$. These values are found by numerical experimentation for a given e, γ and μ_s, and are used to plot the lower boundary of the immediate hopping region in Figure 7.13 in the next section.

e	$\mathcal{P}_0 = \{\gamma,\ \mu_s,\ \omega_0\}$	θ_*	$\mathcal{H}_{O_{max}}$	Phases	$\hat{\omega}_0$
200	{ 0.9, 0.05, 2.0 }	6.2°	0.88	RDH$_i$	0.75
20	{ 0.5, 0.20, 1.0 }	57.6°	0.0003	RDH$_i$	1.0

Table 7.2 : Two examples of immediate hopping

7.6.4 Backspin Hopping

Backspin hopping is characterised by the unusual situation that the hoop is rotating backwards because of the negative angular velocity during the hop. This occurs only for hoops with very large eccentricities, as shown in later phase diagrams.

After adjusting the solution algorithm to allow for negative angular velocity, the graphs shown in Figure 7.12 are obtained. In Figure (a) the graph of the $\mathcal{F}/\mathcal{N}$-ratio is shown as a function of θ as before. Also shown are the curves for δ and ω, the latter reduced by a factor of 10. The graphs clearly show that ω becomes zero and then negative, resulting in a backwards rotation. The graphs end at position $\theta_* = 203°$, shown by the dotted vertical line. This is slightly less than the maximum value of theta where ω becomes zero.

Figure 7.12(b) shows the path of the point O, as given by $\mathcal{H}_O$ in (7.24) and plotted here as a function of X/r.

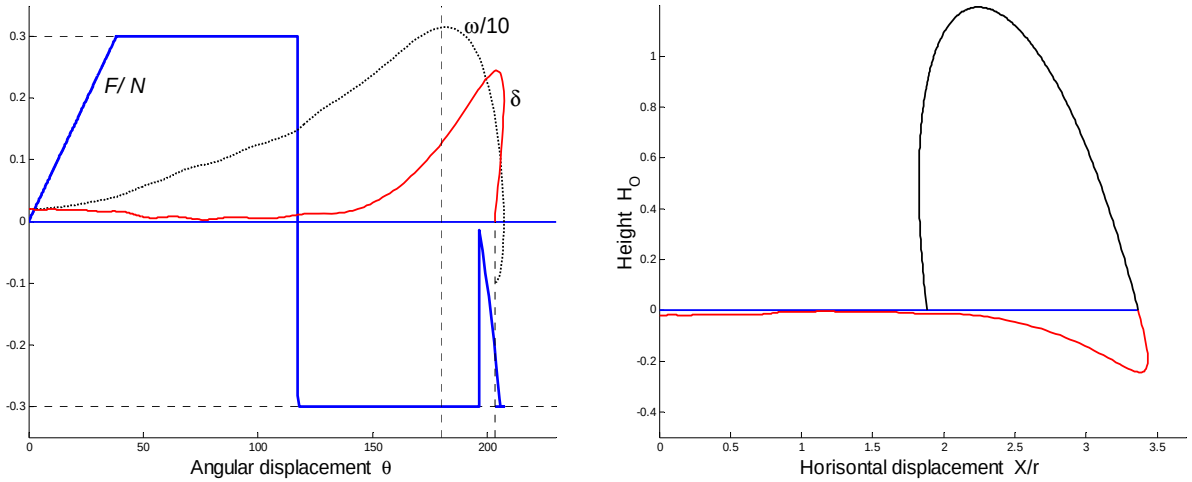

(a) (b)

Figure 7.12 : An example of Backspin hopping for $\mathcal{P}_0 = \{0.9,\ 0.3,\ 0.2\}$ and $e = 50$

7.7 Phase diagrams for the final conditions

7.7.1 Phase diagrams in (μ, ω_0)-space

In the case of the rigid hoop, the three possible final conditions for any motion are `Z`, signifying zero angular velocity, `T`, signifying that the hoop rotates through 360°, or `H`, signifying that a hop occurs. Similar regions for the elastic hoop are shown in the phase diagrams in Figure 7.13, where the region for hopping is divided into the sub-regions of normal, early and immediate hopping.

In Figure 7.13(a) the parameters are $\gamma = 2/3$ and $e = 50$, and the hoop hops for all values of μ and ω_0. In Figure 7.13(b) a stiffer elasticity, $e = 200$, is used together with a lighter particle to give $\gamma = 0.6$. For these parameters a reasonably large Z-region is found round the lower left corner, and a large T-region for the lower velocities. The heavy black curves demarcate the regions of light, medium and heavy friction as before.

In contrast to the rigid hoop, immediate hopping does not occur at $\theta = 0$, but at a small angle which depends on the parameters. Using numerical experimentation it is possible to find a value of $\hat{\omega}_0$ for a given set of parameters such that immediate hopping will occur if $\omega_0 \geq \hat{\omega}_0$. This region is shown as the upper region on the phase diagrams in Figure 7.13. The diagram shows that the friction coefficient has no effect on this value; in case (a) $\hat{\omega}_0 = 0.86$ for all values of μ, and in case (b) $\hat{\omega}_0 = 0.92$.

The region of early hopping is shown as a narrow region immediately below $\hat{\omega}_0$, with normal hopping occurring for still lower initial velocities.

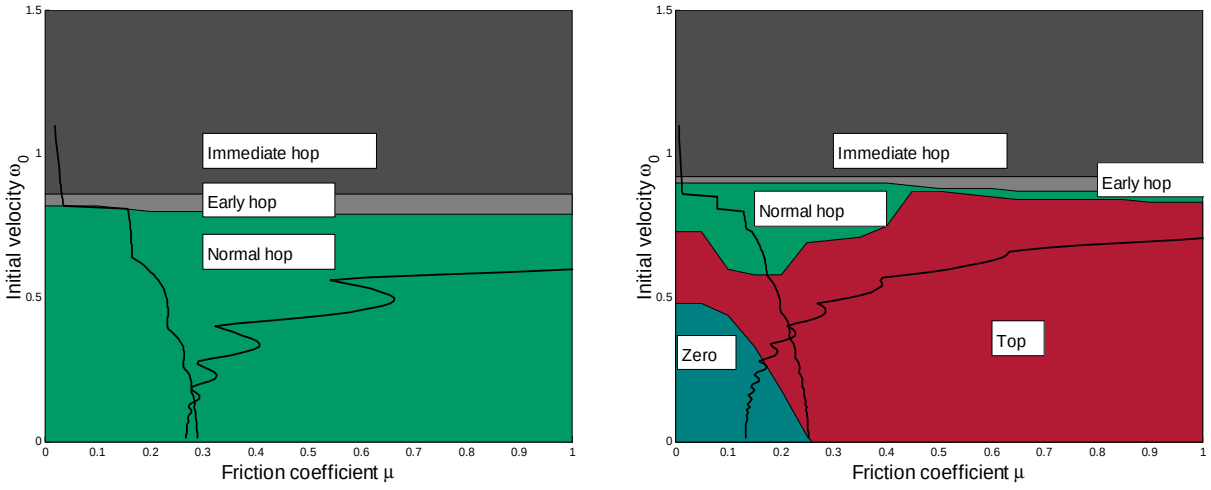

(a) : $\gamma = 2/3$ and $e = 50$ (b) : $\gamma = 0.6$ and $e = 200$

Figure 7.13 : Phase diagrams in (μ, ω_0) space showing the final conditions

7.7.2 Phase diagrams in (γ, ω_0)-space

The phase diagrams in (γ, ω_0)-space in Figure 7.14 show the regions that produce the four different types of hopping and the other two final conditions, for the case of a fairly smooth surface, $\mu = 0.2$. In case (a) a medium soft spring with $e = 50$ is used, and in case (b) a stiff spring with $e = 200$.

Also shown as white curves in case (a) are the corresponding regions for a rigid hoop with $\mu = 0.2$, as shown in Figure 6.1(a). For the elastic case, the Top-region where the hoop rotates a full 360° is found for all initial velocities and small eccentricities and corresponds reasonably closely to the region of heavy friction for the rigid model. A small triangular Z-region where the angular velocity becomes zero and the hoop starts rotating backwards is found for very small initial velocities near $\gamma = 0.5$.

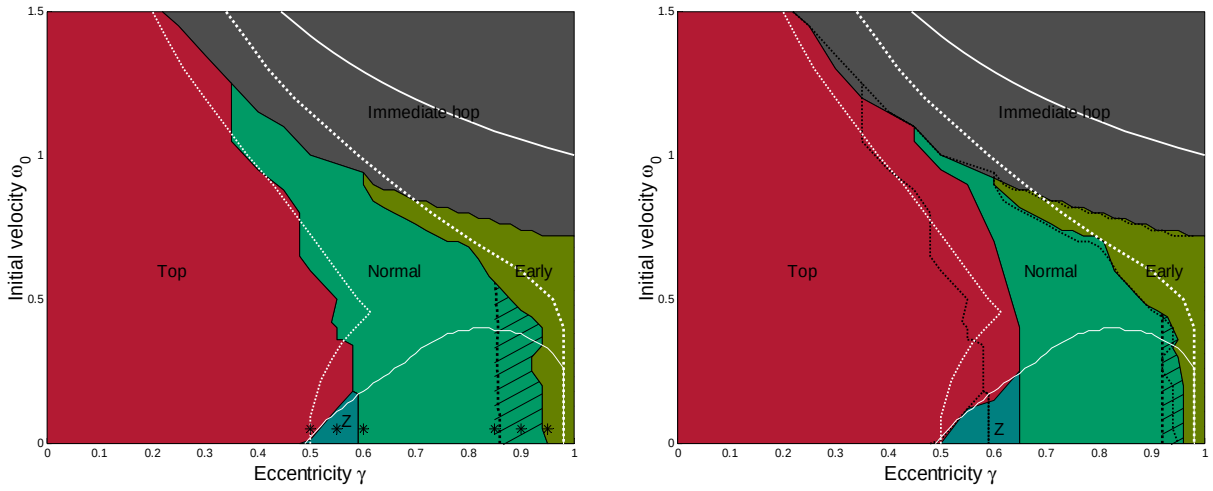

(a) : $e = 50$ (b) : $e = 200$

Figure 7.14 : Phase diagrams showing the different final conditions in (γ, ω_0)-space for $\mu = 0.2$ and two elasticities

The remainder of the area results in the four types of hopping, with immediate hopping occurring with high initial velocities, and early hopping with very large eccentricities. Backspin hopping was discussed in section 7.6.4. The region in which this type of hop occurs is shown as the hashed region of normal hopping to the right of the dotted curve. The dotted curve demarcating the start of this region is almost at a constant value of γ; when drawn to a larger scale with a very fine grid the value varies from $\gamma = 0.852$ at the top to 0.860 at $\omega_0 = 0$.

In Figure 7.14(b) the boundaries of the regions for case (a) are shown as dotted black lines, to facilitate the comparison between cases (a) and (b). Clearly the stiffer elasticity causes larger T- and Z- regions and smaller regions for normal and backspin hopping.

Six data points are marked by *'s on the line $\omega_0 = 0.05$ in Figure 7.14(a). The graphs showing the types of motion for each of these points are shown in Figure 7.15, to illustrate the different

situations. The $\mathcal{F}/\mathcal{N}$-ratio is shown by the solid curves in Figure 7.15 and the dotted curves represent d and ω as labelled. The angular velocity is scaled by a factor 0.1.

In case (a), $\gamma = 0.5$, the motion is labelled `RSRDR T`; clearly d is oscillating but positive, and ω is approaching zero as θ reaches 360°.

By increasing γ slightly to 0.55, the angular velocity becomes zero at 341° and the motion is `RSRSRDR Z`, as shown in Figure 7.15(b). Further increases to $\gamma = 0.6$ and 0.85 result in normal hopping, occurring at 268° and 213° respectively, as shown in Figure 7.15(c) and (d). Note that in case (d) the angular velocity is fast approaching zero.

A further increase to $\gamma = 0.9$ results in the unusual case where the angular velocity is negative and the hoop is rotating backwards at the moment of the hop, as can be seen by careful scrutiny of Figure 7.15(e). The hop occurs at $\theta = 203°$, whereas the angular velocity became zero at 207°. This type of normal hopping will be referred to as *backspin hopping* and is illustrated further in the next section.

The sixth case shows an example of early hopping. Note that the first minimum is scarcely detectable at the scale used, and that there is very little difference between early and immediate hopping.

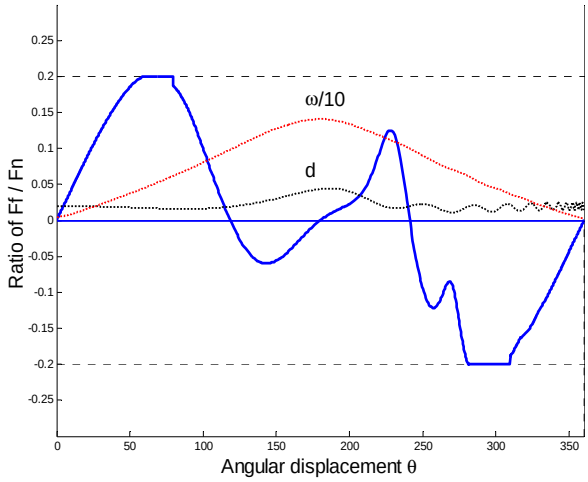

(a) : $\gamma = 0.5$; No hop, T

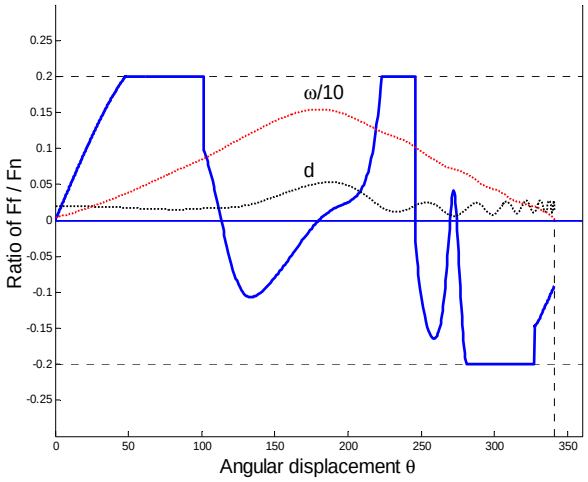

(b) : $\gamma = 0.55$; No hop, Z

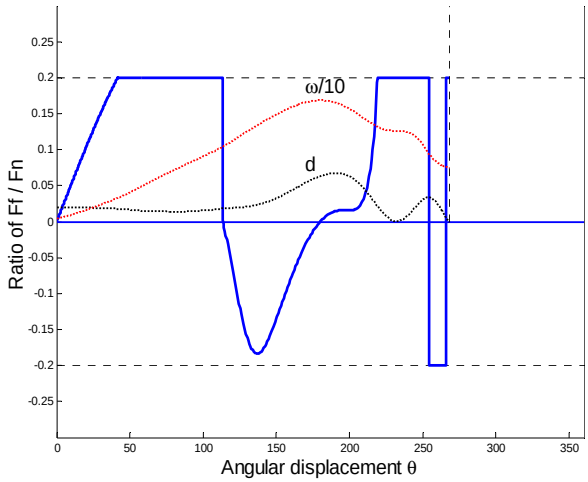

(c) : $\gamma = 0.6$; Normal hop

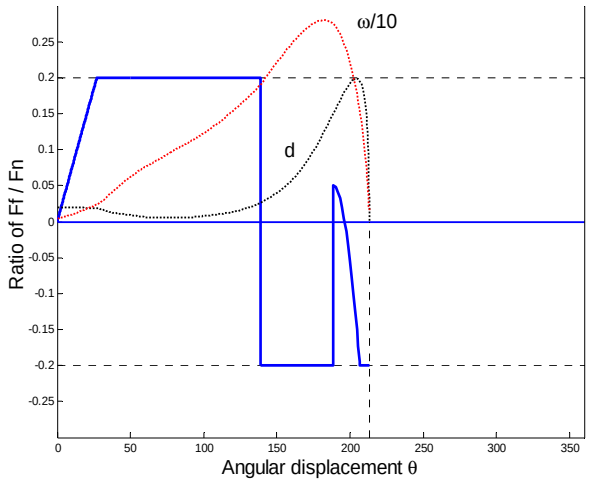

(d) : $\gamma = 0.85$; Normal hop

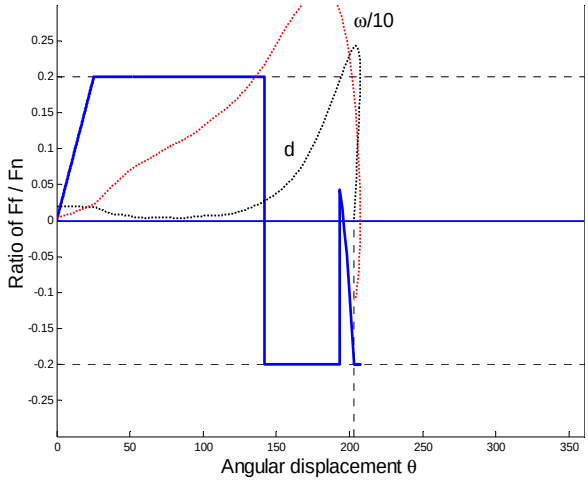

(e) : $\gamma = 0.9$; Backspin hop

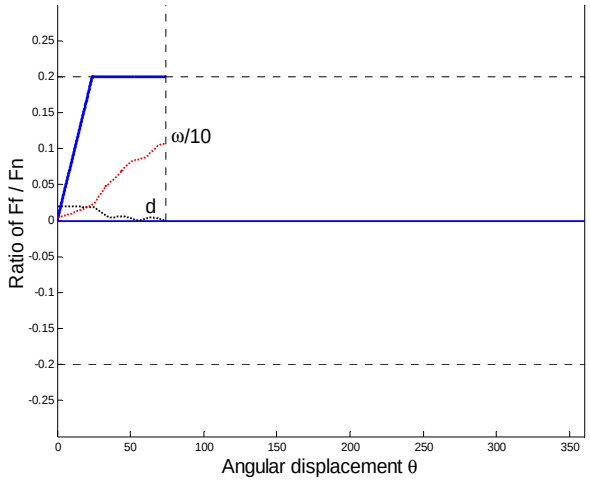

(f) : $\gamma = 0.95$; Early hop

Figure 7.15 : Graphs showing the different final conditions for $e = 50$, $\mu = 0.2$ and $\omega_0 = 0.05$ for different γ

7.8 Magnitude and path of the hops

As a final result we investigate the actual path of the hops, and the magnitude as conveniently measured in terms of the maximum height, $\mathcal{H}_{O_{max}}$.

In Figure 7.16 one example is shown for each of immediate, normal and backspin hopping, shown as cases (a), (b) and (c) respectively.

The first figure for each case shows $\mathcal{F}/\mathcal{N}$ and $\mathcal{H}_O$ as functions of θ as before, in for example figures 7.8 and 7.10. The characteristics of immediate and normal hopping can clearly be recognised in cases (a) and (b). In case (c) the same graphs for the case of backspin show that here the negative angular velocity results in a hop which starts at $\theta_* = 202°$ and ends at $\theta_+ = 49°$. The magnitude of this hop is $\mathcal{H}_{O_{max}} = 1.1$, approximately three times the magnitudes of the first two cases.

The second figure for each case shows the actual paths of points O and G during the hop. The solid curve represents the path of point O, and the dotted curve the parabolic path of G. Also shown is the hoop in three positions, together with the radius from O to P. The lightly dotted hoop is drawn in the position where the hop starts, with point O at co-ordinates $(0,\ 1)$. The hoop drawn as a solid circle is drawn at the end of the hop, with point O at $(\mathcal{S}_h,\ 1)$, where $\mathcal{S}_h$ is the span as previously defined. The intermediate hoop is drawn at the highest point of the hop.

In the immediate hop example, the second figure clearly shows the rotation of the OP-radius, progressing from $\theta = \theta_* = 14°$ to $\theta \approx 90°$ to $\theta = \theta_+ = 155°$ while point G is following a parabolic path which was started with an initial velocity which is almost horizontal; in this example the calculated values are $\mathbf{v}_G = \{2.62,\ -0.06\}$.

In the example of a normal hop, the initial velocity for the parabolic path of point G is $\mathbf{v}_G = \{0.54,\ 1.64\}$, resulting in a much narrower parabola and smaller span for the hop when compared to the previous case. Also, because of the clockwise rotation around G, point O starts moving backwards; during the last stage of the hop $\mathcal{V}_x$ is negative.

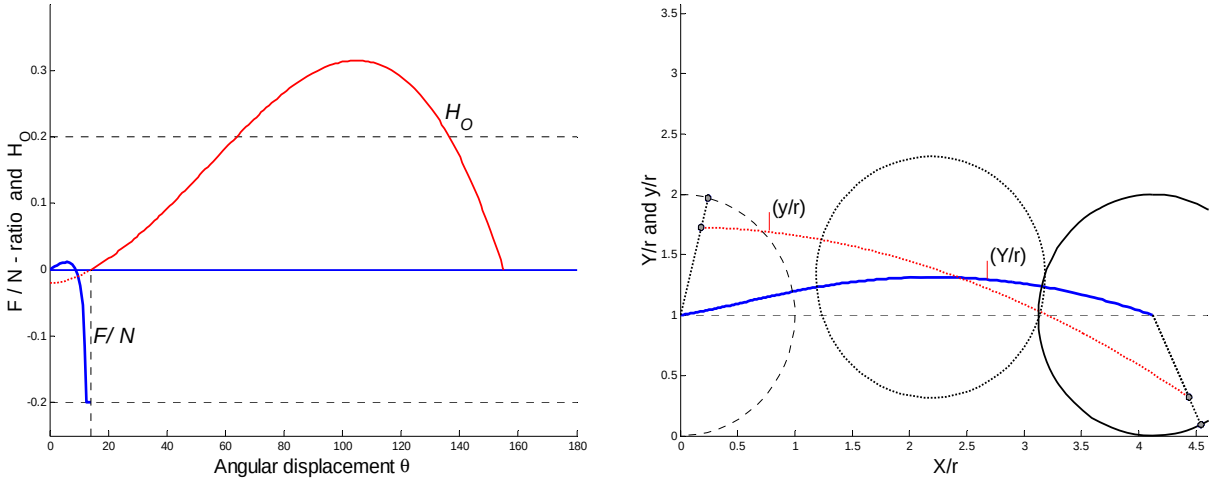

(a) : Immediate hop $\gamma = 3/4,\ \omega_0 = 1.5$

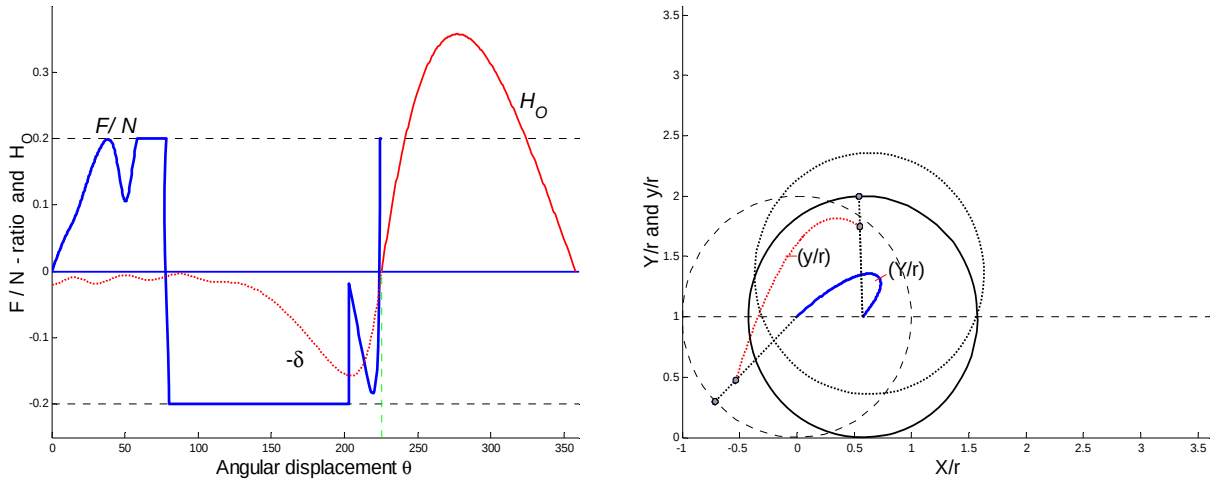

(b) : Normal hop $\gamma = 3/4$, $\omega_0 = 0.6$

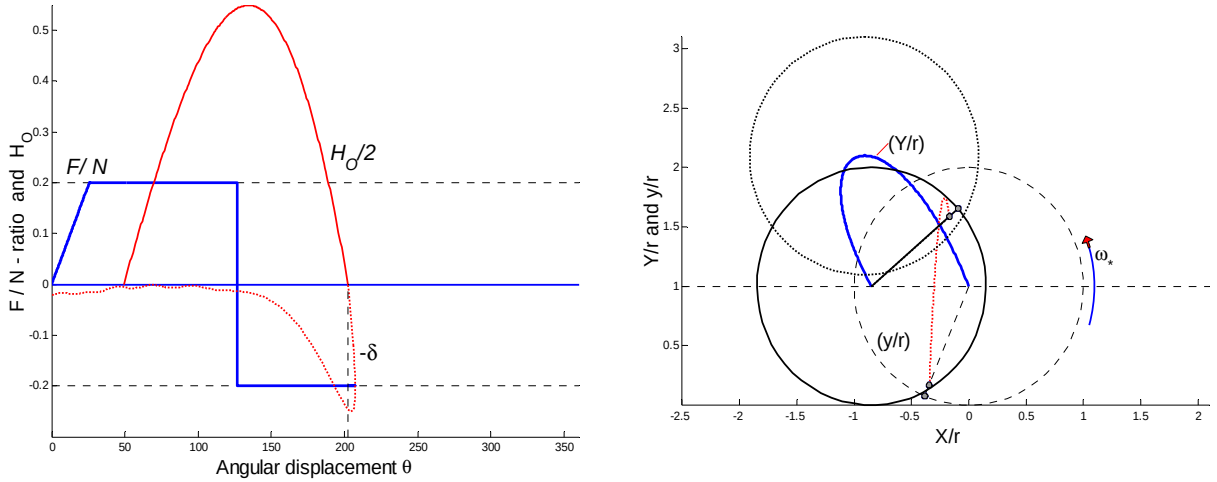

(c) : Backspin $\gamma = 0.9$, $\omega_0 = 0.3$

Figure 7.16 : Graphs showing examples of immediate, normal and backspin hops for $e = 50$ and $\mu = 0.2$

The angular velocities and maximum heights for the first two cases are the same order of magnitude, being $\omega_* = 1.51$ and 1.15 respectively, and $\mathcal{H}_{O_{max}} = 0.315$ and 0.357.

In the third case, the hoop is rotating backwards with $\omega_* = -1.15$, and $\mathbf{v}_G$ is almost vertical. The combined effect is a large backwards hop with a maximum height exceeding 1 and negative span.

Finally, in Figure 7.17 a few contours of equal maximum height are shown on the (γ, ω_0) phase diagram. The contours shown are for $\mathcal{H}_{O_{max}} = 0.05, 0.2, 0.5, 1.0$ and 1.6, as labelled. Also shown as heavy dotted curves are the boundaries between the different types of hopping as in Figure 7.14.

A large region, which includes nearly all of the early hopping region, produces very small hops with $\mathcal{H}_{O_{max}} < 0.05$. In the immediate hopping region the magnitude of the hop increases as γ and ω_0 increase, reaching a value of $\mathcal{H}_{O_{max}} = 0.62$ at point $(0.98,\ 1.5)$. In the normal hopping region the magnitude of the hop increases as γ increases, reaching a maximum at $\gamma = 0.86$, the curve where backspin hopping starts. A very large maximum of $\mathcal{H}_{O_{max}} = 1.86$ occurs at point $(0.864,\ 0.52)$, which is near the top of the backspin region. Further increase in γ through the backspin region causes a decrease in the hop magnitude, with a very sharp drop at the boundary between backspin and early hopping.

The data points for the three examples in Figure 7.16 are indicated by *'s.

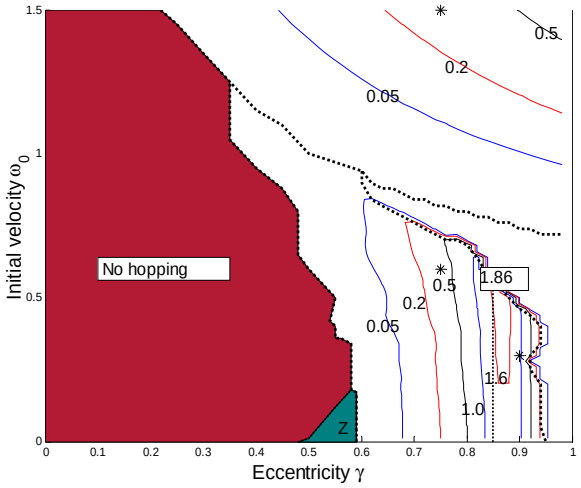

Figure 7.17 : Phase diagram showing contours of constant $\mathcal{H}_{O_{max}}$ in $(\gamma,\ \omega_0)$-space for $e = 50$ and $\mu = 0.2$

7.9 Summary and conclusions

Two elastic models have been developed, and no essential difference in the behaviour of the two models has been found. Nearly all the results shown are for the external model, in which a rigid hoop rolls on an elastic surface.

An important assumption regarding the initial value of the elastic deformation needs to be made. In this dissertation it has been assumed that this value equals the static deformation, and this assumption results in initial oscillations with significant implications for the subsequent motion. Alternative assumptions regarding this initial value can be made, but the effect of these alternatives has not been investigated.

The major difference in the behaviour of the elastic models when compared to the rigid model is the vertical oscillations that occur in the elastic case. These oscillations and the associated elastic forces cause a number of significant results:

- The primary classification of the behaviour of the hoop, namely light, medium and heavy friction, is still applicable after small adjustments to the definitions. Because of the oscillations, the curves separating the different regions on the (μ, ω_0) phase diagrams are no longer smooth, as seen for example in Figure 7.7.
- The Z-region is much smaller than the corresponding region for rigid hoops, and the motion ends with a hop in most cases, provided the eccentricity is reasonably large as shown in the phase diagrams in Figure 7.14.
- Immediate hopping occurs for hoops with a large eccentricity when the initial angular velocity is high and this can cause large hops, as shown for example in the phase diagram in Figure 7.17.
- A fundamental difference is noted between normal hopping, which occurs when $\theta_* > 180°$, and early hopping, when $\theta_* < 90°$.
- An unusual sub-class of normal hopping, referred to as backspin hopping, occurs when the angular velocity is negative at the time of the hop. This occurs for hoops with very large eccentricities and results in hops with very large height and negative span.

Chapter 8

Experimental examples of loaded hoops

Finally, some aspects of the behaviour of two examples of actual hoops are described in the following sections.

8.1 A demonstration model of a rigid hoop

The simple model shown in the photograph in Figure 8.1 was used very successfully during lectures to demonstrate that the motion of a rigid hoop can end with either zero angular velocity or roll to the top or with a hop. The hoop was cut from a plastic pipe, and the load is a steel cylinder which is screwed to the rim.

Figure 8.1 : Photograph of a demonstration model of a rigid hoop

Here the load can clearly not be considered to be a particle, and the ϵ-factor in the equations for the moment of inertia takes on a new meaning. In the following ϵ is used as a correction factor to obtain the correct value for I_G. Because the centre of the load is not located at a distance r from the centre of the hoop, ϵ turns out to be negative and the eccentricity γ is no longer equal to the mass ratio m_p/m.

The physical details of the model are summarised in Table 8.1, with all masses in gram and dimensions in mm. The inner and outer diameters of the hoop are denoted by d_1 and d_2 respectively, and the diameter of the cylindrical load by d_p.

No initial deformation due to the weight of the cylinder is discernable, and the hoop can be considered to be rigid.

Hoop			Cylinder		Loaded hoop			
m_h	d_1	d_2	m_p	d_p	m	r	γ	ϵ
209	238	251	598	50	807	125.5	0.555	-0.324

Table 8.1 : Physical values of the loaded rigid hoop

The calculations and assumptions made to obtain the values for the loaded hoop are:

Total mass $m = m_h + m_p = 807$ g; radius $r = d_2/2 = 125.5$ mm.
Dimensions : (OP) $= (238/2 - 50/2) = 94$ mm; $r_{av} = 238/2 + (251 - 238)/4 = 122.25$ mm.

Moments around O : $m\gamma r = m_p(\text{OP})$; $\gamma = (m_p/m)(OP)/r = 0.555$.

The hoop : $I_{O_h} = m_h r_{av}^2 = 0.003124$ kg m^2.

The cylinder : $I_p = \frac{1}{2} m_p (d_p/2)^2 = 0.000187$ kg m^2.

The loaded hoop : $I_O = I_{O_h} + I_p + m_p(\text{OP})^2 = 0.008594$ kg m^2.

W.r.t G : $I_G = I_O - m(\gamma r)^2 = 0.004679$ and $I_G = mr^2(1 - \gamma^2 + \epsilon)$; therefore $\epsilon = -0.3238$.

In any experiment the values of μ and ω_0 are of course unknown and difficult to obtain. Assuming a value of $\mu = 0.1$, the phase diagram on the (θ, ω_0)-plane shown in Figure 8.2(a) is obtained by using the equations of Chapter 4 with the values of γ and ϵ from Table 8.1. Figure 8.2(b) shows the phase diagram for the same parameter values, but taking $\epsilon = 0$ as in Chapter 5. The large negative value for ϵ has the effect of "raising the humps", similar to the effect of decreasing the moment of inertia by using a smaller particle (i.e. reducing γ) - see discussion in section 6.6.4.

The lowest horizontal line represents the motion for zero initial velocity and shows a motion labelled `RS-----D- Z` in case (a) and `RSR----D- Z` in case (b). The dotted lines at $\omega_0 = 0.6$ and $\omega_0 = 1.0$ show the limits for which the demonstration model rotates the full 360°. The upper line represents the motion for maximum initial velocity $\hat{\omega}_0 = 1.342$ and shows a motion labelled `RD-S--- H` for both cases.

To summarise, Figure 8.2(a) shows that for $\omega_0 < 0.6$ the motion will end with zero angular velocity, and that hopping occurs for $\omega_0 > 1$. For initial velocities between these values, the hoop rotates through a full 360°. Each of these situations can be demonstrated with the model.

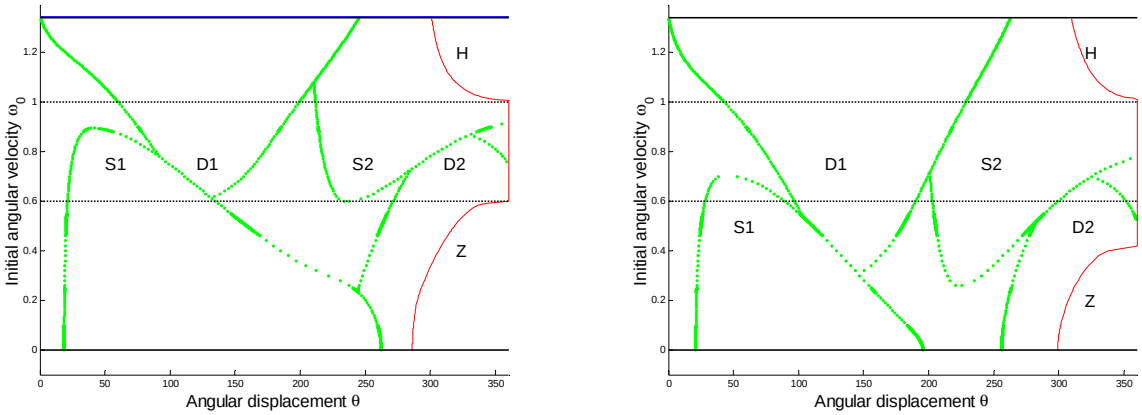

(a) : $\epsilon = -0.324$ (b) : $\epsilon = 0$

Figure 8.2 : Phase diagrams in (θ, ω_0)-space for $\gamma = 0.555$, and $\mu = 0.1$

A demonstration of hopping is shown in Figure 8.3, which shows three consecutive frames from a movie. The first frame shows the hoop just before the hop, with the load at approximately 350°. The second frame, 0.08 seconds later, shows the hoop just after take-off, and the last frame shows the hoop at approximately its maximum height.

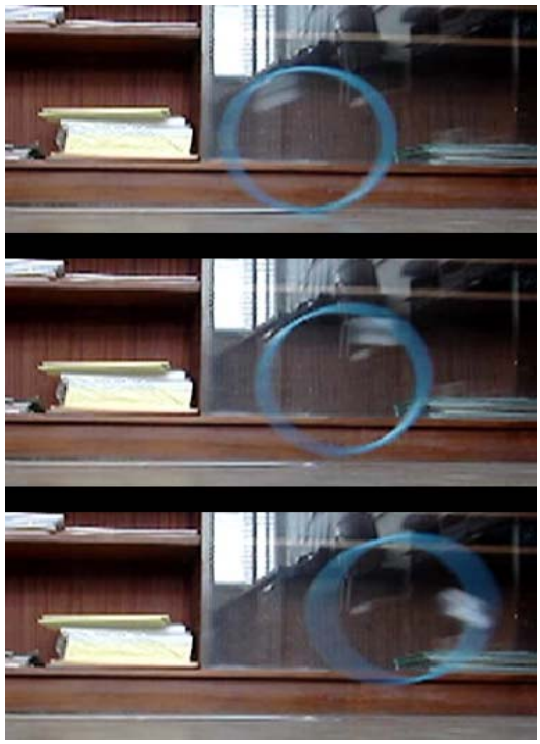

Figure 8.3 : Three frames from a movie [1] showing a rigid hoop executing a normal hop

[1]Taken and processed by Milton Maritz on a digital camera filming at 12.5 frames per second.

8.2 A loaded hula-hoop

As mentioned in the Introduction to this thesis, the literature on hopping hoops includes two references to loaded hula-hoops, namely the demonstration by Almgren and Tokieda, [11], and the stroboscopic photograph by Schwalbe and Wagon in Pritchett's article, [13]. These two references were the initial motivation for most of the research in this dissertation.

Shown in Figure 8.4 is the photograph in Pritchett's paper [13], reproduced here with permission of the publishers of *The American Mathematical Monthly.*

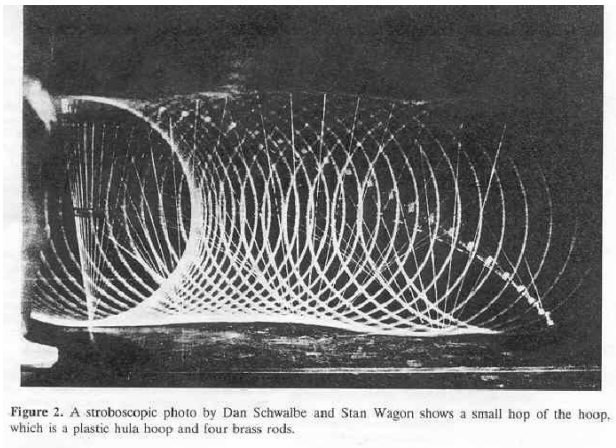

Figure 2. A stroboscopic photo by Dan Schwalbe and Stan Wagon shows a small hop of the hoop, which is a plastic hula hoop and four brass rods.

Figure 8.4 : Stroboscopic photograph of a hopping hula-hoop, from [13], with the caption: "A stroboscopic photo by Dan Schwalbe and Stan Wagon shows a small hop of the hoop, which is a plastic hula hoop and four brass rods."

An attempt will now be made to obtain numerical results that correspond with the measured values in Figure 8.4, which were found to be

$$\theta_* \approx 35^\circ; \quad \theta_+ \approx 112^\circ; \quad \mathcal{H}_{O_{max}} \approx 1/15 = 0.067; \quad \mathcal{S}_h \approx 2.$$

Clearly the equations for the internal model should be used in preference to the external model. A hula-hoop suggests a large static deformation; a small value of $e = 9$ gives the desired result. Figure 5.15, case (a), suggests that this is a case of immediate hopping; therefore reasonably large values are required for the eccentricity and initial velocity. Using $\gamma = 0.8$, $\mu = 0.2$ and $\omega_0 = 1.1$, the calculated values are

$$\theta_* = 34.3^\circ; \quad \theta_+ = 113^\circ; \quad \mathcal{H}_{O_{max}} = 0.135; \quad \mathcal{S}_h = 2.0$$

With the exception of the maximum height of the hop, this is an extremely close fit of the measured values. These results are shown in Figure 8.5. In Figure 8.5(a) the hop is drawn to the same scale as in Figure 5.15, showing the hoop at the beginning, at the highest point, and at the end of the hop. In figure (b) a larger scale is used, and only half the hoop is shown for the sake of clarity. Also shown as dotted lines are the corresponding positions of the hoop in the photograph; the first and last positions are indistinguishable, but at the highest point the calculated height is substantially greater than the height in the photograph.

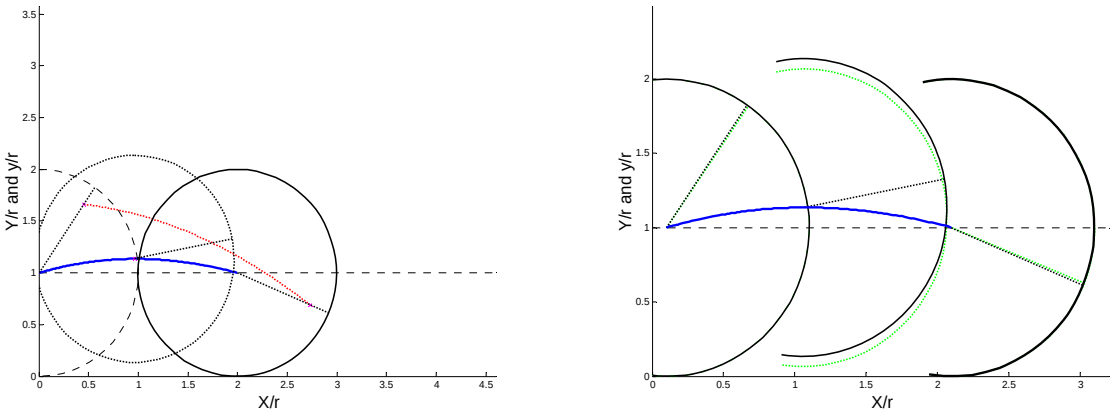

(a) (b)

Figure 8.5 : Hopping of a loaded hula hoop, for $e = 9$, $\gamma = 0.8$, $\mu = 0.2$ and $\omega_0 = 1.1$

All the calculations in the previous chapters, including the results just obtained, were based on the assumption that the initial displacement equals the static displacement; i.e. that $d_0 = d_s$, resulting in (7.7), $\delta_0 = d_0/r = d_s/r = 1/e$. By freeing this constraint, and considering δ_0 to be a second initial value to be input, it is possible to obtain an even better fit of the values of the photograph. It seems intuitive that reducing the value of δ_0 will reduce the height of the hop. After extensive numerical searching to find the best fit, the following was obtained.

The best fit is found by using small values of e and μ, and $e = 5$ and $\mu = 0.1$ are arbitrarily taken as the minimum values to be used. Assuming a hoop with 900 mm diameter ($r = 0.45$ m), $e = 5$ converts to a static displacement of 90 mm.

Also, $\omega_0 = 1.5$ is arbitrarily taken as the maximum value for the initial angular velocity. For $r = 0.45$ m this converts to an initial angular velocity of 7 rad/s and corresponding initial horizontal velocity of the centre of the hoop of 3.15 m/s.

It is found that for these values, $\gamma = 0.6$ gives the best fit. Finally, the best value for δ_0 is found to be $\delta_0 = 0.035$; for $r = 0.45$ m this converts to an initial displacement $d_0 = 15.75$ mm.

Figure 8.6 is obtained when these values for the parameters and initial values are used. Only small differences between the calculated values (solid curves) and the measured values (dotted curves) are now discernible. The calculated values are

$$\theta_* = 33.3^\circ; \quad \theta_+ = 113.6^\circ; \quad \mathcal{H}_{O_{max}} = 0.0699; \quad \mathcal{S}_h = 1.944.$$

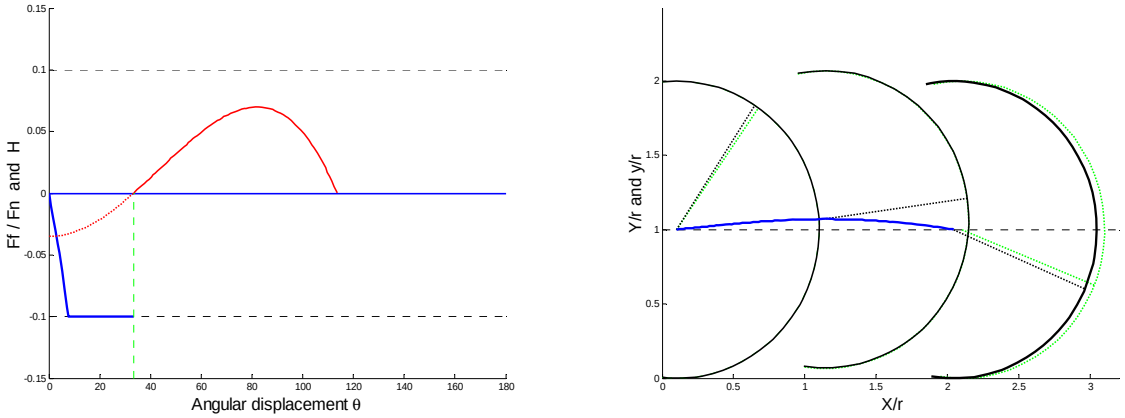

(a) (b)

Figure 8.6 : Hopping of a loaded hula hoop, for $e = 5$, $\gamma = 0.6$, $\mu = 0.1$, $\omega_0 = 1.5$ and $\delta_0 = 0.035$

The result in Figure 8.6 can be considered to be almost optimal, in the sense that the deviation from the measured values is almost zero. The values used were found by devising an error function that consists of the weighted sum of the deviations between the measured and calculated values of θ_*, $\mathcal{H}_{O_{max}}$ and $\mathcal{S}_h$, and then searching for the combination of parameters that minimised the error. The precise 'optimal values' depend on the arbitrary weights in the error function, which were chosen to give the best fit from an optical point of view. To obtain the values used in Figure 8.6, the error function used was defined as

$$\text{error} = (1/60)\|(35 - \theta_*)\| + 25\|((1/15) - \mathcal{H}_{O_{max}})\| + \|(2 - \mathcal{S}_h)\|;$$

this gives a value of 0.139.

A small reduction in δ_0 reduces the values of θ_* and θ_+, and vice cersa.

Chapter 9

Final remarks and conclusions

This dissertation is a detailed report on the results of a research project on the behaviour of a dynamical system consisting of a hoop to which a heavy particle is fixed at the rim. This hoop-and-particle system rolls in the vertical plane on a rough surface. A general mathematical model is developed, consisting of a system of second order ordinary differential equations, one for each of the three degrees of freedom. Analytic solutions are obtained in some cases; otherwise numerical solutions are used.

In all cases the final equations are written in non-dimensional form, using well-defined non-dimensional variables. This reduces the number of parameters required for the numerical calculations, and results in neater, less cluttered, equations.

Specialised models are derived for:

- *A massless hoop*, being a hypothetical hoop-and-particle system in which the hoop is rigid and the entire mass is concentrated in the particle.
- *A rigid hoop*, being a hoop-and-particle system in which the hoop is rigid and the mass of the particle is usually greater than the mass of the hoop.
- *Two elastic models*, being hoop-and-particle systems containing elasticity. In the external model the hoop is rigid and the surface deforms elastically. The internal model is defined as an elastic hoop rolling on a rigid surface.

Three main issues are investigated in the results presented, namely the conditions under which hopping occurs, the various patterns of motion, and the effect of the simplifying assumptions.

The issue of hopping includes the following aspects:

- One of the key issues addressed is the hypothetical question of how a massless hoop behaves after the normal reaction becomes zero while the particle is still moving downwards. Other authors have stated that the hoop will hop. The conclusion is reached here that a well defined skimming motion, in which the hoop continues to move horizontally while rotating around the free-falling particle, can occur. This implies inter alia that zero normal reaction is a necessary but not sufficient condition for hopping.

- It is shown analytically that:
  - a massless hoop will hop on a horizontal plane at $\theta = 0$ if $\omega_0 > 1$;
  - a rigid hoop will hop immediately if the initial angular velocity is greater than a critical initial velocity which is a function of the eccentricity and of the slope.
- The numerical results show that for initial angular velocities less than the critical initial velocity a rigid hoop can never hop while the particle is moving downwards. This is in agreement with the intuitive interpretation of the dynamics of such a system, and is backed up by considering D'Alembert diagrams.
- A rigid hoop can only hop while the particle is moving *upwards*, provided that both the eccentricity and the initial angular velocity are large enough. The parameter values for which this "normal" hopping occurs are shown clearly on phase diagrams.
- The initial oscillations caused by the elasticity and the initial conditions of elastic models can result in hopping during the early stages of the motion while the particle is moving *downwards*, provided that both the eccentricity and the initial angular velocity are large enough.

The numerical results for rigid hoops show that a rather amazing number of different patterns of motion can be obtained by varying the parameters. This is also the topic of a paper [6] recently accepted for publication. Thirty-nine patterns are tabulated, and categorised in seven primary types of motion. Various phase diagrams in different parameter spaces are used to show the regions that result in the different types of motion.

The number of variables affecting the behaviour of a hoop is reduced by making the following assumptions:

- The initial conditions are selected to ensure initial rolling.
- The load is modelled as a particle with zero dimensions and with the centre on the rim of the hoop. The only exceptions to this are the analysis of Pritchett's hoop in section 6.4.2 and the examples in Chapter 8. This affects the position of the centre of gravity, but the results show that the change in the moment of inertia due to the dimensions of the load has very little effect on the behaviour of the hoop.
- The surface on which the hoop rolls is horizontal. The behaviour of the hoop on a sloping surface is investigated in section 6.3, and basically the same behaviour is observed.
- In the general mathematical model a distinction is made between static and kinetic friction. This distinction is however ignored in obtaining nearly all the numerical results, the only exception being section 6.2, where it is shown that this assumption has one small side effect.

With the above assumptions, the behaviour of a loaded hoop depends on the non-dimensional parameters listed below:

- The eccentricity, defined as γ = length OG divided by the radius.
  In all cases where the centre of the particle is on the rim of the hoop,
  γ = the particle mass divided by the total mass.

- The friction coefficient μ.
- The initial angular velocity ω_0.
- In the elastic models, the elastic constant is required. This dimensionless parameter is defined as e = radius of the hoop divided by the static deformation due to the load.

Three aspects that have not been investigated and are considered to be outside the scope of this dissertation are:

- In nearly all cases the analysis is terminated when the angular velocity becomes zero. An exception is the case of the elastic hoop where it is found that under certain conditions the hoop can hop while rotating backwards, the so-called backspin hop. However, it is clear that for all hoops the motion does not end at this point, and that some type of oscillatory motion will occur.
- Initial conditions other than initial rolling have not been investigated. In particular, the initial motion on a slope with a small friction coefficient presents a number of interesting problems.
- The elastic models have been assumed to be in initial static equilibrium; i.e. it is assumed that $\delta_0 = 1/e$ in nearly all examples. The only exception is the attempt to simulate the values measured in the photograph in section 8.2. Here it was seen that the value for δ_0 does have some influence on the motion.

A number of instances of issues that have some pedagogic interest are included in the dissertation. Examples are the use of the moment of inertia factor κ introduced in Chapter 2, and the issues relating to the torque equation as discussed in Appendices A and B as well as the summary of the Lagrange method in Appendix C.

Finally, we return to the articles that provided the original impetus for the research on loaded hoops:

- The phenomenon of "The Hopping Hoop" was recently analysed by Tokieda [9], based on the problem first published by J.E. Littlewood [8] in 1953. They describe the rolling motion of a massless hoop loaded with a particle and *hopping* when the radius to the particle becomes horizontal. In the research by Theron it is shown that a more probable motion after the normal reaction becomes zero is a *skimming motion* in which the massless hoop whips round the particle at just the right angular velocity to ensure horizontal motion of point O while the particle is falling along a parabolic trajectory. The hoop maintains geometric contact with the surface even though the normal reaction is zero.
- Two cases of experiments with hula hoops have been reported.
  First Tokieda and Almgren reported that they observed a loaded hula hoop hopping as predicted. [11]
  Pritchett [13] shows a stroboscopic photograph of the same phenomenon, also using a plastic hula-hoop.
  The work in this dissertation shows that rigid hoops cannot hop in this position, but that a system with elasticity can.

========== FINIS ==========

References

[1] W.F.D. Theron, (2000) "The rolling motion of an eccentrically loaded wheel", *Am. J. Phys.* **68**, 812-820.

[2] W.F.D. Theron & N.M. du Plessis, (2001) "The dynamics of a massless hoop", *Am. J.Phys.* **69**, 354-359.

[3] W.F.D. Theron, (2002) "The Dynamics of an Elastic Hopping Hoop", *Mathl. Comput. Modelling* **35**, 1135-1147.

[4] W.F.D. Theron, (1995) "Analysis of a loaded elastic wheel rolling down a circular track", *Mathl. Comput. Modelling* **21**, 1-15.

[5] W.F.D. Theron, (1995) "Bouncing due to the infinite jerk at the end of a circular track", *Am. J. Phys.* **63**, 950-955.

[6] W.F.D. Theron and M.F. Maritz, "The amazing variety of motions of a loaded hoop", *Mathl. Comput. Modelling*, accepted for publication.

[7] W.F.D. Theron, "Torque around the instantaneous center, revisited", to be submitted.

[8] J.E. Littlewood, (1953) *Littlewood's Miscellany*, Cambridge University Press.

[9] T.F. Tokieda, (1997) "The Hopping Hoop", *Am. Math. Monthly* **104**, 152-153.

[10] T.F. Tokieda, Personal communication, January 2004.

[11] D. Mackenzie, (1997) "Fred Almgren (1933-1997)", *Notices of the Am. Math. Society* **44**, 1102-1106.

[12] J.P. Butler, (1999) "Hopping Hoops Don't Hop", *Am. Math. Monthly* **106**, 565-568.

[13] T. Pritchett, (1999) "The Hopping Hoop Revisited", *Am. Math. Monthly* **106**, 609-617.

[14] W.F.D. Theron and N.M. du Plessis, (1998) The hopping hoop revisited, *Departmental Report TW98/1*, Department of Applied Mathematics, University of Stellenbosch, Stellenbosch.

[15] W.F.D. Theron, (1988) "The 'faster than gravity' demonstration revisited", *Am. J.Phys.* **56**, pp. 736-739.

[16] W.F.D. Theron and J.M. de Villiers, (1988) "Faster than gravity accelerations and the resulting trajectories in a sliding particle and wedge system", *Mathl. Comput. Modelling* **10**, 747-764.

[17] Y.Z. Liu and Y.Xue, (2004) "Qualitative analysis of a rolling hoop with mass unbalance", *Acta Mechanica Sinica* **20** (6), 672-675.

[18] A. Carnevali and R. May, (2005) "Rolling motion of non-axisymmetric cylinders", *Am. J.Phys.* **73** (10), pp. 909-913.

[19] MATLAB, The Mathworks, Inc., 3 Apple Hill Drive, Natick, Massachusets 01760-2098.

.

Supplementary bibliography for Appendix B

[20] F.S. Crawford, (1989) "Problem : Moments to remember",
Am. J. Phys. **57**, 105; 177.

[21] F.R. Zypman (1990) "Moments to remember - The condition for equating torque and rate of change of angular momentum", *Am. J. Phys.* **58**, 41-43.

[22] M.S. Tiersten (1991) "Moments not to forget - The conditions for equating torque and rate of change of angular momentum around the instantaneous center", *Am. J. Phys.* **59**, 733-738.

[23] E.A. Desloge, (1982) *Classical Mechanics*, Wiley, New York, p.230.

[24] L. Rodriguez, (2003) "Torque and the rate of change of angular momentum at an arbitrary point", *Am. J. Phys.* **71**, 1201-1203.

[25] S.L. Loney, (1909) *Dynamics of a particle and of rigid bodies*, Cambridge University Press, p.257 (1946).

[26] C.G. Lambe, (1958) *Applied Mathematics for Engineers and Scientists*, The English Universities Press, p.155.

[27] A.P. Boresi & R.J. Schmidt, (2001) *Engineering Mechanics -Dynamics*, Brooks/Cole.

[28] P. Jansson & R. Grahn, (1995) *Engineering Mechanics - Dynamics*, Prentice Hall.

[29] A. Pytel & J. Kiusalaas, (1999) *Engineering Mechanics - Dynamics*, Second edition, Brooks/Cole.

[30] R.C. Hibbeler, (1998) *Engineering Mechanics - Dynamics*, Eighth edition, Prentice Hall.

[31] B.I. Sandor, (1987) *Engineering Mechanics - Dynamics*, Second edition, Prentice Hall.

[32] D.J. McGill & W.W. King, (1989) *Engineering Mechanics - An Introduction to Dynamics*, Second edition, PWS-Kent.

[33] J.L. Meriam & L.G. Kraige, (1998) *Engineering Mechanics -Dynamics*, Fifth edition, Wiley.

[34] Den Hartog, (1948) *Mechanics*,

[35] Grinter, (1953) *Engineering Mechanics*, MacMillan.

[36] Clifford Truesdell, (1969) *Rational Thermodynamics*, McGraw-Hill.

.

German textbooks

[37] Jens Wittenburg, (1977) *Dynamics of Systems of Rigid Bodies*, B.G. Teubner, Stuttgard.

[38] R. Markert, (2002) *Technische Mechanik, Teil B*, Technische Universitt Darmstadt.

[39] F. Herrmann, (2000) "The Karlsruhe Physics Course", *Eur. J. Phys.* **21**, 49-58.

[40] Rudiger & Kneschke, (1964) *Kinematik and Kinetik - Band 3*, B.G. Teubner Verlagsgesellschaft, Leipzig.

.

Supplementary bibliography for Appendix C

[41] D.T. Greenwood, *Principles of Dynamics*, Second Edition, Prentice Hall, 1988.

[42] J.L. Synge & B.A. Griffiths, *Principles of Mechanics*, Third Edition, McGraw-Hill, 1959.

Appendix A

Alternative derivations

Different methods to derive the equations of motion for rolling of a rigid hoop

It is of some academic interest to consider the different methods available for deriving the equations of motion of a loaded hoop. In this appendix three methods are given for obtaining the equations for rolling (without slipping) of a rigid hoop. These methods are based on Newton's laws. A fourth method based on the Lagrange approach is discussed in Appendix C.

In contrast to previous chapters, the equations in this appendix are derived in terms of real time without using non-dimensional variables.

The kinematic equation (2.8) is repeated here for ease of reference :

$$\ddot{x} = \ddot{X} + \gamma\, r\ddot{\theta}\, \cos\theta - \gamma\, r\dot{\theta}^2\, \sin\theta; \qquad \ddot{y} = \ddot{Y} - \gamma\, r\ddot{\theta}\, \sin\theta - \gamma\, r\dot{\theta}^2\, \cos\theta.$$

For rolling of a rigid hoop, $\ddot{X} = r\ddot{\theta}$ and $\ddot{Y} = 0$ and the above equation becomes

$$\ddot{x} = (1 + \gamma\, \cos\theta)\, r\, \ddot{\theta} - \gamma\, \sin\theta\, r\, \dot{\theta}^2; \qquad \ddot{y} = -\gamma\, \sin\theta\, r\, \ddot{\theta} - \gamma\, \cos\theta\, r\, \dot{\theta}^2. \tag{A.1}$$

Referring to Figure A.1 and using Newton's second law, components in the transverse direction are $mg\sin\psi + F_f = m\ddot{x}$, or dividing by m and using (A.1)

$$F_f/m = (1 + \gamma\, \cos\theta)\, r\, \ddot{\theta} - \gamma\, \sin\theta\, r\, \dot{\theta}^2 - g\sin\psi. \tag{A.2}$$

Similarly for components perpendicular to the plane, $F_n - mg\cos\psi = m\ddot{y}$, or

$$F_n/m = -\gamma\, \sin\theta\, r\, \ddot{\theta} - \gamma\, \cos\theta\, r\, \dot{\theta}^2 + g\cos\psi. \tag{A.3}$$

The geometry of a rigid hoop is summarised by (4.1), repeated here :

$$\mathcal{H} = 1 + \gamma\, \cos\theta\ ; \quad \kappa_G = 1 + \epsilon - \gamma^2\ ; \quad \kappa_C = 2\mathcal{H} + \epsilon = 2(1 + \gamma\, \cos\theta\ + \epsilon/2). \tag{A.4}$$

At this stage $\dot{\theta}$ and $\ddot{\theta}$ are unknown, and the following three sections describe three different methods of obtaining these values, all using Figure A.1.

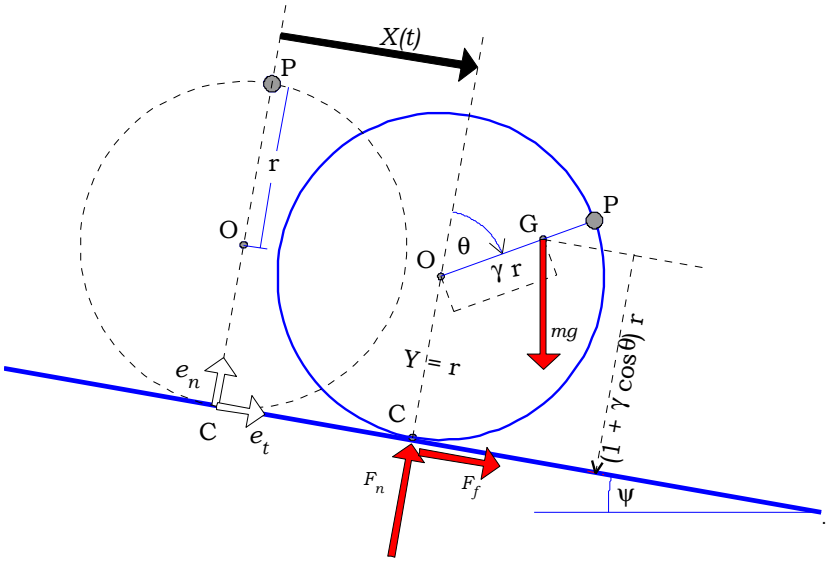

Figure A.1 : The rigid hoop - geometry and forces

A.1 The standard method

The standard method was used in Chapter 2 and is repeated here specifically for the rigid model. This method is characterised by taking moments around the centre of mass.

Newton's second law for clock-wise moments around the centre of mass is

$$F_n\,\gamma\,r\,\sin\theta - F_f\,r\,\mathcal{H} = I_G\,\ddot{\theta}.$$

Dividing by mr and using $I_G = \kappa_G m r^2$,

$$(F_n/m)\,\gamma\,\sin\theta - (F_f/m)\,\mathcal{H} = \kappa_G\,r\ddot{\theta}. \tag{A.5}$$

Substituting (A.2) and (A.3), this torque equation becomes

$$\gamma\,\sin\theta\,(-\gamma\,\sin\theta\,r\,\ddot{\theta} - \gamma\,\cos\theta\,r\,\dot{\theta}^2 + g\cos\psi) - \mathcal{H}\,((1+\gamma\,\cos\theta)\,r\,\ddot{\theta} - \gamma\,\sin\theta\,r\,\dot{\theta}^2 - g\sin\psi) = \kappa_G\,r\ddot{\theta}.$$

Collecting terms and simplifying, this becomes

$$\kappa_C\,\ddot{\theta} = \gamma\,\sin\theta\,\dot{\theta}^2 + (g/r)\,(\gamma\,\sin(\theta+\psi) + \sin\psi). \tag{A.6}$$

Note that $\kappa_G + (\gamma\sin\theta)^2 + \mathcal{H}^2 = \kappa_C = 2(1+\gamma\,\cos\theta\ + \epsilon/2)$ as shown in the derivation of (2.4). This is equivalent to the non-dimensional form of the torque equation as derived as (2.26) and (4.11). Noting that $\frac{\mathrm{d}\dot{\theta}^2}{\mathrm{d}\theta} = 2\ddot{\theta}$, (A.6) can be written as the linear first order differential equation in $\dot{\theta}^2$

$$\frac{\mathrm{d}\dot{\theta}^2}{\mathrm{d}\theta} = \frac{2}{\kappa_C}\,(\gamma\,\sin\theta\,\dot{\theta}^2 + (g/r)\,(\gamma\,\sin(\theta+\psi) + \sin\psi)).$$

Using (A.4), and noting that $\frac{\mathrm{d}\mathcal{K}_C}{\mathrm{d}\theta} = -\gamma \sin\theta$ so that the integrating factor $e^{\int(-2\gamma\sin\theta/\mathcal{K}_C)\mathrm{d}\theta}$ is simply κ_C, this can be integrated with respect to θ to give the analytic solution

$$\dot{\theta}^2 = \frac{2}{\mathcal{K}_C}\left((g/r)(-\gamma\,\cos(\theta+\psi) + \theta\,\sin\psi) + C_0\right), \tag{A.7}$$

where $C_0 = (1+\gamma+\epsilon/2)\,\dot{\theta}_0^2 + (g/r)\,\gamma\,\cos\psi$ from the initial condition that $\dot{\theta}(0) = \dot{\theta}_0$ is given.

All the variables in the problem of a rolling rigid hoop are therefore known as functions of the position θ, with $\dot{\theta}$ from (A.7), $\ddot{\theta}$ from (A.6) and the acceleration and reactions from (A.1) to (A.3).

A.2 Moments about the Instantaneous Centre

For the case of rolling motion, the contact point C is also the centre of instantaneous zero velocity, abbreviated as the IC. In this case the torque equation from Newton's second law is written in the form

$$M_C = I_C\,\ddot{\theta} + \tfrac{1}{2}\,\dot{I}_C\,\dot{\theta}, \tag{A.8}$$

where M_C denotes the total moment about point C, and I_C is the corresponding moment of inertia which is *not* constant in this case. A detailed discussion and derivation of this equation is given in Appendix B, where it is referred to as Loney's equation.

Using Figure A.1, the moment about C is

$$M_C = mg\,\cos\psi\,\gamma r\sin\theta + mg\,\sin\psi\,\mathcal{H}r = mgr(\gamma\sin(\theta+\psi) + \sin\psi).$$

Using (A.4), the right hand side of (A.8) simplifies to

$$mr^2(\kappa_C\,\ddot{\theta} + \tfrac{1}{2}\,\dot{\kappa}_C\,\dot{\theta}) = mr^2(\kappa_C\,\ddot{\theta} - \gamma\sin\theta\,\dot{\theta}).$$

Substituting in (A.8) and cancelling mr^2, the torque equation becomes

$$\kappa_C\,\ddot{\theta} - \gamma\sin\theta\,\dot{\theta} = (g/r)(\gamma\sin(\theta+\psi) + \sin\psi),$$

which is the same as (A.6).

A.3 Conservation of energy

This method has previously been used in section 3.3.2 to obtain the solution for the case of a massless hoop on a horizontal surface. It will now be applied to the hoop shown in Figure A.1.

The Principle of Energy conservation for a system such as that shown in Figure A.1 states that the sum of the Potential and Kinetic energies is constant.

The total kinetic energy of the system during rolling is $T = \frac{1}{2}mv_G^2 + \frac{1}{2}I_G\dot{\theta}^2 = \frac{1}{2}I_C\dot{\theta}^2$.

Taking the origin of the axes in Figure A.1 as reference, the total initial energy is

$$E_1 = mg(r+\gamma r)\cos\psi + mr^2(1+\gamma+\epsilon/2)\dot{\theta}_0^2.$$

The total energy after a rotation θ, using Figure A.1 and $X = r\theta$, is

$$E = mg(-r\theta \sin\psi + r\cos\psi + \gamma r\cos(\theta+\psi)) + \tfrac{1}{2}\kappa_C m r^2\dot{\theta}^2.$$

Energy conservation implies that $E = E_1$, therefore

$$mg(-r\theta \sin\psi + r\cos\psi + \gamma r\cos(\theta+\psi)) + \tfrac{1}{2}\kappa_C m r^2\dot{\theta}^2 = mg(r+\gamma r)\cos\psi + mr^2(1+\gamma+\epsilon/2)\dot{\theta}_0^2.$$

After cancelling mr^2 and re-arranging,

$$\tfrac{1}{2}\kappa_C\dot{\theta}^2 = (g/r)(\theta\sin\psi - \cos\psi - \gamma\cos(\theta+\psi)) + (g/r)(1+\gamma)\cos\psi + (1+\gamma+\epsilon/2)\dot{\theta}_0^2.$$

or

$$\dot{\theta}^2 = \frac{2}{\kappa_C}\left((g/r)(\theta\,\sin\psi - \gamma\,\cos(\theta+\psi) + \gamma\cos\psi) + (1+\gamma+\epsilon/2)\dot{\theta}_0^2\right).$$

This is exactly the same as (A.7).

The angular acceleration is obtained by differentiating the above w.r.t. time,

$$\kappa_C\,\dot{\theta}\,\ddot{\theta} + \dot{\theta}^2\,(-\gamma\sin\theta\dot{\theta}) = (g/r)\left(\dot{\theta}\,\sin\psi + \gamma\,\sin(\theta+\psi)\,\dot{\theta}\right)$$

and simplifying to obtain (A.6)

$$\kappa_C\,\ddot{\theta} = \gamma\,\sin\theta\,\dot{\theta}^2 + (g/r)\,(\gamma\,\sin(\theta+\psi) + \sin\psi).$$

A.4 Conclusion

All three methods give the same solution, confirming the correctness thereof.

There is no definite advantage in using any of the three methods, as they all require more or less the same amount of effort.

Appendix B

The Loney equation

B.1 Introduction

The purpose of this appendix is to discuss in some detail a number of issues relating to the torque equation, especially with reference to the concepts of angular momentum and the instantaneous centre of rotation. In particular, the torque equation that is obtained when taking moments about the instantaneous centre of rotation is discussed in detail. It is convenient to refer to a special form of this equation as the *Loney equation*.

All the references to German textbooks [37] to [40], and the corresponding influence on the contents of this appendix, are the result of a study tour in November 2005 during which several Universities and Technical Universities in Germany were visited. [1]

The contents of this appendix have been condensed into an article that is to be presented for publication in a journal for engineering education [7].

B.1.1 Historical background

It is generally accepted that great care must be exercised when taking moments about a point other than point G or a fixed point - the so-called "safe points". During 1989 to 1991 the American Journal of Physics published three articles, [20, 21, 22] relating to this issue.

Two points of view are discussed. On the one hand there is a strong body of thought against the use of "special points" in general, and the instantaneous centre in particular, when taking moments. Both Zypman [21] and Tiersten [22] quote Desloge [23], who suggested that readers forget such special cases because " ... the convenience that might be gained by retaining this case in one's repertoire is outweighed by the possibility of error it encourages." This viewpoint was also encountered in a number of instances at the universities visited in Germany.

However, Tiersten suggests that " ... quick and elegant solutions of many problems in plane motion of a rigid body may be obtained by taking moments around the instantaneous centre of rotation " [22]. The article [7] that is based on this appendix aims to remind practitioners of dynamics of this method, or possibly to introduce them to it.

[1] I would like to thank the Department of Applied Mathematics and the University of Stellenbosch most sincerely for the financial support which made this possible.

Articles [21, 22] followed an interesting little puzzle posed by Crawford [20], in which two problems are "solved" by taking moments about the contact point. In the case of a rolling cylinder the correct solution is obtained; in the case of a rotating rod the solution obtained is incorrect. The reasons for this are discussed in the three papers quoted.

In a more recent paper by Rodriguez [24], the author gives a number of examples where neat solutions are obtained by taking moments about an arbitrary point, provided that the acceleration of this point is known or prescribed.

The Loney equation used by Tiersten [22] is found in old classics like Loney [25] and Lambe [26]. However, it would seem that modern textbook writers subscribe to the first viewpoint, as it is not found in, for example, [27] to [31].

In our department we have used the Loney equation for many years to solve problems in rigid body dynamics, and it came as quite a surprise when we realized that very few such applications are found in the modern textbooks. This discovery was the driving force behind the research that went into the writing of this appendix.

B.2 Concepts and terminology

In this section a number of concepts that are related to the issue of the Loney equation are defined and briefly discussed.

B.2.1 Notation

There are a few instances where the notation in this appendix differs slightly from that in the main text of the thesis.

Figure B.1 shows a fixed point O, taken as the origin of fixed axes defined by unit vectors $\mathbf{i}$ and $\mathbf{j}$ and $\mathbf{k} = \mathbf{i} \times \mathbf{j}$. A rigid body is moving in the plane defined by $\mathbf{i}$ and $\mathbf{j}$. Here $\boldsymbol{\omega} = \omega\,\mathbf{k}$ denotes the angular velocity (in rad/s), and $\boldsymbol{\alpha} = \dot{\boldsymbol{\omega}}$ the angular acceleration (in rad/s^2) and not the corresponding non-dimensional values of the main text.

The mass centre is located at point G and is located by position vector $\mathbf{r}_G$. Point P is an arbitrary point on the body and is located by position vector $\mathbf{r}_i$. In general, $\mathbf{r}_{*/*}$ denotes a position vector relative to a selected point; for example, $\mathbf{r}_{i/G}$ denotes the position vector of point P relative to G. Therefore

$$\mathbf{r}_i = \mathbf{r}_A + \mathbf{r}_{i/A} \quad \text{or} \quad \mathbf{r}_i = \mathbf{r}_G + \mathbf{r}_{i/G}; \qquad \mathbf{r}_G = \mathbf{r}_A + \mathbf{r}_{G/A}.$$

As before, $\mathbf{v}_* = \dot{\mathbf{r}}_*$ denotes the absolute velocity of a point,
and $\mathbf{a}_* = \dot{\mathbf{v}}_* = \ddot{\mathbf{r}}_*$ denotes the absolute acceleration.

Also, $\mathbf{M}_*$ denotes torque, I_* the moment of inertia, and $\mathbf{L}_*$ denotes the angular momentum, taking moments about an axis through point $*$.

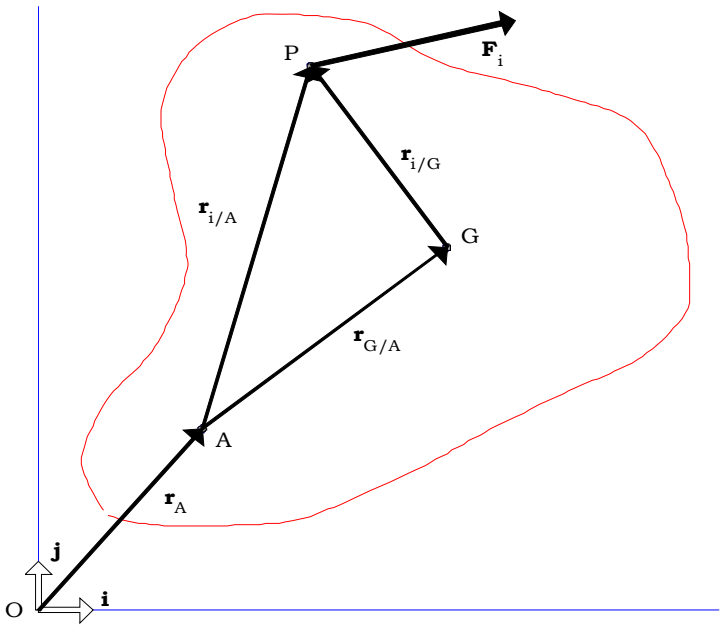

Figure B.1 : Position and force vectors on a rigid body

B.2.2 Fixed reference frame

Newton's second law is formulated in an *inertial* reference frame, which implies that the origin has zero acceleration but may have constant velocity. It also implies zero rotation of the axes.

However, when angular momentum is used, it simplifies the relationships if the origin is *fixed*; i.e. if

$$\mathbf{v}_O = \mathbf{0}.$$

This will be assumed to be the case for the rest of this appendix.

B.2.3 The torque equation

In this appendix the term *torque equation* refers to the relationship between the torque exerted by the external forces on a rigid body, and the kinematic quantities associated therewith. This is derived from Newton's second Law for a particle and taking moments about a specified point. For example, when taking moments about the mass centre G, the torque equation can be written in the well known form of

$$\mathbf{M}_G = I_G\, \boldsymbol{\alpha}.$$

Variations of this equation for situations where the moments are taken around points other than

G can be derived. Only in certain special cases the torque equation reduces to the form

$$\mathbf{M}_* = I_*\boldsymbol{\alpha};$$

this will be referred to as the *simple form* of the torque equation.

Many authors, and the German authors in particular, summarise the kinematic quantities in the torque equation in terms of the time derivative of the angular momentum. This aspect is discussed in the next two sections, but is not used for the derivation of the Loney equation.

B.2.4 Angular momentum

The *momentum of a particle* is defined as the vector quantity $m_i\mathbf{v}_i$. Then the *angular momentum* with respect to any point A is the moment of this vector around A; i.e. $\mathbf{L}_A = \mathbf{r}_{i/A} \times (m_i\mathbf{v}_i)$, where $\mathbf{L}$ is used to denote angular momentum. Many authors call this quantity the moment of momentum.

The concept of angular momentum is of fundamental importance when solving problems involving particle systems, and also for 3-dimensional motion of rigid bodies. It is not essential when formulating the torque equation for planar motion of a rigid body, but, as already mentioned, it can be used to summarise the kinematic quantities of the torque equation.

Therefore, for a system of particles and for a rigid body respectively, the angular momentum with respect to point A is defined as

$$\mathbf{L}_A = \sum \mathbf{r}_{i/A} \times (m_i\mathbf{v}_i); \quad \mathbf{L}_A = \int (\mathbf{r}_{i/A} \times \mathbf{v}_i)\, \mathrm{d}m.$$

This is not the only definition ! Some authors, e.g. Boresi [27], Desloge [23], Zypman [21], use the relative velocity $\mathbf{v}_{i/A} = \boldsymbol{\omega} \times \mathbf{r}_{i/A}$ in the definition. This simplifies certain expressions, but will not be discussed any further in this appendix. Here the absolute velocity $\mathbf{v}_i$ is always used, as in for example Meriam [33].

This is also not the only notation used; there would seem to be no other concept for which so many different symbols are used in the textbooks.
Prof. Wittenburg [37] claims that $\mathbf{L}$ is the universally used symbol, and I will use this here. It is also used in [21], [24], [38] and others. However, certain German textbooks and class notes also use $\mathbf{D}$. The symbol $\mathbf{H}$ is used in [23], [32], [33] and others; $\mathbf{A}$ is used in [27], and no symbol is used by Loney [25] or Lambe [26].

Incidentally, the concept that momentum is one of the basic physical quantities is strongly promoted by Prof. Friedrich Herrmann of the "Abteilung fur Didaktik der Physik", and the "father" of the Karlsruhe Physics Course, [39]. One of the basic issues in this course is defining (linear) momentum as a fundamental Kinematic quantity for learners at school. The suggested unit is the huygens (Hg), 1Hg = 1 N.s. Mass is then defined in terms of momentum and velocity.

B.2.5 Euler's Laws

The well known law for translation of a rigid body is $\mathbf{F} = m\,\mathbf{a}_G$, where $\mathbf{F}$ is the resultant of the external forces acting on the system or body.

Most modern textbooks refer to this equation as Newton's second law. Two exceptions are McGill [32] and Wittenburg [37], who refer to this as Euler's first law or axiom, both quoting Truesdell's Essays in the history of Mechanics [36]. According to this approach, Newton's laws were formulated for particles, and the generalisation to include rigid bodies was due to Leonhard Euler in 1776.

An alternative and more general formulation of this law is given in terms of momentum, namely $\mathbf{F} = \frac{\mathrm{d}}{\mathrm{dt}}(m\,\mathbf{v}_G)$. Note that this reduces to the first formulation only if the mass is constant.

Euler's formulation is in terms of momentum, and is given as follows by Truesdell [36], p. 128.

Law 1 : "The total force acting upon the body equals the rate of change of the total momentum."

Law 2 : "The total torque acting upon the body equals the rate of change of the total moment of momentum, where both the torque and the moment are taken with respect to the same fixed point."

Euler's second law is therefore one form of the torque equation. This formulation of the second law will be broadened slightly in this appendix, by removing the restriction that the reference point must be fixed. Here we will refer to a relationship in the form

$$\mathbf{M}_* = \dot{\mathbf{L}}_*$$

as Euler's second law, for *any reference point for which this relationship is true.* The different points for which this is true will be pointed out in section B.5. The simple form of this law occurs when $\mathbf{L}_* = I_*\boldsymbol{\omega}$ and $\mathbf{M}_* = I_*\boldsymbol{\alpha}$.

B.2.6 The instantaneous centre

At any specific instant a two-dimensional motion of a rigid body (other than pure translation) can be considered to be a rotation around an axis perpendicular to the plane of the motion. This axis is located at a geometric point known as the *the instantaneous centre of rotation* or *the instantaneous centre of zero velocity*; this point will be abbreviated as the IC. (In the case of translation, this point is at infinity; in the case of a pendulum, this point is fixed).

Incidentally, Johann Bernoulli was the first to define the IC, in 1742. [40]

It is necessary to differentiate between two points in connection with the IC. The geometric point is denoted by C' and has position vector $\mathbf{r}_{C'}$, and in general is not stationary. At any instant, a point C which "belongs" to the body and coincides with point C' for that instant has the fundamental property that its velocity is zero. Therefore

$$\mathbf{r}_C = \mathbf{r}_{C'}; \qquad \mathbf{v}_C = 0; \qquad \mathbf{v}_i = \boldsymbol{\omega} \times \mathbf{r}_{i/C}; \qquad \mathbf{v}_G = \boldsymbol{\omega} \times \mathbf{r}_{G/C}.$$

However, the acceleration of point C is not necessarily zero. For example, in the case of a rolling hoop, point C is the point on the hoop which corresponds with the contact point, and its acceleration is directed from C to the centre of the hoop.

At each instant a different point on the body corresponds with C'; therefore $\mathbf{r}_{i/C}$ is not necessarily constant, but may be a function of time. Similarly $\mathbf{r}_{G/C}$ is not necessarily constant and therefore I_C may be a function of time.

Nearly all textbooks use the IC in solving problems in Kinematics, a few use it to calculate the Kinetic energy, but very few use it in the context of the torque equation for solving problems in Dynamics. As already mentioned, this last observation came as a bit of a surprise because lecture notes in our department have used this concept for many years.

B.2.7 Reference points

Quantities such as the torque or angular momentum are always calculated with respect to a specified reference point, which is the point around which the moments are taken. In this appendix the following notation is used for reference points with specific properties.

Point A is any point, which may or may not be connected to the body.

Point B is a *body point*, defined as any point on a rigid body, or a point that "belongs" to the body in the sense that it is fixed in a local coordinate system connected to the body. The important implication is that a line connecting this point to any point on the body must rotate with the same angular velocity as the body. A second property is that the moment of inertia with respect to the body point is constant. To summarise the properties of a body point B :

$$\mathbf{r}_i = \mathbf{r}_B + \mathbf{r}_{i/B}; \quad r_{i/B} = \text{constant}; \quad I_B = \text{constant}; \quad \mathbf{v}_i = \mathbf{v}_B + \boldsymbol{\omega} \times \mathbf{r}_{i/B}. \tag{B.1}$$

An example of a body point that falls outside the body is the centre of mass of a hoop or an angle iron.

Point C is the IC defined in section B.2.6.

Three "special points" are used, namely
point O for any fixed point in or outside the body;
point O_B for a fixed point attached to the body;
point G for the centre of mass.

B.2.8 Loney's equation

The main result of this appendix is a special form of the torque equation that can be derived by using the IC as reference point. It is convenient to refer to this special torque equation as *Loney's equation* or the Loney equation, because the first reference to it which we could find is in Loney's book, [25], first published in 1909.

This is the equation used in our department and is also found in Lambe [26]. It is derived and used by Tiersten [22], but we have not been able to find any other references to it.

B.3 The torque equation with respect to the IC

The torque equation is one of the trickier forms of Newton's second law to use, and it is well known that the simple form of the torque equation is obtained only for certain points which may be used as the reference point for taking moments. Various different expressions for the angular momentum, and different forms of the torque equation, are obtained by taking moments about different points.

In the following sections the torque equation with respect to the IC will be derived in detail.

B.3.1 Some useful relationships

A number of useful relationships involving triple products of vectors are frequently used in the derivations in the later sections.

In general, it can be shown that the *triple vector product* can be calculated by the rule

$$\mathbf{a} \times (\mathbf{b} \times \mathbf{c}) = \mathbf{b}(\mathbf{a} \cdot \mathbf{c}) - \mathbf{c}(\mathbf{a} \cdot \mathbf{b}) \tag{B.2}$$

for any three vectors.

The following relationships hold for the *triple scalar product* of any three vectors.

$$\mathbf{a} \cdot (\mathbf{b} \times \mathbf{c}) = \mathbf{b} \cdot (\mathbf{c} \times \mathbf{a}) = \mathbf{c} \cdot (\mathbf{a} \times \mathbf{b}). \tag{B.3}$$

In the planar motion under consideration, the angular velocity, angular acceleration and all the moments are perpendicular to all the position vectors, velocities and accelerations; therefore, for any position vector for example

$$\mathbf{r}_* \cdot \boldsymbol{\omega} = 0; \quad \mathbf{r}_{*/*} \cdot \boldsymbol{\alpha} = 0. \tag{B.4}$$

This simplifies (B.2) substantially in all the applications where $\boldsymbol{\omega}$ (or $\boldsymbol{\alpha}$) is one of the vectors.

For point P on a rigid body, the *velocity relative to the centre of mass* can always be written as

$$\mathbf{v}_{i/G} = \dot{\mathbf{r}}_{i/G} = \boldsymbol{\omega} \times \mathbf{r}_{i/G}. \tag{B.5}$$

Also, the acceleration of P relative to G, after using (B.5), (B.2) and (B.4), is

$$\mathbf{a}_{i/G} = \dot{\mathbf{v}}_{i/G} = \boldsymbol{\alpha} \times \mathbf{r}_{i/G} - \omega^2 \, \mathbf{r}_{i/G}. \tag{B.6}$$

Because the velocity of point C is zero, the velocity of any other point on a rigid body can be written as

$$\mathbf{v}_i = \mathbf{v}_C + \mathbf{v}_{i/C} = \boldsymbol{\omega} \times \mathbf{r}_{i/C} \tag{B.7}$$

when using the IC as reference. However, $\mathbf{a}_C$ is not necessarily zero.

The integral over the whole body is often used in the following sections. The total mass is $m = \int \mathrm{d}m$, where $\mathrm{d}m$ is the mass of an element at position P. Note that the fundamental definitions imply that

$$\int \mathbf{r}_{i/A} \, \mathrm{d}m = m \, \mathbf{r}_{G/A}; \qquad \int \mathbf{r}_{i/G} \, \mathrm{d}m = 0; \qquad \int r_{i/G}^2 \, \mathrm{d}m = I_G. \tag{B.8}$$

B.3.2 Moments around the IC

In most textbooks the most general form of the torque equation is usually derived by taking moments about an arbitrary point A; for example [26, 33, 27]. This point is not necessarily fixed to the body, and may be moving independently of the body.

Referring to figure B.1, an element with mass dm is located at point P with position vector $\mathbf{r}_i$. Using (B.5) and (B.6), the position vector, velocity and acceleration of point P can be defined by

$$\mathbf{r}_i = \mathbf{r}_G + \mathbf{r}_{i/G}; \qquad \mathbf{v}_i = \dot{\mathbf{r}}_i = \mathbf{v}_G + \boldsymbol{\omega} \times \mathbf{r}_{i/G}; \qquad \mathbf{a}_i = \dot{\mathbf{v}}_i = \mathbf{a}_G + \boldsymbol{\alpha} \times \mathbf{r}_{i/G} - \omega^2\, \mathbf{r}_{i/G}. \tag{B.9}$$

The resultant external force on this element is $\mathbf{F}_i$ and Newton's second law for the element is $\mathbf{F}_i + \sum \mathbf{f}_{i/j} = \mathbf{a}_i \mathrm{d}m$, where $\mathbf{f}_{i/j}$ are the internal forces.

In all the derivations that follow, internal forces between particles or elements are ignored. This issue is discussed thoroughly in most textbooks, for example [33] and [37], and is based on the very reasonable assumption that the internal forces occur as equal but opposite pairs with the same line of action, this being the line connecting the two particles. Therefore the internal forces disappear when the sum over all elements is taken.

Taking moments around point A and taking the sum over all elements, $\mathbf{M}_A = \sum(\mathbf{r}_{i/A} \times \mathbf{F}_i)$. Using (B.9), the total moment of the accelerations is

$$\int (\mathbf{r}_{i/A} \times \mathbf{a}_i)\, \mathrm{d}m = \int (\mathbf{r}_{G/A} + \mathbf{r}_{i/G}) \times (\mathbf{a}_G + \boldsymbol{\alpha} \times \mathbf{r}_{i/G} - \omega^2\, \mathbf{r}_{i/G})\, \mathrm{d}m.$$

After simplifying, and using (B.2) to (B.8), the torque equation simplifies to

$$\mathbf{M}_A = \mathbf{r}_{G/A} \times m\, \mathbf{a}_G + I_G\, \boldsymbol{\alpha}. \tag{B.10}$$

When the reference point is a fixed point O, the acceleration in the first term in (B.10) is zero and the above equation leads to

$$\mathbf{M}_O = I_O\, \boldsymbol{\alpha}.$$

When the reference point is the centre of mass G then $\mathbf{r}_{G/A} = \mathbf{0}$ and (B.10) simplifies to

$$\mathbf{M}_G = I_G\, \boldsymbol{\alpha}.$$

These are the two forms of the torque equation that are generally used.

When the reference point is the IC, equation (B.10) does not simplify :

$$\mathbf{M}_C = \mathbf{r}_{G/C} \times m\, \mathbf{a}_G + I_G\, \boldsymbol{\alpha}. \tag{B.11}$$

This is not a particularly useful form of the torque equation, as it requires knowledge of $\mathbf{a}_G$ in order to find $\boldsymbol{\alpha}$.

B.4 The Loney equation

It will be shown below that a special and useful form of the torque equation can be obtained when using the IC as reference point. As previously mentioned, this special form is referred to as the Loney equation.

B.4.1 Derivation using the general torque equation

The vector equivalent of the derivations by Loney [25] and Lambe [26] takes the scalar product of $\boldsymbol{\omega}$ with each term of (B.11) :

$$\boldsymbol{\omega} \cdot \mathbf{M}_C = I_G \, \boldsymbol{\omega} \cdot \boldsymbol{\alpha} + m \, \boldsymbol{\omega} \cdot \mathbf{r}_{G/C} \times \mathbf{a}_G.$$

The last term can be simplified by using (B.3) and (B.26),

$$\boldsymbol{\omega} \cdot \mathbf{r}_{G/C} \times \mathbf{a}_G = \mathbf{a}_G \cdot \boldsymbol{\omega} \times \mathbf{r}_{G/C} = \mathbf{a}_G \cdot \mathbf{v}_G = \tfrac{1}{2} \tfrac{\mathrm{d}}{\mathrm{dt}} (\mathbf{v}_G \cdot \mathbf{v}_G) = \tfrac{1}{2} \tfrac{\mathrm{d}}{\mathrm{dt}} (v_G^2).$$

Similarly, the second term simplifies to $\boldsymbol{\omega} \cdot \boldsymbol{\alpha} = \tfrac{1}{2} \tfrac{\mathrm{d}}{\mathrm{dt}} (\boldsymbol{\omega} \cdot \boldsymbol{\omega}) = \tfrac{1}{2} \tfrac{\mathrm{d}}{\mathrm{dt}} (\omega^2)$.
Scalar components can be used as all the final vectors are perpendicular to the plane of motion, and the first term simplifies to $\boldsymbol{\omega} \cdot \mathbf{M}_C = \omega \cdot M_C$.

Using these results, the torque equation becomes

$$\omega \cdot M_C = \tfrac{1}{2} \tfrac{\mathrm{d}}{\mathrm{dt}} (I_G \, \omega^2 + m \, v_G^2) = \dot{T},$$

where $T = \tfrac{1}{2} (I_G \, \omega^2 + m \, v_G^2)$ is the total Kinetic energy.
This can also be written as $T = \tfrac{1}{2} (I_G + m \, r_{G/C}^2) \, \omega^2$ because $v_G = \omega \, r_{G/C}$;
therefore, using Steiner's theorem,

$$T = \tfrac{1}{2} I_C \, \omega^2 \quad \text{and} \quad \dot{T} = I_C \, \omega \, \alpha + \tfrac{1}{2} \dot{I}_C \, \omega^2.$$

After cancelling ω, the torque equation becomes

$$M_C = I_C \, \alpha + \tfrac{1}{2} \dot{I}_C \, \omega, \quad \omega \neq 0. \tag{B.12}$$

This is the form referred to as Loney's equation.

In cases where I_C is constant, this simplifies to

$$M_C = I_C \, \alpha. \tag{B.13}$$

This simple form of the equation is used in, inter alia, [27], [34] and [35].

Note that Loney's equation is *valid only if* $\omega \neq 0$. This point is not mentioned by Loney [25] or Lambe [26], and is ignored by Tiersten [22], who makes the rather debatable claim that (B.13) can always be used to find the initial angular acceleration if the initial angular velocity equals zero, by implication using (B.12).

B.4.2 Derivation using the Power equation

Recognising that Loney's equation contains the derivative of the kinetic energy, it is possible to derive the equation more directly by using energy principles. This is the method used by Tiersten [22]. [2]

A seldom-used form of the energy equation equates the total power to the time derivative of the kinetic energy :

$$P = \dot{T}. \tag{B.14}$$

[2] The author however recognised this method independently, before being aware of Tiersten's article.

Here $P = \sum(\mathbf{F}_i \cdot \mathbf{v}_i)$ is the total power generated by all the external forces, and T is the total kinetic energy. Therefore

$$\begin{aligned} P &= \sum(\mathbf{F}_i \cdot \mathbf{v}_i), \\ &= \sum(\mathbf{F}_i \cdot (\boldsymbol{\omega} \times \mathbf{r}_{i/C})), && \text{using (B.26)}, \\ &= \sum(\boldsymbol{\omega} \cdot (\mathbf{r}_{i/C} \times \mathbf{F}_i)), && \text{using (B.3)}, \\ &= \sum(\boldsymbol{\omega} \cdot \mathbf{M}_i), && \text{where } \mathbf{M}_i \text{ is the torque } (\mathbf{r}_{i/C} \times \mathbf{F}_i). \end{aligned}$$

Therefore $P = \omega M_C$, where $M_C = \sum(\boldsymbol{\omega} \cdot \mathbf{M}_i)$ is the total torque about C.

Also, as shown in the previous section and in for example [33], [28], [29], the total kinetic energy of the body can be written as $T = \frac{1}{2} I_C \omega^2$.

Using these expressions in (B.14), $\omega M_C = I_C\, \omega\, \dot{\omega} + \frac{1}{2} \dot{I}_C\, \omega^2$.
Cancelling ω if $\omega \neq 0$, and using $\alpha = \dot{\omega}$, the Loney equation (B.12) is once again obtained in the form

$$M_C = I_C\, \alpha + \tfrac{1}{2} \dot{I}_C\, \omega; \quad \omega \neq 0.$$

Loney's equation is not a true torque equation, in the sense that it cannot be derived directly from basic principles or Euler's laws. It is in fact derived from energy principles utilising the concept of kinetic energy, as shown above. However, it is written in the traditional form of a torque equation, namely relating the total torque to kinematic quantities, and could therefore be considered to be a "quasi" torque equation.
The relationship with energy methods is reinforced by the solution shown as equation (B.16) in the next section.

B.4.3 The general solution of Loney's equation

Loney's equation (B.12) can be re-written as a differential equation for which the general solution can be found as shown below.

Assume that $I_C = I_C(\theta)$, where $\dot{\theta} = \omega$. Then $\dot{I}_C = I'_C\, \omega$, where $(.)'$ denotes the derivative with respect to θ. Also, note that

$$\alpha = \frac{\mathrm{d}\omega}{\mathrm{d}t} = \frac{\mathrm{d}\omega}{\mathrm{d}\theta}\, \omega = \tfrac{1}{2} \frac{\mathrm{d}\omega^2}{\mathrm{d}\theta}.$$

Now (B.12) can be re-written as the linear first order differential equation

$$I_C\, \frac{\mathrm{d}\omega^2}{\mathrm{d}\theta} + I'_C\, \omega^2 = 2M_C$$

with the very simple integrating factor $e^{\int \frac{I'_C}{I_C}\, \mathrm{d}\theta} = I_C$ and solution

$$\omega^2 = \frac{2}{I_C} \int M_C\, \mathrm{d}\theta + C_1, \tag{B.15}$$

where C_1 is a constant of integration found from the initial conditions.

Alternatively, equation (B.15) can be re-written as

$$\tfrac{1}{2}\, I_C\, \omega^2 = \int M_C\, \mathrm{d}\theta + C_2. \tag{B.16}$$

This can be recognized as the relationship between kinetic energy and work.

B.4.4 Applying Loney's equation - a sliding rod

Loney's equation can be used to obtain the equation of motion for a rolling wheel or hoop, as shown in section A.2. The well-known textbook problem of a rigid rod sliding down a smooth vertical wall along a smooth horizontal floor is a second example where taking moments about the IC can be used to good advantage to obtain the solution for the angular velocity and acceleration as functions of position.

The rod is shown in figure B.2. The rod AB has mass m and length L, and is assumed to be eccentrically loaded so that the centre of mass is at point G with AG $= \gamma L$.

The moment of inertia with respect to G, I_G, is written as $I_G = \kappa_G\, mL^2$, with κ_G a known constant.
(For example, if a uniform rod with mass m_r is loaded with a particle at B with mass $m_B = 2m_r$, then $m = 3m_r$ and standard calculations show that $\gamma = 5/6$ and $\kappa_G = 1/12$).

The rotation of the rod is measured by θ as shown, and the angular velocity and acceleration are $\omega = \dot\theta$ and $\alpha = \ddot\theta$, taking anticlockwise as positive. The forces acting on the rod are the weight mg and the normal reactions N_A and N_B.
The IC is located at point C as shown, this point being the intersection of lines AC and BC which are perpendicular to the velocities of points A and B respectively.

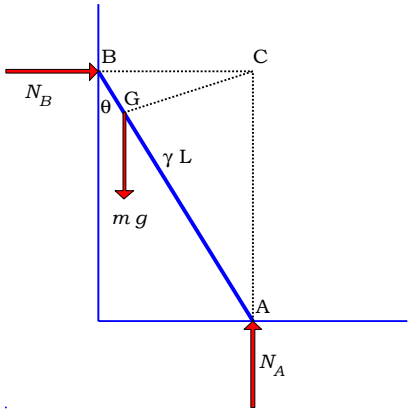

Figure B.2 : A sliding rod - geometry and forces

Using the law of cosines and simplifying,

$$(\mathrm{GC})^2 = L^2(\gamma^2 + (1-2\gamma)\,\cos^2\theta).$$

Using the parallel axis formula, the moment of inertia with respect to C is

$$I_C = \kappa_C\, mL^2, \quad \kappa_C = (\kappa_G + \gamma^2 + (1-2\gamma)\,\cos^2\theta),$$

and the derivative is

$$I'_C = mL^2\,\kappa'_C = mL^2\,(2\gamma - 1)\,\sin 2\theta.$$

Note that for an unloaded uniform rod with $\gamma = \frac{1}{2}$, GC $= L/2$ and the moment of inertia around C is constant; in this case (B.13) is applicable.

Using figure B.2, the total moment of the external forces around C is simply

$$M_C = mg\,\gamma L\,\sin\theta.$$

Using the above in (B.15) and simplifying gives the solution

$$\omega^2 = 2\gamma\,(g/L)\,(C_2 - \cos\theta)/\kappa_C,$$

where C_2 is obtained from the initial conditions.

B.5 Euler's second law

In section B.2.5 a slightly generalised form of Euler's second law was formulated as $\mathbf{M}_* = \dot{\mathbf{L}}_*$. In this section the reference points for which this applies will be derived without going into all the detail.

In section B.3.2 the centre of mass G was used in equation (B.9),

$$\mathbf{r}_i = \mathbf{r}_G + \mathbf{r}_{i/G}; \qquad \mathbf{v}_i = \dot{\mathbf{r}}_i = \mathbf{v}_G + \boldsymbol{\omega} \times \mathbf{r}_{i/G}; \qquad \mathbf{a}_i = \dot{\mathbf{v}}_i = \mathbf{a}_G + \boldsymbol{\alpha} \times \mathbf{r}_{i/G} - \omega^2\, \mathbf{r}_{i/G}.$$

This was then used as the starting point in deriving the torque equation in the form (B.10),

$$\mathbf{M}_A = \mathbf{r}_{G/A} \times m\, \mathbf{a}_G + I_G\, \boldsymbol{\alpha}.$$

Using similar methods, the angular momentum with respect to A is found to be

$$\mathbf{L}_A = \int (\mathbf{r}_{i/A} \times \mathbf{v}_i)\, \mathrm{d}m = \int (\mathbf{r}_{G/A} + \mathbf{r}_{i/G}) \times (\mathbf{v}_G + \boldsymbol{\omega} \times \mathbf{r}_{i/G})\, \mathrm{d}m.$$

Integrating term-by-term and simplifying, using (B.2) and (B.8), this is

$$\mathbf{L}_A = \mathbf{r}_{G/A} \times m\, \mathbf{v}_G + I_G\, \boldsymbol{\omega}. \tag{B.17}$$

The rate of change of the angular momentum is obtained by taking the time derivative of (B.17), using $\dot{\mathbf{r}}_{G/A} = (\mathbf{v}_G - \mathbf{v}_A)$ and noting that I_G is constant :

$$\dot{\mathbf{L}}_A = -\mathbf{v}_A \times m\, \mathbf{v}_G + \mathbf{r}_{G/A} \times m\, \mathbf{a}_G + I_G\, \boldsymbol{\alpha}. \tag{B.18}$$

The torque equation (B.10) is therefore

$$\mathbf{M}_A = \mathbf{r}_{G/A} \times m\, \mathbf{a}_G + I_G\, \boldsymbol{\alpha} = \dot{\mathbf{L}}_A + \mathbf{v}_A \times m\, \mathbf{v}_G.$$

Therefore Euler's second law does not apply when the moments are taken around an arbitrary point A. However, when the reference point is a fixed point O, the first term in (B.18) is zero and the above approach leads to

$$\mathbf{M}_O = \mathbf{r}_G \times m\, \mathbf{a}_G \; + \; I_G\, \boldsymbol{\alpha} = \dot{\mathbf{L}}_O. \tag{B.19}$$

This is of course the original formulation of Euler's second law by Truesdell [36].
If the fixed point is a body point as defined in section B.2.7, then $\mathbf{a}_G = \mathbf{r}_G \times \boldsymbol{\alpha}$, and (B.19) simplifies to

$$\mathbf{M}_{O_B} = I_{O_B}\, \boldsymbol{\alpha} = \dot{\mathbf{L}}_{O_B}.$$

Note that this does not apply to the IC, because $\mathbf{a}_C \neq 0$ even though $\mathbf{v}_C = 0$.

Similarly, if the centre of mass G is used as the reference point, (B.17) simplifies to $\mathbf{L}_G = I_G\, \boldsymbol{\omega}$ and the torque equation is again in the form of Euler's second law :

$$\mathbf{M}_G = I_G\, \boldsymbol{\alpha} = \dot{\mathbf{L}}_G.$$

When the IC is used as reference point, (B.17), (B.18) and (B.10) are simplified by using $\mathbf{v}_C = 0$ and result in the following expressions for the angular momentum and the torque equation

$$\mathbf{L}_C = \mathbf{r}_{G/C} \times m\, \mathbf{v}_G + I_G\, \boldsymbol{\omega} \quad \text{and} \quad \mathbf{M}_C = \mathbf{r}_{G/C} \times \; m\, \mathbf{a}_G + I_G\, \boldsymbol{\alpha} = \dot{\mathbf{L}}_C. \tag{B.20}$$

This is also in the form of Euler's second law.

A different set of equations is obtained if point P is located with respect to the reference point A; i.e. if $\mathbf{r}_i = \mathbf{r}_A + \mathbf{r}_{i/A}$ is used. However, this reference is now selected as a *body point* as defined in section B.2.7, and with the properties summarised by (B.1) This point will be denoted by point B. With this assumption, the velocity of any point relative to B can be written as

$$\mathbf{v}_{i/B} = \dot{\mathbf{r}}_{i/B} = \boldsymbol{\omega} \times \mathbf{r}_{i/B}; \quad \text{also} \quad \dot{\mathbf{r}}_{G/B} = \boldsymbol{\omega} \times \mathbf{r}_{G/B}. \tag{B.21}$$

Then, in stead of using (B.9), we use (B.21) and (B.2) to obtain the velocity and acceleration of any point P on the body as

$$\mathbf{r}_i = \mathbf{r}_B + \mathbf{r}_{i/B}; \qquad \mathbf{v}_i = \mathbf{v}_B + \boldsymbol{\omega} \times \mathbf{r}_{i/B}; \qquad \mathbf{a}_i = \mathbf{a}_B + \boldsymbol{\alpha} \times \mathbf{r}_{i/B} - \omega^2\, \mathbf{r}_{i/B}. \tag{B.22}$$

Using (B.22) and simplifying, the angular momentum relative to B is

$$\mathbf{L}_B = \int \mathbf{r}_{i/B} \times (\mathbf{v}_B + \boldsymbol{\omega} \times \mathbf{r}_{i/B}) \mathrm{d}m = m\mathbf{r}_{G/B} \times \mathbf{v}_B + I_B\, \boldsymbol{\omega}. \tag{B.23}$$

The rate of change of the angular momentum is obtained by taking the time derivative of (B.23) and noting that $\dot{\mathbf{r}}_{G/B} \times \mathbf{v}_B = (\boldsymbol{\omega} \times \mathbf{r}_{G/B}) \times \mathbf{v}_B = \mathbf{0}$, after using (B.21) and (B.2) :

$$\dot{\mathbf{L}}_B = m\mathbf{r}_{G/B} \times \mathbf{a}_B + I_B\, \boldsymbol{\alpha}. \tag{B.24}$$

The moment of the acceleration around B, using (B.22), is

$$\mathbf{r}_{i/B} \times \mathbf{a}_i = \mathbf{r}_{i/B} \times \mathbf{a}_B + \mathbf{r}_{i/B} \times \boldsymbol{\alpha} \times \mathbf{r}_{i/B} - \omega^2\, \mathbf{r}_{i/B} \times \mathbf{r}_{i/B} = \mathbf{r}_{i/B} \times \mathbf{a}_B + r_{i/B}^2\, \boldsymbol{\alpha},$$

and, after integrating over the body as before and using (B.24), the torque equation is once again in the form of Euler's second law.

$$\mathbf{M}_B = \mathbf{r}_{G/B} \times m\, \mathbf{a}_B + I_B\, \boldsymbol{\alpha} = \dot{\mathbf{L}}_B. \tag{B.25}$$

This form of the equation is especially useful in cases where the acceleration of the reference point is known; such an example is given by Meriam and Kraige [33], Sample Problem 6/8, p. 457. Rodriguez [24] also gives a number of similar examples.

The special cases of a fixed point O and the mass centre G are again easily obtained from (B.23) and (B.25), after noting that $\mathbf{v}_O = \mathbf{0}$, $\mathbf{a}_O = \mathbf{0}$ and $\mathbf{r}_{G/G} = \mathbf{0}$.

Noting that equation (B.21) is also applicable to the IC, with $\mathbf{v}_{i/C} = \boldsymbol{\omega} \times \mathbf{r}_{i/C}$, and, with $\mathbf{v}_C = \mathbf{0}$, the velocities are

$$\mathbf{v}_i = \boldsymbol{\omega} \times \mathbf{r}_{i/C}; \qquad \mathbf{v}_G = \boldsymbol{\omega} \times \mathbf{r}_{G/C}. \tag{B.26}$$

Therefore, (B.23) and (B.24) become :

$$\mathbf{L}_C = m\mathbf{r}_{G/C} \times \mathbf{v}_C + I_C\, \boldsymbol{\omega} = I_C\, \boldsymbol{\omega}; \quad \dot{\mathbf{L}}_C = m\mathbf{r}_{G/C} \times \mathbf{a}_C + I_C\, \boldsymbol{\alpha} + \dot{I}_C\, \boldsymbol{\omega}.$$

As pointed out previously, I_C is not necessarily constant because $r_{G/C}$ may be a function of time. Remembering that $\mathbf{a}_C \neq \mathbf{0}$, the acceleration of point P is obtained by differentiating (B.26)

$$\mathbf{a}_i = \mathbf{a}_C + \boldsymbol{\alpha} \times \mathbf{r}_{i/C} + \boldsymbol{\omega} \times \mathbf{v}_{i/C} = \mathbf{a}_C + \boldsymbol{\alpha} \times \mathbf{r}_{i/C} - \omega^2 \mathbf{r}_{i/C}$$

and the torque equation becomes

$$\mathbf{M}_C = \mathbf{r}_{G/C} \times m\, \mathbf{a}_C + I_C\, \boldsymbol{\alpha}. \tag{B.27}$$

Clearly, in this formulation $\mathbf{M}_C \neq \dot{\mathbf{L}}_C$.
In general $\mathbf{a}_C$ is unknown, and this form of the torque equation is not really useful.

In the special case of a rolling cylinder with C at the contact point and G at the centre of the cylinder, the first term in the torque equation in (B.27) is zero because $\mathbf{a}_C$ is directed from C to G. Also, the length C-G is constant, therefore I_C is constant, and the simple form of Euler's second law is obtained :

$$\mathbf{M}_C = \dot{\mathbf{L}}_C = I_C\, \boldsymbol{\alpha}. \tag{B.28}$$

This is the special case of which the use is discouraged by (inter alia) Desloge [23] and Zypman [21].

Equation (B.28) can also be seen as a special case of Loney's equation.

B.6 Summary

The previous section accentuates the large number of different variations of the torque equation. This diversity strengthens the arguments of those writers opposed to using points other than O or G as reference points. This writer would like to join Tiersten [22] in adding Loney's equation as the only other form of the torque equation to be used in practice.

All the different forms of the torque equation are listed below, and the cases where Euler's second law applies are shown.

It can be shown that Euler's second law is valid for a particle system :
$\mathbf{L}_O = \sum(\mathbf{r}_i \times m_i \mathbf{v}_i)$; $\quad \mathbf{M}_O = \sum(\mathbf{r}_i \times m_i \mathbf{a}_i) = \dot{\mathbf{L}}_O$, for any a fixed point O.

The following nine variations of the torque equation apply to rigid bodies.

a/. $\mathbf{L}_O = \mathbf{r}_G \times m\,\boldsymbol{\omega}_G + I_G\,\boldsymbol{\omega}$; $\quad \mathbf{M}_O = \mathbf{r}_G \times m\,\mathbf{a}_G + I_G\,\boldsymbol{\alpha} = \dot{\mathbf{L}}_O$, (B.19), any fixed point.

The simple form of Euler's second law is obtained in three cases :

b/. $\mathbf{L}_{O_B} = I_{O_B}\,\boldsymbol{\omega}$; $\quad \mathbf{M}_{O_B} = I_{O_B}\,\boldsymbol{\alpha} = \dot{\mathbf{L}}_{O_B}$, for rotation round a fixed axis O_B.
c/. $\mathbf{L}_G = I_G\,\boldsymbol{\omega}$; $\quad \mathbf{M}_G = I_G\,\boldsymbol{\alpha} = \dot{\mathbf{L}}_G$, for the mass centre G.
d/. $\mathbf{L}_C = I_C\,\boldsymbol{\omega}$; $\quad \mathbf{M}_C = I_C\,\boldsymbol{\alpha} = \dot{\mathbf{L}}_C$, (B.28) for the IC, *provided that I_C is constant.*

Loney's equation is not in the form of Euler's second law :
e/. $M_C = I_C\,\alpha + \frac{1}{2}\dot{I}_C\,\omega$, $\omega \neq 0$, (B.12).

It is suggested that the above equations be used in practical problem solving.

The following four variations of the torque equation are listed for the sake of completeness.

Euler's second law does *not* apply for an arbitrary point A :
f/. $\mathbf{L}_A = \mathbf{r}_{G/A} \times m\,\mathbf{v}_G + I_G\,\boldsymbol{\omega}$; $\quad \mathbf{M}_A = \mathbf{r}_{G/A} \times m\,\mathbf{a}_G + I_G\,\boldsymbol{\alpha}$, (B.17), (B.18) and (B.10).

The more general form of Euler's second law does apply for any "body point" B :
g/. $\mathbf{L}_B = m\mathbf{r}_{G/B} \times \mathbf{v}_B + I_B\,\boldsymbol{\omega}$; $\quad \mathbf{M}_B = \mathbf{r}_{G/B} \times m\,\mathbf{a}_B + I_B\,\boldsymbol{\alpha} = \dot{\mathbf{L}}_B$, (B.23), (B.25).

Two more forms of the torque equation are obtained for moments about the IC, in which only the first is a form of Euler's second law :
h/. $\mathbf{L}_C = I_C\,\boldsymbol{\omega}$; $\quad \mathbf{M}_C = \mathbf{r}_{G/C} \times m\,\mathbf{a}_G + I_G\,\boldsymbol{\alpha} = \dot{\mathbf{L}}_C$, (B.20);
i/. $\mathbf{L}_C = I_C\,\boldsymbol{\omega}$; $\quad \mathbf{M}_C = \mathbf{r}_{G/C} \times m\,\mathbf{a}_C + I_C\,\boldsymbol{\alpha}$, (B.27), $\neq \dot{\mathbf{L}}_C$ for I_C not constant.

Appendix C

The Lagrange method

In this appendix the Lagrange method for solving problems of dynamics is used to obtain the equations of motion for loaded hoops. The Lagrange equations are first given in general terms, and then applied to a general elastic loaded hoop

C.1 The Lagrange equations

The Lagrange method is an alternative to Newton's second law for deriving the equations of motion of a system of bodies. For simple problems there is little to choose between the two approaches; for complex systems, especially where there are a number of constraints, the Lagrange method is frequently simpler to apply. Whereas the Newton approach is based on the force and acceleration vectors, the Lagrange approach uses expressions for the energy. Whereas the Newton approach frequently requires " ... searching for ingenious special devices for getting the equations of motion for any particular system. ... The method of Lagrange .. provides a systematic plan for writing down these equations." [42].

The notation used in this appendix for the Lagrange method mainly follows that used by Greenwood [41], chapter 6, with some reference to Synge & Griffiths [42], chapter 15. The notation used here is however adjusted in certain respects for the purpose of this appendix.

Given below is a very brief and synoptic summary of the method. The concepts are defined more precisely in the next section when being applied to the problem of a loaded hoop. This summary is confined to motion in two dimensions of systems that are scleronomic and non-conservative and which may include non-holonomic constraints. (These concepts are defined later). The Lagrange approach depends on the correct use of the concepts listed below.

- **Degrees of freedom** The number of degrees of freedom of a system is the minimum number of independent coordinates that are required to specify the configuration of the system, and will be denoted by N :

$$N = \text{number of degrees of freedom.}$$

- **Generalised coordinates** It is frequently convenient to specify a configuration using more than N coordinates; say n coordinates in total. These need not be coordinates in the usual sense of, for example, cartesian or polar coordinates. The *generalised coordinates*

are defined as n quantities which are used to specify the configuration and the energy of the system.

A generalised coordinate is denoted by $q_i,\ i = 1, \ldots, n$, and the set of generalised coordinates by

$$\mathsf{q} = \{q_1, q_2, \ldots, q_n\}, \quad \text{or, in vector form, by} \quad \mathbf{q} = \begin{bmatrix} q_1 & q_2 & \ldots & q_n \end{bmatrix}^t.$$

The coordinates that are selected as the degrees of freedom are always placed first in $\mathbf{q}$, and are denoted by $\mathbf{q}_d$;

$$\mathbf{q}_d = \begin{bmatrix} q_1 & q_2 & \ldots & q_N \end{bmatrix}^t.$$

- **Constraints** In cases where $n > N$, independent equations of constraint are required. The number of constraints is denoted by m, with

$$m = n - N, \quad n \geq N.$$

Certain constraints are classified as *holonomic* and may be used to eliminate the corresponding coordinates from the equations. The remaining coordinates are then termed the *free coordinates*, and the number of free coordinates is denoted by N_f. The sub-set of free coordinates is always placed first in $\mathbf{q}$, includes $\mathbf{q}_d$, and is denoted by

$$\mathbf{q}_f = \begin{bmatrix} q_1 & \ldots & q_N & q_{N+1} & \ldots & q_{N_f} \end{bmatrix}^t.$$

Further classification of the different types of constraint is discussed later.

The difference $N_f - N$ is termed the *redundancy* and is denoted by r. Therefore

$$N_f = N + r, \quad r \geq 0.$$

The free coordinates that are not degrees of freedom are termed *redundant coordinates*.

- **The Lagrange function** The kinetic energy of a system is formulated in terms of the generalised coordinates and the first derivatives :

$$T = T(\mathbf{q},\ \dot{\mathbf{q}}) = T(q_1, q_2, \ldots, q_n, \quad \dot{q}_1, \dot{q}_2, \ldots, \dot{q}_n).$$

The potential energy associated with the conservative forces in the system is

$$V = V(\mathbf{q}) = V(q_1, q_2, \ldots, q_n).$$

The Lagrange function, or simply the *Lagrangian*, L, is defined as

$$L = T - V = L(\mathbf{q},\ \ \dot{\mathbf{q}}).$$

A partial derivative function of L is calculated for each free variable. These partial derivatives are denoted by S_i and are defined as

$$S_i = \frac{\mathrm{d}}{\mathrm{dt}} \left(\frac{\partial L}{\partial \dot{q}_i} \right) - \frac{\partial L}{\partial q_i}, \quad (i = 1, \ldots, N_f). \tag{C.1}$$

- **Generalised forces and forces of constraint**

  A *generalised force* Q_i is found for each free coordinate. These generalised forces are formulated in terms of the virtual work of the forces not included in the expression for the potential energy; this concept will be illustrated in the next section.

  A *constraint force* C_i is found for each free coordinate, as described below. Each redundant coordinate in q_f has associated with it a non-holonomic constraint equation. This set of constraint equations can be written in matrix form as

$$\mathbf{A}_f \, \mathrm{d}\mathbf{q}_f = 0, \quad \text{or} \quad \mathbf{A}_f \, \dot{\mathbf{q}}_f = 0, \tag{C.2}$$

  where $\mathbf{A}_f$ is an r x N_f matrix of coefficients of the constraint equations. Then the vector of constraint forces, $\mathbf{c}$, is defined as

$$\mathbf{c} = \mathbf{A}_f^t \, \boldsymbol{\lambda}, \tag{C.3}$$

  where

$$\mathbf{c} = \left[\; C_1, \; \ldots \; , C_{N_f} \; \right]^t,$$

  and

$$\boldsymbol{\lambda} = \left[\; \lambda_1, \; \ldots \; , \lambda_r \; \right]^t$$

  is the vector of *Lagrange multipliers*.

  In many applications the λ's can be interpreted in terms of physical quantities.

- **The Lagrange equations**

  The *Lagrange equations* are defined as the set of equations :

$$S_i = Q_i + C_i, \;\; (i = 1, \ldots, N_f). \tag{C.4}$$

  Note that whereas the Lagrangian L may be formulated in terms of the full set of n coordinates, one Lagrange equation is formulated for each free coordinate.

  This set of equations contains the N_f unknown free coordinates as well as the r unknown Lagrange multipliers. In order to solve the problem, the r constraint equations must be solved simultaneously with the N_f Lagrange equations (C.4).

  It will usually be possible to eliminate the λ's and the redundant coordinates by means of the constraint equations, leaving a set of N equations in the N coordinates in q_d.

Use of the Lagrange equations (C.4) depends entirely on the correct formulation of the expressions for the energy, the generalised forces and the forces of constraint. The Lagrange approach is flexible, in the sense that the user has some freedom in the selection of the free coordinates to be used. Two such choices are illustrated in the application to loaded hoops, resulting in different paths to the final solution.

C.2 The Lagrange method applied to elastic hoops

In order to demonstrate the power of the Lagrange method, the equations for a loaded *elastic* hoop on an *elastic* surface are derived below; in other words, a combination of the internal and elastic models is considered. This will be referred to as the *general model*.

C.2.1 Coordinates and constraints

The dynamic system being considered here is shown in Figure C.1. As before, $(X\ ,\ Y)$ are the coordinates of the centre O, and $(x\ ,\ y)$ the coordinates of the mass centre G. The geometric parameters are m, g, r and γ with $I_G = \kappa_G m r^2 = (1-\gamma^2)mr^2$.

Now the external elastic force due to deformation of the surface is denoted by $k_1 d_1$, and the internal force due to the deformation of OC in the hoop by $k_2 d_2$. The two elastic forces are in sequence, therefore

$$F_n = k_1 d_1 = k_2 d_2; \quad \text{and} \quad d_1 = (k_2/k_1) d_2. \tag{C.5}$$

The holonomic constraint on Y now becomes $Y = r - d_1 - d_2 = r - ((k_2/k_1)+1)d_2$, and it is convenient to define the parameter $\beta = ((k_2/k_1)+1)$. Writing $d = d_2$ for the general model,

$$Y = r - \beta\, d; \quad \beta = (1 + k_2/k_1); \quad d = d_2. \tag{C.6}$$

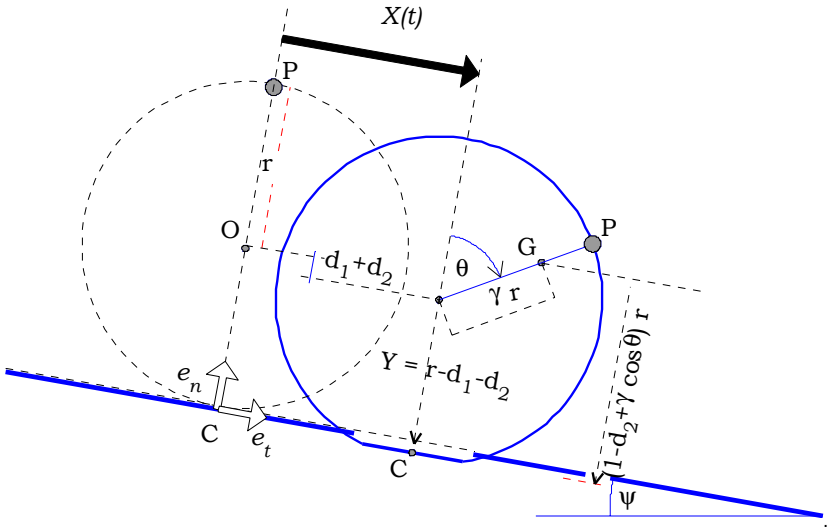

Figure C.1 : The general model : elastic hoop on an elastic surface

Also from Figure C.1, $\mathcal{H} r = r - d_2 + \gamma r \cos\theta$ and $I_C = I_G + mr^2\,(\mathcal{H}^2 + (\gamma \sin\theta)^2)$.
Using $\delta = d_2/r$ for the general model, this simplifies to

$$\mathcal{H} = 1 - \delta + \gamma\cos\theta; \quad \kappa_C = 1 + 2(1-\delta)\gamma\cos\theta + (1-\delta)^2. \tag{C.7}$$

The internal elastic model is obtained from the general model by assuming a rigid surface, i.e. $k_1 \to \infty$ and $\beta = 1$. Also $d_1 = 0$, $d_2 = d$ and $k = k_2$.

The external model is obtained from the general model by first re-defining β in C.6 as $\beta = (1 + k_1/k_2)$ and using $d = d_1$. Then the rigid hoop is modelled by taking $k_2 \to \infty$ and $\beta = 1$, with $d_1 = d$, $k_1 = k$ and $d_2 = 0$, therefore $\delta = 0$.

Table C.1 summarises the geometry of the three elastic models.

General model	Internal elastic model	External elastic model
$d = d_2 \;\; ; \;\; k = k_2$	$d = d_2 \;\; ; \;\; k = k_2$ $d_1 = 0 \;\; ; \;\; k_1 \to \infty$	$d = d_1 \;\; ; \;\; k = k_1$ $d_2 = 0 \;\; ; \;\; k_2 \to \infty$
$\beta = 1 + k_2/k_1$	$\beta = 1$	$\beta = 1$ $\delta = 0$
$Y = r - d_1 - d_2 = r - \beta d$	$Y = r - d_2$	$Y = r - d_1$
$\mathcal{H} = 1 - \delta + \gamma \cos\theta$	$\mathcal{H} = 1 - \delta + \gamma \cos\theta$	$\mathcal{H} = 1 + \gamma \cos\theta$
$\kappa_C = 1 + 2(1-\delta)\gamma\cos\theta$ $+(1-\delta)^2$	$\kappa_C = 1 + 2(1-\delta)\gamma\cos\theta$ $+(1-\delta)^2$	$\kappa_C = 2\mathcal{H}$

Table C.1 : Geometry of the three elastic models

As before, the assumed rigidity of radius OP enforces the constraints

$$x(t) = X(t) + \gamma\, r\, \sin\theta(t), \qquad y(t) = Y(t) + \gamma\, r\, \cos\theta(t), \tag{C.8}$$

and differentiation with respect to time results in

$$\dot{x} = \dot{X} + \gamma\, r\, \cos\theta\, \dot{\theta}, \qquad \dot{y} = -\beta\dot{d} - \gamma\, r\, \sin\theta\, \dot{\theta}. \tag{C.9}$$

Note that (C.8) is also the transformation from the generalised coordinates (X , Y) to the cartesian coordinates.

C.2.2 The Lagrangian for the general model

The total kinetic energy is

$$T = \tfrac{1}{2} m v_G^2 + \tfrac{1}{2} I_G \dot{\theta}^2 = \tfrac{1}{2} I_G \dot{\theta}^2 + \tfrac{1}{2} m \dot{x}^2 + \tfrac{1}{2} m \dot{y}^2. \tag{C.10}$$

Using the origin of the axes as reference, the potential energy for the weight is

$$V_g = mg\left(-X \sin\psi + Y \cos\psi + \gamma r \cos(\psi + \theta)\right). \tag{C.11}$$

The potential energy for the elastic forces is

$$V_k = \tfrac{1}{2} k_1 d_1^2 + \tfrac{1}{2} k_2 d_2^2 = \tfrac{1}{2} \beta k d^2. \tag{C.12}$$

Using the holonomic constraint (C.6), the Lagrangian, $L = T - V$ is

$$L = \tfrac{1}{2} I_G \dot{\theta}^2 + \tfrac{1}{2} m \dot{x}^2 + \tfrac{1}{2} m \dot{y}^2 + mg\left(X \sin\psi - (r - \beta d)\cos\psi - \gamma r \cos(\psi + \theta)\right) - \tfrac{1}{2}\beta k d^2. \tag{C.13}$$

The set of generalised coordinates (in vector form) for the general elastic model is therefore

$$\mathbf{q}_d = \begin{bmatrix} \theta & d & X & x & y \end{bmatrix}^t.$$

C.2.3 The Lagrange equations (i) - without pre-elimination

In this section (C.9) is used as a non-holonomic constraint; therefore the set of free generalised coordinates is

$$\mathbf{q}_f = \mathbf{q}_d = \begin{bmatrix} \theta & d & X & x & y \end{bmatrix}^t.$$

In this application therefore, $N_f = 5$, $N = 3$ and the redundancy $r = 2$.

The partial derivatives of the Lagrangian are next obtained for each free coordinate, using (C.1) $S_i = \frac{\mathrm{d}}{\mathrm{dt}} \left(\frac{\partial L}{\partial \dot{q}_i}\right) - \frac{\partial L}{\partial q_i}$.

For the first coordinate, θ, $S_1 = I_G\ddot{\theta} - mg\gamma r \sin(\psi + \theta)$.

For d this becomes $S_2 = -mg\beta \cos\psi + \beta k d$.

For X, this is $S_3 = -mg \sin\psi$.

For x : $S_4 = m\ddot{x}$.

For y : $S_5 = m\ddot{y}$.

The next step is to obtain expressions for the generalised forces, Q_i. This is defined in terms of the concept of virtual work, calculated for each of the non-conservative forces during a virtual displacement.

Without going into further detail, we note that here the friction force F_f is the only non-conservative force and that the virtual work is simply $F_f\ \delta X - F_f\ (r - d_2)\delta\theta$. Note that d_1 does not affect the virtual work. The vector of generalised forces is therefore

$$\mathbf{Q} = \begin{bmatrix} -(r-d)F_f & 0 & F_f & 0 & 0 \end{bmatrix}^t.$$

Equations (C.2) and (C.3) are now used to obtain expressions for the forces of constraint. Taking x and y as the redundant coordinates and noting that (C.9) can be written in the standard form for the non-holonomic constraint equation, namely $\mathbf{A}_f\ \dot{\mathbf{q}}_f = \mathbf{0}$, or

$$\begin{bmatrix} -\gamma r\cos\theta & 0 & -1 & 1 & 0 \\ \gamma r \sin\theta & \beta & 0 & 0 & 1 \end{bmatrix} \begin{bmatrix} \dot{\theta} \\ \dot{d} \\ \dot{X} \\ \dot{x} \\ \dot{y} \end{bmatrix} = \begin{bmatrix} 0 \\ 0 \end{bmatrix}. \tag{C.14}$$

The vector of constraint forces, $\mathbf{c}$ is defined as $\mathbf{c} = \mathbf{A}_f^t\ \boldsymbol{\lambda}$; therefore

$$\begin{bmatrix} C_1 \\ C_2 \\ C_3 \\ C_4 \\ C_5 \end{bmatrix} = \begin{bmatrix} -r\gamma\cos\theta & r\gamma\sin\theta \\ 0 & \beta \\ -1 & 0 \\ 1 & 0 \\ 0 & 1 \end{bmatrix} \begin{bmatrix} \lambda_1 \\ \lambda_2 \end{bmatrix}. \tag{C.15}$$

Then the *Lagrange equations* (C.4), $S_i = Q_i + C_i$, $(i = 1, \ldots, N_f)$ can be written in vector

form as

$$\begin{bmatrix} I_G\ddot{\theta} - mg\gamma r\sin(\psi+\theta) \\ -mg\,\cos\psi + kd \\ -mg\,\sin\psi \\ m\ddot{x} \\ m\ddot{y} \end{bmatrix} = \begin{bmatrix} -(r-d)F_f \\ 0 \\ F_f \\ 0 \\ 0 \end{bmatrix} + \begin{bmatrix} -\gamma r\cos\theta\,\lambda_1 + \gamma r\sin\theta\,\lambda_2 \\ \lambda_2 \\ -\lambda_1 \\ \lambda_1 \\ \lambda_2 \end{bmatrix} \tag{C.16}$$

after cancelling β from the second equation.

The third equation defines the first Lagrange multiplier as $\lambda_1 = F_f + mg\sin\psi$.
Therefore λ_1 is the transverse component of the resultant force.

Similarly, $\lambda_2 = -mg\,\cos\psi + kd$ is the normal component of the resultant force.

The first equation is $I_G\ddot{\theta} - mg\gamma r\sin(\psi+\theta) = -rF_f - \gamma r\cos\theta\,\lambda_1 + \gamma r\sin\theta\,\lambda_2$.
After eliminating the λ's by using the second and third equations and using $F_n = kd$, this simplifies to

$$I_G\ddot{\theta} = -\mathcal{H}rF_f + F_n\gamma r\sin\theta.$$

This is equivalent to the torque equation (2.12).

The fourth equation is $m\ddot{x} = \lambda_1 = F_f + mg\sin\psi$, which is Newton's second law for the transverse components.

Similarly, the fifth equation leads to Newton's second law for the normal components :
$m\ddot{y} = kd - mg\,\cos\psi$.

To summarise : here the Lagrange equations supply the three equations of motion that can be obtained more directly from Newton's second law. The solution is now obtained by differentiating the rigidity constraints (C.9) with respect to time and following the same procedures as in Chapters 2 and 5.

Note that the five Lagrange equations above do not include explicit equations for the first and second degrees of freedom, X and d. The reason for this is that the expression for the kinetic energy did not include these coordinates explicitly. In the next section these coordinates are included by eliminating $\dot{x}$ and $\dot{y}$ from the expression for the kinetic energy.

C.2.4 The Lagrange equations (ii) - with pre-elimination

In the derivation of the Lagrange equations in the previous section the redundant coordinates x and y are eliminated *after* applying the Lagrange equations. In this section, they are pre-eliminated.

Using (C.9), the total kinetic energy (C.10) is

$$T == \tfrac{1}{2}I_G\dot{\theta}^2 + \tfrac{1}{2}m(\dot{X} + \gamma\,r\,\cos\theta\,\dot{\theta})^2 + \tfrac{1}{2}m(-\beta\dot{d} - \gamma\,r\,\sin\theta\,\dot{\theta})^2,$$

or

$$T = \tfrac{1}{2}I_G\dot{\theta}^2 + \tfrac{1}{2}m\gamma^2\,r^2\,\dot{\theta}^2 + m\,\dot{X}\,\dot{\theta}\,\gamma\,r\cos\theta + m\,\beta\dot{d}\,\dot{\theta}\,\gamma\,r\sin\theta + \tfrac{1}{2}m\,\dot{X}^2 + \tfrac{1}{2}m\,\beta^2\dot{d}^2.$$

Noting that $I_G = (1-\gamma^2)mr^2$ and that the potential energy is again given by (C.11) and (C.12), the Lagrangian becomes

$$\begin{aligned} L \;=\; & \tfrac{1}{2}m\,r^2\,\dot{\theta}^2 + m\,\dot{X}\,\dot{\theta}\,\gamma\,r\cos\theta + m\,\beta\dot{d}\,\dot{\theta}\,\gamma\,r\sin\theta + \tfrac{1}{2}m\,\dot{X}^2 + \tfrac{1}{2}m\,\beta^2\dot{d}^2 \\ & + mg\,(X\sin\psi - (r-\beta d)\cos\psi - \gamma r\cos(\psi+\theta)) - \tfrac{1}{2}\beta k d^2. \end{aligned} \tag{C.17}$$

Now L is a function of θ, d and X and the first time derivatives; therefore the vector of free coordinates consists only of the degrees of freedom; i.e. $N_f = N = 3$ and there is no redundancy so that

$$\mathbf{q}_f = \mathbf{q}_d = \begin{bmatrix} \theta & d & X \end{bmatrix}^t.$$

The partial derivatives of the Lagrangian are obtained next for each free coordinate, using (C.1) $S_i = \frac{\mathrm{d}}{\mathrm{dt}} \frac{\partial L}{\partial \dot{q}_i} - \frac{\partial L}{\partial q_i}$. For the first coordinate, θ, this simplifies to

$$S_1 = mr^2\,\ddot{\theta} + m\gamma r \sin\theta\,\beta\ddot{d} + m\gamma r\cos\theta\,\ddot{X} - mg\gamma r\sin(\psi+\theta).$$

For coordinates d and X these partial derivatives simplify to

$$S_2 = m\beta\gamma r\sin\theta\,\ddot{\theta} + m\beta^2\ddot{d} + m\beta\gamma\, r\cos\theta\,\dot{\theta}^2 + \beta k d - mg\beta\cos\psi;$$

$$S_3 = m\gamma r\cos\theta\,\ddot{\theta} + m\ddot{X} - m\gamma\, r\sin\theta\,\dot{\theta}^2 - mg\sin\psi.$$

The expression for the virtual work is the same as before, $F_f\ \delta X - F_f\ (r-d)\delta\theta$, and the vector of generalised forces is

$$\mathbf{Q} = \begin{bmatrix} -r(1-\delta)F_f & 0 & F_f \end{bmatrix}^t.$$

The solution of the problem requires an additional constraint, because the three Lagrange equations contain three unknown coordinates plus the unknown friction force. This additional constraint relates to whether the hoop is rolling or slipping.

C.2.5 Equations of motion for rolling

The constraint for rolling motion for the general model, using Figure C.1, is

$$\dot{X} = (r - d_2)\,\dot{\theta}, \tag{C.18}$$

or, in the standard form for non-holonomic constraints, as

$$\begin{bmatrix} r(1-\delta) & 0 & -1 \end{bmatrix}.\dot{\mathbf{q}}_f = 0.$$

Therefore the forces of constraint are

$$\begin{bmatrix} C_1 \\ C_2 \\ C_3 \end{bmatrix} = \begin{bmatrix} r(1-\delta) \\ 0 \\ -1 \end{bmatrix} \lambda_3,$$

and the Lagrange equations $S_i = Q_i + C_i$ are

$$\begin{bmatrix} S_1 \\ S_2 \\ S_3 \end{bmatrix} = \begin{bmatrix} -r(1-\delta) \\ 0 \\ 1 \end{bmatrix} F_f + \begin{bmatrix} r(1-\delta) \\ 0 \\ -1 \end{bmatrix} \lambda_3.$$

By eliminating λ_3 from the first and third equations, this becomes

$$\begin{bmatrix} S_1 + r(1-\delta)S_3 \\ S_2 \end{bmatrix} = \begin{bmatrix} 0 \\ 0 \end{bmatrix}.$$

Note that the friction force has disappeared from the equations, as expected because it does not influence the accelerations during rolling.

Substituting S_1 and S_3, the first equation becomes

$$\begin{aligned} mr^2\,\ddot{\theta} + m\gamma r\sin\theta\,\beta\ddot{d} + m\gamma r\cos\theta\,\ddot{X} - mg\gamma r\sin(\psi+\theta) \\ +r(1-\delta)\,\Big(m\gamma r\cos\theta\,\ddot{\theta} + m\ddot{X} - m\gamma\, r\sin\theta\,\dot{\theta}^2 - mg\sin\psi\Big) = 0. \end{aligned}$$

Substituting S_2 and cancelling β the second Lagrange equation is

$$m\gamma r\sin\theta\,\ddot{\theta} + m\beta\ddot{d} + m\gamma\, r\cos\theta\,\dot{\theta}^2 + kd - mg\cos\psi = 0.$$

The third equation is obtained by differentiating the rolling constraint (C.18) to obtain

$$\ddot{X} = r(1-\delta)\,\ddot{\theta} - \dot{\theta}\,\dot{d}.$$

After cancelling a factor mr from the first equation and m from the second, the equations of motion can be written as

$$\begin{bmatrix} (1+(1-\delta)\gamma\cos\theta) & \gamma\sin\theta & (\gamma\cos\theta+1-\delta) \\ \gamma\sin\theta & 1 & 0 \\ -(1-\delta) & 0 & 1 \end{bmatrix} \begin{bmatrix} r\ddot{\theta} \\ \beta\ddot{d} \\ \ddot{X} \end{bmatrix} =$$

$$r\dot{\theta}^2 \begin{bmatrix} (1-\delta)\gamma\sin\theta \\ -\gamma\cos\theta \\ 0 \end{bmatrix} + \begin{bmatrix} 0 \\ 0 \\ -\dot{\theta}\,\dot{d} \end{bmatrix} + (k/m)\,d \begin{bmatrix} 0 \\ -1 \\ 0 \end{bmatrix} + g \begin{bmatrix} \gamma\sin(\theta+\psi) + (1-\delta)\sin\psi \\ \cos\psi \\ 0 \end{bmatrix}. \quad \text{(C.19)}$$

This is a well defined set of three second order differential equations which, together with the necessary initial conditions, can be solved numerically. However, it is normal in cases of rolling motion to eliminate $\ddot{X}$ before solving the differential equations, as was done in Chapters 2 and 5. When this is done, the equations for rolling simplify to

$$\begin{bmatrix} \kappa_C & \gamma\sin\theta \\ \gamma\sin\theta & 1 \end{bmatrix} \begin{bmatrix} r\ddot{\theta} \\ \beta\ddot{d} \end{bmatrix} =$$

$$r\dot{\theta}^2 \begin{bmatrix} (1-\delta)\gamma\sin\theta \\ -\gamma\cos\theta \end{bmatrix} + \begin{bmatrix} \mathcal{H}\dot{\theta}\,\dot{d} \\ 0 \end{bmatrix} + (k/m)\,d \begin{bmatrix} 0 \\ -1 \end{bmatrix} + g \begin{bmatrix} \gamma\sin(\theta+\psi) + (1-\delta)\sin\psi \\ \cos\psi \end{bmatrix}. \quad \text{(C.20)}$$

Note that the vectors on the right hand side are the contributions of the ' centrifugal force', a type of 'Coriolis force', the elastic force and gravity respectively.

After setting $\beta = 1$ to obtain the internal elastic model, these are the same as the non-dimensional set of equations obtained in Section 5.3.2 for the case $\psi = 0$.

To obtain the external model, $\beta = 1$, $\delta = 0$ and the 'Coriolis' term disappears when the rolling constraint C.18 is differentiated. Then (C.20) is the same as the non-dimensional equations in Section 5.2.3 for the case $\psi = 0$. Also, after simplifying the last term, the first equation corresponds with (2.25) as obtained in Section 2.4.

C.2.6 Equations of motion for slipping

The friction force during slipping is $F_f = \mu F_n$, where it is convenient to define $\mu = +\mu_k$ for spinning and $\mu = -\mu_k$ for skidding, as in Chapters 2, 4 and 5. Using $F_n = kd$ for the general model, the vector for the generalised forces becomes

$$\mathbf{Q} = \mu k d \begin{bmatrix} -r(1-\delta) & 0 & 1 \end{bmatrix}^t.$$

Now there are no additional constraints or redundancies, so that the three Lagrange equations are simply $S_i = Q_i$. After cancelling mr from the first equation, $m\beta$ from the second and m from the third, the equations can be written in matrix form as

$$\begin{bmatrix} 1 & \gamma\sin\theta & \gamma\cos\theta \\ \gamma\sin\theta & 1 & 0 \\ \gamma\cos\theta & 0 & 1 \end{bmatrix} \begin{bmatrix} r\ddot{\theta} \\ \beta\ddot{d} \\ \ddot{X} \end{bmatrix} = r\dot{\theta}^2 \begin{bmatrix} 0 \\ -\gamma\cos\theta \\ \gamma\sin\theta \end{bmatrix} + (kd/m) \begin{bmatrix} -\mu(1-\delta) \\ -1 \\ \mu \end{bmatrix} + g \begin{bmatrix} \gamma\sin(\theta+\psi) \\ \cos\psi \\ \sin\psi \end{bmatrix}. \tag{C.21}$$

The matrix in (C.21) may be interpreted as a mass matrix and denoted by $\mathbf{M}$. The determinate of $\mathbf{M}$ is found to be $1-\gamma^2$, i.e. κ_G, and the inverse is the symmetric matrix

$$\mathbf{M}^{-1} = \frac{1}{\kappa_G} \begin{bmatrix} 1 & -\gamma\sin\theta & -\gamma\cos\theta \\ -\gamma\sin\theta & 1-\gamma^2\cos^2\theta & \gamma^2\sin\theta\cos\theta \\ -\gamma\cos\theta & \gamma^2\sin\theta\cos\theta & 1-\gamma^2\sin^2\theta \end{bmatrix}. \tag{C.22}$$

Pre-multiplying with this inverse matrix, and using the notation of the slip factor

$$S = \gamma\sin\theta - \mu\,\mathcal{H},$$

as defined in (2.27), the first Lagrange equation simplifies to

$$r\ddot{\theta} = (1/\kappa_G)\,(k/m)\,S\,d.$$

This is equivalent to the non-dimensional equation (7.13) used previously.

Similarly, the second Lagrange equation simplifies to the equivalent of (7.14),

$$\beta\ddot{d} = -\gamma\cos\theta\, r\dot{\theta}^2 - (k/m)(1 + (1/\kappa_G)\,S\,\gamma\sin\theta)d + g\,\cos\psi.$$

The third equation was previously used without eliminating $\ddot{\theta}$; therefore the third Lagrange equation in (C.21) can be written as

$$\ddot{X} = -\gamma\cos\theta\, r\ddot{\theta} + \gamma\sin\theta\, r\dot{\theta}^2 + \mu(k/m)\,d + g\sin\psi.$$

This is equivalent to the non-dimensional equation used before in Chapter 5.

Alternatively, $\ddot{\theta}$ can be eliminated by pre-multiplying the third equation in (C.21) by $\mathbf{M}^{-1}$. However, the different factors in this equation do not simplify and are not given here.

C.3 Conclusions

There is little difference between the Lagrange and Newtonian approaches as regards the amount of effort required to obtain the equations of motion for the loaded hoops that have been considered in this dissertation.

Appendix D

Moment of inertia of an elastic hoop

In the model for the internal elastic model of a hoop, section 7.3, the assumption was made that the moment of inertia of a rigid hoop could also be used for the deformed hoop, namely that I_G is given by

$$I_G = (1 - \gamma^2)\, mr^2. \tag{D.1}$$

. The validity of this assumption is investigated in this appendix.

The figure shows the deformed hoop, with the deformed section spanning an angle 2ϕ.
Noting that $\mathrm{OC} = r - d = r(1 - \delta) = r\cos\phi$,

$$\cos\phi = 1 - \delta.$$

The figure is drawn for a large deformation with value $\delta = 0.1$.
The deformed hoop consists of a circular part (part 1), and the straight section (part 2). The masses of the two parts are

$$m_1 = (1 - \phi/\pi)m_h;$$

$$m_2 = (\phi/\pi)m_h,$$

assuming that all the mass that was in the circular arc is now compressed uniformly into a shorter line segment of length L_2, where

$$L_2 = 2r\sin\phi.$$

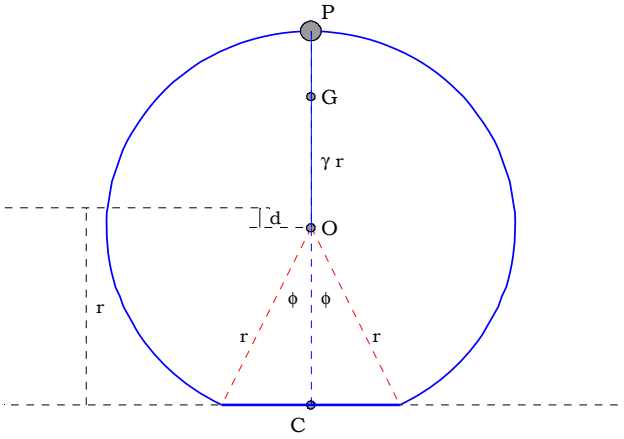

Deformed hoop

For the hoop the moment of inertia about O is $I_{Oh} = m_1 r^2 + (1/12)m_2 L_2^2 + m_2(r\cos\phi)^2$.
This simplifies to

$$I_{Oh} = m_h r^2 \left[1 - \frac{2}{3}\frac{\phi}{\pi}\sin^2\phi\right].$$

The error term in I_{Oh} is denoted by

$$E_h = \frac{2}{3}\frac{\phi}{\pi}\sin^2\phi.$$

The total moment of inertia (of the elastic hoop plus the particle) about O is
$I_O = m_h r^2[1 - E_h] + m_p r^2 = mr^2 - m_h r^2 E_h$, and about G this becomes
$I_{Ge} = mr^2 - m_h r^2 E_h - m(\gamma r)^2$, where $m = m_h + m_p$ and $m_h = (1-\gamma)m$ as before. Therefore

$$I_{Ge} = mr^2 \left[1 - \gamma^2 - (1-\gamma)E_h\right]. \tag{D.2}$$

. The % error in I_G due to the assumption (D.1) is $E_G = 100(I_{Ge} - I_G)/I_{Ge}$, or

$$E_G = 100\,\frac{-(1-\gamma)E_h}{(1-\gamma^2) - (1-\gamma)E_h}\,\% = \frac{100}{1 - (1+\gamma)/E_h}\,\%. \tag{D.3}$$

.

Table D.1 shows the values of ϕ for a range of values for δ. The tabulated values for e are calculated from the relationship $\delta_0 = 1/e$; i.e. these are the values of e that would result in an initial deformation equal to δ. Also shown are the corresponding values for the moment of inertia I_{Ge} and the % error using (D.2) and (D.3). A typical value of $\gamma = 2/3$ is used, with $I_G = 0.5556\,mr^2$ from (D.1).

δ	0.005	0.01	0.02	0.05	0.1	0.2	0.5
e	200	100	50	20	10	-	-
ϕ°	5.7	8.1	11.5	18.2	25.8	36.9	60
$I_{Ge}/(mr^2)$	0.5555	0.5554	0.5550	0.5534	0.5495	0.5392	0.5
$E_G\%$	-0.013	-0.036	-0.10	-0.4	-1.10	-3.04	-11.1

Table D.1 : Error in the moment of inertia of a deformed hoop for $\gamma = 2/3$

The results in Chapter 7 show that:

- In cases of immediate and early hopping the deformation is always less than δ_0, and that column 6 shows the maximum possible deformation for $e \geq 10$.
- In cases of normal and backspin hopping δ reaches a maximum in the region of $\theta = 180^\circ$. This maximum can be much greater than δ_0.
- Figure 7.12 for backspin hopping shows a maximum value of $\delta \approx 0.2$. Column 7 in Table D.1 shows the corresponding values, with an error of 3%.
- The last column shows the case where the compression is half the radius and results in $\phi = 60^\circ$. Even in this extreme case the error is just over 11%.

It is therefore reasonable to conclude that the error made by using $I_G = (1-\gamma^2)mr^2$ is small and may be ignored.

Appendix E

Listings of computer programs

In this appendix the most important functions of the MATLAB implementation of the algorithms are listed for the elastic models.

E.1 The main program

All the parameters and initial values and control parameters are set in the calling program.

```
% ----------------------------
pi = 4*atan(1);  r2d=180/pi;  d2r=pi/180;   % define pi; convert degrees to radians
maxTh = 360;  maxThR = maxTh*d2r;           % stop analysis when theta = 360 deg

% model parameters
eps = 0.0; muKfactr = 1.0; psi=0; psiR=psi*d2r; % fixed parameters
gamma = input(' gamma = ?');                    % input the eccentricity
     KG = 1 + eps - gamma*gamma;
muS = input(' \mu = ? ');                   % Friction;  muK = muKfactr*muS
e1 = 50;                                    % Assign elastic constant
par = [gamma, KG, muS, muKfactr, maxThR, eps, psiR, e1]
% ----------------------------------------------------
% Initial values
Emodl='Ea';     %External model  - flag to choose between internal or external model
[initL, CondnCode]=E_InitialValues(e1, Emodl);   % function to assign/input initial values
% initL = [ theta0, omega0, X0, Vx0, delta0, Vd0 ]

% Control paramaters
inc=0.01; epsilon=1.0E-12;  Tf =2*maxThR/0.3;  % max time for numerical integration
maxStep=0.01; % used in ODE45
Cpar=[inc, epsilon, Tf, maxStep];         % Control parameters required by various functions

ZF=0;  % Zero Flag : 1='on' = test for w=0 and stop; 0='off'= do not test, allow w<0;
% ============================================================
```

The following function is used to assign and input the initial values.

```
function[initL, CondnCode]=E_InitialValues(e1,Emodl);
% ------------------------------------------------
th0=0;  X0=0; Vd0=0;
w0 = input(' omega0 = ? ');
d0 = 1/e1; % alternative : input(' d0 = ? ');
if Emodl=='Ea'; Vx0=w0;  end        % External model - rolling
if Emodl=='Eb'; Vx0=(1-d0)*w0; end  % Internal model - rolling
initL=[th0, w0, X0, Vx0, d0, Vd0];
CondnCode = 'R';                    % Always start with Rolling
% ------------------------------------------------
```

The main program then calls the solution function and processes the values that are returned in various ways, for example to plot a graph or a phase diagram. The detail of these processes will not be discussed here. The main solution function is based on the algorithm in section 4.4

E.2 The main solution function

This function receives a single set of parameters and initial values, then calculates and returns the complete solution up till the final position.

In the following functions the variable 'eta' is used for omega squared ($\eta = \omega^2$.

```
function[X, Z, PhI, PR, Angles]=E_SingleSolution(par,initL,CondnCode,Cpar,Emodl,ZF);
% ------------------------------------------------------------------------------------
%   Calculates all phases for a single set of parameters & initial values
%   Returns X = [theta, omega, X, Vx, delta, Vd]
%           Z = [alpha, Ax, Ad, N, F];
%         PhI = index where phase changes; Pr = PhaseRecord : labels of each phase
%      Angles = angle where each phase change occurs
% ------------------------------------------------------------------------------------
% Initialise
X = [0, 0, 0, 0, 0, 0];  Z = [0, 0, 0, 0, 0, 0]; PhI=[0]; PR=[0]; Angles=[0];
lastX=initL; %[lastTh, lastW, lastXx, lastVx, lastD, lastVd];
% Solve for any sequence of  Roll or slip
for J=1:15   % more than maximum number of possible repetitions
if CondnCode == 'R'
  if(J==1); PR='R'; else PR=[PR, CondnCode]; end;
  [X1, CondnCode]=E_SingleRoll(par, lastX, Cpar, Emodl,ZF);
  if Emodl=='Ea'; [eta, alpha, Ax, Ad, N, F] = Ea_valRoll(par,X1); end
  if Emodl=='Eb'; [eta, alpha, Ax, Ad, N, F] = Eb_valRoll(par,X1); end

  Z1=[eta, alpha, Ax, Ad, N, F]; th=X1(:,1); ie1=length(th);
   if ie1 > 1
       X=[X;X1]; Z=[Z; Z1]; PhI=[PhI, ie1] ; Angles=[Angles, th(ie1)];
       lastX=X1(ie1,:);  % initial values for next phase
     else %did not roll
```

```
       L=length(PR); PR(L)='_';
   end  % if ie1
end  % CondnCode == 'R'

if ((CondnCode == 'S')|(CondnCode == 'D'))
  PR=[PR, CondnCode];  Code2=CondnCode;
  [X1, Z1, CondnCode]=E_SingleSlip(par, lastX, Code2, Cpar, Emodl,ZF);
  th=Z1(:,1); ie1=length(th);
  if ie1 > 1
     X=[X; X1]; Z=[Z; Z1]; PhI=[PhI, ie1]; Angles=[Angles, th(ie1)];
       lastX=X1(ie1,:);
   end  % else did not slip
end

if (( CondnCode == 'Z')|( CondnCode == 'H')|( CondnCode == 'T'))
       PR=[PR, CondnCode];
       break
end

end % for J = 1:15

% Strip first row (= zeros)
L=length(Z(:,1)); r=[2:L]; X=X(r,:); Z=Z(r,:);

% Test for negative omega when ZF=0
w=X(:,2); PRf=PR(end);
if ((ZF==0) & (w(end)<0))
    if PRf ~= 'H'; PR(end)='Z'; end
end
% ================================================================
```

E.3 Functions for a rolling phase

Only the functions relating to the external model will be listed. The corresponding functions for the internal model are very similar.

The following function calculates and returns the complete solution for one rolling phase.

```
function[X2, CondnCode]=E_SingleRoll(par, initL, Cpar, Emodl,ZF);
% ----------------------------------------------------------------
muS=par(3); muK=muS*par(4); maxTh=par(5); w0=initL(2);
inc=Cpar(1); epsilon=Cpar(2); Tf=Cpar(3); maxStep=Cpar(4);
Tspan2=[0:inc:Tf];  options2=odeset('events','on','MaxStep',maxStep); % for ODE45

% Calc first value to check for large discontinuities at end of slipping
if Emodl=='Ea'; [eta, alpha, Ax, Ad, N1, F1] = Ea_valRoll_1(par,initL); end;
if Emodl=='Eb'; [eta, alpha, Ax, Ad, N1, F1] = Eb_valRoll_1(par,initL); end;
if abs(F1) > muK*N1  % immediate slipping
    X2=initL; if F1 > 0; CondnCode='S'; else CondnCode='D';  end
else
 if Emodl=='Ea'
  [T2,X2,te2,Xe2] = ODE45('Ea_ModERoll',Tspan2, initL, options2,par,ZF); % event = (muS*N-abs(
  [eta, alpha, Ax, Ad, N, F] = Ea_valRoll(par,X2);
 end
 if Emodl=='Eb'
  [T2,X2,te2,Xe2] = ODE45('Eb_ModERoll',Tspan2, initL, options2,par,ZF); % event = (muS*N-abs(
  [eta, alpha, Ax, Ad, N, F] = Eb_valRoll(par,X2);
 end
  ie1=length(T2);  theta = X2(:,1);  w=X2(:,2);  Vx=X2(:,4); d=X2(:,5);
    Z1=[0]; Z1 = [eta, alpha, Ax, Ad, N, F];
    lastTh=theta(ie1);  lastEta=eta(ie1); lastN=N(ie1); lastF=F(ie1); %lastVx=Vx(ie1);
% Assign CondnCode for next phase
  CondnCode ='?';
  if ((abs(maxTh-lastTh) <= epsilon) |(lastTh > maxTh) )
    CondnCode='T';
  else
   if (muS*lastN-abs(lastF)) <= epsilon ;
      if lastF > 0; CondnCode='S'; else CondnCode='D'; end;
   end;
  end
  if (lastEta <= epsilon ); CondnCode='Z';  end;
  if (lastN <= epsilon ); CondnCode='H';  end;
end % if immediate slip

%Last_th_N=[lastTh*r2d, lastN]
%CondnCode
% ------------------------------------
```

The following functions are used by the MATLAB function ODE45 to solve the set of differential equations. These functions represent the mathematical model developed in Chapter 5.

```
function varargout = Ea_ModERoll(t, x, flag,par,ZF)
%            called by ode45 - event used to find end of Rolling
% ---------------------------------------------------------------
switch flag
   case ''
      varargout{1} = Ea_Roll(t,x,par);  % define the ode
   case 'events'
     [varargout{1:3}] = Ea_eventRoll(t,x,par,ZF);  % define the event
   otherwise
      error(['Unknown flag']);
   end
% ---------------------------------------------

function [value,ist,dir]=Ea_eventRoll(t,x,par,ZF);  % define the event
%
   th=x(1);  wi=x(2); di=x(5);
   gamma = par(1); KG=par(2); muS=par(3); maxTh=par(5); e1=par(8);
%    === Only for eps=0; psi =0;  !!!!!!!!!!
    gst=gamma*sin(th);  gct=gamma*cos(th);  eta=wi^2;
    h = 1 + gct;   D1= KG + h^2;  N = e1*di;
    alpha=(eta*h + N)*gst/D1;
    F = h*alpha - gst*eta;
%
  dir = -1;  % negative slope through the zero point
  if th < maxTh
    if ZF==1; value = (muS*N-abs(F))*wi*di;end;
    if ZF==0; value = (muS*N-abs(F))*di;end;
  else
    value = maxTh - th;  %dir=-1;
  end
  ist = 1;                % terminates execution : on=1; off=0;
% ------------------------------------------------

function rk = Ea_Roll(t,x, par)   % define the ode
%
  th = x(1);  w  = x(2);  Xx= x(3); Vx=x(4);  d=x(5); Vd=x(6);
  gamma=par(1);  KG=par(2); e1=par(8);
    gst=gamma*sin(th);  gct=gamma*cos(th);  eta=w^2;
    h = 1 + gct;   D1= KG + h^2;  N = e1*d;
    alpha=(eta*h + N)*gst/D1;
    Ad = 1 - N - eta*gct - alpha*gst;  Ax = alpha;
%
  rk = [w;  alpha;  Vx; Ax;  Vd; Ad];  % Column vector x'
%------------------------------------------------
```

The following function calculates the values $\eta = \omega^2$, α, the accelerations X'' and δ'', and the forces F_n/mg and F_f/mg, for a single solution vector $\mathbf{x} = [\theta, \omega, X/r, (X/r)', \delta, \delta']$.

```
function[eta, alpha, Ax, Ad, N, F] = Ea_valRoll_1(par,x);  % single x
% ------------------------------------------------------------------------
gamma = par(1); KG=par(2); e1=par(8);
thi = x(1);  wi=x(2);  di = x(5); Vdi=x(6);
%    === Only for eps=0; psi =0;  !!!!!!!!!!
    gst=gamma*sin(thi);  gct=gamma*cos(thi);  eta=wi.^2;
    h = 1 + gct;   D1= KG + h.^2;
    N = e1*di;
    alpha=(eta.*h + N).*gst./D1;
    Ad = 1 - N - eta.*gct - alpha.*gst;
    Ax = alpha;
    F = h.*alpha - gst.*eta;
% ========================================================================
```

E.4 Functions for a slipping phase

A similar set of functions is required for the slipping phases.

```
function[X2, Z1, CondnCode]=E_SingleSlip(par, initL, Code2, Cpar, Emodl,ZF);
% ------------------------------------------------------------------------
muS=par(3); muKfactr=par(4); maxTh=par(5); e1=par(8);
% Rolling finished
  if Code2=='S';  muK =  muKfactr*muS; end
  if Code2=='D';  muK = -muKfactr*muS; end
% Control parameters
Tf=Cpar(3); maxStep=Cpar(4); Tspan2=[0:inc:Tf];
options2=odeset('events','on','MaxStep',maxStep);
%
% Find end of slipping : event = (Vx-w)*w*N or (maxTH-th)
if Emodl=='Ea'
  [T2,X2,te2,Xe2] = ODE45('Ea_ModESlip',Tspan2, initL, options2,par,muK,ZF);
  [eta, alpha, Ax, Ad, N, F] = Ea_valSlip(X2,par, muK);
end;
if Emodl=='Eb'
  [T2,X2,te2,Xe2] = ODE45('Eb_ModESlip',Tspan2, initL, options2,par,muK,ZF);
  [eta, alpha, Ax, Ad, N, F] = Eb_valSlip(X2,par, muK);
end;
%
  ie1=length(T2);   theta = X2(:,1);  w=X2(:,2);  Vx=X2(:,4);  d=X2(:,5);
  Z1=[0]; Z1 = [eta, alpha, Ax, Ad, N, F];
  lastX=X2(ie1,:); lastTh=lastX(1);  lastW=lastX(2); lastD=lastX(5); lastVx=lastX(4);
\newpage
if ((abs(maxTh-lastTh) <= epsilon) |(lastTh > maxTh) );  CondnCode='T';
 else
 if ( abs(lastD) <= epsilon);  CondnCode='H';
   else
   if ( abs(lastW) <= epsilon);  CondnCode='Z';
    else
    if ( abs(lastW-lastVx) <= epsilon); CondnCode='R';
      else
        display(' Error in E_SingleSlip - no minimumevent')
        CondnCode='?';
      end
    end
   end
end
% ========================================================================
```

The following functions are used by the MATLAB function ODE45 to solve the set of differential equations used for slipping. These functions represent the mathematical model developed in Chapter 5.

```
function varargout = E_ModESlip(t, x, flag,par,muK,ZF)
% ------------------------------------------------------------
switch flag
   case ''
      varargout{1} = Ea_Slip(t,x,par,muK);  % define the ode
   case 'events'
     [varargout{1:3}] = Ea_event(t,x,par,muK,ZF);  % define the event
   otherwise
      error(['Unknown flag']);
   end
% ---------------------------------------------
function [value,ist,dir]=Ea_event(t,x,par,muK,ZF);    % define the event
%
maxTh=par(5); th=x(1);  w=x(2); Vx=x(4);  d=x(5);
if muK > 0   % spin,  Vx < w
  Sd = (w-Vx);  % to find where the hoop stops slipping  Vx = w
else        %skid, Vx > w
  Sd = (Vx-w);
end
%
dir = -1;
  if th < maxTh
    if ZF==1; value = d*w*Sd;  end; % Zero flag is on, test for omega = 0.
    if ZF==0; value = d*Sd;  end; %
  else
    value = maxTh - th;  %dir=-1;
  end
ist = 1;                % terminates execution : on=1; off=0;
% -------------------------------------------------
function rk = Ea_Slip(t,x, par, muK)  % define the ode
  th=x(1);  w  = x(2); Xx=x(3);  Vx=x(4); d=x(5); Vd=x(6);
  gamma = par(1); KG=par(2);  e1=par(8);
  gct = gamma*cos(th);        gst = gamma*sin(th);
  S = gst - muK*(1 + gct);    SoK=S/KG;
  N = e1*d;   F =  muK*N;
%
  eta = w*w;  alpha = N*SoK;
  Ad = 1  - eta*gct - N*(1 + SoK*gst);
  Ax = F - gct*alpha + gst*eta; % + sin(psi);  % Ax = (X/r)'' - eq.74

  rk = [w; alpha; Vx;  Ax;  Vd;  Ad];
%-------------------------------------------------
```

The following function calculates the values $\eta = \omega^2$, α, the accelerations X'' and δ'', and the forces F_n/mg and F_f/mg, for a matrix of solution vectors $\mathbf{x} = [\theta, \omega, X/r, (X/r)', \delta, \delta']$.

```
  function [eta, alpha, Ax, Ad, N, F] = E_valSlip(X,par, muK)
%  Calculates the values for theta-vector - External Model; Slip
%  ASSUME psi = 0
  gamma = par(1); KG=par(2);  e1=par(8);
  th = X(:,1);  w  = X(:,2); d=X(:,5);
  gct = gamma*cos(th);        gst = gamma*sin(th);
  S = gst - muK*(1 + gct);    SoK=S/KG;
%
  N = e1*d;   F =  muK*N;
  eta = w.*w;
  alpha = N.*SoK;
  Ad = 1  - eta.*gct - N.*(1 + SoK.*gst);
  Ax = F - gct.*alpha + gst.*eta; % + sin(psi);  % Ax = (X/r)'' - eq.74
% ========================================================================
```